

POLYMERIC MICELLES FOR SOLUBILIZATION AND TARGETING OF HYDROPHOBIC DRUGS

Dissertation zur Erlangung des Doktorgrades
der Naturwissenschaften (Dr. rer. nat.)
der Fakultät für Chemie und Pharmazie
der Universität Regensburg



vorgelegt von
Tobias Miller aus Potsdam

Juni 2012

Diese Doktorarbeit entstand in der Zeit vom April 2009 bis Juni 2012 bei der Merck KGaA, Exploratory Pharmaceutical Developement, Darmstadt, in Zusammenarbeit mit dem Institut für Pharmazeutische Technologie der Universität Regensburg.

Die Arbeit wurde von Prof. Dr. Achim Göpferich betreut.

Promotionsgesuch eingereicht am:	04.06.2012
Datum der mündlichen Prüfung:	27.06.2012
Prüfungsausschuss:	Prof. Dr. Sigurd Elz (Vorsitzender) Prof. Dr. Achim Göpferich (Erstgutachter) PD Dr. Rainer Müller (Zweitgutachter) Prof. Dr. Frank-Michael Matysik (Drittprüfer)

To try and fail is at least to learn; to fail to try is to suffer the inestimable loss of what might have been.

Chester Barnard

Contents

1	Introduction	1
1.1	Academic research vs industrial development	2
1.2	Stress factor analysis: implications on drug targeting	5
1.2.1	Abstract	6
1.2.2	Introduction	7
1.2.3	Analysis of stress mechanisms occurring immediately upon injection of polymeric micelles	9
1.2.3.1	Physical events during injection - formulations entering the body	9
1.2.3.2	Biophysical events upon injection	10
1.2.4	Implications for passive targeting	20
1.2.4.1	Evidence of EPR effect for macromolecules	20
1.2.4.2	The EPR effect in case of nanoparticles	21
1.2.4.3	Additional factors shaping EPR effect	23
1.2.5	Conclusion	25
1.2.6	Future perspective	26
1.3	Research objectives of the thesis	27
2	Drug loading of polymeric micelles	29
2.1	Abstract	30
2.2	Introduction	31
2.3	Materials and methods	32
2.3.1	Materials	32
2.3.2	Methods	32
2.3.2.1	Preparation of drug loaded micelles	32
2.3.2.2	Drug load determination	33
2.3.2.3	Particle size measurement	34
2.3.2.4	Lyoprotector screening via Differential Scanning Calorimetry (DSC)	34
2.3.2.5	Lyoprotector screening via lyophilization of placebo micelles .	34
2.3.2.6	Influence of lyoprotector concentration on micelle reconstitution	35

2.3.2.7	Cryo-Transmission Electron Microscopy (cryo-EM)	35
2.4	Results	35
2.4.1	Solvents for cosolvent evaporation	35
2.4.2	Preparation of drug loaded micelles	36
2.4.3	Lyoprotector screening via DSC and lyophilization of placebo micelles	36
2.4.4	Optimum concentration of lyoprotector	39
2.4.5	Morphological and size analysis by cryo-EM	40
2.5	Discussion	42
2.6	Conclusions	50
3	<i>In vitro</i> serum stability	51
3.1	Abstract	52
3.2	Introduction	53
3.3	Materials and methods	55
3.3.1	Materials	55
3.3.2	Polymer characterization by differential scanning calorimetry (DSC) .	55
3.3.3	Micelle preparation	55
3.3.3.1	Samples for determination of critical association concentration (CAC)	55
3.3.3.2	Samples for serum incubation studies, Asymmetrical Flow Field Flow Fractionation (AF4) experiments, and Transmis- sion Electron Microscopy (TEM)	56
3.3.4	Micelle characterization	56
3.3.4.1	Determination of critical association concentration (CAC) . .	56
3.3.4.2	Particle size measurements	57
3.3.4.3	Transmission Electron Microscopy (TEM)	57
3.3.5	Determination of micelles' <i>in vitro</i> serum stability	57
3.3.5.1	Sample incubation, FRET ratio determination, calculation of stability parameters	57
3.3.5.2	Asymmetrical Flow Field Flow Fractionation (AF4)	58
3.4	Results	59
3.4.1	Polymer and micelles characterization	59
3.4.2	FRET stability assay	61
3.4.3	Asymmetrical Flow Field Flow Fractionation (AF4)	65
3.5	Discussion	66
3.6	Conclusion	69
4	Cytotoxicity and immunogenicity	71
4.1	Abstract	72

4.2	Introduction	73
4.3	Materials and methods	74
4.3.1	Materials	74
4.3.2	Methods	74
4.3.2.1	Synthesis of PEG-PEI as reference material	74
4.3.2.2	Micelle preparation	75
4.3.2.3	Particle size measurements	77
4.3.2.4	Cell incubation experiments	77
4.3.2.5	Determination of complement scission products upon serum incubation	78
4.4	Results	78
4.4.1	PEG-PEI synthesis	78
4.4.2	Particle size of test materials	78
4.4.3	Cytotoxicity assay	78
4.4.4	Complement activation assays	81
4.5	Discussion	81
4.6	Conclusion	84
5	Drug encapsulation and biodistribution	87
5.1	Abstract	88
5.2	Introduction	89
5.3	Materials and methods	89
5.3.1	Materials	89
5.3.2	Methods	90
5.3.2.1	Solvent screen prior to cosolvent evaporation	90
5.3.2.2	Polymer screen to load compound A into micelles	90
5.3.2.3	Preparation of study materials	91
5.3.3	Particle size measurements	91
5.3.4	Biodistribution experiments of micelles vs. solution	92
5.3.5	Preparation of radiolabeled H ₂ N-PEG-PLGA and bioimaging	92
5.4	Results	93
5.4.1	Solvent screen for cosolvent evaporation	93
5.4.2	Drug loading, particle sizes and size distributions for compound A loaded micelles	94
5.4.3	Injected formulations for biodistribution purposes	94
5.4.4	Biodistribution of compound A-loaded PEG-PLGA micelles	96
5.4.5	Synthesis of H ₂ N-PEG-PLGA and bioimaging	97
5.4.5.1	Synthesis	97

5.4.5.2	Bioimaging	98
5.5	Discussion	100
5.6	Conclusions	103
6	PEG-PVPy labeling and biodistribution	105
6.1	Abstract	106
6.2	Introduction	107
6.3	Materials and methods	107
6.3.1	Materials	107
6.3.2	Methods	108
6.3.2.1	PEG-PVPy quaternization and labeling with radioactive io- dine isotopes	108
6.3.2.2	Bioimaging of labeled PEG-PVPy micelles	109
6.3.2.3	Biodistribution of labeled PEG-PVPy micelles	109
6.4	Results	109
6.4.1	Preparation of labeled PEG-PVPy	109
6.4.2	Bioimaging of labeled PEG-PVPy micelles	110
6.4.2.1	IFF in unlabeled PEG-PVPy micelles	110
6.4.2.2	Labeled PEG-PVPy micelles	110
6.4.2.3	Elucidation of PEG-PVPy body clearance	111
6.5	Discussion	112
6.6	Conclusions	113
6.7	Outlook	113
7	The fate of carrier and ecapsulated drugs	115
7.1	Abstract	116
7.2	Introduction	117
7.3	Materials and methods	118
7.3.1	Materials	118
7.3.2	Methods	118
7.3.2.1	Synthesis of H ₂ N-PEG-PDLLA	118
7.3.2.2	Polymer analytics	119
7.3.2.3	Radioactive labeling of H ₂ N-PEG-PLA	119
7.3.2.4	Radiolabeling of H ₂ N-PEG	120
7.3.2.5	Formulation preparation for biodistribution and bioimaging .	120
7.3.2.6	Animal preparation and <i>in vivo</i> studies	121
7.4	Results	122
7.4.1	Polymer synthesis, analytics and micelle characterization	122

7.4.2	Bioimaging	123
7.4.2.1	Drug-loaded polymeric micelles	123
7.4.2.2	^{111}In -DOTA-NH-PEG-PLA solution	124
7.4.2.3	^{111}In -DOTA-NH-PEG solution	125
7.4.3	Biodistribution of dual-labeled polymeric micelles with ^{131}I FF payload in several animal groups of tumor-bearing mice	126
7.5	Discussion	128
7.6	Conclusion	131
8	Summary and conclusion	133
	Bibliography	138
	List of abbreviations	164
	List of figures	167
	List of tables	169
	Appendix	171
	Curriculum vitae	172
	List of publications	173
	Acknowledgements	175

Chapter 1

Introduction

1.1 Drug delivery at the interface of academic research and industrial development

Pharmaceutical companies underwent massive economic pressure in the last decades. The major reasons for this were and still are varying challenges which comprise of 1) increasing regulatory hurdles to enhance drug safety, 2) decreasing effectiveness of industrial research and development processes in receiving drug approvals and 3) decreasing financial resources of the society which is less able to fund drug innovations.

The less effective efficacy of development processes was impressively shown by Mullard [1]. From 1996 to 2010 the number of the yearly drug approvals by the Food and Drug Administration (FDA) declined from 53 (in 1996) to 15 (in 2010) in a time period of only 14 years. Simultaneously the development costs and the market entry time for each new drug candidate were continuously rising resulting in less profitability of the newly approved medicines [2]. In this connection the questions becomes relevant: Why do so many novel drugs fail? Kola and Landis [3] reviewed this issue in 2004 and presented the most prominent reasons for drug attrition upon approval. These comprised of factors such as 1) insufficient clinical efficacy, 2) undesirable pharmacokinetics and low bioavailability, 3) unexpected toxic side effects, 4) insufficient formulation stability as well as economical reasons like 5) low marketing success or 6) unjustifiable cost of goods. It can be suggested that these issues were not limited to drug attrition but also were important factors for the failure of discovery compounds in early phases.

Looking again at the facts 1) to 6) that Kola and Landis reported, the question arises which impact novel drug delivery technologies might have to reduce drug failure rates. Based on the idea of targeted, organ specific delivery, nanoparticles have the potential to change drug disposition in the body compared to freely administered small molecules [4]. The controllable size, charge and material properties of nanoparticles allowed for potential changes in biodistribution of the encapsulated drugs. Consequently by controlling the pharmacokinetic properties of the drug by the carrier system, the drugs' efficacy, bioavailability and toxicology profile can be altered (factors 1, 2 and 3 reported by Kola and Landis [3]). Summarizing all these factors, by increasing the efficacy of development processes, all participants, pharmaceutical companies and society, will benefit.

Polymeric micelles present a promising tool to increase bioavailability and alter the toxicological profile of the encapsulated drug. Based on above suggestions, the topics of this thesis comprised of solubilization of hydrophobic drugs combined with *in vitro* and *in vivo* approaches to investigate the micelles' targeted delivery potential. As many discovery compounds in pharmaceutical industry are hydrophobic [5, 6], polymeric micelles are a highly interesting drug delivery system which requires intensive fundamental research prior to their

implementation in industrial development processes. Specific knowledge gaps to date are in the fields of drug-polymer, micelle-blood and body-polymer interactions. The thesis will focus on some aspects of these interactions such as 1) drug loading, 2) stability in biofluids, 3) potential cytotoxic and immunogenic reactions and finally 4) *in vivo* performance regarding pharmacokinetics.

Despite the specific gaps in fundamental understanding of micellar systems, a few products already entered the market: the anticancer drugs Paclitaxel/Docetaxel containing micellar drugs Genexol-PM[®] and Nanoxel-PM[®]. Both drugs reduce the toxicity of the original formulation Taxol[®] containing a mixture of Cremophor EL[®] and ethanol as solubilizers. Finally these novel formulations led to increased tolerated doses and therefore higher efficacy compared to the original one [7].

To pick up the thoughts outlined above, the multiple interactions of colloidal carriers with the biological systems to which they are applied, determine efficacy and safety of nanomedicine. The fate of nanoparticles upon injection is still quite unknown but definitely will have a strong influence on both, the particles and the biological system. Enlightenment regarding this topic will be delivered by analyzing the stress mechanism which colloidal carriers encounter upon injection. For this purpose, literature was revisited and analyzed in section 1.2 which finally led to the question what factors can be made responsible for successful accumulating colloidal carriers in tumor tissue.

1.2 Analysis of immediate stress mechanisms upon injection of polymeric micelles and related colloidal drug carriers: implications on drug targeting

Tobias Miller^{1,3}, Alexandra Hill^{1,2}, Senta Uezguen¹, Markus Weigandt¹, Achim Goepferich³

¹ Merck KGaA, Exploratory Pharmaceutical Development, Frankfurter Str. 250, 64293 Darmstadt, Germany

² Martin-Luther-University of Halle-Wittenberg, Department Pharmaceutical Technology and Biopharmaceutics, Wolfgang-Langenbeck-Straße 4, 06120 Halle, Germany

³ University of Regensburg, Department of Pharmaceutical Technology, Universitätsstrasse 31, 93040 Regensburg, Germany

Published in: *Biomacromolecules* (2012)

1.2.1 Abstract

Polymeric micelles are ideal carriers for solubilization and targeting applications using hydrophobic drugs. Stability of colloidal aggregates upon injection into the blood stream is mandatory to maintain the drugs' targeting potential and to influence pharmacokinetics. In this review the most relevant stress mechanisms that polymeric micelles and related colloidal carriers encounter upon injection are analyzed and discussed (Fig. 1.1), including: 1) dilution, 2) interactions with blood components and 3) immunological responses of the body. In detail the opsonin-dysopsonin hypothesis was analyzed that points at a connection between a particles' protein-corona and its tissue accumulation by the enhanced permeability and retention (EPR) effect. In the established theory size is seen as a necessary condition to reach nanoparticle accumulation in disease modified tissue. There is, however, mounting evidence of other sufficient conditions (e.g. particle charge, receptor recognition of proteins adsorbed onto particle surfaces) triggering nanoparticle extravasation by active mechanisms. In conclusion, the analyzed stress mechanisms are directly responsible for *in vivo* success or failure of the site-specific delivery with colloidal carrier systems.

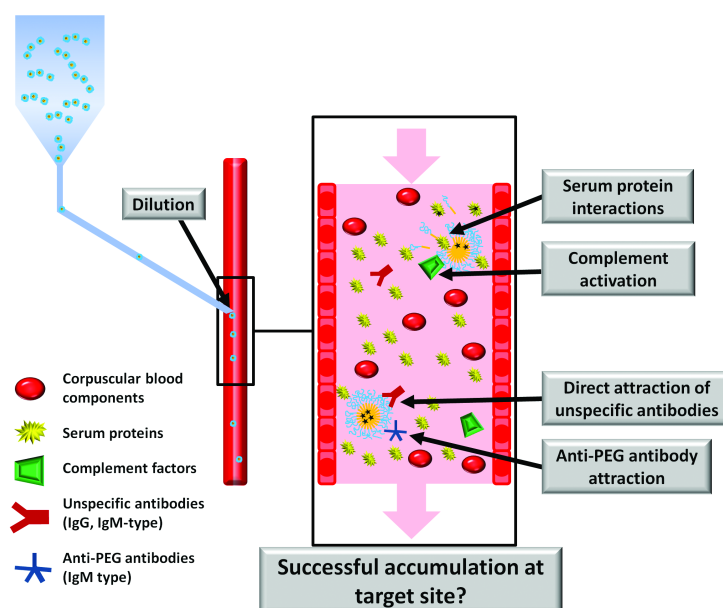


Figure 1.1: Summary of stress factors which colloidal carriers encounter upon injection.

1.2.2 Introduction

Polymeric micelles currently receive the widespread attention of the scientific community as a drug carrier system for parenteral delivery. This technology is seen to be as equally promising compared to the well-investigated liposomes in terms of the two major driving forces for their development: solubilization and site-specific delivery. Compared to other nanoparticulate drug delivery systems, polymeric micelles exhibit many unique properties that make them an ideal approach in the treatment of unmet medical needs. These properties generally comprise of 1) particle sizes below 150 nm (preferentially 100 nm), which allows for escape of the mononuclear phagocyte system (MPS) [8], 2) multiple possible core properties and morphologies due to a variety of applicable chemistries which can increase drug loading and circulation half-life of the systems [9], and 3) stimulus responsive release of the drug payload in dependence of particle environment [10]. However, the first micellar products on the market (Genexol-PM[®], Nanoxel-PM[®]) and ongoing clinical investigations (e.g., NK-105, NK-911, DACH-Platin, Lipotecan) seem to justify this view on the superiority of polymeric micelles. But only few of these products alter drugs' pharmacokinetics significantly and successfully target their site of action. Reaching both goals by formulation approaches still remains highly challenging. The main reason for this is that some of the most urgent questions in the application of nanoparticulate delivery systems have not yet been sufficiently addressed: 1) the idea of drug targeting is based on the questionable stability of cargo incorporation and consequently protection from premature release and from circulation elimination, 2) the mechanisms that accelerate particle accumulation into target tissue are still not fully understood and 3) the body's responses to nanoparticle therapies seem unpredictable and exhibit high inter- and inpatient variability. Moreover, the interactions between colloidal carriers and living organisms are very complex and many of them will change the integrity and structure of such systems in the bloodstream. Dominant stress factors among these interactions comprise of the following: 1) immediate high dilution of the formulation, 2) interaction with blood components, as well as 3) rapid responses by the immune system. All of these factors play a key role in nanomedicines' safety and efficacy. A powerful protective tool against the influences of stress factors is a nanoparticle design that reduces the rapid remodeling of the drug delivery system. In the special case of polymeric micelles, cargo protection is achieved by encapsulation of the active pharmaceutical ingredient in the hydrophobic particle core which is surrounded by a hydrophilic shell that prevents rapid clearance by the MPS from the bloodstream [11]. Consequently, the drug-loaded particles exhibit a prolonged circulation time. This necessary condition is seen to be responsible for site-specific delivery into tumors [12, 13, 14] or arthritic tissue [15] based on the enhanced permeability and retention effect (EPR) [16, 17, 18]. In the EPR concept, particle sizes are assumed to be the decisive factor for this passive type of drug targeting. Maintaining colloidal stability to allow for passive guiding of drugs by the carrier

system led to a number of micellar products. However, many of these products have not been approved yet by the health regulatory authorities, although some of them are subject to clinical trials. A micelle-related colloidal drug delivery system that successfully targets the drug to tumors received FDA approval in 1995: this liposomal product is marketed as Doxil[®] or Caelyx[®]. It contains the anticancer agent doxorubicine encapsulated in liposomes made from a mixture of PEGylated and non-PEGylated lipids of 1,2- distearoyl-sn-glycero-3-phosphoethanolamin (mPEG-DSPE/DSPE) that exhibits excellent *in vitro* stability [19]. A number of pharmacokinetic studies with this product have been conducted in animals and humans. The resulting data contribute significantly to the understanding of nanoparticle biodistribution and its underlying mechanisms. It was found that a rapid primary blood clearance of nanoparticles occurred within the first 2 h and was followed by a terminal clearance after 26 h [20]. In the discussion of these biphasic pharmacokinetics, opsonization and dysopsonization came into play. Both terms rely on the fact that plasma proteins adsorb onto nanoparticle surfaces. Opsonins ultimately lead to enhanced phagocytosis of the tagged particle, whereas dysopsonins prevent particle uptake [21, 22]. Depending on the nanoparticle properties, one of these species was preferentially attracted onto the surfaces [23]. This balanced composition is known to be time-dependent [24]. In the case of Doxil[®], one explanation for its pharmacokinetics was thought to be rapid complement activation [25, 26] combined with opsonization within the first 2 h leading to increased liver uptake of the liposomes. However, it was found that the adsorption of opsonins was saturable and incomplete so dysopsonins could attach onto the particle surfaces [20]. Finally the dysopsonins were seen to be responsible for the increased circulation time. Apart from nonspecific serum protein interactions another important aspect was revealed for PEGylated nanoparticles: upon multiple dosing of placebo liposomes, anti-PEG-antibodies were produced as a bodily response, this phenomenon is also known to arise from the multiple-dosing of PEGylated drugs [27]. This example makes it quite clear, that a colloidal system undergoes significant changes once it is exposed to biological systems that lead to alterations in its surface chemistry completely. This will have a strong impact on the *in vivo* disposition of such systems. It is, therefore, the intention of this review to analyze these rapidly occurring mechanisms upon injection of colloidal systems with special emphasis on polymeric micelles. Furthermore, it is aimed to revisit the impact of such stress mechanisms on current hypotheses regarding passive particle targeting in the last section of this article. Such a detailed analysis can contribute to a better understanding of nanoparticle biodistribution, premature clearance mechanisms and *in vivo* failure of targeting. It is intended to renew the views on the design of *in vitro* and *in vivo* experiments when working with colloidal drug delivery systems.

1.2.3 Analysis of stress mechanisms occurring immediately upon injection of polymeric micelles

1.2.3.1 Physical events during injection - formulations entering the body

The most relevant physical stress factor appearing upon injection is immediate dilution of the formulation. Dilution effects of colloid dispersions are highly crucial to the integrity of micellar formulations. In regards to this, the most important ones are the thermodynamic and kinetic stabilities of colloidal associates. Thermodynamic stability is related to the critical association concentration (CAC) of the micelle forming block copolymers. Upon immediate dilution which obviously takes place during injection, low molar mass surfactant micelles disintegrate very quickly [28]. It is well-known that block copolymer micelles exhibit much lower CACs compared to these low molar mass surfactant micelles [29, 30]. Another advantage of block copolymers is the possibility to modify the hydrophobic core: an increase in the length of the hydrophobic block generally leads to a decrease in CAC [31]. Consequently, block copolymer micelles with long hydrophobic blocks typically exhibit an enhanced thermodynamic stability and therefore dilution has less of an impact on their stability. These are results from experiments conducted by Kang et al. who synthesized varying PEGylated polylactic acid (PEG-PLA) block copolymers and studied their micellar association and kinetic stability [32]. Specific interactions between hydrophobic blocks increased association tendency as studied with mixed micelles composed of PEGylated poly-D-lactic acid (PEG-PDLA) and PEGylated poly-L-lactic acid (PEG-PLLA) [33]. Other groups made similar observations and based the increased stability on an increased number of hydrogen bonds in the core forming blocks [34, 35], π - π -stacking [36], hydrophobic interactions [37], ionic interactions in the core [38], and core cross-linking [39, 40]. Typically CAC values of block copolymers are between 1 and 5 mg/L [41]. Consequently, maintenance of polymer blood concentrations above the CAC level requires a minimum polymer dose between 6 and 30 mg for an average adult (6 L blood volume assuming immediate complete distribution). These numbers clearly demonstrate the importance of association properties especially at low concentrations. Another point is the kinetic stability of micelles upon dilution in the bloodstream. If micelles are kinetically stable, dilution below CAC does not necessarily lead to an immediate dissociation of the polymeric associates. This has been proven by Hans et al. who investigated the *in vitro* drug release from micelles upon dilution below CAC in PBS buffer [42]. In this study, mPEG-PLA micelles with varying hydrophilic/ hydrophobic ratios were loaded with haloperidol physically or by combining covalent coupling with physical incorporation. Depending on the core-shell ratio, the physically incorporated drug haloperidol was released immediately upon dilution (55% w/w PEG) or released in a sustained fashion over days (68% w/w PEG). These observations were confirmed by fluorescence probe studies that measured the integrity of micellar associates and found that 55% w/w PEG ratio micelles disassembled into unimers

whereas 68% w/w PEG ratio micelles remained intact. Interestingly the group concluded from the combination of drug physical and chemical coupling that an initial burst release even from the 68% w/w PEG ratio micelles occurred from intact micelles. In their experiments an enhancement of the hydrophobic block lengths of the polymer did not lead to a decrease in the burst release as expected. Apart from dilution, kinetic stability also implies stability against detergents like surfactants [43] or proteins [44, 45]. In this field, the physicochemical status of the micellar core plays a key role besides the properties of the micellar shell. Micelles with cores that exhibit high glass transition temperatures, a high degree of crystallinity, or low interfacial tension of the hydrophobic block with water (“frozen micelles”) [46] reduce the tendency of disassembly into single polymer chains upon dilution. Another micelle-like carrier system is dendritic “unimolecular micelles” [47], which exhibit a hydrophobic core as well as a hydrophobic shell. Due to their unimolecular nature, they do not show disassembling properties upon dilution but are similarly effective in drug loading of hydrophobic compounds [48, 49]. Furthermore, they are stable against shear forces and show drug release in a sustained fashion [50]. To summarize, the existing strategies to increase micellar stability and reduce premature disassembly upon dilution are based on the following: 1) increasing hydrophobic block lengths, 2) altering hydrophobic/hydrophilic ratios, 3) selection of the type of hydrophobic block in terms of physical status and 4) core cross-linking. Another strategy to overcome the disadvantages of stability upon dilution of such self-assembling systems could be the preparation of the above mentioned unimolecular micelles. For all of the above mentioned strategies when fine-tuning the micellar properties, one has to consider an altered drug release and drug loading capacity [42]. Existing products in clinical testing that have shown to be successfully at targeting, currently rely on ionic interactions in the micellar core for stabilization (NK-105, NK-911) by using PEG-polyamino acids [51, 52]. Biodegradability and biocompatibility are excellent for these systems. Evaluations of the other stabilization strategies such as particle crosslinking seem to strongly increase particle stability and require further investigations *in vitro* (drug load, release) as well as *in vivo* (degradability and compatibility).

1.2.3.2 Biophysical events upon injection

Apart from immediate dilution of the applied formulation during its injection, polymeric micelles come in contact with corpuscular blood ingredients as well as humoral components such as serum proteins, enzymes, electrolytes, lipid particles, and cells. Indeed, these factors represent a strong stress for micelles and challenge the maintenance of stability. Consequently, a detailed understanding of the processes appearing at the interface between nanoparticle surfaces and surrounding biological media is of high relevance. While dealing with this question the major blood components with strong interaction potential have been identified:

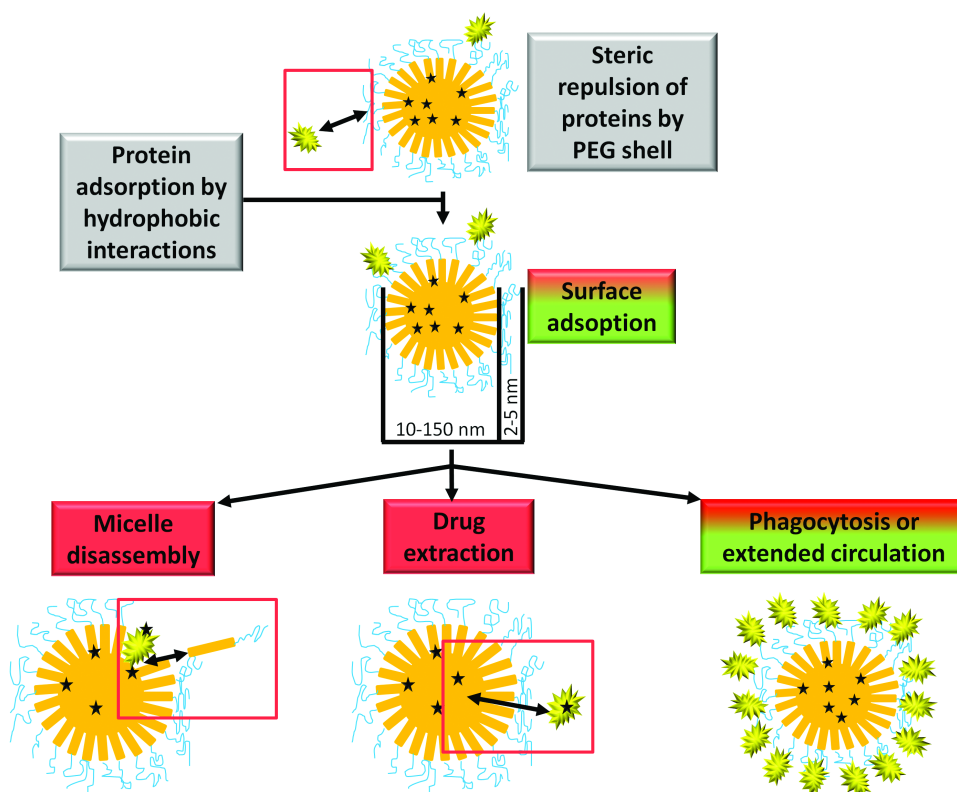


Figure 1.2: Scenario analysis of micelle-protein interactions. PEG-coating of the particles was made to avoid protein adsorption. Nevertheless, this seems to happen not entirely. However, proteins can 1) destabilize the colloidal aggregates, 2) extract the drug from the micellar core due to small diffusion length or 3) completely cover the nanoparticle. The latter mechanism might lead to a prolonged circulation and decreased MPS uptake or extended phagocytosis.

certain fractions of serum proteins seem to have a very deep impact on micellar stability and carrier properties whereas several studies revealed the low influence of corpuscular blood ingredients [45, 53]. As summarized in Figure 1.2, multiple interaction scenarios of serum proteins with micelles are possible: 1) destabilization followed by disintegration, 2) drug distribution from particle core toward proteins by maintaining particle stability, and 3) opsonization/dysopsonization of particles leading to phagocytosis by the MPS or to extended circulation.

Stability against serum proteins

Theories of nanoparticle-protein interactions as explanation for disassembly of micelles

The prevention of premature disassembly of the nanoparticles is extremely important for their *in vivo* success. A number of studies in the past years have focused on this analytically

challenging issue. Recently, some progress has been made due to the development of easy to access *in vitro* experiments for screening the colloidal carrier systems' serum stability. These techniques focus on 2D-PAGE analysis [54, 55, 56], Foerster Resonance Energy Transfer [53, 57], dialysis against serum proteins [58], and separation-based approaches such as size exclusion chromatography [59], asymmetrical field flow fractionation [57], or fast protein liquid chromatography [45]. One of the first investigations of interactions between hydrophobic surfaces and proteins was carried out by Leo Vroman [60]. The Vroman effect describes protein adsorption onto a limited number of hydrophobic surfaces and a competition was found between various protein types depending on their affinity to this surface. Directly upon exposing the surface to serum or plasma, proteins with low affinity adsorb rapidly and are replaced later by proteins with higher affinity to this surface. This phenomenon had been studied with fibrinogen [61] that exhibited high initial adsorption onto surfaces, which decreased over contact time. The adsorptive properties depended on serum concentration (dilution) [62, 63]. High serum concentrations led to low fibrinogen adsorption, whereas low concentrations exhibited the opposite effect. Destabilization of colloidal aggregates by proteins can only take place when proteins are allowed to adsorb onto the surfaces of the nanoparticles. The suppression of serum protein adsorption from the particle surface is typically thought to be achieved by a PEG shielding. Complete particle surface coverage and a minimal thickness in a "brush"-like conformation of PEG chains is seen as the ideal condition to obtain long circulating particles [64]. If the surface is perfectly protected, thermodynamically triggered repulsion [64] forces and entropically mediated interfacial water layers [65] prevent proteins from adsorption. Additionally, Lasic et al. [66] developed an extension of the DLVO theory for liposomes which helps to explain the repulsive effects of non-ionic surfaces. This theory already considers colloidal particle surfaces of micelles or liposomes that exhibit a dynamic equilibrium of associated macromolecules with rather fluidic surfaces. Another theory to explain extended circulation properties denies the stealthiness of particles themselves and speaks of a saturable protein opsonization phenomenon. This opsonin–dysopsonin theory was formulated first by Moghimi and Patel [67] in 1989 based on experimental observations from 1983 with liposomes [68]. It was found that cholesterol-rich liposomes exhibited longer blood circulation times due to lower protein opsonization compared to liposomes with lower or no cholesterol content. Furthermore, once the particles were opsonized they showed preferred accumulation in the liver or spleen [69]. Interestingly, opsonization experiments with serum from healthy and tumor-bearing rats showed remarkable differences in terms of their blood clearance by liver and spleen macrophages [70], indicating altered pharmacokinetics in diseased animals. However, the nature of proteins that act in a similar way to opsonins/dysopsonins remains partly unknown. Studies have reported calcium-dependent proteins as opsonins [71], whereas other investigations limited the knowledge of dysopsonins to their molar masses above 100 kDa [22]. Fibrinogen was found to be an opsonin [72] and albumin was believed to

be a dysopsonin [23]. In theory, after clearing the pool of protein-opsonins in the bloodstream, the remaining particles showed prolonged circulation. This hypothesis was used to explain the biphasic pharmacokinetic of the liposomal drug Doxil[®] [20]. Other studies with liposomes supported this hypothesis [73]. Doubts on the perfect stealth properties of PEG surfaces have arisen from several groups in the past: Vert et al. [74] showed the high compatibility of serum albumin to PEG of certain molar masses. For specific PEG molar masses (<8 kDa), the group postulated perfectly albumin covered surfaces. Consequently, the resulting particle mimicked “native” albumin particles. This hypothesis is supported by the recent studies of Tenzer et al. [75]. The group investigated the protein-corona of modified silica nanoparticles and identified albumin as the most abundantly absorbed protein on the surface. Furthermore, they impressively showed the major influence of particle size and the minor role of particle surface charge on protein adsorption. In total, more than 125 different proteins could be identified on the surfaces. Emmenegger et al. investigated anti-fouling properties of PEG-coated gold chips in the presence of serum proteins. They found that a certain serum fraction (>350 kDa) was adsorbed onto the surface of PEG with varying molar masses [76]. Also, a similar yet unusual behavior of fibrinogen on hydrophilic surfaces was found to be modulated by high molecular weight kininogens [24, 77]. Fibrinogen, albumin, and complement adsorption were also found on PEG surfaces in dependence of PEG density, as studied by Unsworth et al. with PEGylated gold nanoparticles [78]. This effect was also observed on other particle species, such as solid lipid nanoparticles [79, 80]. Summarizing these studies on the stealthiness of PEG surfaces, legitimate doubts could arise if this material is able to completely prevent protein adsorption and consequently allows for selective opsonization/dysopsonization. In this connection, the observations of Vroman can be used to explain time-dependent changes of opsonin and dysopsonin adsorption. Moreover, many different proteins participate in the formation of this effect and it is not completely clear which role each species plays with regard to opsonization-dysopsonization. In this context, the questions arise how stealthy PEGylated micelles are and what impact the repulsive properties have on micellar stability. However, once proteins are allowed to adsorb to the surface, cohesive forces of the micellar core decide about the particle stability. Again, similar issues are responsible for nanoparticle stability as previously discussed for thermodynamic and kinetic stability. Furthermore, it is remarkable that this physicochemical status can be altered by residual solvents [81] from preparation and water, as well as drug incorporation. These moieties can act as plasticizers and increase or decrease carrier stability. For example, Chen et al. identified α - and β -globulines that led to fast disassembly of PEG-PDLLA micelles [53]. Similar observations and impacts of these serum fractions were found by Diezi et al. who investigated PEG-DSPE micelles that showed rapid disintegration [82]. In the same study, PEG-block-poly-(N-hexylstearate-aspartamide) (PEG-b-PHSA) micelles exhibited high stability against serum proteins. As indicated by these studies, micellar architectures are very heterogeneous, and there seems to be no direct

correlation between a particular physicochemical parameter and serum stability [57]. Apart from this, the mechanism of micellar disassembly upon contact with serum proteins has not been fully understood yet. However, the examples above make it clear that the results concerning influence of the PEG shell on micellar stability are quite heterogeneously shown and discussed in literature. Prediction seems to be challenging if the protein coating acts as stabilizer or increases the tendency of the system to disassemble.

Stability of drug incorporation against extraction As previously analyzed, protein binding to nanoparticle surfaces is an important event upon injection. The most abundant protein in serum is albumin. Generally the diffusion pathways of small molecules between micellar core and proteins adsorbed on nanoparticle surfaces are short because PEG shieldings exhibit typical thicknesses of about 1–5 nm [83]. Consequently, the question arises if additional distribution phenomena from nanoparticle cores toward adsorbed serum proteins play a role. In the following section it is intended to point out drug properties that are associated with nanoparticle design to finally clarify the role of such distribution phenomena. Originally, the motivation for developing polymeric micelles was solubilization and bioavailability enhancement for poorly soluble drugs. However, most drugs in pharmaceutical development with solubility issues are hydrophobic as well and therefore eligible for encapsulation into nanocarriers. But, in line with hydrophobicity, the drug’s protein binding affinity is increasing: Ritchie and Macdonald [84] have shown by analyzing ~8000 drugs in the GlaxoSmithKline library that the probability of low aqueous solubility increases with the number of aromatic rings in the drug molecule and simultaneously goes along with stronger albumin binding. On average, albumin binding of these compounds is heavily increased, up by 75% when 1–3 aromatic rings are present and even up to 95% or more when 4 aromatic rings appear in the drug molecule structure. Consequently, drug disposition within colloidal carriers toward extraparticulate acceptors like proteins pose a dynamic equilibrium. Especially in the case of polymeric micelles, this equilibrium can shift upon injection from the hydrophobic particle core toward surrounding proteins depending on the affinity of the drug. Generally, in the circulating bloodstream the number of proteins that could serve as a drug acceptor exceeds the reservoir of nanoparticles. Concluding from this it would be an appropriate scenario that long circulating particles can lose their drug payload due to simple distribution toward serum proteins and continue circulating as “empty carriers”. First observations of this issue were made by Burt et al. [85]. The group loaded ^3H -labeled Paclitaxel into ^{14}C -labeled mPEG-PDLLA micelles and followed biodistribution in rats. As a result of their studies the authors found a discrepancy between drug and micelle biodistribution even after a couple of minutes upon injection. The group concluded that Paclitaxel was rapidly released from the micelles, while the carrier system was circulating for a longer time (~15 h). Later Burt’s group investigated the Paclitaxel plasma distribution *in vitro* in dependence of drug formulation. Drug solution

was compared to 2 PEG-poly-(ϵ -caprolactone) (PEG-PCL) formulations [86]. After 1 h of incubation with human plasma, the drug encapsulated in mPEG₁₁₄-b-PCL₁₉ micelles showed a similar protein distribution compared to drug solution. Prolonging the hydrophobic block to mPEG₁₁₄-b-PCL₁₀₄ led to the majority of drug remaining in the micelles. A highly interesting finding came from the inverse designed experiment in which Paclitaxel solution was incubated with plasma and blank mPEG₁₁₄-b-PCL₁₀₄ micelles were added. Unexpectedly, the results showed that drug distribution from plasma proteins toward micelles appeared in the other direction as well. The group suggested from their findings that the redistribution and accumulation of Paclitaxel from proteins took place at the interface between PCL core and PEG shell. The recent investigation of Letchford and Burt [87] proved this hypothesis of drug extraction *in vivo*. The authors included the previously described block copolymers in their study and investigated mPEG₁₁₄-b-PCL₁₀₄ and mPEG₁₁₄-b-PCL₁₉ on *in vitro* serum stability and *in vitro* drug release, as well as *in vivo* biodistribution. As expected, the polymer with the longest hydrophobic block exhibited higher *in vitro* serum stability assessed by the FRET technique [53], which had been previously used to study micelles on their stability in biofluids. Moreover, the particles from this polymer species released the drug Paclitaxel in a more sustained fashion compared to the polymer with shorter hydrophobic block length. By employing radiolabeling of polymer and analyzing the distribution combined with the drug, the *in vivo* biodistribution revealed rapid dissociation of the micellar adducts: independently of their *in vitro* properties, 99% of the drug was eliminated from plasma within 15 min upon injection, whereas the polymeric carrier systems remained circulating for several hours. These results were very awakening and questioned the overall concept of drug targeting with drugs encapsulated in self-assembling systems. However, as shown in the studies of Burt et al., drug distribution from micelles to protein fractions in blood is a dynamic equilibrium. The investigated drug Paclitaxel is highly lipophilic with $\sim 95\%$ protein binding affinity, primarily to albumin and α -1-acid glycoprotein [88]. Liu et al. [89] observed similar distribution phenomena with PEG-poly-(5-benzoyloxytrimethylene carbonate) (PEG-PBTMC) micelles loaded with ellipticine. In this study, drug release was found to be strongly dependent on protein concentration. A similar observation of drug extraction from carriers was made by Chen et al. who investigated PEG-PDLLA micelles loaded with two dyes exhibiting a FRET pair (DiI and DiO) [53]. After a short period of time (15 min) upon injection into mice, the FRET effect decreased strongly, indicating loss of dye payload. The group also investigated the *in vitro* serum stability of these micelles with the same dyes and found them to be quite stable. A possible explanation for this observation could be the high lipophilicity of the dyes and, consequently, a high affinity to lipid bilayers. Furthermore, in systemic circulation, the amount of proteins is certainly higher than in *in vitro* experiments. Summarizing the cited studies above it is clear that the relevance of drug distribution between nanoparticles and serum proteins is highly important. According to the contemporary literature, it seems as if

this problem is underestimated. A strong drug–polymer interaction is essential for stable drug incorporation into nanoparticles. In the case of low interaction forces between the drug and the nanoparticle core, premature drug release combined with continued “empty” particle circulation could occur. As previously shown in published literature, this effect takes place and has two major consequences on the results of *in vivo* experiments: 1) the highly hydrophobic drug is released and can be distributed toward serum proteins that are able to carry it to the target site and 2) if biodistribution of the carrier is followed, an accumulation of the carrier at the target site does not necessarily lead to an accumulation of its cargo. Consequently, carrier and payload follow completely different biodistribution patterns. As indicated by the studies of Burt et al., the distribution effect is very fast. This generally questions the application of self-assembling systems with physically incorporated drugs that rely on weak interaction forces such as hydrophobic interactions for altering drugs’ pharmacokinetics. A strategy to avoid this release was shown by the product NC-6004, which incorporated Cisplatin in a coordinative complex with a polyglutamine micellar core. Pharmacokinetic studies showed an incredible extension of circulation time compared to drug solution [90].

Immunological responses Strong immunological responses of the body upon nanoparticle injection is a major mechanism that triggers rapid particle clearance from circulation. In Figure 1.3 the most relevant interactions are portrayed. In the following sections of the article, the most relevant effects will be highlighted.

Complement activation Introduction of foreign macromolecular materials into a living body leads to an activation of the humoral immune system [91, 92, 93]. As a part of this system, complement activation is an efficient mean for the immune system to recognize and initiate clearance of particle-like organisms such as viruses or bacteria from the bloodstream [94]. It is worth mentioning the fact that typical sizes of viruses are equal to that of colloidal systems [95]. As discussed above, PEG is a widely used material to achieve stealthiness that aims at avoiding opsonization and, consequently, rapid uptake by the MPS. The mode of binding of complement factors onto the particle surface was nicely reviewed by Karmali and Simberg [93]. Furthermore, the investigations of Szebeni and Moghimi contributed to the knowledge and understanding of complement activation by PEGylated surfaces. The authors revealed that, as a special type of hypersensitivity reaction, CARPA (C-activation related pseudoallergy) is associated with nanoparticles [96]. This reaction is known to be non-IgE based but initiated by the classical, alternative, or lectin pathway of complement activation (C3a-, C5a-activation). Upon injection of nanoparticles, complement activation appears rapidly which finally activates immune competent cells such as mast cells or other granulocytes. In sensitive patients this could lead to anaphylactic reactions [97]. Several *in vitro* tests were proposed for screening the tendency of nanoparticulate formulations on

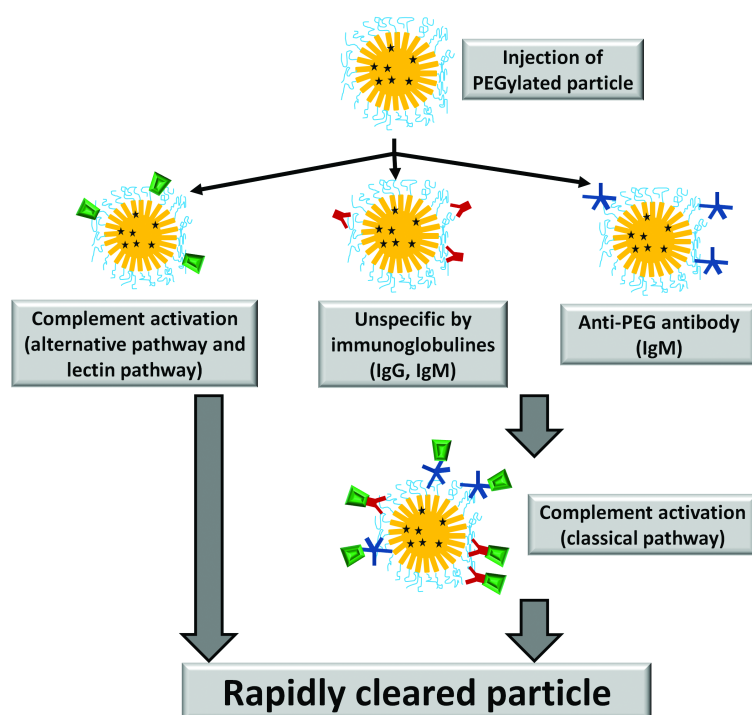


Figure 1.3: Immunological effects that are responsible for premature nanoparticle clearance. The most impacting mechanisms are shown: 1) complement activation, 2) unspecific antibody attraction and 3) anti-PEG antibody attraction.

complement activation [98, 99], as well as a porcine *in vivo* test [25]. The high relevance of complement activation in humans was already investigated with the liposomal drug delivery system Doxil® [100]. Apart from severe hypersensitivity reactions complement activation plays an important role in particle opsonization followed by phagocytosis in the MPS and is therefore an important mechanism that can alter particle biodistribution and circulation kinetics. Once “detected” by the complement system, rapid clearance can occur.⁹⁴ Considering this idea, Yang et al. performed an *in vitro* study to answer the question of complement activation and phagocytotic uptake in relation to PEG block lengths on the particle surfaces [101]. The group prepared PLGA nanoparticles with and without varying PEG chains and incubated them with different sera types. The incubated and opsonized particles were studied on phagocytosis by murine peritoneal macrophages. To distinguish between effects caused by 1) antibodies or 2) the complement system, the authors applied murine anti-IgG (model protein for inhibiting antibody response), EGTA (inhibits classical complement pathway), and EDTA (inhibits both pathways). As a result of their study, decreasing phagocytotic uptake of nanoparticles was found less dependent on anti-IgG but more on complement system. Furthermore, widely accepted “stealth” PEG block lengths (2 and 5 kDa) and hydrophilic/hydrophobic ratios (from 2.5% to 10%) played a significant role in reducing

adsorption of opsonins due to complement activation onto particle surfaces. The influence of the PEG chain on nanoparticle distribution compared to bare PCL nanoparticles dependent on complement activation was also studied by Shan et al. [102]. Although PEG is known as a complement activator, lower opsonization and phagocytotic rates by macrophages (bare NP, 90% phagocytosed 5 min upon injection; PEGylated NP, 45% phagocytosed 5 min upon injection) were found for the PEGylated species that reduced complement activation significantly and finally increased circulation time of PEG-PCL particles. Polymeric micelles also present PEG at their surfaces and therefore could be able to activate the complement system. As indicated by the cited studies, complement activation upon nanoparticle injection plays an important role in their safety and biodistribution. Although the liposomal product Doxil® showed strong complement activation *in vitro* [98] and most likely *in vivo* by causing anaphylactic reactions in certain patient groups [26], these liposomes showed a prolonged circulation time in the second part of their biphasic pharmacokinetics [20]. Consequently, the influence on circulation times of nanoparticles seems to be more or less unpredictable. Opsonization by complement can lead to rapid particle phagocytosis and the underlying mechanisms have not been fully understood yet.

Unspecific antibody attraction and opsonization Apart from antibody opsonization upon complement activation, very little is known about the direct interaction between circulating, unspecific antibodies and nanoparticle surfaces. Some studies reported in the past an influence of Immunoglobulin G [103, 104, 105] and M [106] on particle opsonization. From the cited studies it is very speculative to make a conclusion on the relevance of this phenomenon. Finally, it is hard to distinguish in experiments between complement activation followed by immunoglobulin attraction or immediate immunoglobulin attraction without any complement activation. Nevertheless, it has been shown in these studies that PEGylated surfaces can inhibit very strong immunoglobulin attraction and, consequently, maintain the stealth effect of the particles.

Anti-PEG-antibodies When PEGylation arose as a strategy to prolong circulation and decrease degradation of therapeutic proteins, in 1983 Richter and Akerblom found an anti-PEG antibody formation in rabbits and mice by coupling different PEG chain lengths with varying adjuvant proteins [107]. As a result of their study, they could harvest anti-PEG antibodies and concluded that a sequence of 6–7 ethylenoxide units was the “antigen determinant”. One year later, in 1984, the same authors investigated the natural occurrence of anti-PEG antibodies in allergic and healthy patients and identified them mainly as IgM isotype [108]. The prevalence in allergic patients was significantly higher than that in healthy ones. Nevertheless, upon PEG-hyposensitization nearly 50% of the patients showed an anti-PEG antibody response. This number declined over 2 years of treatment to ~28%. Overall, titer of these anti-PEG

antibodies in patients' serum was very low. Therefore, the authors concluded that their findings were of no clinical significance. By increased usage of PEGylated drugs, knowledge on clinical relevance increased simultaneously. Ganson et al. described the formation of IgM and IgG anti-PEG antibodies in a phase I clinical study with PEG-uricase upon a single s.c. injection [109]. The authors identified two patient collectives: the first with high drug titers after 3 weeks of injection and the second with no detectable drug titers after 10 days of treatment. Consequently, the second specific patient group was more susceptible to antibody formation that led to rapid clearance of the drug. Interestingly, the analyzed anti-antibodies were of two species: one against the drug uricase and the other against PEG. Armstrong et al. analyzed serum samples from patients treated with PEG-asparaginase [110]. It was previously reported that therapy with this drug could fail due to antibody formation in 25% of the patients. Armstrong et al. found a strong positive correlation between antibody formation and rapid drug clearance and finally advised an anti-PEG antibody screening prior to the therapy for every patient. Nowadays the formation and appearance of anti-PEG antibodies upon multiple dosing of nanoparticles is still intensely discussed in literature; it has been found that such antibodies have a huge impact on nanoparticle distribution: The effect is called "accelerated blood clearance (ABC) phenomenon", and is caused by anti-PEG IgM formation and was first observed for nanoparticles in rodents and rhesus monkeys [27, 111]. This antibody formation takes place in the spleen where a certain amount of all nanoparticles, depending on their size, accumulate [112]. Recent studies in B- and T-cell deficient mice make splenic B-cells responsible for this IgM secretion, whereas the detailed mechanisms of this phenomenon yet remain unclear [113]. The studies of Ishida et al. with liposomes revealed a dose dependency of the lipid inducing antibody formation. Predosing low lipid amounts (1 μmol per kg) without drug (blank liposomes) induced increased antibody concentrations, whereas higher doses (5 μmol per kg) of lipids showed lower IgM response. When doxorubicine-loaded liposomes were applied, even in low lipid doses, the IgM formation was decreased compared to empty liposomes. Upon injection of the liposomal drug Doxil[®] for several times into animals, blood concentrations of doxorubicine, as expected, did not decrease with every injection [113]. It was suggested in this study that the encapsulated anticancer drug led to an inhibition of antibody induction by reducing the number of B-cells as a result of cytotoxic effects. Similar observations of this ABC phenomenon were also made by the group of Romberg et al. [114] with liposomes and by Ishida et al. for PEG-PLA nanoparticles [115], as well as for siRNA-loaded cationic liposomes [116]. The relevance for polymeric micelles was investigated and a strong size dependency was found. For micelles $< \sim 30$ nm in diameter it was believed that the ABC phenomenon has no relevance [117]. The question remains as to what extent these results are unexpected and what impact they have on multiple dosing in humans. From the current point of view, the probability and clinical significance of anti-PEG antibody formation seems to be underestimated. A

detailed understanding of the formation mechanisms is the basis for the avoidance of therapy failures. The results from further studies could give an answer to the question if PEG was the only highly suitable material to achieve stealth properties. Development of ELISA test kits to screen anti-PEG antibodies state the upcoming clinical relevance of this issue [118]. Furthermore, Koide et al. [113] argued that this phenomenon is not seen for the liposomal Doxil[®] due to cytotoxic effects of the anticancer agents on antibody producing splenic cells. If this hypothesis is true, then the question is, if nanomedicine is only applicable for cancer treatment or for other indications too?

1.2.4 Implications for passive targeting

Generally, there are two strategies available that allow for drug targeting to disease-modified tissue. Active targeting focuses on the coupling of targeting moieties onto nanoparticulate surfaces. The moieties represent ligands to cell-specific antigens that mediate coupling and uptake of colloidal associates into the target cells [119, 120]. Contrary to this concept is the passive targeting that utilizes the unique size properties of colloidal carriers. In the following sections it will be focused on the passive targeting concept because the above stress factor analysis contributed most to this concept.

1.2.4.1 Evidence of EPR effect for macromolecules

Accumulation of macromolecules in disease-modified tissue like tumors or arthritic tissue is believed to be based on the Enhanced Permeability and Retention (EPR) effect. The concept of EPR was formulated in 1986 by Maeda and Matsumura based on the observations that macromolecules (e.g., albumin, dyes attached to albumin, IgG) show an enhanced tumor accumulation and could sustain in tumor tissue for long periods of time [16]. The group of Maeda et al. [18, 121, 122, 123, 124] named the following anomalies that could be found in various disease-modified tissues “EPR”: 1) high vascularization density, 2) leaky vasculature, 3) decreased lymphatic drainage, and 4) participation of certain tissue inflammation mediators (e.g., NO, Bradykinin, VEGF, Prostaglandins) that support the formation of 1) and 2). Further studies showed that a minimum molar mass for this tumor accumulation is mandatory: macromolecules above 40 kDa cannot be excreted via free filtration from the kidneys and represent the molar mass minimum [16]. The EPR effect with macromolecules has been shown numerous times in diverse disease models and has been reviewed extensively [12, 17, 125, 122, 126]. Apart from molar mass considerations, the group of Dellian et al. [127] reported differences in tumor accumulation of BSA and IgG that were chemically modified. The modifications changed the electrical charges of the proteins by keeping their molar mass nearly constant. The results of their study showed,

that the cationic particles of BSA and IgG exhibited the shortest serum half-life yet and the highest tumor accumulation compared to the anionic species. Simultaneous uptake in healthy tissue increased as well. This observation corresponded to the anionic surface charge of endothelium cells in healthy and tumor tissue, which consequently increased the retention of cationic particles. An often cited experiment in this context to prove the accumulation of macromolecules in tumor tissue is based on experiments with the SMANCS adduct consisting of poly-(styrene-co-maleic acid) (SMA) copolymer coupled to neocarzinostin (NCS) [18]. Maeda et al. compared tumor accumulation of the polymer adduct with the unbound NCS. It was shown that the SMANCS adduct (16 kDa) was retained more effectively in the tumor tissue compared to NCS (12 kDa) due to the SMANCS' high affinity to albumin [128, 129]. Consequently, the efficacy of SMANCS was based on the utilization of albumin as a "ferry" (final molar mass: ~ 92 kDa). This hypothesis was supported by Pimm and Hudecz [130] who compared the tumor accumulation of varying serum proteins with that of synthetic macromolecules. The results were acquired from radiolabeling natural proteins (albumin, IgG, transferrin) and synthetic macromolecules (polypeptides with poly-L-lysine backbone). The protein and macromolecular species were injected into tumor bearing mice (subcutaneously implanted tumors) and tumor/blood concentration ratios were utilized to evaluate the accumulation efficiency. As expected, the results showed a strong accumulation of transferrin and albumin in the tumor tissue. Compared to the accumulation values of these natural macromolecules, the synthetic macromolecules accumulated to a lesser extent in the tumor tissue, even when exhibiting long blood circulation times (~ 26 h and more). The authors were aware of the fact that their polymers might not be suitable for such distribution experiments, but according to the EPR theory, long circulating macromolecules should invade the tumor extensively. Charge effects were included in the study by utilizing two different labels (Iodine-125 and Indium-111). The authors raised the question how permeability "enhancement" can be defined and what factor one could use to evaluate this (organ/blood concentration ratios, control groups with serum proteins). The group concluded that enhancing tumor uptake of macromolecules could simultaneously enhance uptake in the liver, spleen, or kidneys as well. The authors stress the need for consideration of this matter when deliberating passive tumor delivery of macromolecules. So far, there has been no evidence of nanoparticle formation in the studies mentioned above yet.

1.2.4.2 The EPR effect in case of nanoparticles

It is generally believed that similarly to macromolecule accumulation in tumors one can conclude that nanoparticle accumulation is based on similar effects, especially that long circulation necessarily leads to superior tumor accumulation [131]. However, this remains questionable due to the high molar mass differences between macromolecules in the several

hundred kDa range and nanoparticulate associates with masses of possibly several millions of kDa. In this context, the investigations of Dreher et al. [132] revealed that, for dextran macromolecules, the optimal tumor accumulation molar masses range between 40 and 70 kDa. Although the plasma half-life of dextrans with higher molar masses up to 2 MDa resulted in an extended blood circulation time, it still led to a less-effective extravasation and penetration into tumor tissue. In detail, 2 MDa dextran exhibited the longest circulation time but did not reach the extravasal tumor accumulation of 70 kDa dextran. Consequently, the often described paradigm [12, 18, 122] that long blood circulation relates to high tumor accumulation of macromolecules does not necessarily work. When high molar mass macromolecules show a decreased extravasation compared to low molar mass species, then what does this mean for nanoparticles? Many studies have revealed without any doubts that increased accumulation of nanoparticulate formulated drugs is related to the EPR effect [133, 134]. Other authors that investigated particulate tumor accumulation were much more reserved in concluding and supporting the existence of an EPR effect [135, 136] based on their observations. So far, the proposed mechanisms leading to nanoparticle extravasation from bloodstream comprise of leakage from blood vessels through fenestrations, transendothelial channels, and anomalies in the endothelial basement membrane [137, 138]. When talking about nanoparticle tumor accumulation, the question of size ranges for the tumor blood vessel fenestrae comes up. Due to the varying expression of tissue anomalies in different tumor models, the information reported in the literature is strongly scattered. The proposed size ranges for particles utilizing the EPR effect range from several nanometers for macromolecules over 200–300 nm [134] to 2 μm [139]. Yuan et al. [140] proposed pore cutoff sizes between 400 and 600 nm. Hobbs et al. [138] investigated the leaky vasculature extensively and revealed intercellular gaps between 200 nm and 1.2 μm . The group also found an impact of hormones on the vascular leakiness of hormone-dependent tumors. As an example, in a testosterone-dependent tumor hormone withdrawal led to a decrease in the pore size from 200 to 7 nm within 48 h. Another discrepancy was found between the same tumors in different locations within the animal. Tumors grown in the cranial environment had smaller pore sizes compared to subcutaneously implanted ones. Interestingly leakiness for albumin was found to be equal in all investigated tumor models [138]. Xiao et al. [141] showed dependence of tumor size on the extent of accumulation of polymeric micelles. Larger tumors showed a higher extent of particle accumulation compared to smaller tumors which were related to “underdeveloped vasculature” [141] in small tumors. Apart from this Feng et al. [142] found that tumor vessel fenestration was highly dependent on the tumor model. It was previously shown by Maeda et al. [122] that a vascular endothelial growth factor (VEGF) was of high relevance for the EPR effect. The group of Feng et al. [142] investigated two well-known VEGF-secreting tumor models and revealed fenestrations in only one of these models. By checking both tumor models on vascular permeability with a plasma protein, extravasation was found in both models.

The group especially argued for and proved the presence of endothelial cell vesiculo-vacuolar organelles that allowed macromolecules to extravasate from vessels.

1.2.4.3 Additional factors shaping EPR effect

Upon discussing morphological and physiological issues of tumor tissue the question now arises which additional mechanisms could play a role in accumulation of nanoparticles in disease modified tissues? A point which has not been highlighted in this article yet is the role of tumor nutrition: Rapidly proliferating cells obviously have an increased need of nutrients. The review of Stehle et al. [143] nicely summarized tumor uptake of varying nutrients from the bloodstream. The group concluded that glucose and albumin were the most relevant molecules that maintain rapid cell growth in tumor tissue. The authors proposed that the high albumin consumption of the tumor cells provided a negative nitrogen balance in a late tumor state and that, therefore, tumors were often called “nitrogen traps”. In this case, the effect could lead to cachexia. Additionally, the group described the accumulation of albumin in the well oxygenated periphery of the tumor tissue due to the lack of lymphatic drainage. Evidence for this phenomenon was provided by radiolabeled serum albumin, which showed enhanced tumor accumulation [144], leading to increased osmotic pressure in tumor tissue based on this natural macromolecule accumulation. Consequently, in the tumor periphery, cell energy is generated from protein metabolism. It was presented by Stehle et al. that uptake of albumin in tumor cells took place by pinocytosis, indicating a nonspecific mechanism. Albumin accumulation in other disease modified tissue plays an important role too, for example, in rheumatoid arthritis. Patients in their acute disease state exhibited a hypoalbuminemia and an extremely high accumulation of albumin in inflamed joints [145]. However, this physiology could favor the delivery of nanoparticles into disease regions by utilizing proteins as “ferries”. The underlying physiology in arthritis and therefore the retention of colloidal carriers were found to be based on a different mechanism compared to the EPR effect: the reason for extravasation was seen in “leaky vasculature and subsequent inflammatory cell-mediated sequestration (ELVIS)” [146]. Depending on the disease state (acute vs chronic), lymphatic drainage is counterbalanced: in acute states the lymphatic flow was increased, whereas in the chronic state the number of mainly leaky lymphatic vessels increased [147, 148]. Consequently, the overall lymphatic flow is not decreased as it was found in solid tumors. Therefore, enhanced retention in arthritic joints was found to be increased by the uptake of colloidal systems into synovial cells [149]. Coming back to the original discussion on tumor accumulation and retention, recent investigations with Paclitaxel-coupled albumin nanoparticles (Abraxane[®]) suggest the involvement of active mechanisms that guide albumin nanoparticles into the tumor region. According to Desai et al. [150, 151], the following two mechanisms are involved: 1) transcellular uptake by

gp-60 receptor on endothelial cell surfaces and 2) SPARC (secreted protein acidic and rich in cysteine) overexpression in tumor cells with increased albumin retention. The group [150] came to this conclusion on the gp-60 receptor mechanisms by performing *in vitro* uptake experiments with Abraxane[®] compared to Taxol[®] (Cremophor EL[®]/ ethanol formulation). Inhibition of gp-60/caveolar transport by addition of β -cyclodextrin decreased the transcytotic transport of Abraxane[®]. SPARC was found to be secreted in many different tumor cell lines [152] and to be a strong affinity albumin binding protein [153]. The group of Desai et al. [151] investigated tissue samples from patients suffering from head and neck cancer that were treated with Abraxane[®] on SPARC expression levels. They showed a correlation of enhanced SPARC expression in head and neck cancer patients with increased response rate of Abraxane[®] nanoparticles (83% responders in SPARC overexpression group vs 25% in SPARC normal expression group). As indicated by this analysis of mechanisms upon injection, it is highly unlikely that injected nanoparticles arrive at the tumor tissue in their original form. Greish et al. [154] investigated styrene-maleic acid micelles for encapsulation of pirarubicin and confirmed the high albumin binding capacities of the micelles. Upon albumin adsorption the micelles reached a molar mass of around 94 kDa and were found to accumulate successfully in tumors. So what role does the protein corona play in tumor accumulation? Walczyk et al. published in 2009 their results on the “rigidity” of the protein corona adsorbed onto nanoparticle surfaces. From studying several modified polystyrene (PS) and SiO₂ particles concerning their protein surface adsorption properties they revealed a “hard” corona (protein double or single layer) protein species pattern that was highly dependent on the particle type [155]. Due to the high stability of attached proteins they proposed that biodistribution could be altered by protein adsorption and that this corona might change again once it has reached the target cells. Most likely the target cells did not “see” the bare nanoparticles but most likely these highly complex protein shells [156]. Ehrenberg et al. [157] investigated the relation of nanoparticle surface properties (e.g., charge) and protein adsorption patterns on the particle binding to a human endothelium cell line *in vitro*. The group found a direct correlation between surface properties, protein content adsorbed onto the particles and binding to endothelium cells. Upon depletion of the most abundant proteins from serum and incubation with this depleted serum, the adsorption pattern on the surfaces changed as expected. Unexpectedly, the binding properties to endothelium cells remained unchanged. From their experiments the group concluded on the high relevance of unspecific uptake mechanisms for particles with high protein coverage. For particles with low protein coverage active receptor-mediated uptake could not be excluded. The dysopsonic [158] properties of albumin were subject of further investigations by Furumoto et al. [159]. The group coupled albumin onto the surfaces of PEG-liposomes and investigated biodistribution in rats. In fact, albumin coupling prolonged circulation time of albumin-PEG-liposomes compared to bare PEG-liposomes. Simultaneously, liver deposition of the albumin-bound PEG-liposomes

decreased. The investigations of Crielgaard et al. are in contrast to these, they utilized surface plasmon resonance to elucidate PEG-liposome attachment on protein-coated chips [160]. They revealed high affinity of PEG-liposomes to apolipoprotein E and α_2 -macroglobulin and a low affinity to human serum albumin. Both proteins are known to be opsonins. In *in vivo* experiments, the interaction of several proteins with liposomes were successfully correlated with plasma clearance. Considering these studies, there is strong evidence that target accumulation of nanoparticles in tumor tissue is not only a matter of particle size, but also depends on the protein corona adsorbed onto the particle surface. Albumin and other proteins seems to play a highly important role as dysopsonins by prolonging the circulation of nanoparticles and might present a nutrient for tumors or inflamed tissue, thus, being preferentially phagocytosed by rapidly proliferating cells. The importance of other serum proteins on tumor accumulation needs to be further elucidated. Furthermore, extended circulation times of particles seem not to be a prerequisite to making use of the EPR effect; it is rather a matter of surface attached dysopsonins that finally guides the particles to the target organs. Apart from this, there are successfully targeting drugs on the market or in research that are bound to albumin (Abraxane[®]) or bind to the protein *in situ* (e.g., Doxo-EMCH) [161]. Overall, the dysopsonin theory is not that new and was used to explain the biphasic pharmacokinetics of Doxil[®] [20].

1.2.5 Conclusion

In this review it was analyzed relevant and important stress factors that colloidal drug delivery systems encounter upon injection with special emphasis on polymeric micelles. High dilution, multiple interactions with serum proteins, complement activation, and antibody attraction can accelerate premature particle and drug clearance from the bloodstream. The mechanisms involved are rather complex but should be considered when designing nanoparticles and eventually in evaluating the failure of nanomedicines during *in vivo* experiments. In this context it seems that protein adsorption has a strong impact on nanoparticle biodistribution and their uptake into diseased tissue. Due to advances in analytical techniques, interactions of nanoparticles with serum proteins can be monitored *in vitro*. The role of premature drug redistribution from nanoparticles toward serum proteins remains unknown. In the case of drugs with high protein binding affinities, successful transport to the target site of action could be carried out by such drug–protein adducts. However, some studies indicate that nanoparticle sizes and the selection of an appropriate tumor model state were necessary conditions but not the only factors that affect the EPR effect. It is suggested to consider the opsonin–dysopsonin model to explain the pharmacokinetics and tumor uptake of existing successfully targeting systems as well.

1.2.6 Future perspective

The performance of nanoparticles for intravenous drug delivery should be carefully evaluated in terms of their 1) colloidal stability upon dilution and contact with serum proteins, 2) drug incorporation stability, and 3) relevance of immunological responses of the human body. Most of these questions can only be answered *in vivo* (preferentially human), but *in vitro* approaches could give valuable hints (e.g., *in vitro* complement activation, serum incubation). A subject of future investigations will be the appearance of nanoparticles (protein corona) at their target site of action. A detailed understanding of all relevant uptake mechanisms into tissue is extremely important. Additionally, future clinical trials must reveal the relevance of the EPR effect in humans for colloidal nanoparticles to give evidence, if the promising developments and theories from the past decades contribute significantly to the efficacy and safety of drug therapies.

1.3 Research objectives of the thesis

The research focus of this thesis was the preparation, characterization and investigation of polymeric micelles for organ specific drug delivery purposes. This challenging issue was to be clarified based on the following pillars:

1. **Drug loading efficacy:** Concerning therapeutic efficacy of colloidal carriers their loading with the drug (drug/polymer ratio) is a crucial parameter [8]. Typically drug loads in polymeric micelles are quite low and need enhancement by novel polymer architectures or drug loading techniques. One example for this are griseofulvin loaded PEG-PLA micelles with a load of 0.65% [162]. Other systems were more successful and there are reports in literature which describe impressive loading rates e.g. of 10% for taxane derivatives [163] or 19% for cyclosporin A [164]. Consequently one goal of the thesis was the investigation of drug loading mechanisms into micelles which finally could enhance the drug/polymer ratio (**chapter 2**).
2. **Stability of polymeric micelles in biofluids:** Stability of colloidal carriers is essential to assure the long-circulating properties and to prevent premature drug release upon injection. This issue can be addressed *in vitro* by incubation with relevant media. One approach from literature is an analytical technique based on Foerster Resonance Energy Transfer (FRET) [165, 53]. This method was selected as a starter. One aim was to find a correlation between serum stability and physicochemical properties of polymeric micelles and to select suitable candidates for *in vivo* applications (**chapter 3**).
3. **Toxicological concerns and immunological responses against colloidal carriers:** Acute and chronic toxicity as well as reactions by the immune system prominently by the complement system are severe drawbacks of micellar systems [166, 167, 168, 93]. For this purpose particle toxicity was to be elucidated *in vitro* on primary cells/cell lines and in presence of serum. The goal was to discriminate between different polymeric compositions in terms of cytotoxicity and complement activation. Both issues deliver valuable information about drug safety of nanomedicines (**chapter 4**).
4. **Drug targeting into tumor tissue:** In case of high colloidal stability of drug-loaded polymeric micelles upon injection it is believed that such PEGylated nanoparticles with sizes below 200 nm were very effective in tumor targeting [131]. This passive targeting concept was originally invented for macromolecules by Maeda and Matsumura [16] and should allow for superior cancer treatment. Both assumptions, 1) colloidal stability upon injection (**chapter 6**) and 2) passive targeting by size, were followed *in vivo* by radiolabeling of carrier and payload. If both species, carrier and payload, reach their target site of action in sufficient concentrations compared to other organs, this would

indeed show rationale for improved cancer treatment (**chapter 5 and 7**). So far, only a couple of studies were dealing with this extremely relevant question [53, 87].

Summarizing these research objectives, it is obvious that for addressing the open scientific questions *in vitro* as well as *in vivo* experiments were necessary to conduct. Moreover, this thesis could deliver the answer if the existing micellar technologies were sufficient for targeted delivery or if further modifications of the systems have to be considered.

Chapter 2

Drug loading of polymeric micelles

Tobias Miller^{1,5}, Gwenaëlle van Colen¹, Bjoern Sander^{2,3}, Mariola Monika Golas^{3,4}, Senta Uezguen¹, Markus Weigandt¹, Achim Goepferich⁵

¹ Merck KGaA, Exploratory Pharmaceutical Development, Frankfurter Str. 250, 64293 Darmstadt, Germany

² University of Aarhus, Stereology and EM Laboratory, Department of Clinical Medicine, Wilhelm Meyers Allé 3, 8000 Aarhus C, Denmark

³ University of Aarhus, Centre for Stochastic Geometry and Advanced Bioimaging, Wilhelm Meyer Allé 3, 8000 Aarhus C, Denmark

⁴ University of Aarhus, Department of Biomedicine, Wilhelm Meyers Allé 3, 8000 Aarhus C, Denmark

⁵ University of Regensburg, Department of Pharmaceutical Technology, Universitätsstrasse 31, 93040 Regensburg, Germany

Submitted to: *Pharmaceutical Research* (2012)

2.1 Abstract

With this study it was intended to gain mechanistic insights into drug loading and lyophilization of polymeric micelles. PEGylated poly-4-(vinylpyridine) micelles were loaded with the model drug dexamethasone. Three different methods were applied and compared: 1) O/W emulsion technique, 2) direct dialysis and 3) cosolvent evaporation (Fig. 2.1). Micellar dispersions with the highest drug load were lyophilized with varying lyoprotectors, including polyols like sucrose, trehalose, maltose, a polyvinylpyrrolidone derivative as well as β -cyclodextrin derivatives. For comparison other PEGylated block copolymers (PEGylated polylactic acid, polylactic acid-co-glycolic acid, poly- ϵ -caprolactone) were freeze-dried. Drug loading via direct dialysis from acetone was a less effective loading method which led to dexamethasone loads $<2\%$ (w/w). O/W emulsion technique from dichloromethane increased the drug load up to $\sim 13\%$ w/w whereas the optimized cosolvent evaporation increased the load up to $\sim 19\%$ w/w. An important step for the cosolvent evaporation was the solubility screen of the drug prior to preparation. The high drug load was maintained upon lyophilization with β -cyclodextrins which proved to be excellent, versatile stabilizers for other block copolymer micelles as well. In conclusion careful solvent selection prior to cosolvent evaporation was a beneficial approach to load hydrophobic drugs into polymeric micelles. Moreover, β -cyclodextrins could be used as versatile lyoprotectors for these micelles.

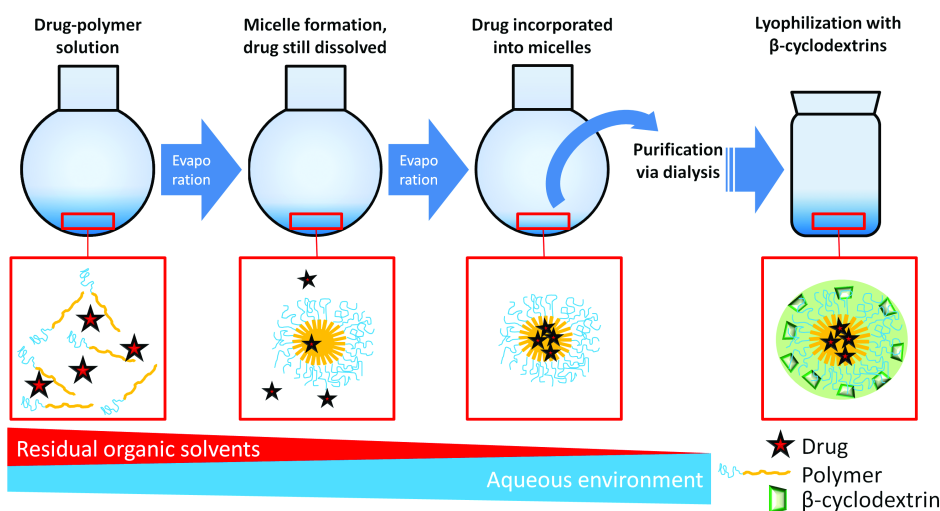


Figure 2.1: Summary of the most successful micellar preparation approach in the study: cosolvent evaporation followed by lyophilization.

2.2 Introduction

High Throughput Screening (HTS) of drug candidates increased the number of hydrophobic new molecular entities in drug discovery [169, 170]. The amount of hydrophobic drugs among development compounds was estimated by Lipinski in 2002 to be around 40% [5]. Recent investigations showed that the actual number of drug candidates which can be categorized in class II or IV in the Biopharmaceutics Classification System (BCS) [171] was 75% and higher. However, low aqueous solubility resulting from HTS remains a challenge in pharmaceutical industry leading to higher costs in development and drug attrition rates upon approval [6]. Despite huge progress in advanced solubilization technologies, the options for hydrophobic compounds aiming on intravenous injection are still limited [6] and often bought dearly with toxic side effects of utilized excipients (e.g. Cremophor EL[®]/ethanol in Taxol[®] [172]). Therefore nanosized approaches to overcome solubility issues became more and more important over the last decades. However, encapsulation of therapeutically relevant drug doses are a basic requirement for reasonable treatment and has been regarded as one of the major drawbacks of nanoparticulate delivery systems [173]. Among nanoparticles a very promising technology with high solubilization potential is based on polymeric micelles. However, preparation of such micellar systems with high drug loads remains still challenging [174, 8]. A number of different drug loading procedures were elaborated but often were based on trial and error experiments and lack of a more systematic approach. The major reason is the limited knowledge of the underlying mechanisms leading to sufficiently high drug loadings. The organic solvent by which the drug loading process is initiated plays a key role in all preparation methods: According to the solvent properties (water-miscibility) an appropriate candidate is usually selected which finally defines the processing steps to follow. In this context the following drug loading methods have commonly been used: 1) O/W emulsion techniques [175], 2) W/O/W emulsion techniques [176, 177], 3) direct dialysis [178], 4) cosolvent evaporation techniques [179] and 5) loading via lyophilization [180]. Among those procedures especially 1), 3) and 4) are highly compatible with hydrophobic drugs whereas 2) focuses on the encapsulation of more hydrophilic compounds and 5) has limitations concerning polymer water solubility [180]. In this study the methods 1), 3) and 4) were selected as ideal loading methods for hydrophobic drugs and micelles were prepared by encapsulating the model drug dexamethasone. With its aqueous solubility of 80 µg/mL [181] it is a typical hydrophobic model compound which is in addition highly interesting for parenteral application. For the encapsulation study the PEGylated poly-(4-vinylpyridine) was selected that was known to form stable micelles in water [57]. As micelles are fragile dynamic systems it is highly desirable to stabilize the particles after freeze-drying. It is known from literature that besides classic lyoprotectors like sucrose or trehalose especially β -cyclodextrins are suitable lyoprotection excipients [182, 183]. Consequently the question became relevant

which kind of stabilizing mechanisms cyclodextrins might have compared to classical polyols and if they might be helpful as versatile protectors for PEGylated block copolymer micelles. The purpose of this study was to gain mechanistic insight into the micellar encapsulation process of hydrophobic drugs by applying different preparation techniques using various organic solvents. In addition, β -cyclodextrins were compared to standard lyoprotection agents for their stabilizing properties. Such mechanistic insights in both the loading procedure and lyoprotector stabilization are of immediate relevance for the development of novel preparation techniques for polymeric micelles.

2.3 Materials and methods

2.3.1 Materials

PEGylated poly-(4-vinylpyridine) (PEG-PVPy) [5-b-20], PEGylated poly-(lactic acid) (PEG-PLA) [5-b-23] and PEGylated poly-(ϵ -caprolacton) (PEG-PCL) [5-b-32.5] were purchased from Polymer Source, Inc., Montreal, Canada. PEGylated poly-(lactic-co-glycolic acid) (PEG-PLGA) [5-b-28] (Resomer RGP d 50155) was delivered from Boehringer Ingelheim, Ingelheim, Germany. Dichlormethane (DCM), tetrahydrofuran (THF), acetonitrile (ACN), methanol, ethanol, dimethylsulfoxide (DMSO) were obtained from VWR, Darmstadt, Germany. Dexamethasone (Ph.Eur.) was delivered by Euro OTC Pharma from a local pharmacy store. Dulbeccos Saline PBS buffer concentrate was obtained from Sigma Aldrich, Rossdorf, Germany. Float-A-Lyzer G2 dialysis tubes (MWCO 8-10 kDa) and standard dialysis tubes (MWCO 6-8 kDa) were obtained from Spectrumlabs Inc., Breda, The Netherlands. For filtration of the micellar dispersions 0.2 μ m Pall Acrodisc syringe filters with GHP membrane were used (Pall Life Sciences, Ann Arbor, MI, USA). Sucrose, trehalose, glucose, lactose, maltose and D-(-)-mannitol were obtained from VWR, Darmstadt, Germany. Kollidon 17PF was delivered from BASF, Ludwigshafen, Germany. Kleptose[®] (HP β CD) was obtained from Roquette, Frankfurt, Germany. Captisol[®] (SBE β CD) was delivered from Cydex, Lenexa, KS, USA. Water was of MilliQ grade.

2.3.2 Methods

2.3.2.1 Preparation of drug loaded micelles

Direct dialysis from acetone 10 and 20 mg of block copolymer and 1 and 4 mg DXM, respectively, were dissolved in 1 mL acetone. This solution was filled into a dialysis bag and sealed. Dialysis was carried out over 24 h against 5 L water which was changed once after 4 h.

The dispersion was filtered through a 0.2 μm membrane to remove drug precipitates. Finally the mass of the resulting micellar dispersion was adjusted to 2 g by dilution with water.

O/W emulsion technique Micelles without DXM were prepared as described above in the section “direct dialysis from acetone” without drug. For drug loading, 2 mg DXM was dissolved in 1 mL DCM. This solution was injected under constant stirring to 2 mL aqueous micellar dispersion containing the “empty” micelles. After stirring over night the resulting dispersion was filtered through a 0.2 μm filter membrane to remove drug precipitates and the mass was adjusted to 2 g by dilution with water.

Selection of appropriate solvent for cosolvent evaporation The following water miscible organic solvents were included in a solvent screen for DXM: THF, ACN, acetone, DMSO, DMF, methanol, ethanol. The screen was carried out by using the following procedure at 25°C: 1) Dissolving 1mg of drug in 100 μL organic solvent, 2) stepwise addition of 10 μL water to this solution, 3) determination of drug precipitation by optical visibility of particles. Precipitation was investigated against a black background with sample illumination by cold light. The solvent in which the drugs exhibited the highest optical solubility was selected for preparation in the solvent evaporation step.

Cosolvent evaporation Drug loaded micelles were prepared by the combination of solvent evaporation followed by dialysis. 10 mg block copolymer and 2 mg drug were dissolved in 6 mL THF or 8 mL acetone; this solution was mixed with 2 mL water. The mixture was transferred into a round bottom flask and evaporated by applying vacuum of 30 mbar at 25°C. To remove the maximum amount of solvent this vacuum was kept constant for 10 min. The remaining aqueous formulation was then transferred into a Float-A-Lyzer G2 tube for dialysis to remove residual solvents. The formulation was dialyzed against 5 L DXM saturated water for 24 h. Finally the formulation was filtered through a 0.2 μm membrane and mass adjusted to 2 g.

2.3.2.2 Drug load determination

100 μL of the final micellar formulation was dissolved in 900 μL acetonitrile. This solution was injected in a HPLC system (Merck Hitachi La Chrom Elite) equipped with a UV detector (detection wavelength: 282 nm) and a Agilent Eclipse Plus C18 column (3.5 μm coarse, 5 cm length) at 35°C. A gradient method was used for separation where the mobile phase A consisted of 90% (v/v) ACN/ 10% (v/v) ammonium acetate buffer (pH 4.5, 10 mM) pH 4.5; mobile phase B had the opposite composition. DXM concentration was determined by drug

substance calibration curve. The polymer concentration was calculated from the initially used polymer feed prior to the preparation of micelles. Drug load was calculated according to equation 2.1:

$$Drug\ load\ [\%] = \frac{Drug\ concentration\ [\frac{mg}{mL}]}{Polymer\ concentration\ [\frac{mg}{mL}]} \cdot 100\% \quad (2.1)$$

2.3.2.3 Particle size measurement

Dynamic light scattering (DLS) was used to determine hydrodynamic diameter of the nanoparticles. Therefore, a Zetasizer-ZS from Malvern Instruments, UK, was selected and used in the backscattering mode. Measurements were performed in triplicate.

2.3.2.4 Lyoprotector screening via Differential Scanning Calorimetry (DSC)

10% w/v aqueous solutions of the selected lyoprotectors served as reference and were filled into 100 μ L aluminum pans. Micellar formulations of DXM-loaded PEG-PVPy (0.5% w/v) were mixed with the lyoprotector solutions (10% w/v) 1:1 to reach a final lyoprotector concentration of 5 % (w/v). Each aluminium pan was filled with 80 μ L and sealed. Thermoanalysis was performed on a Mettler Toledo DSC 821e (Mettler Toledo GmbH, Giessen, Germany). The samples were frozen from 25°C to -50°C with a cooling rate of 10 K/min followed by an isothermal step of 5 min. The samples were heated to 25°C with a heating rate of 10 K/min. After an isothermal step at 25°C of 5 min the whole procedure was repeated. Onset of glass transitions were evaluated in the thermograms of the heating step. For stabilizer screening each experiment was carried out in triplicate.

2.3.2.5 Lyoprotector screening via lyophilization of placebo micelles

Polymeric micelle formulations (0.5% w/v polymer) were prepared employing the cosolvent evaporation method from THF, including either the DXM-loaded PEG-PVPy micelles or unloaded PEG-PDLLA, PEG-PLGA and PEG-PCL micelles. The dispersions were premixed with adequate amounts of β -cyclodextrin derivative solutions to reach final lyoprotector concentrations of 5% w/v. The prepared solutions were transferred into 2R-glas vials; filling height was adjusted to 1.0 mL for all samples. Lyophilization was carried out on a Christ Epsilon 2-6 D freeze-dryer (Martin Christ GmbH, Osterode am Harz, Germany). The samples were frozen over 2 h to -40°C, primary drying was achieved at -38°C (according to previous T_g determination) and 0.05 mbar over 48 h and followed by secondary drying step at 30°C and 0.005 mbar for 24 h. After drying was finished, all sample vials were sealed under nitrogen atmosphere at 500 mbar. The lyophilized samples were reconstituted with 500 μ L water

and analyzed by DLS measurements. Data evaluation was carried out by the calculation of a particle size increase factors as proposed by Abdelwahed et al. [184]. Following their proposal the size increase factors were calculated as the ratio between initial particle sizes prior to lyophilization and particles sizes upon reconstitution of the samples.

2.3.2.6 Influence of lyoprotector concentration on micelle reconstitution

Investigation of the influence of lyoprotector concentrations on the drug-loaded micelles was carried out by preparation of lyophilizates with varying β -cyclodextrin concentrations. For this purpose the dexamethasone-loaded PEG-PVPy micelles were freeze-dried with 0.5%, 1%, 2.5% and 5% of HP β CD and SBE β CD. Reconstitution properties were investigated by DLS.

2.3.2.7 Cryo-Transmission Electron Microscopy (cryo-EM)

Drug-free and DXM-loaded PEG-PVPy nanoparticles as well as nanoparticles upon reconstitution of the lyophilizates with SBE β CD as cryoprotector were subjected to cryo-EM analysis. To this end, 4 μ l of sample were pipetted onto a glow-discharged holey-carbon copper grid, blotted with filter paper and plunge-frozen in liquid ethane. EM grids were stored in liquid nitrogen until imaging. Images were taken under cryo conditions in a Tecnai T12 (FEI, Eindhoven, The Netherlands) electron cryomicroscope equipped with a MultiScan 794 CCD camera (Gatan, Pleasanton, CA, USA) using a side-entry cryoholder (Gatan). Individual nanoparticles were selected from the raw images, and the dimensions of the nanoparticles were determined by comparing with reference binary discs of different diameters using a multi-reference alignment [185]. The determined particle sizes were used to calculate cumulant frequency curves for each sample. From these cumulant curves, the d_{10} , d_{50} , d_{90} values as the size distribution parameters of the samples were calculated as the size distribution parameters of the samples.

2.4 Results

2.4.1 Solvents for cosolvent evaporation

Based on previous reports that the preparation of drug loaded-micelles [179] requires a high solubilization capacity of the selected organic solvents, the drug solubility was screened in common fully water-miscible organic solvents. Fig. 2.2 shows the maximum volume of water which could be added to 7 solvents without drug precipitation. From this screening it was obvious that THF had the best solubilization properties in connection with water. Consequently this solvent as the most appropriate one was selected for the cosolvent evaporation.

However, for comparison purposes the preparation was additionally carried out using acetone which has a still reasonable solubilization capacity and low toxicity [186].

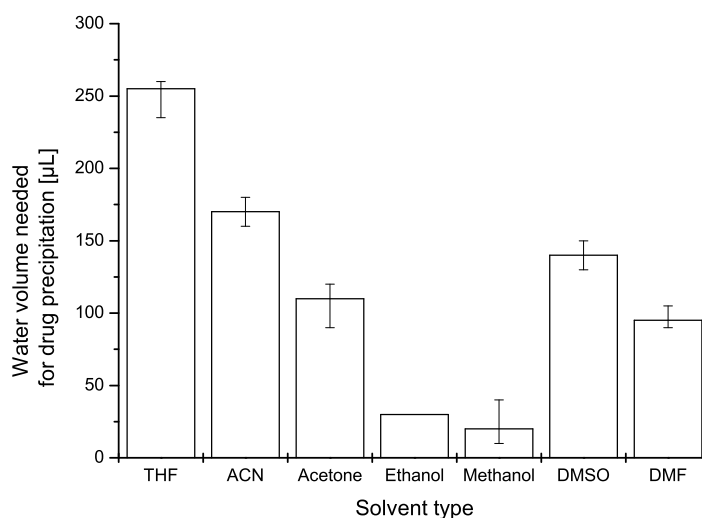


Figure 2.2: Solubility screening of 1 mg DXM in 100 μL of varying organic solvents upon addition of water. Drug precipitation was detected visually against a black background and illumination of the sample with cold light. The experiments were carried out in triplicate (mode \pm range).

2.4.2 Preparation of drug loaded micelles

The micelles were prepared and drug loaded according to the 3 selected methods. Table 2.1 reports the analytical results for the drug load determined by HPLC-UV, particle sizes and size distributions obtained from DLS technique.

2.4.3 Lyoprotector screening via DSC and lyophilization of placebo micelles

DXM-loaded PEG-PVPy micelles prepared by cosolvent evaporation technique from THF were selected for freeze-drying due to their high drug content compared to micelles made by other methods. Prior to lyophilization the lyoprotector solutions were prepared, mixed with micelles and analyzed by DSC measurements for their thermal properties. The thermograms revealed the glass transition temperatures of the maximally freeze concentrated solutions T_g' [187] (Fig. 2.3).

Table 2.1: Loading results of DXM incorporated in PEG-PVPy [5-b-20] micelles in dependence of the preparation techniques. All experiments were done in triplicate (mean \pm SD). * indicated drug precipitation during preparation.

Polymer	Polymer conc. w/v [%]	Drug/pol ratio feed [%]	Preparation technique	Solvent and conditions	Drug load [%]	d_h [nm]	PdI
PEG-PVPy [5-b-20]	0.5	1:10	O/W emulsion	DCM, preformed micelles from acetone DCM,	8.74 \pm 0.03*	52 \pm 2	0.15 \pm 0.01
PEG-PVPy [5-b-20]	1.0	1:10	O/W emulsion	preformed micelles from acetone DCM,	7.81 \pm 0.18*	69 \pm 4	0.19 \pm 0.03
PEG-PVPy [5-b-20]	0.5	4:10	O/W emulsion	preformed micelles from acetone	13.50 \pm 5.05*	52 \pm 1	0.19 \pm 0.02
PEG-PVPy [5-b-20]	0.5	1:10	Direct dialysis	Acetone	1.71 \pm 0.15*	56 \pm 7	0.18 \pm 0.06
PEG-PVPy [5-b-20]	1.0	1:5	Direct dialysis	Acetone	0.62 \pm 0.60*	67 \pm 2	0.16 \pm 0.01
PEG-PVPy [5-b-20]	0.5	1:5	Cosolvent evaporation	Acetone	12.07 \pm 1.21*	41 \pm 3	0.14 \pm 0.01
PEG-PVPy [5-b-20]	1.0	1:5	Cosolvent evaporation	Acetone	10.84 \pm 2.64*	45 \pm 5	0.12 \pm 0.01
PEG-PVPy [5-b-20]	0.5	1:5	Cosolvent evaporation	THF	18.67 \pm 0.21	37 \pm 1	0.21 \pm 0.01
PEG-PVPy [5-b-20]	1.0	1:5	Cosolvent evaporation	THF	19.25 \pm 0.54	52 \pm 1	0.26 \pm 0.01

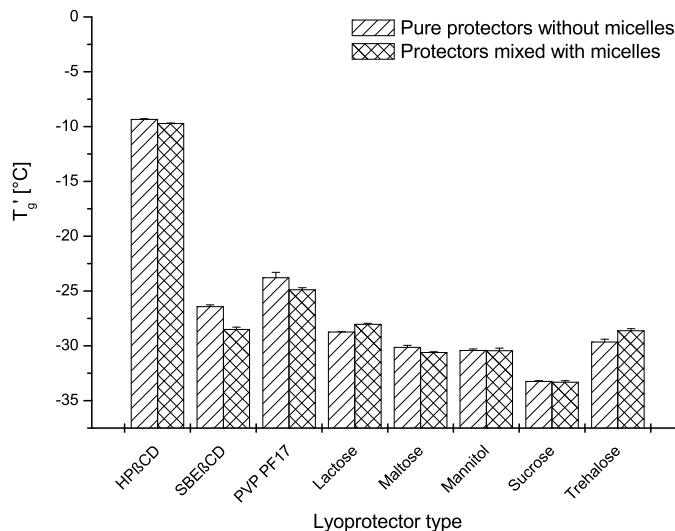


Figure 2.3: T_g' determination for the lyoprotectors included in the study (results: mean \pm SD, $n=3$) determined by DSC.

The T_g' values of the pure excipient solutions and of the excipient micelle mixtures are reported. Sucrose had the lowest T_g' with $\sim -32^\circ\text{C}$; the highest was reached with $\text{HP}\beta\text{CD}$ at $\sim -9^\circ\text{C}$. When the influence of nanoparticle presence was investigated by mixing DXM-loaded PEG-PVPy micelles with lyoprotector solutions, the maximum deviation in T_g' comparing with and without micelles was found for $\text{SBE}\beta\text{CD}$, where the micelles led to 2 K lower glass transition temperatures. Based on these results the primary drying temperature for a generic lyophilization process was set to -38°C (-33°C for lowest T_g' and 5 K safety margin). This maintained the “glassy” state of the freeze-dried solution and prevented influence of physical changes in the lyoprotector structure which could lead to micellar rupture and non-redispersibility. The DXM-loaded PEG-PVPy micelles were dried in a lyophilization process and screened with the selected lyoprotectors for reconstitution properties. The screening results are shown in Fig. 2.4A. As a quality parameter the particle size increase factor was calculated to compare the stabilizing properties of each lyoprotector with the investigated micelles, a method that was proposed by Abdelwahed et al. [184]. As evaluation criteria a change of hydrodynamic diameter of 10% compared to the micellar size before lyophilization was considered to be acceptable. The PEG-PVPy micelles increased in size by more than a factor of two when sucrose or Kollidon 17PF was used for stabilization. Maltose led to non-redispersible lyophilizates whereas trehalose did not stabilize the micelles sufficiently which can be seen by an increase in the size factor to 1.4. The investigation revealed that $\text{HP}\beta\text{CD}$ and $\text{SBE}\beta\text{CD}$ stabilized micelles quite well, apart from $\text{HP}\beta\text{CD}$ that

decreased particle size by $\sim 30\%$ after reconstitution. SBE β CD was able to stabilize the micelles excellently. The question became relevant if the results of lyoprotector screening were only valid for PEG-PVPy micelles and each polymeric micellar species requires a new screening.

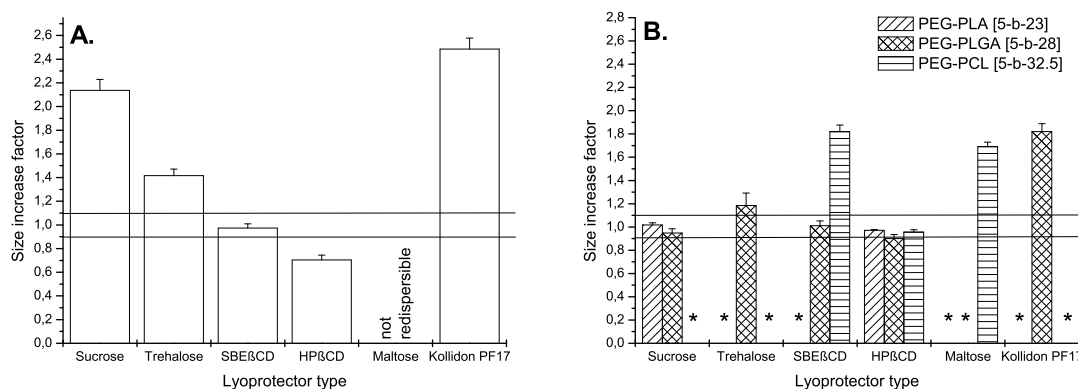


Figure 2.4: **A.** Size increase factors of micelles upon reconstitution of the lyophilizates of DXM-loaded PEG-PVPy [5-b-20] micelles prepared with varying lyoprotectors (results: mean \pm SD, n=3). **B.** Size increase factors of drug-free micelles upon reconstitution of the lyophilizates of PEG-PDLLA [5-b-23], PEG-PLGA [5-b-28] and PEG-PCL [5-b-32.5] micelles prepared with varying lyoprotectors (results: mean \pm SD, n=3).

To answer this question three different micelle forming block copolymers were selected and screened accordingly on their reconstitution properties (Fig. 2.4B). The results showed that HP β CD stabilized PEG-PLA, PEG-PLGA and PEG-PCL micelles excellently whereas SBE β CD were only sufficient for PEG-PLGA micelles. Moreover, sucrose led to full reconstitution of freeze-dried PEG-PLA and PEG-PLGA but could not stabilize PEG-PCL micelles. Trehalose, maltose and the Kollidon derivative did not stabilize any of the investigated micelles. Based on these results further mechanistic investigations of DXM loaded PEG-PVPy micelles with both β -cyclodextrin derivatives HP β CD and SBE β CD in varying concentrations were performed.

2.4.4 Optimum concentration of lyoprotector

Lyoprotector concentration played an important role for particle reconstitution. Consequently varying concentrations of HP β CD and SBE β CD were screened to determine the optimal ratio. As a result drug loaded PEG-PVPy micelles were reconstitutible in the selected concentration range between 0.5% and 5.0% (w/v) of lyoprotectors concentrations (Fig. 2.5).

The hydrodynamic diameter of the reconstituted micelles decreased for both stabilizers from 0.5% to 5.0%. It was remarkable that the micelles stabilized with 0.5% HP β CD exhibited strongly scattering particle sizes (reported as size increase factors) upon reconstitution whereas the micelles with 5.0% HP β CD were found to have strongly scattering particle size distributions widths. Lyoprotector concentrations between 1.0% and 2.5% were ideal to achieve reproducible hydrodynamic diameter and particle size distribution values. The question remained which influence the presence of β -cyclodextrins have on the recovery of dexamethasone before and after lyophilization. The results (data not shown) revealed the robustness of the HPLC method against the presence of β -cyclodextrins in liquid formulation (recovery: $\sim 102\%$). Moreover, upon reconstitution of lyophilizates the recovery decreased to $\sim 93\%$ - 95% from the initial liquid formulation.

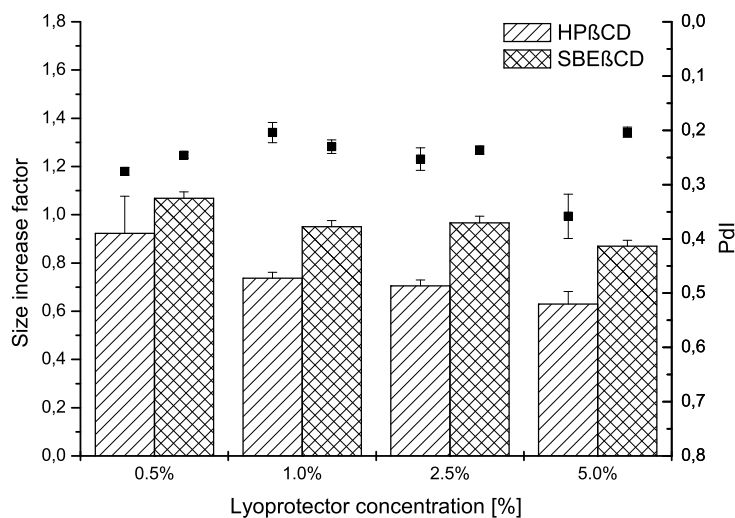


Figure 2.5: Size increase factors of micelles DXM-loaded PEG-PVPy micelles upon reconstitution of lyophilizates with varying HP β CD and SBE β CD concentrations (results: mean \pm SD, $n=3$).

2.4.5 Morphological and size analysis by cryo-EM

Previous studies indicated that the PEG-PVPy material was able to form various particle morphologies [188, 189]. For elucidation of the particle morphologies in the experiments cryo-EM as the method of choice was selected. As shown in Fig. 2.6A-C (left and middle) cryo-EM revealed spherical particles in the nanometer range for all analyzed samples.

Drug-free and DXM-loaded particles revealed a similar morphology, and the shape of the micelles was independent of the particle processing steps, i.e drug-loading and lyophilization

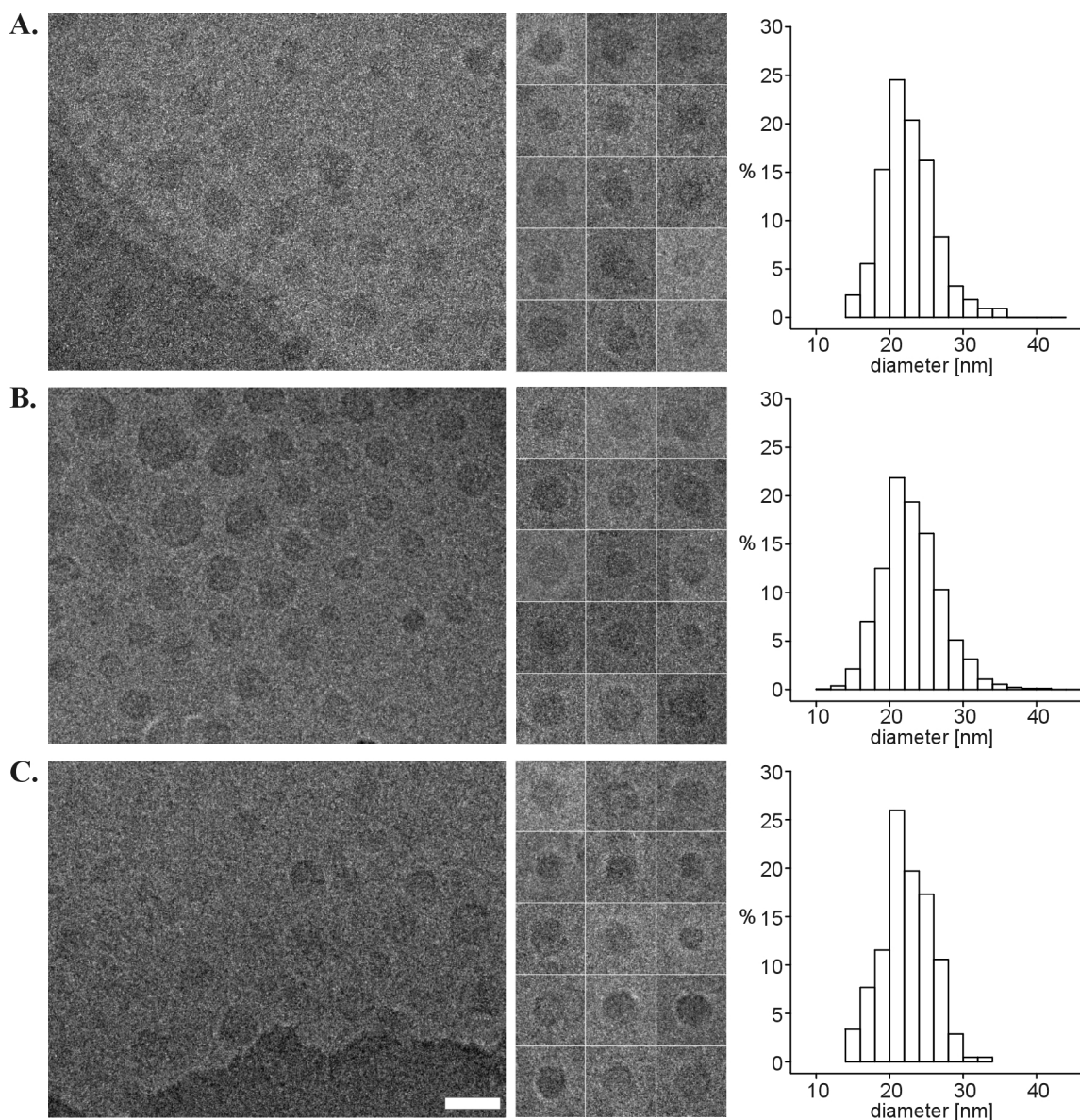


Figure 2.6: Cryo-EM analysis of PEG-PVPy micelles. The scale bar of the overview images (left) corresponds to 40 nm, and the box length of the single-particles (middle) corresponds to 53 nm. The size distribution of the respective sample is provided on the right. **A.** Drug-free PEG-PVPy micelles. **B.** DXM-loaded PEG-PVPy micelles. **C.** PEG-PVPy micelles loaded with DXM upon reconstitution of lyophilizates stabilized with SBE β CD.

with lyoprotectors. Upon computational measurement of the particles, the distribution of sizes was plotted. In line with the visual impression, this analysis confirmed that drug-free, drug-loaded and reconstituted PEG-PVPy micelles exhibited comparable sizes (Fig. 2.6A-C, right and Fig. 2.7). In particular, particles obtained by lyophilization and reconstitution of

particles revealed similar particle sizes and size distributions. Size distributions obtained from micrograph analysis are summarized in Table 2.2.

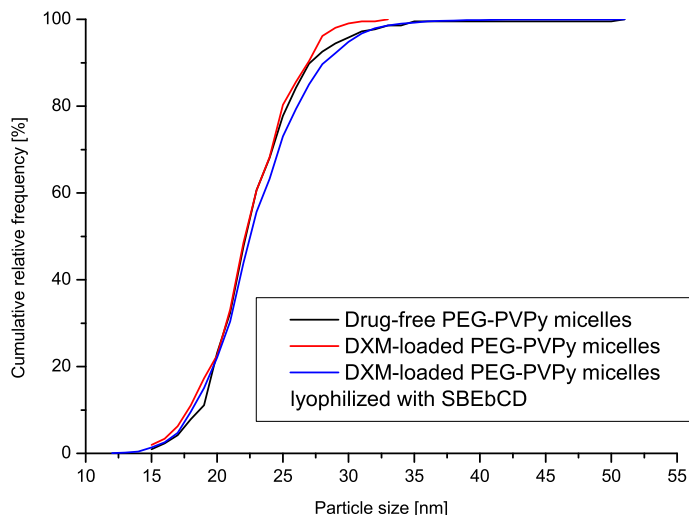


Figure 2.7: Cumulant frequency curves of particle sizes obtained from cryo-EM image analysis. Drug-free PEG-PVPy micelles (black), DXM-loaded micelles (red) and DXM-loaded micelles upon reconstitution of lyophilizates stabilized with SBE β CD (blue).

2.5 Discussion

The purpose of this study was to gain mechanistic insights into the drug-loading procedure and the stabilizing mechanisms of β -cyclodextrins during lyophilization of polymeric micelles. Three different preparation techniques for the DXM-loading of PEG-PVPy micelles were studied. All these methods had in common that organic solvents were used to load the micelles whereas the loading principles were completely different. The relevance of the organic solvent during micellization process was subject of previous investigations in the literature: Self-association of amphiphilic block copolymers in mixtures of organic solvents with water was first described by Selb and Gallot in 1975 [190]. The authors investigated the influence of the methanol/water ratio on the association properties of a polystyrene-poly-(vinyl-N-alkylpyridiniumbromide) copolymer. From their results they concluded that decreasing the methanol/water ratio led to the formation of star-shaped micelles due to the reduced solubility of the hydrophobic part of the polymer in the more aqueous solvent mixture. A change in intrinsic viscosity depending on the solvent composition (methanol/water) was additionally highlighted. Intrinsic viscosity of the micellar core also played an important role during drug

Table 2.2: Particle size distribution parameters obtained from cryo-EM micrograph analysis.

Sample	d ₁₀ [nm]	d ₅₀ [nm]	d ₉₀ [nm]	Number of particles evaluated from micrograph analysis
Drug-free PEG-PVPy	19	22	27	216
DXM-loaded PEG-PVPy	18	22	28	1881
DXM-loaded PEG-PVPy SBE β CD lyo	18	22	27	208

loading process. Organic solvents could act as plasticizers, making the core susceptible for hosting drugs. This phenomenon was described by Cinelli et al. [191]. Furthermore, the group of Zhao et al. [192] studied polystyrene-polyacrylate micelles with a fluorescent probe concerning kinetic effects of molecule encapsulation. To this end, pyrene was selected as a molecule which reported information about the micropolarity of its surrounding environment by changes in fluorescence emission spectra based on the method of Wilhelm et al. [41]. In Zhao’s study solvent mixtures of dimethylformamid/water with varying compositions were used to reveal the partitioning of the probe into the micelles. By calculating the drug load of pyrene as “number of molecules per micelle”, the authors concluded that a gradually change in composition of organic/water solvent mixtures during preparation of the micelles led to higher loading rates in polymeric micelles. Furthermore, the type of organic solvents was known to have an influence on particle sizes of resulting micelles: Vangeyte et al. [193] investigated PEG-poly-(ϵ -caprolactone) and PEG-poly-(γ -methyl- ϵ -caprolactone) in terms of particle sizes as a function of organic solvent type and mixture ratios. In their preparation THF, DMF, dimethylacetate (DMAc) and dimethylsulfoxide (DMSO) was included. The nanoparticles were prepared by 3 different methods: 1.) direct dialysis, 2.) addition of water to organic solution and 3.) addition of organic solution to water. For the methods 2 and 3 the ratio organic solvent/water was fixed (1:4). The group showed, that direct dialysis did not work reproducibly resulting in large particles in submicron range to micron range, whereas the solvent evaporation techniques worked well (sizes < 100 nm). The resulting particle sizes varied in this study depending on the used solvent. A size correlation was found: THF (80-100 nm) > DMSO (70-80 nm) > DMF (30-60 nm) = DMAc. The group of Aliabadi et al. picked up these thoughts about solvent influences and investigated the impact of the solvent type on drug loading into polymeric micelles [179]. Cyclosporine A which was encapsulated into PEG-poly-(ϵ -caprolactone) served as a model payload. Selected cosolvents

were acetone, THF and acetonitrile. The group worked with fixed organic/water mixtures 1:6 and 1:2. For micellar preparation, either the organic/water mixture was injected into water or it was prepared vice versa. In line with the studies of Vangeyte et al. [193], Aliabadi et al. [179] found solvent dependent particle size of drug-free micelles in the order: THF > acetone > acetonitrile. The authors selected acetone as the solvent of choice due to the nearly unimodal size distribution of the formed micelles from this solvent. The system was then investigated for drug loading and highest drug load as well as encapsulation efficiency was found for the preparation method acetone injection in water (final acetone water ratio 1:6). In their discussion the authors argued for a positive effect of gradually increasing the water content in a micellar system during preparation that prevented the hydrophobic drug from precipitation and consequently enabled encapsulation. Jette et al. [59] employed this cosolvent evaporation technique from acetonitrile/water to load fenofibrate into PEG-PCL micelles and drew similar conclusions on this method compared to Aliabadi et al. Summarizing these studies it was obvious that the organic solvent selected for the preparation of a micelle had a strong influence on drug load as well as particle sizes. Furthermore, the preparation technique was decisive for the successful encapsulation even if the solvent was selected appropriately. In this context the cosolvent evaporation technique employed e.g. by Aliabadi et al. [179] seemed to be superior over the other techniques due to the wide spectrum of organic solvents that can be used and its increased controllability by measurable physical factors during preparation. However, while the findings afore mentioned are highly significant there are a number of aspects they do not cover. This inspired us to further look into the drug loading techniques for polymeric micelles. Most important is the influence of organic solvents and preparation methods on the drug load of micelles. It was deemed necessary that it should be clarified if the preparation technique, the organic solvent within the preparation technique or the drug-polymer compatibility is most decisive for successful drug loading of micelles. To address this point three different preparation methods were selected for this purpose: 1) O/W emulsion technique, 2) direct dialysis and 3) cosolvent evaporation technique and assayed their potential for loading polymeric micelles with drug. The O/W emulsion technique is based on the use of water non-miscible solvents. By applying this method the organic phase (Fig. 2.8) which dissolved the drug was injected into an aqueous phase under constant agitation (e.g. stirring, ultrasound). Due to mechanical agitation the organic phase is distributed as small emulsion droplets in the aqueous phase. Consequently this effect increased the surface area of the organic phase. At those interfaces between organic and aqueous phase the distribution of the drug from organic emulsion droplets towards micellar core was possible. Furthermore, the slow evaporation of the organic solvent increased the time for this distribution process compared to simple mixing of both phases with small interface areas.

This method resulted in quite high drug loads for DXM in PEG-PVPy micelles (up to ~13% w/w). Variation of the initial drug-polymer ratio from 1:10 to 4:10 increased the drug load

from $\sim 10\%$ (w/w) to $\sim 13\%$ (w/w). This was concomitantly found to be the upper limit for this method due to the occurring drug precipitation upon solvent evaporation. A completely different loading mechanism exhibited the direct dialysis method (Fig. 2.9): Once the organic drug/polymer solution was filled into the dialysis bag, the overall system immediately came into contact with an aqueous phase during dialysis.

The exchange of organic solvent at the interface of the dialysis tube could be very fast and less controllable. Finally the solution conditions of the drug decreased strongly which led to immediate drug precipitation and resulted in a low drug load ($\sim 2\%$ w/w) independent of the drug-polymer ratio. Once precipitated, the drug was not available for encapsulation anymore. For the cosolvent evaporation mechanism there was a variety of water-miscible organic solvents available in which the drug solubility was screened prior to micelle preparation (Fig. 2.2). Compared to the direct dialysis premature drug precipitation was avoided during the cosolvent evaporation by the selection of a “good” solvent for the drug DXM (Fig. 2.10).

The cosolvent evaporation was carried out from an initial solvent/water ratio which was able to still solubilize both, drug and polymer. During evaporation the micelles were preformed but simultaneously the drug was still dissolved at this point. This procedure enabled the distribution from the outer aqueous/organic phase into the micellar core. By continuing the evaporation the drug solubility decreased in the organic/water phase which finally shifted the distribution equilibrium further towards the micellar core. At the end of this step the formulations contained only low amounts of residual solvents which were further cleared by dialysis. The dialysis step was implemented to overcome the disadvantage of cosolvent formation: azeotropic mixtures [59]. These mixtures made it impossible to evaporate the

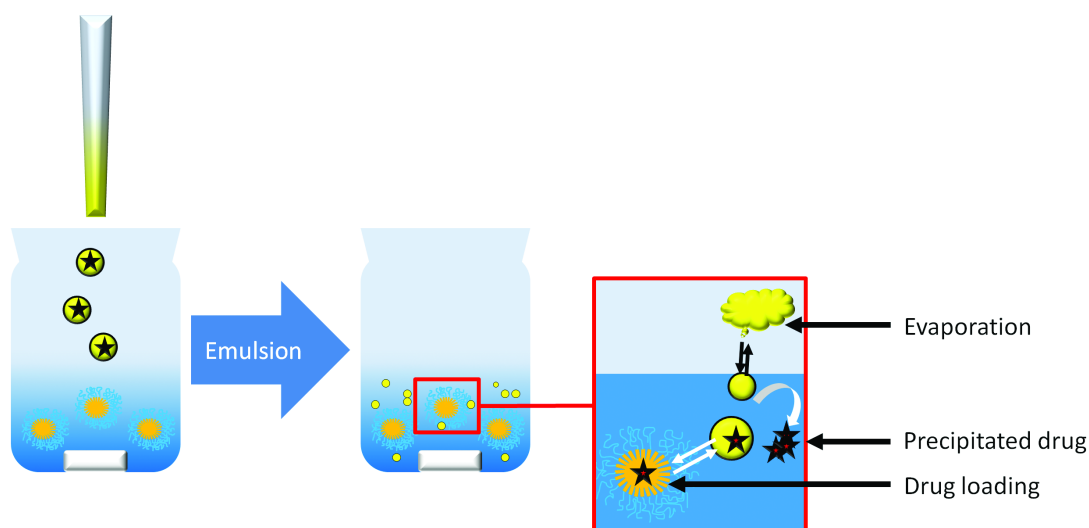


Figure 2.8: Schematic drawing of the O/W emulsion process.

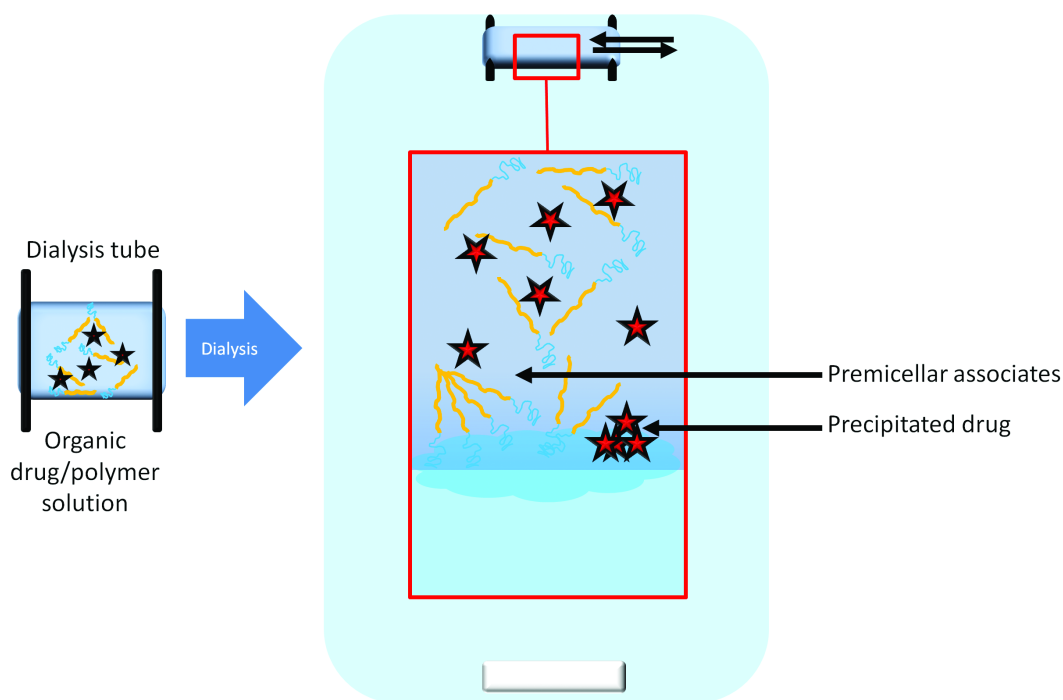


Figure 2.9: Schematic drawing of the direct dialysis process.

solvents completely. Overall the superior properties of cosolvent evaporation are reflected by these results: the drug load of the system increased up to $\sim 19\%$ w/w DXM for $\sim 1\%$ PEG-PVPy (w/v). As a next step, stabilization of this high drug load inside the micelles was a focus of this study. Freeze-drying was selected as the method of choice to gain a storage stable product. Maintaining full reconstitution properties of micelles with high drug load is generally very challenging: during freezing of micellar dispersions varying stress factors could appear which are of physical or chemical nature and which are well investigated for therapeutic proteins [187]. For nanoparticles, they usually comprise: 1) particle aggregation due to the loss of repulsive properties of steric stabilizers [194], 2) nanoparticle reassembly and remodeling after reconstitution [195], 3) loss of encapsulated drug due to changes in the physical status of the nanoparticle [196] as well as 4) chemical degradation of the carrier polymer and the encapsulated drug [184]. Prevention of these stresses and full reconstitution properties can be achieved by the addition of cryo- and lyoprotectors to the formulation [187]. There were two well established hypotheses for the explanation of the efficacy of protectors which were nicely summarized by Abdelwahed et al. [184]: the water substitution model explains protection during the drying step whereas the vitrification model highlights on the stability during freezing [184]. The water substitution model suggests that water molecules are substituted by OH-groups from molecules which are similarly hydrophilic e.g. polyols like sugars which are widely used as lyoprotectors. This is known to assure chemical and physical

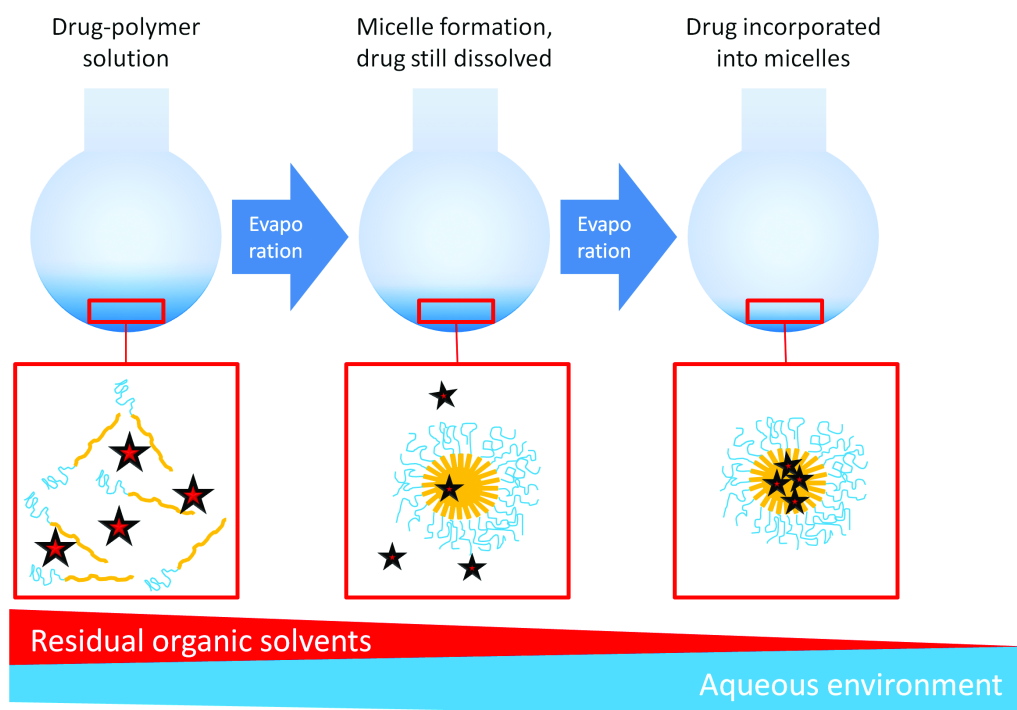


Figure 2.10: Schematic drawing of the cosolvent evaporation process.

integrity of proteins [187] and consequently should be one approach to stabilize nanoparticles. The vitrification model describes nanoparticle embedding into an amorphous stabilizer matrix which finally prevents aggregation [184, 197]. Moreover, Allison et. al [198] brought the “particle isolation hypothesis” [198] into play which argued for the isolation of particles in the non-frozen fraction by polyols. It is worth mentioning that the above cited studies investigated nanoparticles like liposomes or nanocapsules and did not highlight on the mechanisms of freeze-drying of polymeric micelles. Since this is an important issue it will be discussed below in more detail. Abdelwahed et al. [184] selected various sugars (maltose, sucrose, trehalose) as cryo- (prevents from freezing stress) and lyoprotectants (prevents from drying stress), a stabilizer and “collapse temperature modifier” [184] vinylpyrrolidin macromolecule (PVP PF 17) and cyclic oligosaccharides (HP β CD, SBE β CD) (also “collapse temperature modifier” [184]) for a lyoprotector screening. As a first step all considered lyoprotectors were screened via DSC concerning their optimal freezing-properties. T_g' was selected as a reporting parameter for the optimization of the lyophilization process. Whereas HP β CD revealed a T_g' of $\sim 10^\circ\text{C}$ which could assure a short, effective and less costly lyophilization process all the T_g' values for the other investigated lyoprotectors scattered between $\sim 22^\circ\text{C}$ and $\sim 33^\circ\text{C}$. Consequently to run a generic lyophilization process for all stabilizers the primary drying temperature was selected at -38°C . Interestingly the presence of micelles did not strongly change the freezing properties of lyoprotectors. Obviously β -cyclodextrin derivatives seemed to

have excellent stabilization properties for various micellar species (Fig. 2.5B) and seemed to be versatile lyoprotectors. Support of this hypothesis came from the investigations of the other pegylated block copolymers PEG-PDLLA, PEG-PLGA and PEG-PCL (Fig. 2.5B). HP β CD stabilized all investigated micelles very well and led to completely redispersable formulations while SBE β CD excellently stabilized PEG-PLGA and PEG-PVPy micelles. Especially the results acquired from HP β CD led to the assumption that for β -cyclodextrin derivatives there might be an additional mode of action concerning stabilization besides the water molecule substitution and vitrification model. All the investigated polymeric micelles present PEG chains on their surfaces. It is known from the literature that PEG and cyclodextrins are able to form inclusion complexes called pseudopolyrotaxanes [199, 200]. Less was known if this phenomenon appeared on micellar surfaces as well. Joseph et al. described inclusion complexes of a cyclodextrin derivative with Pluronic[®] block copolymer molecules which they proved by small angle neutron scattering (SANS) experiments [201]. The authors hypothesized that the β -cyclodextrin derivative preferentially covered the more hydrophobic PPO block of the polymer. This observation was found for single polymer chains and for micellar aggregates, but increasing β -cyclodextrin concentrations led to increased complexation and finally to dissociation of the micelles. These phenomena were highly temperature dependent; below room temperature pseudopolyrotaxane formation appeared whereas above 50°C precipitation/gelation occurred. Qin et al. investigated the interaction of β -cyclodextrin with varying Pluronic[®] derivatives as well and confirmed the pseudopolyrotaxane formation by two-dimensional NMR spectroscopy [201]. A strong dependency of cyclodextrin concentration and temperature on the aggregate size was found. Moreover, such an inclusion phenomenon was found to be very fast (< 3 min), preferentially below 25°C and could be disturbed by changing the water cluster structure by chaotropic solutes (e.g. urea) [202]. The presence of pseudopolyrotaxanes on PEG brushes was at first described by He et al. in 2005 [203]. The general question remains if pseudopolyrotaxane formation is beneficial for the lyophilization of polymeric micelles and what makes them superior compared to the other polyols? In this connection the influence of solutes on the water cluster structure comes into play. Generally solutes can have “structure-making (kosmotropic)” [204] and “structure-breaking (chaotropic)” [204] properties on the water cluster structure. Sugars lead to kosmotropic structures as has been shown for trehalose, maltose and sucrose [205]. Trehalose is known to be a very effective cryoprotectant and superior to the other two sugars. Investigation of the reasons for this observation was performed by Lerbret et al. [205]. These three sugars were investigated and compared to each other on their changes in water cluster structure by means of molecular dynamic simulations. As a result the group found trehalose to form larger water cluster sizes compared to the other sugars. Consequently more water atoms were associated by hydrogen bonding to trehalose molecules and the amount of bulk water which induces nucleation during freezing was reduced. The group concluded on less

drying stress and less risky ice formation to explain the superior cryoprotective properties of trehalose. Coming back to the polypseudorotaxane formation of PEGylated block copolymer micelles with β -cyclodextrins, the facts appear in a different light: Generally cyclodextrin derivatives are known to be strong kosmotropic solutes [206]. In contrast, Sano et al. [206] revealed by Raman spectroscopy that the formation of polypseudorotaxane recovered the original cluster structure of pure water and denied a kosmotropic influence of cyclodextrin derivatives. Consequently the water cluster model cannot be used for polypseudorotaxanes to explain the results obtained from lyophilization. An alternate explanation is provided by Liu et al. [207] who investigated the change of material properties of such inclusion complexes. The group prepared guest-host complexes from an ABA triblock copolymer (poly-[(R,S)-3-hydroxybutyrate]-poly(ethylene glycol)-poly[(R,S)-3-hydroxybutyrate] [PHB-PEG-PHB]) containing PEG as block B. They confirmed the selective formation of the inclusion complexes with block B (central block) with an α -cyclodextrin derivative by differential scanning calorimetry (DSC), ^1H -NMR and X-ray diffraction (XRD) studies. As a result the partial degree of crystallinity of PEG was strongly reduced and could not be detected after formation of polypseudorotaxanes. Consequently the material properties were altered and the PEG part was embedded into an amorphous matrix. Therefore it is postulated that the PEG shield which covers the hydrophobic cores in the used systems is undergoing polypseudorotaxane formation. Consequently freezing stress and crystallization of water that challenges the core stability could be prevented by creating this kind of amorphous shield. Furthermore, desiccation stress from the particles can be reduced by the amorphous matrix as well. Based on these results and previous studies from literature there is mounting evidence for a direct interaction between β -cyclodextrins and PEGylated block copolymers (Fig. 2.11) which could explain the excellent results from lyophilization.

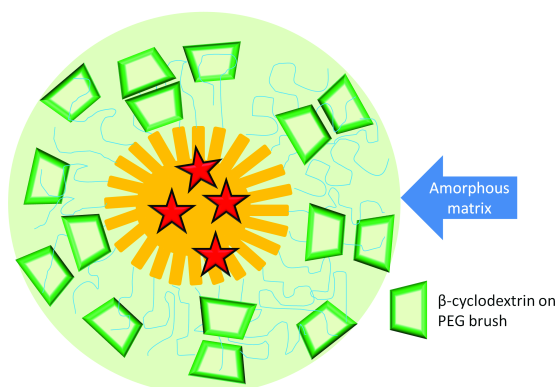


Figure 2.11: Schematic drawing of the β -cyclodextrin inclusion complexes with PEGylated surfaces (pseudopolyrotaxane formation).

The formation of PEG- β -cyclodextrin inclusion complexes had a beneficial effect on the

reconstitution properties of pegylated block copolymer micelles. Consequently these molecules can be proposed as versatile lyoprotectors for such micellar systems.

2.6 Conclusions

In this study three different drug loading mechanisms for hydrophobic drugs into polymer micelles were compared. Among those the cosolvent evaporation technique was superior compared to O/W emulsion technique and direct dialysis technique. The reasons for these observations were the possibility of appropriate solvent selection as well as a better control of the evaporation step during preparation. This combination kept the drug as long as necessary in solution during micelle formation and prevented premature precipitation. This high drug load can be stabilized by final micelle freeze-drying. It was found that β -cyclodextrins are versatile lyoprotectors for pegylated polymeric micelles due to a possible direct interaction between PEG corona chains and the hydrophobic β -cyclodextrin cavity. The special stabilization properties of β -cyclodextrins was seen to be based on 1) embedding of the PEG parts into an amorphous matrix, 2) prevention from formation of crystalline PEG during freezing and 3) stabilization of the hydrophobic core during freezing by prevention of water crystallization in the hydrophilic shell.

Chapter 3

Comparative investigations on *in vitro* serum stability of polymeric micelle formulations

Tobias Miller^{1,3}, Reinhard Rachel², Ahmed Besheer¹, Senta Uezguen¹, Markus Weigandt¹, Achim Goepferich³

¹ Merck KGaA, Exploratory Pharmaceutical Development, Frankfurter Str. 250, 64293 Darmstadt, Germany

² University of Regensburg, Center for Electron Microscopy at the Institute for Anatomy, Universitätsstrasse 31, 93040 Regensburg, Germany

³ University of Regensburg, Department of Pharmaceutical Technology, Universitätsstrasse 31, 93040 Regensburg, Germany

Published in: *Pharmaceutical Research* (2011)

3.1 Abstract

Stability of polymeric micelles upon injection is essential for a drug delivery system but is not fully understood. An analytical test was optimized allowing for quantification of micellar stability in biofluids and applied to a variety of block copolymer micelles with different hydrophobic block architectures. Polymeric micelles were prepared from four different polymers and investigated via encapsulation of two fluorescent dyes. Samples were incubated in human serum; changes in Foerster Resonance Energy Transfer (FRET) were recorded as a function of time. This fluorescence-based approach was supported semi-quantitatively by results from Asymmetrical Flow Field-Flow-Fractionation (AF4). After incubation experiments, micellar stability was determined by calculation of two stability-indicating parameters: residual micellar fractions (RMFs) and *in vitro* serum half-lives. Both parameters showed that PEG-PVPy micelles rapidly destabilized after 3 h (RMF<45%), whereas PEG-PLA, PEG-PLGA and PEG-PCL micelles were far more stable (RMFs 65 to 98%). This FRET-based assay is a valuable tool in evaluating and screening serum stability of polymeric micelles and revealed low serum stability of PEG-PVPy micelles compared to polyester-based micelles.

3.2 Introduction

During the past 20 years of drug research, the number of newly developed poorly soluble compounds has steadily increased. Estimations suggest that 40% of new chemical entities have an aqueous solubility problem that consequently leads to insufficient bioavailability and undesired low therapeutic effects [5]. Varying approaches have been investigated to conquer solubility problems by formulation processes. Several highly fascinating and yet challenging options can be found in the field of nanosized carrier systems. For example, polymeric micelles seem to be highly promising for overcoming the problem outlined above. This drug delivery system can be formed from amphiphilic block copolymers leading to spherical nanosized particles with a hydrophobic core surrounded by a hydrophilic shell. In the core, these particles can host hydrophobic drugs, whereas the shell-forming corona confers the drug delivery system stealth properties and, as a result, a less distinct recognition by the mononuclear phagocyte system (MPS) [208, 8, 209, 210]. Such pegylated nanoparticles could achieve long blood circulation times and, thus, can target tumors passively by the enhanced permeability and retention (EPR) effect [12] or actively using appropriate ligands [211, 14, 212]. Currently, the most advanced micellar formulations encapsulating the hydrophobic taxol-derivatives have already entered the market in India (Nanoxel[®]) and Korea (Genexol-PM[®]) [7]. Generally, when working with polymeric micelles, there are two methods to encapsulate drugs: physical entrapment in the hydrophobic core or chemically linking the drug to the polymer chain by a covalent bond. Both approaches have their advantages. The physical entrapment of the drug is generally easier to prepare and leads to higher loading rates, while the chemical coupling confers the polymer-drug adduct a higher stability upon injection [213]. Consequently, the fate of micelles with physically incorporated drugs after intravenous application is a very critical issue. Generally, micelles are in dynamic equilibrium and tend to disassemble upon dilution below their critical association concentration. Contrary to the low molar mass surfactants, polymeric micelles are known to be kinetically stable, taking hours to disassemble. However, while circulating in the blood, the polymeric micelles can lose their drug payload due to multiple reasons, including: 1) diffusion of the drug due to the small diffusion length; 2) partitioning between the hydrophobic micellar core and the surrounding aqueous phase, as well as binding to serum proteins or lipid membranes; and 3) eventual disassembly of the micelles themselves due to the strong dilution below their critical association concentration (CAC) [174]. Such premature release can lead to undesired pharmacokinetics and/or severe side effects, including the triggering of immunotoxicological cascades [214]. Considering these problems, the aim of this study was to investigate the *in vitro* stability of polymeric micelles made of different block copolymers, namely PEG-PVPy (PEG-poly-4-(vinylpyridine)), PEG-PLA (PEG-poly-(lactic acid)), PEG-PLGA (PEG-poly-(lactic acid-co-glycolic acid)) and PEG-PCL (PEG-poly-(ϵ -caprolactone)) based on an analytical test was adapted from the literature

[53, 165] and then further improved. Additionally, the stability of these polymeric micelles were benchmarked against those of Tween 80[®], which was selected as an ideal reference non-ionic surfactant due to the presence of already published studies in humans. For these *in vitro* studies, the two fluorescent dyes 1,1'-Diocadecyl-3,3',3'-tetramethylindocarbocyanine perchlorate (DiI) and 3,3'-Diocadecyloxacarbocyanine perchlorate (DiO) were incorporated into micelles as a model for physically entrapped drugs. When both dyes are in close proximity, Foerster Resonance Energy Transfer (FRET) can be measured and, hence, be used as a marker for micellar integrity. To study the serum stability of PEG-PVPy micelles *in vitro* and to compare the results with previously investigated block copolymers by other groups, the FRET-based technique was refined in this study. In contrast to the existing studies of Chen et al. [165] that calculate a FRET ratio from fluorescence maximum peak height, in this study the recorded fluorescence spectra were integrated. This minimizes effects caused by changes in Stokes shifts from fluorescence dyes due to hydrophobic interactions of dye and polymer, as shown previously for poly-(4-vinylpyridine) by Kamat and Fox [215]. In addition, it was possible to achieve complete dye release after incubation from the still intact polymeric micelles by addition of 7.5% v/v TritonX-100 at 37°C. This non-ionic surfactant leads to the dissolution of polymeric micelles, as indicated by Cerritelli et al. for PEG-PPS micelles [43]. The resulting FRET ratio after complete dye release and the initial ratio enable the calculation of two parameters reflecting the stability of micelles: the *in vitro* serum half-life and residual micellar fraction (RMF). Some of the investigated materials (PEG-PLA, PEG-PLGA and PEG-PCL) are well-known block copolymers, and their micelles have been thoroughly investigated. Gref et al. studied the influence of PEG chain length, PEG surface density, and different types of hydrophobic cores (PLA, PLGA and PCL) on plasma protein absorption by two-dimensional electrophoresis. This group identified a pattern of different proteins adsorbing onto the nanoparticulate surfaces [216]. The different micellar hydrophobic cores showed qualitatively similar adsorption patterns with varying degrees in quantity of each serum protein fraction. Additionally, PEG-PCL micelles were investigated by Aliabadi et al. concerning their *in vivo* pharmacokinetic behavior [58]. This was correlated with an *in vitro* serum stability experiment in which micelles were dialyzed against serum proteins to determine the non-encapsulated drug fraction. The authors correlated high micellar *in vivo* stability with the occurrence of low unbound drug fraction. As previously mentioned, Chen et al. [53] have already shown by using a FRET-based method for PEG-PDLLA micelles that the stability depends on the influence of varying serum proteins and red blood cells. This group calculated FRET ratios from the emission maxima in the fluorescence spectra and discussed the impact of varying serum proteins and red blood cells on stability qualitatively. Furthermore, this technique has been applied to trace cellular uptake of intact micelles which physically encapsulate the dyes by confocal laser microscopy [165]. Savic et al. conjugated a fluoresceine derivative covalently to PEG-PCL micelles and performed cellular uptake studies.

They were able to distinguish between intact micelles and single polymer chains [217]. These existing methods, however, lack the possibility to quantify the micelles in human serum and to directly compare between formulations composed of block copolymers with different architectures.

3.3 Materials and methods

3.3.1 Materials

The following block copolymers were purchased from Polymer Source Inc., Montreal, Canada: mPEG-PLLA [5-b-4.7], mPEG-PDLLA [5-b-23], mPEG-PCL [5-b-32.5], mPEG-Poly-(4-vinylpyridine) [mPEG-PVPy] [2-b-5.5], mPEG-PVPy [2-b-10] and mPEG-PVPy [5-b-20]. mPEG-PLGA [5-b-28] (Resomer RGP d 50155) was obtained from Boehringer Ingelheim, Ingelheim, Germany. Pyrene, tetrahydrofuran (THF) and acetone were delivered by VWR, Darmstadt, Germany. Tween 80[®], human serum from male (blood group AB), and fluorescent dyes DiI and DiO were obtained from Sigma Aldrich, Rossdorf, Germany. SpectraPor dialysis tubing with MWCO 3.5 kDa was delivered by Spectrum Laboratories Inc., Breda, The Netherlands. Water was of MilliQ grade.

3.3.2 Polymer characterization by differential scanning calorimetry (DSC)

Thermoanalysis was performed on a Mettler Toledo DSC 821e scanning calorimeter to investigate glass transition temperatures and melting points of the polymers. All dry block copolymers were weighed into 100 μ L aluminium pans. These samples were heated two times from -50°C to 100°C (PEG-PVPy samples to 200°C) with a heating and cooling rate of 10 K/min. After each heating or cooling ramp, an isothermal step of 5 min was implemented. The first heating and cooling cycle was used to clear thermal history of the polymers; the second heating cycle was used to evaluate thermal events. All experiments were performed in triplicate.

3.3.3 Micelle preparation

3.3.3.1 Samples for determination of critical association concentration (CAC)

For the determination of the CAC, the pyrene probing method described by Wilhelm et al. was used and further adapted to the requirements of the tested polymer types [41]. This method is based on the change of vibrational fine structure of the fluorescence light emission spectra, which depends on the polarity of the probe environment [218]. Micelles were prepared

by dissolving the polymers in acetone, reaching a final concentration of 0.5% w/v. This organic solution was directly dialyzed against 5 L water for 7 h. The water was changed twice. This preparation step forms dye-free micelles with very low residual solvent (data not shown). In the second step, a pyrene stock solution was prepared and added to the dye-free polymeric micelles in a third step. The pyrene solution was prepared by dissolving the dye in tetrahydrofuran (THF, 6×10^{-2} mol/L). This solution was injected into water with a final pyrene concentration of 6×10^{-6} mol/L (stock solution). THF was removed by evaporation at 40°C and 50 mbar over 1 h. As a third step, the dye-free polymeric micelles were diluted corresponding to a polymer concentration range from 1.0 mg/mL to 5×10^{-4} mg/mL. The samples were incubated over 12 h with the pyrene stock solution, enabling the partition of pyrene into the micellar core. The pyrene concentration was kept constant in all samples at 1.2×10^{-7} mol/L.

3.3.3.2 Samples for serum incubation studies, Asymmetrical Flow Field Flow Fractionation (AF4) experiments, and Transmission Electron Microscopy (TEM)

DiI- and DiO-loaded polymeric micelles were prepared by solvent evaporation and finally a dialysis technique. Both dyes and the polymer were dissolved in acetone and added to water under stirring to reach a polymer target concentration of 2 mg/mL loaded with 0.0015% w/v of each dye. PEG-PVPy-based micelles were loaded with 0.0045% w/v donor (DiO) and 0.0015% w/v acceptor (DiI). The latter donor/acceptor (d/a) ratio was selected due to the light absorption properties of the vinylpyridine part in the block copolymer in contrast to the nonabsorbing aliphatic polymers, such as PEG-PLLA, and is in line with investigations of Berney and Danuser [219]. After evaporation overnight, the resulting micellar dispersion was filled into a dialysis bag and dialyzed over 4 h against 5 L water. This step was carried out to remove untrapped fluorescence dye and residual solvent. Finally, the dispersion was filtered through a 0.2 μ m celluloseacetate filtermembrane.

3.3.4 Micelle characterization

3.3.4.1 Determination of critical association concentration (CAC)

Fluorescence excitation spectra of the pyrene-loaded micelles were recorded on an Aminco Bowman luminescence spectrometer (Aminco Bowman, Urbana, Illinois) at 390 nm emission wavelength and excitation wavelengths ranging from 300 nm to 360 nm using a spectral bandwidth of 1 nm and 2 nm for fluorescence excitation and emission, respectively. The scan rate was 0.5 nm/s. According to the method of Wilhelm et al., the $I_{338 \text{ nm}}/I_{334 \text{ nm}}$ ratio was evaluated for the determination of CAC [41]. Each experiment was performed in triplicate.

3.3.4.2 Particle size measurements

The dynamic light scattering (DLS) technique was used to investigate the micellar average diameter. For the measurements, a Zetasizer Nano ZS90 from Malvern, UK, was set to 173° backscattering mode. The mean size and polydispersity index (PDI) were calculated by cumulants analysis using ZetasizerNano[®] software.

3.3.4.3 Transmission Electron Microscopy (TEM)

Micellar size and morphology were investigated by transmission electron microscopy using a negative staining technique. The samples were dried on the surface of carbon-coated copper grids (400 mesh; Plano, Wetzlar, Germany) for electron microscopy. For staining of PEG-PDLLA [5-b-23], a solution of 2% uranyl acetate solution in water (pH 4.5) was used, while all the other samples were stained using an aqueous solution of 2% phosphor tungstic acid (PTA; titrated to pH 7, using NaOH). The PEG-PLLA [5-b-4.7] sample was incubated with TritonX-100 for 20 min to examine the micellar destruction process as used in the FRET assay. All electron micrographs were digitally recorded using a CCD camera (TVIPS, Gauting) on a CM12 transmission electron microscope (FEI Electron Optics, Eindhoven, The Netherlands). For particle size determination, 100 particles in a predefined area of the electron micrograph were measured. Statistical evaluation was performed by calculation of arithmetic mean and standard deviation.

3.3.5 Determination of micelles' *in vitro* serum stability

3.3.5.1 Sample incubation, FRET ratio determination, calculation of stability parameters

Set-ups of fluorescence experiments were similar to the CAC determination. In contrast, excitation wavelength was set to 484 nm, and emission was scanned from 495 nm to 600 nm (for PEG-PVPy samples to 620 nm). All samples were incubated at 37°C over 3 h. Emission spectra were recorded after 0, 15, 30, 45, 60, 90, 120, and 180 min of incubation. Additionally, for PEG-PLGA [5-b-28] micelles, spectra at 4, 5, 6, 9, 12, 15, 18, and 26 h were recorded. After the last recording time point, micelles were dissolved by adding 7.5% v/v TritonX-100. The incubation was maintained for 20 min and a final spectrum was recorded. Each single spectrum was integrated using Origin[®] software to determine the peak area of FRET-acceptor maximum and donor maximum. Calculating the FRET was done according to Eq. 3.1:

$$FRET\ ratio = \frac{\frac{\int_{D/A\ border}^{Spectrum\ end} intensity}{c[Acceptor]}}{\frac{\int_{Spectrum\ start}^{D/A\ border} intensity}{c[Donor]} + \frac{\int_{Spectrum\ end}^{D/A\ border} intensity}{c[Acceptor]}} \quad (3.1)$$

For each polymer, the interception point of the time-resolved fluorescence emission spectra was determined. By overlaying the recorded spectra, this interception point is defined before the emission peak of FRET acceptor dye (varying around 545 nm). “Spectrum start” was 495 nm emission wavelength for all DiO/DiI loaded micelles, whereas “spectrum end” was 600 nm apart from the PEG-PVPy micelles. For the latter, the spectra were integrated to 620 nm due to a wavelength shift caused by quenching effects of the dyes’ fluorescent emission from pyridines’ aromatic rings. For quantitative evaluation of the data, the resulting FRET ratios were normalized to the TritonX-100 FRET ratio and the initial ratio at t=0 min by Eq. 3.2:

$$Residual\ micellar\ fractions\ [\%] = 100 \cdot \frac{FRET\ ratio_{t=x\ min} - FRET\ ratio_{TritonX-100}}{FRET\ ratio_{t=0\ min} - FRET\ ratio_{TritonX-100}} \quad (3.2)$$

Residual micellar fractions (RMFs) were plotted and analyzed by Origin[®] software using the first-order decay curve-fitting function. From the fitted curves at RMF_{50%}, the serum half-life was calculated if possible. Additionally, the RMF_{180 min} was analyzed.

3.3.5.2 Asymmetrical Flow Field Flow Fractionation (AF4)

Due to the great versatility of AF4 concerning particle and protein separation [220], this method was selected to confirm the hypothesis of micellar disassembly in the presence of human serum. Therefore, dye-loaded PEG-PVPy [5-b-20] micelles, which showed intermediate stability in the described FRET assay, were incubated with human serum at 37°C. The incubation sample was prepared with a polymer concentration of 2 mg/mL and diluted with human serum (1:2). The samples were injected into a Wyatt Eclipse F module (Wyatt Inc., Santa Barbara, USA) with a 26.5 cm separation channel using a 350 µm polycarbonate spacer and polyethersulfone membrane with 5 kDa molecular weight cut-off (MWCO). The pump system consisted of an Agilent 1100 HPLC pump and degasser; detection was performed on a Wyatt DAWN EOS MALS detector and a Shodex RI-101 detector. A 50 mmol NaCl solution with 0.05% NaN₃ served as a mobile phase. The detector flow rate was 1.0 mL/min using a cross flow gradient from 3.0 mL/min to 0 mL/min, and the injection volume was 100 µL. The original incubated sample was separated using AF4 0, 90, 180, 270, and 1,440 min after the beginning of incubation. During each separation run, the micellar fractions were collected (from 28 min to 33 min) and concentrated using Vivaspin 6 tubes. The resulting

5 mL sample volume from the first AF4 experiment was concentrated to 0.5 mL. Finally, this fraction was injected and separated again. The presented size and size distribution equations were performed with Astra[®] 4 software. The particle diameters were calculated from RMS radii (d_{50}) in the particles mode, evaluating the angular dependence of scattered light assuming spherical particles. Based on the Zimm equation [221], the “90° MALS detector signal height” of the second separation step was used for semi-quantitative data evaluation of the concentrated samples.

3.4 Results

3.4.1 Polymer and micelles characterization

The CAC of the tested block copolymers was studied due to its association with micellar thermodynamic stability. The CAC values of the polymeric micelles ranged from 0.41 to 5.71 mg/L (Fig. 3.1), which is considerably low compared to Tween 80[®] micelles (11.16 mg/L) and indicates a high stability upon dilution of block copolymer micelles.

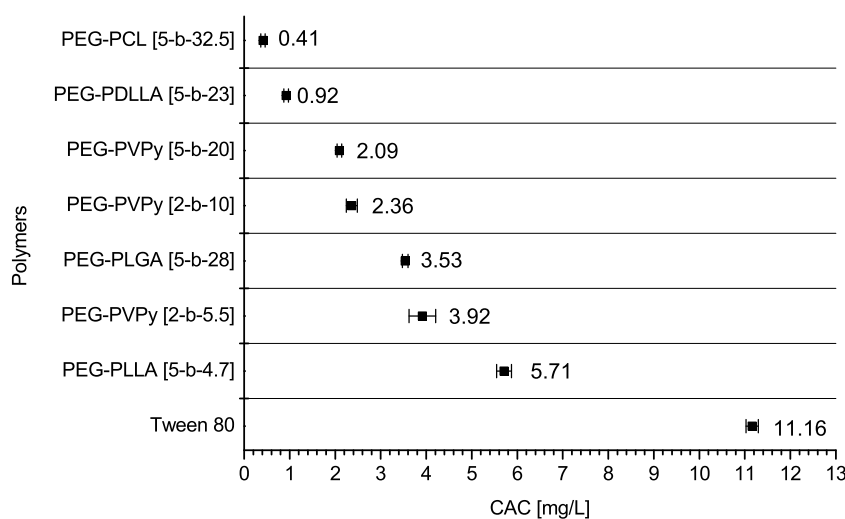


Figure 3.1: CAC values of the investigated polymers determined by the pyrene method. Results are presented as mean \pm SD ($n=3$).

To validate the accuracy of the method used in this study, the CAC value for Tween 80[®] was compared with literature data which determined the CAC value by other methods. A good correlation was observed (e.g., surface tension measurement: 15.7 mg/L [222]). Furthermore, from the CAC data of the different PEG-PVPy micelles, it was obvious that an

increasing hydrophobic block length leads to a lower CAC, in agreement with published data [223]. Comparing CAC values of micelles based on copolymers with similar hydrophobic to hydrophilic ratios, a decrease of CAC from PEG-PLGA to PEG-PVPy and PEG-PDLLA was observed. The architecture of the micellar core, which can be either crystalline or amorphous, plays an important role in the stability of polymeric micelles [223]. Therefore, the thermal properties of the dry polymers were investigated as received (Table 3.1).

 Table 3.1: Physical state of used block copolymers (mean \pm SD (n=3)).

Polymer type	Amorphous	Crystalline	T _g [°C]	T _m [°C]
PEG-PLLA [5-b-4.7]	-	X	-	46.23 \pm 0.24
PEG-PDLLA [5-b-23]	X	-	5.07 \pm 0.13	-
PEG-PLGA [5-b-28]	X	-	6.19 \pm 0.57	-
PEG-PCL [5-b-32.5]	-	X	-	55.84 \pm 1.05
PEG-PVPy [2-b-5.5]	X	-	101.83 \pm 4.58	-
PEG-PVPy [2-b-10]	X	-	109.19 \pm 2.54	-
PEG-PVPy [5-b-20]	X	-	136.36 \pm 1.36	-

Differential scanning calorimetry revealed that PEG-PLLA [5-b-4.7] and PEG-PCL [5-b-32.5] showed crystalline characteristics with melting points above room temperature, whereas for the other investigated polymers glass transition temperatures that are typical for amorphous materials were detected in their thermograms. The glass transition temperatures of PEG-PDLLA [5-b-23] and PEG-PLGA [5-b-28] were below room temperature. In contrast, the investigated PEG-PVPy showed glass transition temperatures above 100°C. It is worth mentioning that the presence of water, encapsulated compounds, or residual solvents can act as plasticizers and greatly affect the nature of the hydrophobic core, changing it from crystalline to amorphous and/or reducing its glass transition temperature. Micellar morphology and diameter were investigated by transmission electron microscopy (TEM) and dynamic light scattering (DLS). Results are summarized in Table 3.2.

DLS revealed that Tween 80[®] forms the smallest micelles with a hydrodynamic diameter of about 10 nm followed by the PEG-PVPy micelles ranging in size from \sim 28 nm to \sim 31 nm. The micelles of PEG-PLA derivatives, PEG-PLLA and PEG-PDLLA were \sim 49 nm and \sim 45 nm in diameter, respectively. PEG-PCL and PEG-PLGA form larger micelles with a diameter of around 80 nm. This trend in size can also be found in the TEM micrographs. They revealed nanosized particles of spherical shape independent of the copolymers used (Fig. 3.2).

The mean particle diameter observed by TEM is either smaller than or equal to the hydrodynamic diameter measured by DLS. Both PEG-PDLLA [5-b-23] and all PEG-PVPy-based micelles showed narrow and homogeneous particle size distribution in TEM micrographs, although the PDI in DLS was relatively high. On the other hand, a wider size distribution

Table 3.2: Particle Sizes and Size Distributions of Polymeric Micelles Resulting from TEM and DLS (Mean \pm SD).

Polymer	TEM size [nm]	DLS size [nm]	DLS PdI
Tween 80 [®]	n.p. ^a	10 \pm 0	0.09 \pm 0.02
PEG-PLLA [5-b-4.7]	17 \pm 6	49 \pm 7	0.26 \pm 0.01
PEG-PDLLA [5-b-23]	23 \pm 4	45 \pm 4	0.12 \pm 0.03
PEG-PLGA [5-b-28]	32 \pm 10	83 \pm 4	0.14 \pm 0.03
PEG-PCL [5-b-32.5]	38 \pm 7	82 \pm 5	0.06 \pm 0.03
PEG-PVPy [2-b-5.5]	19 \pm 4	30 \pm 3	0.10 \pm 0.05
PEG-PVPy [2-b-10]	24 \pm 4	31 \pm 2	0.18 \pm 0.01
PEG-PVPy [5-b-20]	24 \pm 5	28 \pm 1	0.17 \pm 0.01

^a not possible with the used experimental setup: for a Cryo-TEM micrograph of Tween 80[®] micelles please refer to Sagalowicz et al. [224]

was obvious for PEG-PLGA [5-b-28]- and PEG-PCL [5-b-32.5]-based micelles in the TEM micrographs. Taking the negative staining sample preparation technique into consideration, the single particles showed a bright grey micellar core surrounded by a shell-forming corona visible as dark shadows. This observation confirms the well-established core-shell model for polymeric micelles and had been shown also in TEM micrographs for drug-loaded micelles by Wang et al. [225]. The TEM micrographs of TritonX-100 and PEG-PLLA [5-b-4.7] were recorded to document the dissolution of the micelles by this detergent. The micrograph of TritonX-100 alone did not show any visible particles. Particle diameter obtained from DLS for TritonX-100 micelles are below 10 nm (data not shown). Incubation and preparation of PEG-PLLA and TritonX-100 show large particles in the micrograph without the typical core-shell structure. The contrasting agent was able to diffuse inside this larger particle and indicated the principle of micellar disintegration.

3.4.2 FRET stability assay

In this study, FRET as a direct marker of micellar integrity was used. Energy transfer from the fluorescence dyes DiO (emission maximum: 505 nm) to DiI (emission maximum: 575 nm) without light emission of DiO appears only when the distance between both molecules is in the lower nanometer range. Due to overlapping DiO emission and DiI excitation spectra, the DiI emission can be only observed after exciting DiO. This is the case in the micellar core. Results and basic principle of this FRET assay are outlined in Fig. 3.3 for Tween 80[®] micelles. The final data evaluation process is presented in Fig. 3.4. All investigated polymeric micelles were analyzed accordingly, and the resulting data are summarized in Table 3.3 and Fig. 3.5.

The calculation of a half-life after incubation in human serum was possible for Tween 80[®],

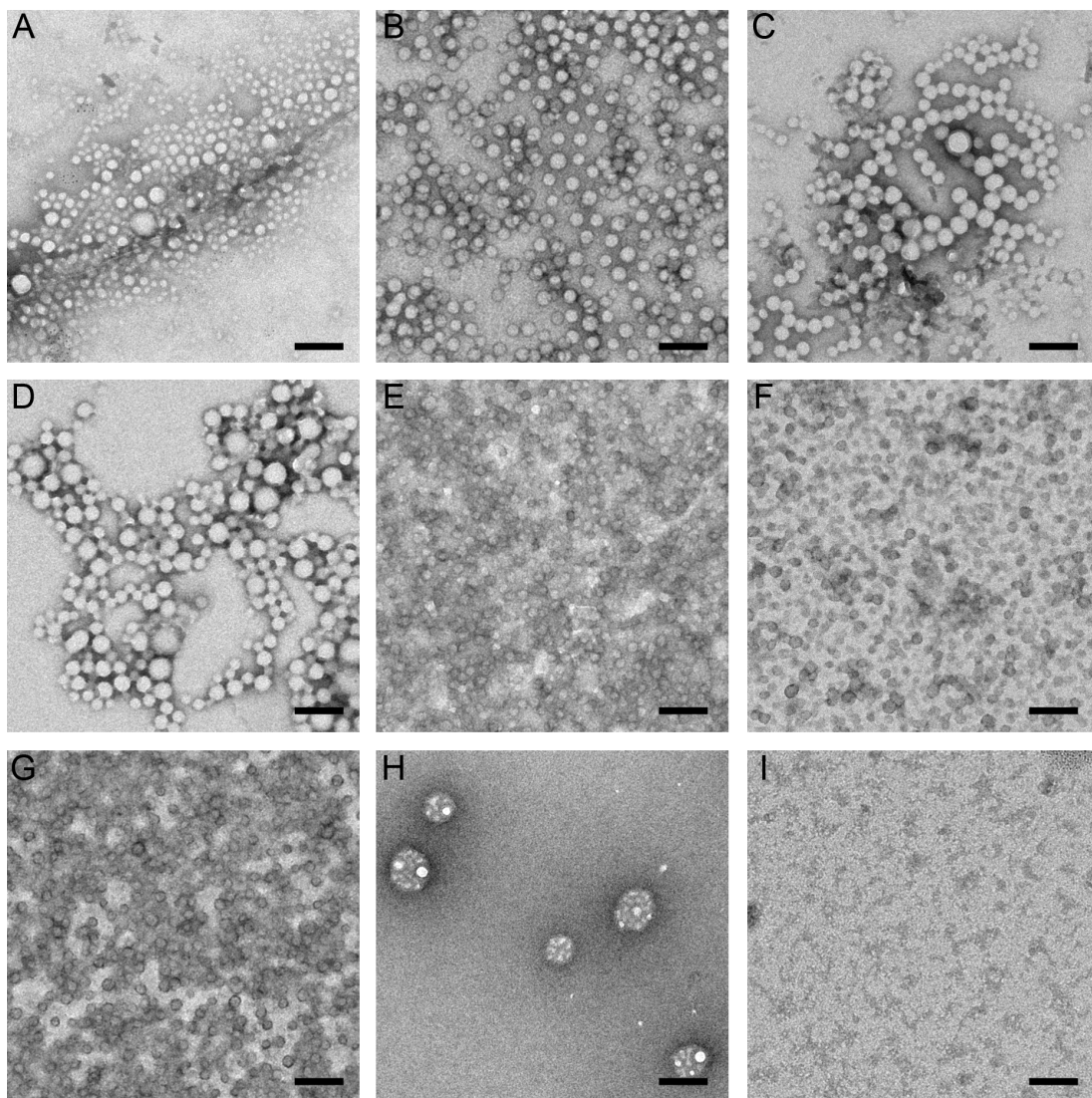


Figure 3.2: TEM micrographs of block copolymer micelles, negatively stained using uranyl acetate (PEG-PDLLA) or phosphor tungstate (all other samples). Scale bar represents 100 nm. (A) PEG-PLLA [5-b-4.7]; (B) PEG-PDLLA [5-b-23]; (C) PEG-PLGA [5-b-28]; (D) PEG-PCL [5-b-32.5]; (E) PEG-PVPy [2-b-5.5]; (F) PEG-PVPy [2-b-10]; (G) PEG-PVPy [5-b-20]; (H) PEG-PLLA [5-b-4.7] incubated with TritonX-100 for 20 min at 37°C; (I) TritonX-100.

PEG-PLGA, and all PEG-PVPy micelles, whereas for the other investigated polymers the calculated RMF values did not fall below 50%. All micellar disassemblies followed a first-order kinetic profile, with a good correlation observed ($R^2 > 0.90$). The PEG-PVPy micelles showed an increase in half-life with increasing molar masses of the hydrophobic part. The longest half-life which could be achieved with PEGPVPy [5-b-20] was similar to Tween 80[®] micelles. In contrast PEG-PLGA formed more stable micelles and exhibited a half-life in

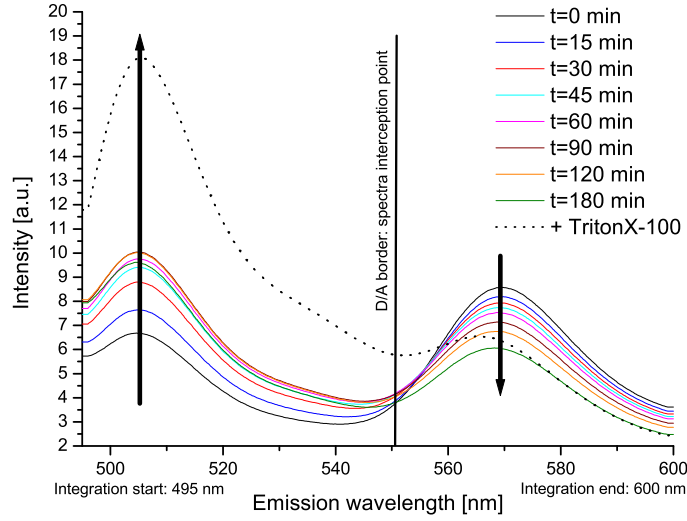


Figure 3.3: Fluorescence spectra overlay for DiI/DiO-loaded Tween 80[®] micelles in human serum. The maximum at 570 nm emission wavelength originally comes from the acceptor DiI, the one at 505 nm from the donor DiO. The decreasing acceptor and increasing donor maximum indicate the micellar disassembly during sample incubation. After 3 h incubation time TritonX-100 was added. This destroys the micelles and leads to a complete dye release.

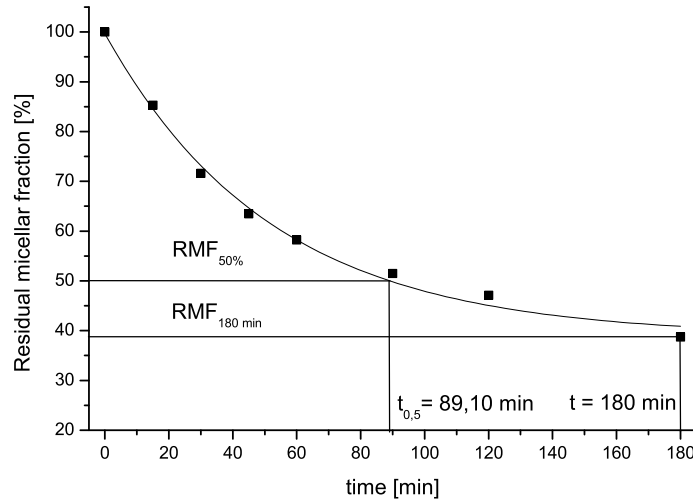


Figure 3.4: RMF at different incubation times of Tween 80[®] micelles. Tween 80[®] micelles show a first-order disassembly kinetic. To compare varying block copolymers from the resulting graphs, the serum half-life ($t_{0.5}$) and the $\text{RMF}_{180 \text{ min}}$ were evaluated.

Table 3.3: Stability of different block copolymers in human serum. All samples follow first-order kinetics.

Polymer	Quality of curve fitting (R^2)	$t_{0.5}$ [h]	RMF _{180 min} [%] (Mean \pm SD)
Tween 80 [®]	0.9924	1.48	38.73 \pm 10.37
PEG-PLLA [5-b-4.7]	0.9886	$>>26^a$	98.38 \pm 1.00
PEG-PDLLA [5-b-23]	0.9901	$>>26^a$	91.60 \pm 1.28
PEG-PLGA [5-b-28]	0.9850	25.07	66.83 \pm 1.23
PEG-PCL [5-b-32.5]	0.9946	$>>26^a$	85.27 \pm 1.24
PEG-PVPy [2-b-5.5]	0.9923	0.68	23.27 \pm 10.37
PEG-PVPy [2-b-10]	0.9389	0.92	34.19 \pm 2.57
PEG-PVPy [5-b-20]	0.9659	1.72	44.19 \pm 4.26

^a These micellar types exhibit very high serum stability in the assay; consequently, serum half-life was not calculated due to necessary extrapolation of the existing data.

this assay larger than 24 h. The more stable micelles are characterized by the RMF values above 50%. PEG-PCL, PEG-PDLLA, and PEG-PLLA micelles were the most stable ones investigated in this study. Moreover, the best stability in human serum was detected using PEG-PLLA-formed micelles showing nearly no influence of serum proteins on stability. Fig. 3.5 further illustrates that the investigated DiI/DiO-loaded polymeric micelles were stable upon dilution in water above CAC over a time period of 180 min at 37°C.

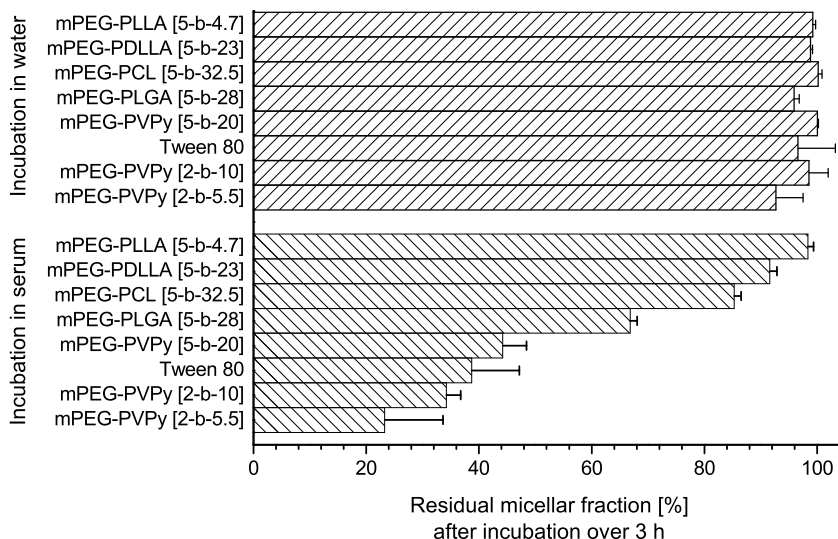


Figure 3.5: Residual micellar fraction [%] of the investigated polymers determined by the FRET method in human serum compared to water. Results are presented as mean \pm SD ($n=3$).

3.4.3 Asymmetrical Flow Field Flow Fractionation (AF4)

AF4 measurements were performed as a reference method to confirm micellar disassembly in the presence of human serum. Fig. 3.6 illustrates the results of the AF4 experiments. First, the behavior of the dye-loaded PEG-PVPy [5-b-20] micelles and human serum under the selected separation conditions was analyzed (Fig. 3.6a). The chromatogram of PEG-PVPy micelles showed a main peak ranging between 24 min to 31 min retention time. A sharp signal observed from the polymeric micelles indicated their high stability upon dilution in AF4 experiments. Although serum and micellar signals are overlapping, Fig. 3.6A shows the detection of micelles in the presence of serum was possible due to slightly different hydrodynamic radii of serum proteins and micelles. Therefore, micelles and serum were mixed and investigated simultaneously in a second experiment (Fig. 3.6B). As shown in Fig. 6a by single micelles and serum fractograms, the micelles are detectable in the mixture at retention time between 28 min and 33 min. This fraction was collected and separated again to improve resolution. Finally, polymeric micelles were incubated in human serum at 37°C, and samples were analyzed at different time periods as described above (Fig. 3.6C). Table 3.4 summarizes the changes in particle sizes of each process step.

Table 3.4: PEG-PVPy [5-b-20] micelles diameter determined by MALS detector signal after incubation in human serum at different time points.

Sample	Sample status	Particle diameter [d_{50} nm]
Micelles (pure)	Not processed	21.8
Micelles and serum t=0 min	Untreated	50.5
Micelles and serum t=90 min	Untreated	182.9
Micelles and serum t=180 min	Untreated	183.8
Micelles and serum t=270 min	Untreated	166.1
Micelles and serum t=1440 min	Untreated	34.6

Pure micelles showed particle diameters of ~ 22 nm, whereas immediately after addition of human serum the particle size increased to ~ 50 nm. During incubation, the particle diameters of the untreated sample increased continuously after 180 min incubation time to ~ 184 nm and declined to ~ 35 nm after 24 h. The particle size of the concentrated samples showed a different trend. During the second separation, the d_{50} -size parameter scatters around $22 \text{ nm} \pm 1.5 \text{ nm}$. This enabled the evaluation of the MALS detector peak height to correlate it with the particle concentration. In Fig. 3.6D, 90° MALS detector signal height is shown for the concentrated samples over time. Its decrease followed a first-order kinetics, which was also observed in the FRET experiments.

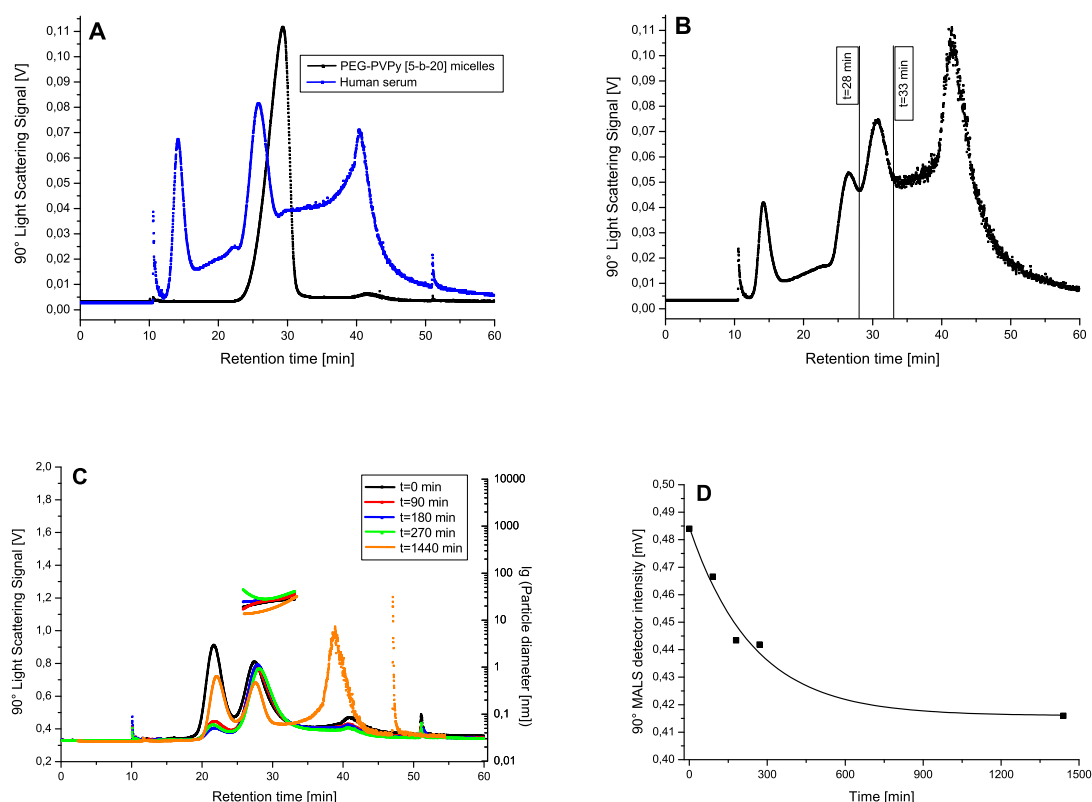


Figure 3.6: **A.** Overlay of light scattering detector trace of dye-loaded micelles and human serum, **B.** dye-loaded micelles mixed with human serum, **C.** concentrated samples of dye-loaded micelles in human serum over time, **D.** intensity decay of light scattering detector signal height over sample incubation time, baseline corrected.

3.5 Discussion

In this study, different block copolymers were investigated for their applicability as a micellar drug delivery system. For its clinical development, it is of high interest to understand the fate of polymeric micelles after intravenous application [174]. This issue is also highlighted by the regulatory authorities, as seen in the current guideline draft released by the EMA in the field of micellar formulations [226]. Block copolymers were composed of different chain lengths of polyethylene glycol as the hydrophilic part and varying hydrophobic parts with different molar masses. Physicochemical characterization revealed that all polymers were able to form nanosized micelles of spherical shape. The results show that particle size obtained from TEM often is much smaller compared to the results from DLS. One explanation for this observation could be the airdrying step involved in TEM sample preparation. The most probable reason is the different measurement principle of DLS and TEM. DLS delivers an intensity weighed

size distribution of hydrodynamic radii based on the Rayleigh approximation (scattering intensity $\sim d^6$), which finally overestimates the presence of larger micelles. Considering this factor, the large discrepancy between the results of both techniques is not unexpected. The recorded TEM micrograph indicated that the addition of TritonX-100 to copolymer micelles led to a fusion of micelles. This goes along with FRET dye release obtained by fluorescence spectroscopy. The lysis of the nanoparticles was responsible for the decrease of the FRET ratio after TritonX-100 incubation. Similar disintegration effects of lipid membranes by detergent interaction have been described previously by Ahyayauch et al. [227]. Consequently, this enabled the investigation of the stability of different polymeric micelles in human serum. Dual dye-loaded polymeric micelles were analyzed with a FRET-based technique. After fluorescence spectra integration and FRET ratio calculation, the two serum stability parameters residual micellar fractions (RMF) and serum half-lives were determined. Both parameters revealed highly relevant properties concerning stability. In the FRET assay, PEG-PLLA [5-b-4.7], PEG-PDLLA [5-b-23], PEG-PLGA [5-b-28], and PEG-PCL [5-b-32.5] micelles exhibited an extended half-life longer than 24 h, whereas Tween 80[®] and PEG-PVPy micelles were more labile, with half-lives below 2 h. Fast disassembly of Tween 80[®] micelles was expected (FRET assay half-life ~ 1.5 h). This non-ionic surfactant was chosen as an ideal reference polymer to compare with the results from the block copolymers due to known very low *in vivo* stability. For instance, Lasseter et al. performed a tolerability and bioequivalency study of fosaprepitant compared to aprepitant, where the prodrug fosaprepitant was encapsulated in Tween 80[®] micelles and applied to healthy subjects [228]. The pharmacokinetic data revealed that after injection the prodrug was completely metabolized to the active drug by ester hydrolysis in less than 45 min, indicating a full micellar destruction and drug release from the Tween 80[®] micelles. Thus, a comparison between Tween 80[®] and the block copolymer micelles in the developed *in vitro* assay was highly interesting and helps to better interpret the obtained stability parameters. Comparing the stability based upon dilution values of the polymers with the serum values, it is obvious that micellar disassembly did not result from simple dilution phenomena as long as the final concentration is above the CAC. A major change in FRET ratio was not detectable after dilution of the samples in water still above CAC (Fig. 3.5). However, in this study it was furthermore investigated which physicochemical properties of these micelle-forming block copolymers were strongly linked with micellar stability: hydrophilic/hydrophobic ratio [229], particle sizes and particle size distributions [229], critical association concentration (CAC) [223], and thermal status of the block copolymers [230, 46]. Riley et al. reported for PEG-PLA micelles a dependence of serum stability on particle size and hydrophilic/hydrophobic ratio [229]. While keeping a constant block length of the PEG part (5 kDa), an increase of hydrophobic block length led to larger micellar cores and finally larger particles. Consequently, the PEG shell had only a minor influence on the properties of micelles and can lead to incomplete coverage

and protection of the core from environmental milieu (as postulated for PLA blocks larger than 30 kDa). According to Riley et al., this partially leads to the presence of PLA carboxyl groups on the surface and confers the particles a surface charge, as indicated by zeta potential measurements. Proteins could thus adsorb onto the less PEG-protected surface. Colloidal stability was investigated by addition of the nanoparticles to different amounts of Na_2SO_4 solution and the determination of the critical flocculation points (CFPT). Interestingly, copolymers with high molar mass PLA blocks (30 kDa and more) exhibited a lower CFPT before protein incubation and similar CFPTs after protein incubation compared to lower molar mass PLA blocks (<30 kDa). Riley et al.'s study revealed that incomplete PEG surface coverage did not lead to lower colloidal stability when designing micelles with larger PLA blocks [229]. This postulated mechanism could be one explanation for the high stability of PEG-PDLLA [5-b-4.7] and PEG-PLLA [5-b-23] micelles, whereas thermodynamic and kinetic approaches could not fully explain the high stability of PLA-based micelles. The FRET assay showed that PEG-PLLA [5-b-4.7] with a molar mass of around 10 kDa and a hydrophobic/hydrophilic ratio of nearly 1:1 exhibited much higher stability than PEG-PVPy [5-b-20] with a molar mass of 25 kDa and a ratio 1:5. The same result was found with PEG-PLGA [5-b-28] (lower stability) and PEG-PLLA [5-b-23] (higher stability). Consequently, the total molar masses and hydrophilic/hydrophobic ratios do not have a direct impact on micelle serum stability when comparing different block copolymers. In contrast, it was shown for the PEG-PVPy micelles with different PEG and vinylpyridine amounts in the molecule that an increasing hydrophobic part also increased the serum stability. Although PEG-PVPy [2-b-10] had a higher hydrophobic/hydrophilic ratio than PEG-PVPy [5-b-20], the latter was more stable, indicating that the size of the hydrophobic part is more decisive in determining the serum stability than the size of the PEG part. The same conclusion was drawn by Toncheva et al. when investigating the stability of PEG-polyorthoester ABA triblock polymers against bovine serum albumin [231]. Thermodynamic stability of polymeric micelles is directly connected with the CAC. Data of CAC determination for the tested polymers showed that PEG-PCL (CAC~0.41 mg/L) micelles had the lowest aggregation onset, whereas PEG-PLLA (CAC~5.71 mg/L) micelles showed the highest CAC in this study. In contrast to the block copolymers, Tween 80[®], as a non-ionic surfactant, had an aggregation onset at a much higher concentration (11.16 mg/L). Therefore, one would expect PEG-PCL micelles to be most stable, and PEG-PLLA micelles would be associated with lowest stability from a thermodynamic point of view. The crystalline and/or amorphous nature of the dry polymer seems to have no connection with its *in vitro* serum stability. For instance, the thermograms of PEG-PLLA [5-b-4.7] (T_m ~46°C) and PEG-PCL [5-b-32.5] (T_m ~56°C) show melting events, while PEG-PLGA [5-b-28] (T_g ~6°C), PEG-PDLLA [5-b-23] (T_g ~5°C), and PEG-PVPy (T_g ~102–136°C) are amorphous. If the hydrophobic core of the micelles was crystalline or frozen due to a high T_g , analogous to the dry polymer, then one

would expect PEG-PVPy to be more stable than the “softer” polylactide copolymers, which was not the case in this study. The effect of micellar stabilities cannot be fully explained by the thermal properties, as is also shown by Jacquin et al. [230]. This is because the presence of water or encapsulated material can act as plasticizer or crystallization inhibitor, thus changing the state of the hydrophobic micellar core compared to the dry polymer. Finally, it was to clarify if the observed time-dependent changes in FRET effects are exclusively due to micellar disassembly in the presence of serum. There is still a possibility that the fluorescent dyes redistribute from the micellar core towards serum proteins. AF4 measurements were used to substantiate the FRET results and exclude the latter possibility. For this experiment, PEG-PVPy [5-b-20] micelles were selected due to their intermediate stability in serum as determined by FRET measurements. The fact that during the elution of the pure micelles no peaks for the polymer appeared in the fractogram (before the micellar peak) shows that the micelles remained intact under the high dilution processes in the AF4 experiments. While incubating the micelles with serum over time, a method for semiquantitative data analysis was identified involving the evaluation of signal height of light scattering. This light scattering intensity decreases over time in a first-order decay, showing similar kinetics to those found for the FRET experiments (Fig. 3.6D). It is highly probable that the effects seen in the FRET experiments were caused by micellar disassembly. Interestingly, the protein adsorption on the micellar shell can be followed via the particle diameter, which increased from the initial particle size of ~ 51 nm to 184 nm after 180 min incubation time and subsequently decreased down to ~ 35 nm after 24 h. FRET experiments confirmed that only minor changes in micellar concentrations can be expected after 120 min due to the observed first-order kinetics (Fig. 3.4). Saturation of micelles with serum proteins is highly probable. AF4 experiments further revealed that there are residual micelles with comparable size to freshly prepared ones still present after 24 h incubation time. Based on this observation, high adsorption of proteins on the micellar surface most likely occurred during the first few hours. However, when the stability influencing protein fraction is saturated with polymer monomers, the reaction rate slows down to a first-order kinetic. Additional data will be needed to confirm this hypothesis. In summary, it was shown that all investigated block copolymer micelles exhibited relatively high thermodynamical stability against dilution, whereas the serum stability differed extremely between the different polymers.

3.6 Conclusion

By using an improved FRET-based assay, it was possible to discriminate between different block copolymers quantitatively in terms of *in vitro* serum stability. PEG-PVPy showed very low serum stability compared to the PEG-PLGA, PEG-PLA, and PEG-PCL. Within the same homologous series, the length of the hydrophobic chain was more decisive regarding

the serum stability than the hydrophobic/hydrophilic ratio or the length of the PEG chain. Additionally, the crystalline/amorphous state of the hydrophobic chain in the dry polymer could not predict the serum stability of the polymeric micelles. AF4 experiments are one approach to confirm that a decrease in FRET ratio is due to micellar disassembly. Although further relevance of these studies has to be carefully investigated in *in vivo* experiments, the presented techniques and results offer the possibility to screen novel polymers in terms of *in vitro* stability.

Chapter 4

In vitro cytotoxicity and interactions with the immune system

4.1 Abstract

In vitro biocompatibility and potential immunological reactions upon application were investigated prior to performing *in vivo* experiments for safety and ethic reasons. Different test polymers of PEGylated poly-(lactic acid) (PEG-PLA), PEGylated poly-(lactic acid-co glycolic acid) (PEG-PLGA), PEGylated poly-(ϵ -caprolactone) (PEG-PCL) and PEGylated poly-4-(vinylpyridine) (PEG-PVPy) were investigated on their potential biological effects. Several benchmark materials which are approved for use in humans were compared to the test materials aiming on the delivery of information concerning toxic effects. These benchmark materials comprise of Tween 80[®] and Cremophor EL[®] for the cytotoxicity studies and Doxil[®] for the complement activation studies. Furthermore, branched PEI [25 kDa] and PEG-PEI 0.1/0.1 which was synthesized from PEI [25 kDa] served as positive controls in the cytotoxicity assays. PEI [25 kDa] and Zymosan were positive controls for complement activation assays. Investigations were carried out in two different setups: 1) cytotoxicity experiments on HepG2 cells (staining and hand-counting) and on primary rat hepatocytes (ATP test readout) as well as 2) elucidation of complement activation (ELISA based). As a result of these studies it was found that the test materials PEG-PVPy was less cytotoxic compared to Tween 80[®] and Cremophor EL[®]. Distinct toxic effects could be detected from metabolically active rat hepatocytes. The other PEGylated block copolymer micelles exhibited no toxicity on these assays. Moreover, Doxil[®] showed stronger complement activation compared to most of the investigated test polymers. Consequently the selected polymeric micelles were not expected to exhibit strong cytotoxic effects and immunological responses *in vivo*.

4.2 Introduction

The biological responses upon injection of nanoparticles can be assessed with various *in vitro* test assays prior to *in vivo* experiments. Such a strategy contributes, therefore, as a major part to drug safety. Although assays for the investigation of drugs' cytotoxicity were standard industrial procedures [232, 233], the relevance for nanoparticles was not well investigated yet. In this connection cytotoxicity can be either of acute [234] or metabolic type [235]: acute toxicity leads to immediate cell death due to high specimen concentrations whereas metabolic toxicity occurs after processing of the specimen by metabolizing cells also in subacute toxic concentrations. Consequently investigation of those cytotoxic effects is very important to ensure safety for further *in vivo* experiments. For this purpose the HepG2 cell line and primary rat hepatocytes were selected as suitable reporter cells for detecting cytotoxicity of the nanoparticles. For the investigation of multiple dosing cytotoxicity, the HepG2 cell line is an established reporter cell line [234]. Both liver cell species are expected to have a comparably high exposure of the micelles *in vivo* due to the strong phagocytotic activity of the reticulo-endothelial system in this organ. The HepG2 cells were derived from human hepatoblastoma and possess only minor metabolic activity for xenobiotics [234]. In contrast to this the primary rat hepatocytes exhibit full metabolic activity [235]. The non-ionic surfactants Cremophor EL[®] and Tween 80[®] were selected for reference purposes. Both excipients have FDA approval for intravenous injectable products and are highly interesting for benchmarking. Interestingly, Cremophor EL[®] for example is approved for iv infusion with an impressively high concentration of 52.75% w/v in Taxol[®].

Apart from toxicity on cells, immunological reactions upon nanoparticle injection could be severe and lead to death of the patient within minutes. Those rapid reactions are mainly caused by responses of the complement system and are called CARPA (C-activation related pseudoallergy) in literature [97, 99, 96, 25]. This allergic reaction is of non-IgE type and therefore called a pseudoallergy. It was well described that liposomal (e.g. Doxil[®]) and micellar encapsulated drugs (e.g. Taxol[®]) could lead to strong responses of the complement system [236]. The *in vitro* complement activation can be monitored by detection of varying complement scission products. For this purpose the readout was focused on: C3a, C5a and SC5b-9. These three scission products are representative for the complement cascade and can be detected by commercial ELISA test kits. Strong complement activation can be a hint for potential immunological reactions which could lead to CARPA upon injection. Therefore, it is essential to gather information about the test micelles in comparison to other approved products. As a reference product Doxil[®] was selected due to the known complement activation *in vitro* and *in vivo* [100, 99].

4.3 Materials and methods

4.3.1 Materials

The following block copolymers were purchased from Polymer Source Inc, Montreal, Canada: mPEG-PLLA [5-b-4.7], mPEG-PDLLA [5-b-23], mPEG-PCL [5-b-32.5], mPEG-Poly-(4-vinylpyridine) [mPEG-PVPy] [2-b-5.5], mPEG-PVPy [2-b-10] and mPEG-PVPy [5-b-20]. PEG-PLGA [5-b-28] (Resomer RGP d 50155) was obtained from Boehringer Ingelheim, Ingelheim, Germany. DMEM F12 buffer, DMEM F12 Glutamax[®] buffer, gentamicin solution (50 mg/mL) and sodium pyruvate solution (100 mM) were delivered by Invitrogen Inc., Darmstadt, Germany. HepG2 cell line was ordered from ATCC, Manassas, VA, USA. Human serum and branched PEI [25 kDa] were purchased from Sigma Aldrich, St. Louis, MO, USA. Penicillin-Streptomycin solution and ITS insulin solution were delivered by Sigma Aldrich, Rosdorf, Germany. mPEG succinimidylester [5 kDa] (mPEG-NHS) was purchased from NANOCS Inc., New York City, NY, USA. ELISA test kits for complement scission product detection were delivered by Quidel Corp., San Diego, CA, USA. Doxil[®] was delivered by Pharmarama Inc., Boston, MA, USA. Tween 80[®] and D₂O were obtained from VWR, Darmstadt, Germany, and Cremophor EL[®] was delivered by BASF, Ludwigshafen, Germany. Pall Acrodisc (GHP membrane) 0.2 µm filters were used for sterile filtration. Water was of MilliQ grade.

4.3.2 Methods

4.3.2.1 Synthesis of PEG-PEI as reference material

PEG-PEI was selected as a reference material for the cytotoxicity studies. For material synthesis the method of Hong et al. [237] was employed. In brief, branched PEI [25 kDa] was PEGylated using a mPEG-NHS ester. The synthetic procedure was described in Fig. 4.1. For this purpose different ratios of mPEG to PEI were selected: 1) 300 mmol PEI to 100 mmol mPEG and (PEG-PEI 0.3/0.1) 2) 100 mmol PEI to 100 mmol mPEG (PEG-PEI 0.1/0.1). Synthesis was carried out in PBS buffer pH 7.4. The appropriate reactants were dissolved in 5 mL PBS buffer each, unified and stirred over 24 h. Finally the micellar dispersion was dialyzed against 5 L water over 24 h for purification purposes. As last step the polymer was lyophilized at -35°C over 48 h to remove water. Polymer analytics was performed via ¹H-NMR spectroscopy in D₂O on a Bruker 400 MHz spectrometer.

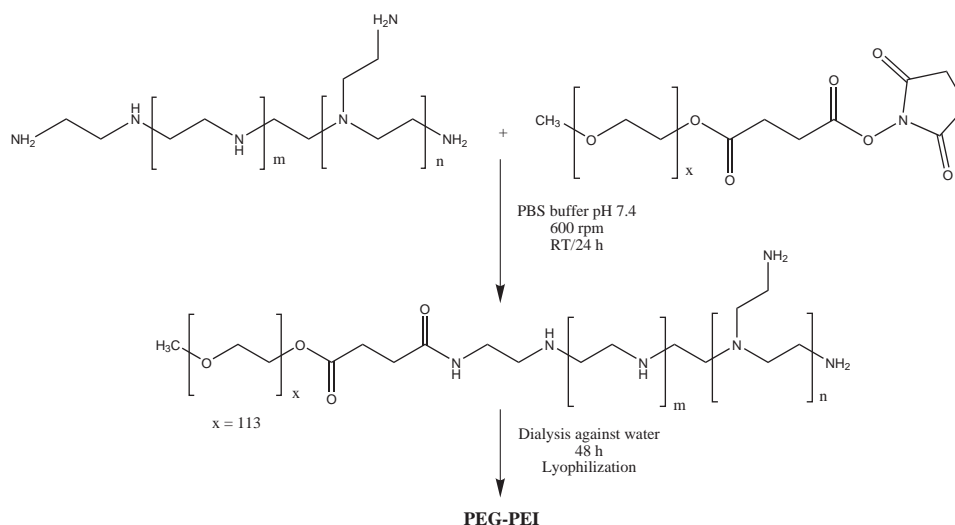


Figure 4.1: Preparation steps for PEG-PEI derivatives.

4.3.2.2 Micelle preparation

For cytotoxicity assays All preparation procedures were carried out under aseptic conditions using sterilized glass ware and equipment where possible. The micelles as well as each of the reference materials for these test assays were prepared in the appropriate cell line buffers for the final cell tests. For the HepG2 cell line DMEM F12[®] buffer was selected as dispersion medium, for the primary rat hepatocytes DMEM F12[®] Glutamax buffer was selected. However, for the micellar preparation a nanoprecipitation technique was employed. In brief, 50 mg polymer was dissolved in 2 mL acetone. This solution was injected into 5 mL of the aqueous buffer phases under constant stirring. The organic solvent was evaporated under normal atmosphere under continued stirring overnight. Finally all micellar dispersions were filtered through a 0.2 µm filter. The exactly resulting polymer concentrations were determined by gravimetry. Dilution with the appropriate buffers was carried out accordingly prior to cell incubation.

For complement activation assays Micelle preparation was performed employing the cosolvent evaporation method (section 2.3.2.1) which was previously developed. Differing from this procedure acetone instead of THF was used for the cosolvent preparation. Dialysis for further purification was performed against 2 L water over 24 h. The micellar dispersions were prepared with polymer concentrations at 10 mg/mL.

Selection and purposes of the investigated materials Table 4.1 summarized the investigated materials with the intended purposes in each study.

Table 4.1: Testing materials/particles in the cytotoxicity and complement assays.

Polymer / particle species	Cytotoxicity assay	Purposes	Complement assay	Purposes
mPEG-PDLLA [5-b-23]	X	Negative control (no cytotoxicity), approved in market products	X	Test micelles
mPEG-PLLA [5-b-4.7]	-	-	X	Test micelles
mPEG-PDLLA [5-b-23] mixture with H ₂ N-PEG-PDLLA [5-b-28]	-	-	X	Test micelles, increased surface charge due to amino-function at surface
mPEG-PLGA [5-b-28]	X	Negative control (no cytotoxicity), approved in market products	X	Test micelles
mPEG-PCL [5-b-32.5]	X	Negative control (no cytotoxicity), approved in market products	X	Test micelles
mPEG-PVPy [2-b-5.5]	X	Test material (unknown tox)	X	Test micelles
mPEG-PVPy [2-b-10]	X	Test material (unknown tox)	X	Test micelles
mPEG-PVPy [5-b-20]	X	Test material (unknown tox)	X	Test micelles
Tween 80 [®]	X	Reference material (approved up to 12.5% w/v for i.v. use by FDA)	-	-
Cremophor EL [®]	X	Reference material (approved up to 52.7% w/v for i.v. use in Taxol [®] by FDA) [238]	-	-
Doxil [®]	-	-	X	Reference particles (FDA approved drug), PEG-liposomes known to exhibit strong complement activation [97]
PEI [25 kDa]	X	Positive control (known high tox) [239]	X	Reference particles, expected high complement activation
mPEG-PEI 0.1/0.1	X	Positive control (known high tox, expected lower compared to PEI)	-	-
Zymosan	-	-	X	Reference standard, yeast enzyme which complement cleaving properties

4.3.2.3 Particle size measurements

The dynamic light scattering (DLS) technique was used to investigate the micellar average diameter. For the measurements, a Zetasizer Nano ZS90 from Malvern, Worcestershire, UK, was set to 173° backscattering mode. The mean size and polydispersity index (PDI) were calculated by cumulants analysis using ZetasizerNano[®] software. The samples were measured in cell culture buffer for the cytotoxicity experiments and in water for the complement activation studies.

4.3.2.4 Cell incubation experiments

Primary rat hepatocytes Rat hepatocytes were taken from male Wistar rats, Charles River Corp., Wilmington, MA, USA. Upon resection of the liver, the cells were seeded into 96 well plates which were previously treated as follows: Type I collagen from rat tail fibers (lyophilizate from Roche Diagnostics Inc., Mannheim, Germany) was dissolved in 0.2% acetic acid to a final collagen concentration of 110 $\mu\text{g}/\text{mL}$. This solution was transferred into each well resulting in a target concentration of 20 $\mu\text{g}/\text{mL}$. Finally the well plate was dried over 48 h prior to seeding the cells.

Approximately 3.5×10^4 cells/well were seeded into the plate and cultivated in a mixture of DMEM/F12 Glutamax[®] buffer with streptomycin (100 $\mu\text{g}/\text{mL}$), penicillin (100 IU/mL), sodium pyruvate (0.5 mM), dexamethasone (100 $\mu\text{g}/\text{mL}$), ITS Insulin (110 $\mu\text{g}/\text{mL}$) as additives. Prior to incubation with the micelles the buffer supernatant was removed and the previously diluted and in buffer formulated micelles were incubated with the cells over 24 h. After incubation the cells were washed three times with buffer and non-vital cells were stained with trypanblue. A representative number of cells was counted in a Fuchs-Rosenthal chamber.

HepG2 cell lines For this experiment the cells were cultivated in a DMEM/F12[®] buffer with streptomycin (100 $\mu\text{g}/\text{mL}$), penicillin (100 IU/mL), sodium pyruvate (0.5 mM), gentamycin (50 $\mu\text{g}/\text{mL}$) as additives. 2×10^4 cells/well were seeded into a 96 well plate 24 h prior to addition of the micelles. The buffer supernatant was removed and the previously diluted and in buffer formulated micelles were incubated with the cells over 24 h. After incubation the cells were washed three times with buffer and detection of vital and non-vital cells was carried out by using an ATP assay (CellTiter-Glo[®] Luminiscent, Promega, Madison, WI, USA).

4.3.2.5 Determination of complement scission products upon serum incubation

Incubation of the micellar dispersions was carried out in human serum. For this purpose, 250 μ L micellar dispersion (10 mg/mL) or MilliQ water and 250 μ L human serum were mixed and incubated at 37°C over 2 h. Zymosan, PEI [25 kDa] and Doxil[®] served as reference materials. A Zymosan solution was prepared at 5 mg/mL (according to Szebeni et al. [99]), whereas PEI [25 kDa] and Doxil[®] concentrations were set to 10 mg/mL polymer and lipid content, respectively. Upon serum incubation the mixtures were immediately centrifuged at 10.000 g for 10 min and the supernatant of these mixtures was taken for further analysis on complement activation.

According to the ELISA test assay description provided by Quidel Corp. the samples were diluted as follows: 1:5000 (C3a), 1:250 (C5a) and 1:100 (SC5b-9). The test was performed according to the manufacturers protocol and finally detection of optical density was carried out at 450 nm. The complement activation of the micellar/liposomal species was referred to the baseline activation detected from water incubation with serum. Complement results are reported as the ratio between baseline and sample activation in percent. According to the ELISA specifications, a test result which scatters below 10% from this baseline activation was not considered to be significant. Each experiment was carried out with n=6.

4.4 Results

4.4.1 PEG-PEI synthesis

The resulting PEG-PEI polymers were investigated on composition and block lengths by ¹H-NMR spectroscopy. Figure 4.2 reports an example spectrum for PEG-PEI 0.1/0.1. Table 4.2 presents the polymer compositions obtained from ¹H-NMR spectroscopy. The low M_n -values (number average molar mass) for the PEG-PEI 0.3/0.1 species was not explainable from the experiments. Therefore, PEG-PEI 0.1/0.1 was selected for further experiments.

4.4.2 Particle size of test materials

All materials were successfully prepared and analyzed for particle sizes and size distributions. Table 4.3 summarized the results for the cell incubation and complement assays.

4.4.3 Cytotoxicity assay

The above described nanoparticles/polymers were assayed on HepG2 cells and primary rat hepatocytes. Evaluation of the recorded data delivered sigmoidal curves from which the

Table 4.2: PEG-PEI characteristics obtained from ^1H -NMR spectroscopy.

Polymer	Feed ratio n/n [mol/mol]	PEG in copolymer [%] w/w	Block ratio (PEG-chains per PEI chain)	M_n [kDa]
PEG-PEI 0.1/0.1	0.1:0.1	16.9	0.20	26.1 (PEG: 4.4, PEI: 21.6)
PEG-PEI 0.3/0.1	0.3:0.1	36.0	0.55	12.2 (PEG: 4.4, PEI: 7.8)

EC_{50} -values (effective concentration of analyte at which 50% of the cells were still viable) were calculated. Fig. 4.3 shows a representative curve for this purpose.

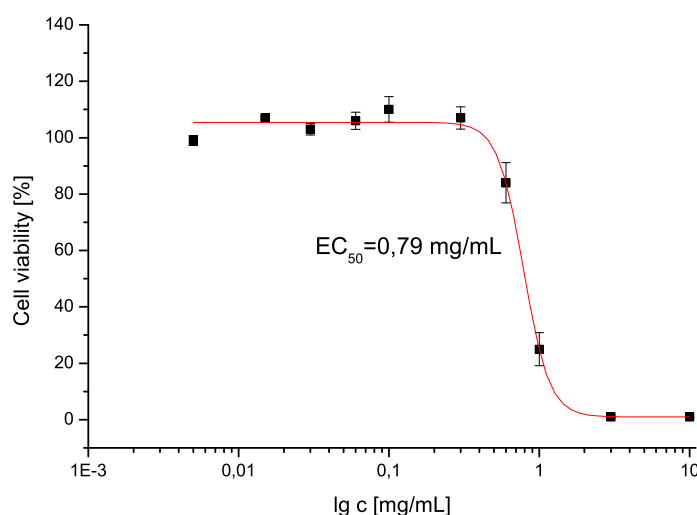


Figure 4.3: Cytotoxicity of Cremophor EL[®] micelles on HepG2 cells. Results were presented in percent cell viability. The curve was representative in shape for the results of the other investigated micelles/polymers.

Table 4.4 summarizes the EC_{50} -values on both cell types for all investigated micelles. Strong differences in cytotoxicity was found for the investigated micellar samples. As expected for the negative control mPEG-PDLLA no toxic events were found up to a concentration of 10 mg/mL on both cell types. The positive controls PEI [25 kDa] and PEG-PEI 0.1/0.1 showed severe cytotoxic effects with effective concentration in the lower $\mu\text{g}/\text{mL}$ ranges on both cell types. The test polymers from the PEG-PVPy series showed very low cytotoxic

Table 4.3: Particle sizes and size distributions for resulting dispersions.

Polymer/product	For cytotoxicity assays		For complement assays	
	d_h [nm] in DMEM F12 (mean \pm SD)	PdI in DMEM F12 (mean \pm SD)	d_h [nm] in water (mean \pm SD)	PdI in water (mean \pm SD)
mPEG-PDLLA [5-b-23]	48 \pm 2	0.144 \pm 0.010	66 \pm 2	0.084 \pm 0.011
mPEG-PLLA [5-b-4.7]	n.a.	n.a.	43 \pm 4	0.322 \pm 0.006
mPEG-PDLLA [5-b-23]				
mixture with H ₂ N-PEG-PDLLA [5-b-28]	n.a.	n.a.	85 \pm 1	0.162 \pm 0.021
mPEG-PLGA [5-b-28]	92 \pm 3	0.092 \pm 0.008	150 \pm 1	0.101 \pm 0.028
mPEG-PCL [5-b-32.5]	67 \pm 1	0.068 \pm 0.014	100 \pm 1	0.108 \pm 0.032
mPEG-PVPy [2-b-5.5]	34 \pm 1	0.101 \pm 0.005	24 \pm 1	0.119 \pm 0.016
mPEG-PVPy [2-b-10]	36 \pm 1	0.201 \pm 0.010	n.a.	n.a.
mPEG-PVPy [5-b-20]	44 \pm 1	0.105 \pm 0.001	42 \pm 1	0.052 \pm 0.005
Tween 80 [®]	10 \pm 0	0.098 \pm 0.010	n.a.	n.a.
Cremophor EL [®]	13 \pm 0	0.034 \pm 0.019	n.a.	n.a.
Doxil [®]	n.a.	n.a.	89 \pm 1	0.056 \pm 0.018
PEI [25 kDa]	11 \pm 0	0.295 \pm 0.008	8 \pm 1	0.297 \pm 0.050
mPEG-PEI 0.1/0.1	19 \pm 1	0.613 \pm 0.018	n.a.	n.a.

n.a.: not applicable; not all polymers were included into both studies, cytotoxicity and complement activation assay.

effects on HepG2 cells whereas distinct toxicities were found on the primary rat hepatocytes. Interestingly, the benchmark micelles composed of Tween 80[®] and Cremophor EL[®] showed comparably toxic effects to the PEG-PVPy samples.

Table 4.4: Summary of the EC₅₀-values for the investigated micelles/polymers. Each EC₅₀-value was determined in triplicate. From the resulting sigmoidal curves the EC₅₀-values were calculated where possible.

Micelle type/polymer	EC ₅₀ HepG2 [mg/mL]	EC ₅₀ rat hepatocytes [mg/mL]
mPEG-PDLLA [5-b-23]	>> 10	>> 10
PEI [25 kDa]	0.0099 ± 0.002	0.015 ± 0.002
PEG-PEI 0.1/0.1	0.0107 ± 0.003	0.028 ± 0.020
Tween 80 [®]	0.49 ± 0.060	1.16 ± 0.182
Cremophor EL [®]	0.79 ± 0.030	1.56 ± 0.087
PEG-PVPy [2-b-5.5]	> 10	1.15 ± 0.115
PEG-PVPy [2-b-10]	>> 10	4.20 ± 0.216
PEG-PVPy [5-b-20]	> 10	4.57 ± 0.404

4.4.4 Complement activation assays

The results delivered by the ELISA tests for the three investigated complement factors C3a, C5a and SC5b-9 are presented in Fig. 4.4. As shown, the selected positive control Zymosan (5 mg/mL) exhibited the strongest complement activation in all setups followed by PEI [25 kDa]. Doxil[®] resulted in comparable complement activation in the SC5b-9 assay and only a slight increase in the C3a compared to water. The test polymers showed lower activation of complement in all three assays compared to the reference materials. A negative value compared to water could result from complement adsorption onto the surfaces of the micelles. This effect was also considered in the graphs.

4.5 Discussion

Cytotoxicity and complement activation assays generally are valuable tools for the elucidation of drug/formulation risks prior to administration to living organisms. In this study cytotoxicity was investigated with two cell types: HepG2 cells and primary rat hepatocytes. Especially the rat hepatocytes with their metabolic activity were taken as important reporter cells for expected toxicity in later *in vivo* studies in rodents. However, the results reported in Table 4.4 revealed very differentiated properties of cytotoxicity for the test and reference polymers: mPEG-PDLLA [5-b-23] did not show any cytotoxic effects on both cell types as expected

for a negative control. The positive controls PEI [25 kDa] and PEG-PEI 0.1/0.1 showed severe cytotoxic effects at very low concentrations [$EC_{50} < 20 \mu\text{g/mL}$]. The expectation that PEGylation of PEI reduced the toxicity [237] was not strongly detectable. PEG-PEI exhibited only slightly lower EC_{50} values compared to PEI. Interestingly the benchmark polymers Tween 80[®] and Cremophor EL[®] showed distinct toxicity on both cell types as certain toxic effects were expected from literature: for Tween 80[®] direct toxic interactions with lipid bilayers were discussed [240] whereas for Cremophor EL[®] the formation of free radicals is assumed to be one potential mechanism of cytotoxicity [241]. It is remarkable that both polymers/surfactants received FDA approval although they are known to exhibit cytotoxic effects. Taking this background into consideration, the cytotoxicity of PEG-PVPy derivatives are to be evaluated. The results showed that a strong toxicity on HepG2 cells could not be detected ($EC_{50} > 10 \text{ mg/mL}$ for all specimen) whereas differential picture was shown on the metabolically active rat hepatocytes: All three polymer derivatives showed a distinct toxicity with EC_{50} values scattering between $\sim 1 \text{ mg/mL}$ and $\sim 5 \text{ mg/mL}$. This could be due to a potential metabolism of the polyvinylpyridine part of the PEG-PVPy: liver enzymes were known to form N-oxides from pyridine [242, 243]. Those N-oxides are reactive species and could induce cell death by forming of DNA adducts. These values were higher compared to Tween 80[®] and Cremophor EL[®] indicating lower cytotoxicity. Consequently strong toxic effects by the PEG-PVPy species were not expected in later animal experiments. However, if extensive, multiple dosing of this polymer would be planned it needs to be evaluated if mutagenic effects could occur from N-oxides formation [244]. The complement activation assay which was employed to assess potential impacts of nanomedicine on severe body side reactions was the complement activation assay. According to the suggestion of Szebeni et al. [99] three readouts C3a, C5a and SC5b-9 for complement activation were selected. Zymosan was suggested as a positive control by Szebeni et al. because this yeast enzyme was known to be a very strong complement activator. In contrast to this, PEI [25 kDa] served as a highly charged positive control. Both positive controls were expected to exhibit very strong complement activation in all three assays. Increase of complement referred to water was between $\sim 350\%$ to $\sim 1500\%$ for Zymosan and $\sim 150\%$ to $\sim 400\%$ for PEI [25 kDa], respectively. However, the reference product Doxil[®] showed its strongest complement activation in the SC5b-9 assay ($\sim 150\%$ referred to water). This was not unexpected because previous studies in humans with Doxil[®] revealed a strong activation in the SC5b-9 readout [100].

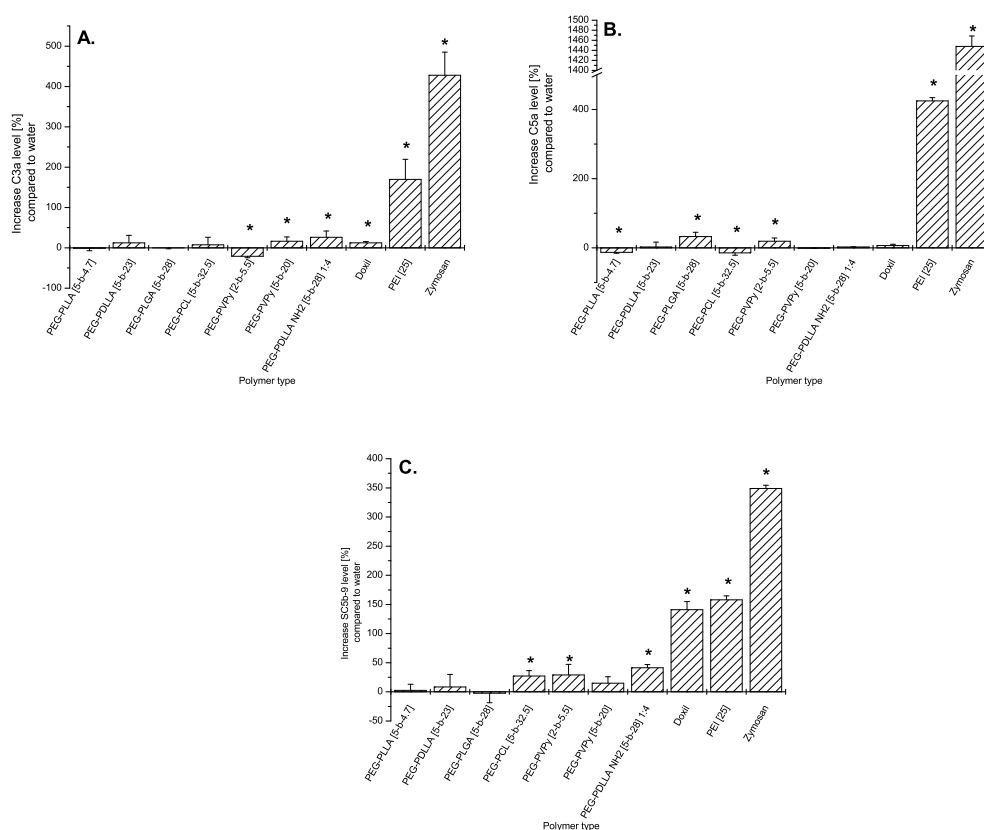


Figure 4.4: Results obtained from the complement activation assays: C3a readout (A), C5a readout (B) and SC5b-9 readout (C). Bars represent increase of complement factor level in percent compared to water baseline levels. Each experiment was carried out $n=6$ (mean \pm SD). The asterisk indicates which samples delivered significantly different results compared to water ($> 10\%$ differences according to manufacturer specifications).

Moreover, an activation $> 10\%$ referred to water was additionally found in the C3a assays, whereas for C5a there was nearly no activation detectable. As liposomal Doxil[®] is a FDA approved product, this complement activation should not be a problem for other low micellar products. A complement activation chart which evaluates the obtained data and puts them into connection was shown in Table 4.5.

Table 4.5: Evaluation of the complement activation results.

Specimen	C3a	C5a	SC5b-9	Evaluation/comment
mPEG-PLLA [5-b-4.7]	-	↓	-	Light C5a adsorption
mPEG-PDLLA [5-b-23]	-	↓	-	Light C5a adsorption
mPEG-PLGA [5-b-28]	-	↑↑	-	Stronger C5a activation
mPEG-PCL [5-b-32.5]	-	↓	↑↑	Stronger activation of SC5b-9, adsorption C5a
mPEG-PVPy [2-b-5.5]	↓	↑	↑↑	C5a and SC5b-9 activation, C3a adsorption
mPEG-PVPy [5-b-20]	-	↑	↑	C5a and SC5b-9 activation
mPEG-PDLLA [5-b-23] mixture with H ₂ N-PEG- PDLLA [5-b-28]	-	↑	↑	C5a and SC5b-9 activation
Doxil[®]	↑	-	↑↑	Light C3a activation, strong SC5b-9 activation
PEI [25 kDa]	↑↑↑	↑↑↑	↑↑↑	Positive control
Zymosan	↑↑↑↑	↑↑↑↑	↑↑↑	Positive control

Legend: complement activation within range $\pm 10\%$ (-), range 10% to 50% (\uparrow or \downarrow), range 50% to 200% ($\uparrow\uparrow$), range 200% to 400% ($\uparrow\uparrow\uparrow$), range $> 400\%$ ($\uparrow\uparrow\uparrow\uparrow$)

4.6 Conclusion

In this study potential effects of micellar carriers on biological systems were investigated. Prominent concerns which could limit the applicability of colloidal systems are 1) cytotoxicity and 2) immunological responses. *In vitro* cytotoxicity and complement assays revealed valuable information about possible interactions of micelles with components of the biological system. The cytotoxicity studies were carried out on HepG2 cells and primary rat hepatocytes. Compared to the benchmark systems such as micellar Cremophor EL[®] or Tween 80[®], the results indicated no enhanced toxicity of the test polymers compared to those already approved systems. Interestingly cytotoxicity was increased for the PEG-PVPy polymers on metabolically active cells whereas on metabolically inactive cells there was no strong toxicity to be found.

For the complement activation studies in comparison to the liposomal market product Doxil[®] it can be concluded that from all investigated test micelles none exhibited stronger complement

activation. Consequently further *in vivo* studies with the materials should not cause any issues in animal welfare or deliver results which are related to toxicity items.

Chapter 5

Application of the developed drug loading technique to a hydrophobic compound: *in vitro* feasibility and *in vivo* biodistribution analysis

5.1 Abstract

The purpose of this study was the achievement of encapsulating compound A into polymeric micelles. Therefore different polymers were screened for compatibility to the drug. These polymers included PEGylated poly-(lactic acid) (PEG-PLA), PEGylated poly-(lactic acid-co-glycolic acid) (PEG-PLGA), PEGylated poly-(ϵ -caprolactone) (PEG-PCL) as well as PEGylated poly-(4-vinylpyridine) (PEG-PVPy). By preparing the micelles with all these polymers, the highest drug solubilization capacity among the biocompatible polymers was achieved by PEG-PLGA. By investigating the compound A loaded PEG-PLGA micelles in an *in vivo* biodistribution experiment, the pharmacokinetic properties were compared to the solution of compound B (salt form of compound A). The results revealed that the drug independently of its formulation in micelles or solution showed nearly the same pharmacokinetic profile. Radiolabeling of the carrier combined with a drug were applied to clarify these observations. Animal experiments with such a system indicated that the model drug IFF dissociated rapidly upon injection from its polymeric carrier.

5.2 Introduction

Polymeric micelles are ideal systems for solubilization purposes and drug targeting of hydrophobic compounds. As many new drugs have severe solubility problems [5, 6], the applicability of these systems was tested by encapsulation of compound A. Besides low aqueous solubility, this drug exhibited a severe off-target toxicity: During animal experiments heart valve failures were observed due to increased drug accumulation in the heart. This unlucky combination between low solubility, organ-specific toxicity and the limitation in solubilizing excipients presented a huge hurdle for this study. It was intended to guide the drug from heart tissue toward other organs: Tumor, liver and spleen. This goal should be reached by applying well-known, biocompatible polymers for encapsulation. Consequently encapsulation studies were carried out with PEGylated poly-(lactic acid) (PEG-PLA), PEGylated poly-(lactic acid-co-glycolic acid) (PEG-PLGA) and PEGylated poly-(ϵ -caprolactone) (PEG-PCL). However, for comparison purposes also the non-biodegradable PEGylated poly-(vinylpyridine) PEG-PVPy was investigated.

The biodistribution study of compound A loaded micelles was performed in tumor bearing animals by recording drug distribution via an LC-MS method. Due to the study design, it was not able to report information about the fate of the polymeric carrier. Consequently a follow up study was started to clarify the fate of each, drug and carrier, within one animal. For this purpose H₂N-PEG-PLGA was synthesized for further labeling with ¹¹¹In-DOTA. As a radiotractable model compound the ¹²⁵I labeled dechloro-4-iodo-fenofibrate (¹²⁵IFF) was selected [245].

In summary, the biodistribution assay with compound A loaded micelles investigated micellar drug distribution vs solution. whereas the radiolabeling experiment revealed additional information about the fate of drug and carrier.

5.3 Materials and methods

5.3.1 Materials

The following amphiphilic block copolymers in research grade were purchased from Polymer Source, Inc., Montreal, Canada: PEGylated poly-(lactic acid) (PEG-PLA) [5-b-23], PEGylated poly-(ϵ -caprolactone) (PEG-PCL) [5-b-32.5], PEGylated poly-(4-vinylpyridine) (PEG-PVPy) [5-b-20]. PEGylated poly-(lactic acid-co-glycolic acid) (PEG-PLGA) [5-b-28] (Resomer RGP 50155d) was delivered from Boehringer Ingelheim, Ingelheim, Germany. The following solvents/chemicals in LC grade were delivered by VWR, Darmstadt, Germany: Tetrahydrofuran (THF), acetonitrile (ACN), acetone, dimethylsulfoxide (DMSO), ethanol,

methanol, dimethylformamide (DMF), trifluoroacetic acid (TFA). Compound A (free drug base, solubility: 1 µg/mL at pH 7.4, weak basic with pK_a 3.2 for corresponding acid, logP 4.6 calculated with ChemDraw 8.0) and compound B (dimesylate salt of compound A) was synthesized and provided from Merck Serono, department of medicinal chemistry, Darmstadt, Germany. Dechloro-4-iodo-fenofibrete (non-acidic, non-basic, logP 5.5 calculated with ChemDraw 8.0, solubility <0.1 µg/mL) was synthesized and provided by Breyer et al. [245]. Dulbeccos Saline PBS buffer concentrate was obtained from Sigma Aldrich, Rossdorf, Germany. Float-A-Lyzer G2 dialysis tubes (MWCO 8-10 kDa) were obtained from Spectrumlabs Inc., Breda, The Netherlands. Water was of MilliQ grade. For sterile filtration the Pall Acrodisc GHP membrane 0.2 µm syringe filters were used.

5.3.2 Methods

5.3.2.1 Solvent screen prior to cosolvent evaporation

According to the developed procedure in chapter 2 in section 2.3.2.1, the encapsulation of the compound was carried out in this study by using the cosolvent evaporation technique. The following water miscible organic solvents were included in the solvent screen for compound A: THF, ACN, acetone, DMSO, DMF, methanol, ethanol. Compound A acts as a base and, therefore, solvent screen was carried out by adjusting “apparent pH” with TFA for determination of the solubility of compound A. The procedure was followed as described in 2.3.2.1. The solvent in which the drug exhibited the highest optical solubility was selected for the cosolvent evaporation step. The screening experiments were carried out with $n=1$ due to the very limited availability to the development compound.

5.3.2.2 Polymer screen to load compound A into micelles

Drug loaded micelles were prepared by a combination of solvent evaporation and dialysis technique. 10 mg block copolymer and 1 mg drug were dissolved in 8 mL ACN/0.1% TFA by ultrasonication and was mixed with 2 mL water. The mixture was transferred into a round bottom flask and evaporated with decreasing pressure to 30 mbar at 25°C. To remove the maximum amount of solvent, this pressure was kept constant for 10 min. The remaining aqueous formulation was then transferred into a Float-A-Lyzer G2 tube for dialysis. The formulation was dialyzed against compound A saturated PBS buffer pH 7.4 for 24 h. Finally the formulation was filtered through a 0.2 µm membrane and volume adjusted to 2 mL with PBS buffer.

5.3.2.3 Preparation of study materials

Micelle preparation To prepare the micelles, a modified cosolvent evaporation method was employed. Briefly, for preparation of 5 mL micellar dispersion, 5 mg compound A and 250 mg PEG-PLGA was dissolved in a mixture of 20 mL acetonitrile/0.1% TFA (v/v). Finally, 5 mL water was added to this organic solution to preform the micelles. Evaporation of acetonitrile was performed under reduced pressure (Buechi rotary evaporator) to load the micelles. Removal of residual solvents was gained by a following dialysis step against drug saturated PBS buffer. As a last step untrapped drug was removed by filtration of the formulation through a 0.2 μm filter membrane.

Drug solution According to the final drug concentration acquired from micellar loading experiments, a solution of compound B was prepared to benchmark against the micelles. For this purpose the drug was dissolved in citrate buffer pH 3 to avoid release of the free base (aqueous solubility of compound A is highly pH dependent).

Drug load determination 100 μL of the final micellar dispersion was dissolved in 900 μL acetonitrile. This solution was injected in a HPLC system (Merck Hitachi La Chrom Elite) equipped with a UV detector (detection wavelength: 254 nm) and a Agilent Eclipse Plus C18 column (3.5 μm coarse, 5 cm length) at 30°C. A gradient method was used for separation where the mobile phase A consisted of 90% ACN (v/v)/10% water with TFA (v/v); mobile phase B had the opposite composition. Compound A concentration was determined by drug substance calibration curve.

Drug load calculation The drug load was calculated according to Eq. 5.1:

$$\text{Drug load [\%]} = \frac{\text{Drug concentration } [\frac{\text{mg}}{\text{mL}}]}{\text{Polymer concentration } [\frac{\text{mg}}{\text{mL}}]} \cdot 100\% \quad (5.1)$$

5.3.3 Particle size measurements

Dynamic light scattering (DLS) technique was used to determine hydrodynamic diameter of the nanoparticles. Samples were diluted 1:100 with water and analyzed with a Zetasizer Nano ZS90 from Malvern, Worcestershire, UK, set to backscattering mode. Particle size calculations were performed via cumulants analysis of the intensity weighed particle distributions.

5.3.4 Biodistribution experiments of micelles vs. solution

Animal model All animal experiments were conducted according to regulations of the German law.

5 weeks old BalbC mice (Charles River Inc., Wilmington, MA, USA) were inoculated with $5 \cdot 10^4$ 4T1 cells (mouse mammary carcinoma) subcutaneously into the right flank of the animal. Tumor growth was supervised over 14 days post injection. Animal selection for the biodistribution study was based on tumor volume (minimum: 300 mm³). 100 μ L of each formulation (compound A in PEG-PLGA micelles, compound B as solution) was injected into the tail vein of the mice and biodistribution was analyzed according to the following time points: 0.5 h, 1 h, 3 h, 6 h, 24 h, 48 h, 72 h post injection. Three animals were sacrificed per treatment group per time point and the organs were resected.

Drug analytics in resected organs The quantitative distribution data were acquired from a HPLC-MS/MS assay. The resulting tissue/organ samples from the animal experiments were treated with ethanol/water 80/20 (v/v) to precipitate proteins. Upon centrifugation, the supernatant was then extracted with water/ACN 10/90 (v/v). 10 μ L of this solution was injected into a HPLC system (Agilent 1100). Separation was carried out on a Cromolith FastGradient RP-18e (50 mm), Merck KGaA, Darmstadt, Germany column using a phase gradient. The mobile phases consisted of water with 0.1% formic acid (phase A) and ACN (phase B) 10/90 (v/v). Detection was performed on a API 4000 MS detector from AB Sciex Instruments (quadrupole detector). Quantification was done by recording a drug substance calibration curve.

5.3.5 Preparation of radiolabeled H₂N-PEG-PLGA and bioimaging

Synthesis Generally the ring opening polymerization (ROP) procedure was employed which is described in section 7.3.2.1. Deviating from this, instead of dilactide alone an equimolar mixtures of dilactide and diglycolide prior to starting the synthesis was used.

Polymer analytics Molar masses and mass distributions of the resulting polymers were determined on a Viscotek GPCmax system equipped with a TDA 302 triple detector system (full system provided by Malvern Instruments Ltd., Worcestershire, UK). 0.1% TBABr in DMF served as a solvent mixture on a Tosoh TSK Gel 3000 HHR column (Tosoh Biosciences GmbH, Stuttgart, Germany). Calibration was carried out with a polystyrene standard. Prior to NMR analysis the polymers were dissolved in CDCl₃. Spectra were recorded on a Bruker 400 MHz NMR spectrometer (Bruker BioSpin GmbH, Rheinstetten, Germany).

Radiolabelling of H₂N-PEG-PLGA and micelle preparation for bioimaging The method described in detail in section 7.3.2.3 was carried out to achieve a ¹¹¹In-DOTA-HN-PEG-PLGA. This polymer was used for bioimaging experiments. The labeled polymeric species was mixed 1:5 (w/w) with mPEG-PLGA [5-b-28]. The polymeric mixtures were dissolved in THF and mixed micelles were prepared by cosolvent evaporation following the protocol previously described in section 2.3.2.1.

Animal experiment via bioimaging Clarification of carrier and drug payload fate *in vivo* was carried out by employing bioimaging for the dual-labeled polymeric micelles. 100 µL of the ¹²⁵IFF loaded ¹¹¹In-mixed micelles were injected into the tail vein of a NMRI mouse (Charles River, Wilmington, MA, USA). The mouse was kept under anesthesia with isoflurane prior to injection. Bioimaging was carried out on a γ -imager SCT. After finishing the bioimaging experiments, the animal was sacrificed and radioactivity of ¹¹¹In and ¹²⁵I was quantified in different organs with a berthold LB951G γ -counter (Berthold Technologies, Bad Wildbad, Germany).

5.4 Results

5.4.1 Solvent screen for cosolvent evaporation

The results from the solvent screen experiment to elucidate the highest optical solubility of the drug was portrayed in Fig. 5.1.

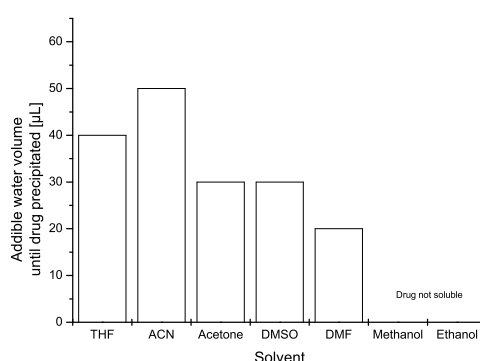


Figure 5.1: Results of the solvent screen for compound A. 1 mg of drug was dissolved in 100 µL of the displayed organic solvents and water was added incrementally. Precipitation was detected by optical turbidity. The screen was carried out with n=1 due to the very limited availability of compound A.

The critical precipitation ratio was ACN/water 2:1. Based on this solvent screen, fixed mixtures of solvents were used for the preparation of drug-loaded micelles from cosolvent evaporation. Due to practical considerations for the cosolvent evaporation the ACN/water containing 0.1% TFA (v/v) was set to 5:1.

5.4.2 Drug loading, particle sizes and size distributions for compound A loaded micelles

Compound A was encapsulated into polymeric micelles with the cosolvents evaporation technique followed by dialysis against drug saturated solution. The preparation results are presented in table 5.1. Due to the very limited availability of the development compound (<100 mg in early stages) the polymer screen was carried out with n=1. The results showed that PEG-PVPy exhibited the best polymer-drug compatibility leading to the highest drug load among the investigated block copolymers. Despite these results, for further experiments one of the polyester based block copolymers was selected due to their known biodegradability. Comparison of PEG-PLA, PEG-PLGA and PEG-PCL revealed PEG-PLGA as the species with the highest drug loads. Moreover, for the finally selected PEG-PLGA combination this experiment was repeated in triplicate. The reasons for preferring PEG-PLGA compared to PEG-PVPy polymers was the known biodegradability and biocompatibility of this polymer [176]. Moreover, this formulation preparation was upscaled and then investigated in the biodistribution experiment which was presented in section 5.4.3.

5.4.3 Injected formulations for biodistribution purposes

5 mL of the compound A loaded PEG-PLGA micelles were prepared. Compound B was dissolved according to the the final drug concentration of compound A. Table 5.2 summarized the acquired formulations upon upscale which finally were used for the biodistribution experiments. 100 μ L of these preparations were injected into each animal.

Table 5.2: Physicochemical characterization of the injected formulations.

Parameter	Compound A	Compound B
Formulation type	Micellar	Solution
Particle size [nm]	112 ± 1	n.a.
Particle size distribution (PdI)	0.216 ± 0.03	n.a.
Drug concentration [μ g/mL]	180	180

Table 5.1: Results from preparation of compound A loaded micelles. Apart from the PEG-PLGA preparation with 5% polymer content, the experiments were carried out with $n=1$ due to the limited availability of compound A. In all cases the drug polymer feed ratio was 1:10. Loading was carried out from cosolvent evaporation by using ACN with 0.1% TFA followed by dialysis.

Polymer	Polymer conc. w/v [%]	Preparation technique	Drug load [%] (w/w)	Drug conc. [$\mu\text{g/mL}$]	d_h [nm]	PdI
PEG- PDLLA [5-b-23]	0.5	Cosolvent evaporation	< LOQ*	< LOQ	n.a.	n.a.
PEG-PLGA [5-b-28]	0.5	Cosolvent evaporation	0.508*	25.4	n.a.	n.a.
PEG-PCL [5-b-32.5]	0.5	Cosolvent evaporation	0.498*	24.9	n.a.	n.a.
PEG-PVPy [5-b-20]	0.5	Cosolvent evaporation	0.812*	40.6	n.a.	n.a.
PEG-PLGA [5-b-28]	5.0	Cosolvent evaporation	0.202 \pm 0.013**	101.90 \pm 6.44	122 \pm 2	0.183 \pm 0.034

* $n=1$; ** $n=3$; LOQ = Limit Of Quantification

5.4.4 Biodistribution of compound A-loaded PEG-PLGA micelles

The micellar formulation of compound A and drug solution of compound B were injected into tumor bearing mice. After determined time points each group of three animals were sacrificed and organs were resected for further LC-MS analysis on drug concentration. Fig. 5.2 reports the time-dependent biodistribution values in varying organs for both formulations. Compared to drug solution, the micellar formulation showed significantly increased accumulation in lungs, liver and spleen. In tumor, heart and kidneys there was no significant difference in drug concentration between micellar formulation to solution. This observation was supported by plasma analysis as reported in Fig. 5.3. Over the investigated time period a significant difference between both formulations has not been found. Tab. 5.3 summarizes the pharmacokinetic data in plasma, tumor and heart. From these values it was clear that overall exposure of drug either in micelles or solution in tumor and heart (AUC values) were similar. Additionally, half life in plasma could be only extended from 0.6 h (solution) to 1.5 h (micelles) but finally resulted in comparable AUC plasma values (Fig. 5.3).

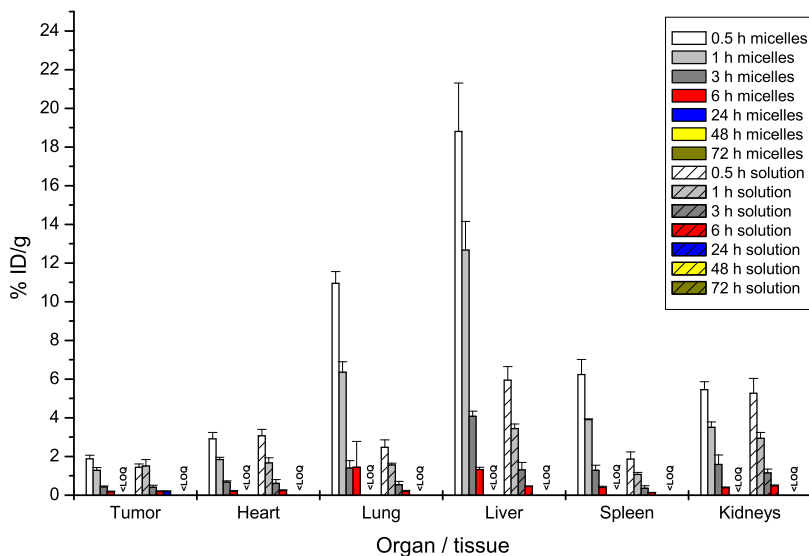


Figure 5.2: Biodistribution of compound A loaded PEG-PLGA micelles compared to compound B solution. Drug concentrations at 48 h and 72 h post injection were not reported in the figure because their values were below the limit of quantification (<LOQ) in the used LC-MS method.

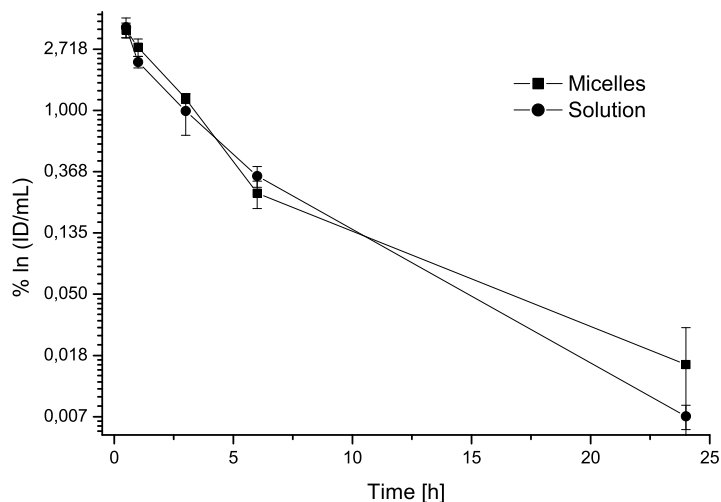


Figure 5.3: Recorded drug plasma concentrations over time upon injection of micellar drug or drug solution.

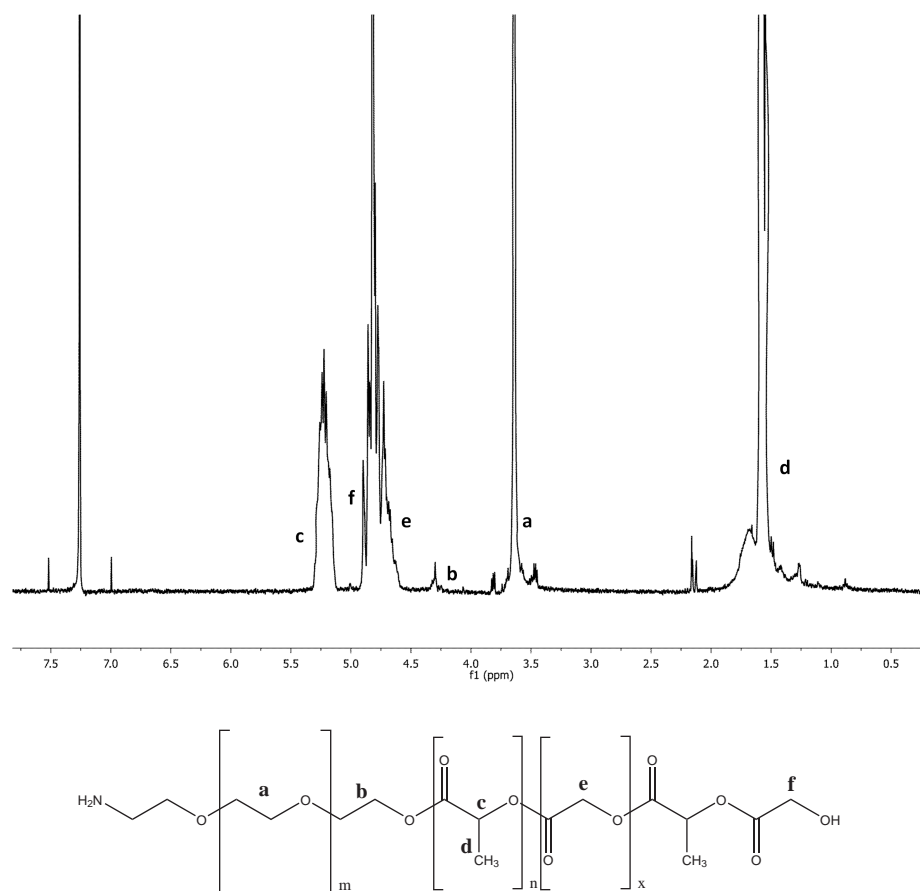
Table 5.3: Pharmacokinetic parameters of compound A and compound B in different tissues/organs. Each value was taken from graph fitting of the pharmacokinetic data.

Tissue/organ	Half life $t_{0.5}$ [h]		AUC [h·%/g]	
	Micelles	Solution	Micelles	Solution
Plasma	1.5	0.6	12.5	12.7
Tumor	1.1	1.0	7.3	9.3
Heart	0.5	0.6	8.8	9.3

5.4.5 Synthesis of H₂N-PEG-PLGA and bioimaging

5.4.5.1 Synthesis

Amino functionalized PEG-PLGA was successfully synthesized by ring opening polymerization with the following characteristics obtained from GPC and NMR (Tab. 5.4). A representative ¹H-NMR spectrum was shown in Fig. 5.4.

Figure 5.4: ^1H -NMR spectrum of H_2N -PEG-PLGA.Table 5.4: Molar mass characterizations of H_2N -PEG-PLGA. $M_n[\text{calc}]$ is the theoretical molar mass of the polymers assuming full conversion of the educts.

	M_n [calc]	M_n [^1H -NMR]	M_n [GPC]	M_w [GPC]	M_w/M_n [GPC]
H_2N -PEG-PLGA	28.000	25.900	20.500	23.500	1.15

5.4.5.2 Bioimaging

Dual-labeled polymeric micelles were prepared by using ^{111}In for carrier tracking (^{111}In -DOTA-HN-PEG-PLGA) and ^{125}I for drug tracking (IFF). This micellar preparation was injected into one NMRI mouse. To reduce the number of animal experiments, bioimaging was carried out with only one animal. The results of this experiment were intended to support

the previous biodistribution study of the compounds A and B.

For this experiment the injected activities for both isotopes were ~ 3.3 MBq. Upon injection into a healthy NMRI mouse, distribution of radioactivity was recorded as a function of time. Fig. 5.5 reported the carrier distribution (^{111}In) whereas Fig. 5.6 presented the drug distribution (^{125}I).

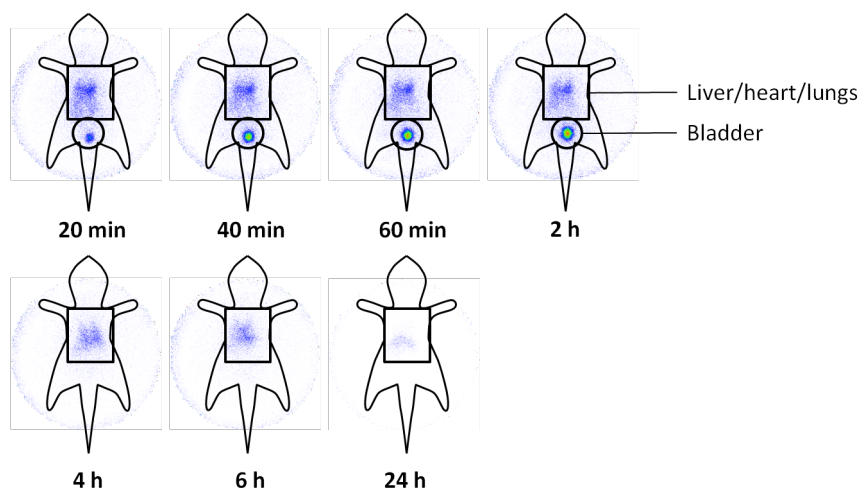


Figure 5.5: Scintigrams of ^{125}I FF loaded ^{111}In -DOTA-HN-PEG-PLGA. Presentation of the ^{111}In traces. Bioimaging was performed by using one NMRI mouse to reduce the number of animals in this study.

As reported by the scintigrams for the drug carrier (Fig. 5.5) the biodistribution of the micelles was preferentially in the heart/lungs and liver region. Obviously shortly upon injection the carrier accumulated in the lungs and liver whereas non-accumulated carrier remained in circulation. This could be detected by the rather diffuse distribution pattern of radioactivity signals in the scintigrams. 2 h upon injection the diffuse pattern declined in the scintigrams, whereas the staining of the lungs/liver remained constant. 24 h upon injection the radioactivity signal could be further detected in the lungs/liver region. Interestingly directly upon injection there was a strong signal of radioactivity in the bladder. After stopping narcosis of the animal, the bladder was obviously emptied and the signal was not found in later experimental imaging time points.

Simultaneously to recording the ^{111}In radioactivity for the carrier system, the ^{125}I activity for the encapsulated IFF drug was detected (Fig. 5.6). For the drug directly upon injection a strong signal in the liver was detectable. Besides the liver signal, a diffuse radioactivity pattern was detected in the heart region indicating still circulating, drug-loaded carriers. 40 min post injection the excretion of the drug via the biliar route into the intestinal system was visible. The excretion visibility continued until 6 h upon injection. 24 h post injection there was nearly no radioactivity remaining in the animal. The scintigrams showed similar

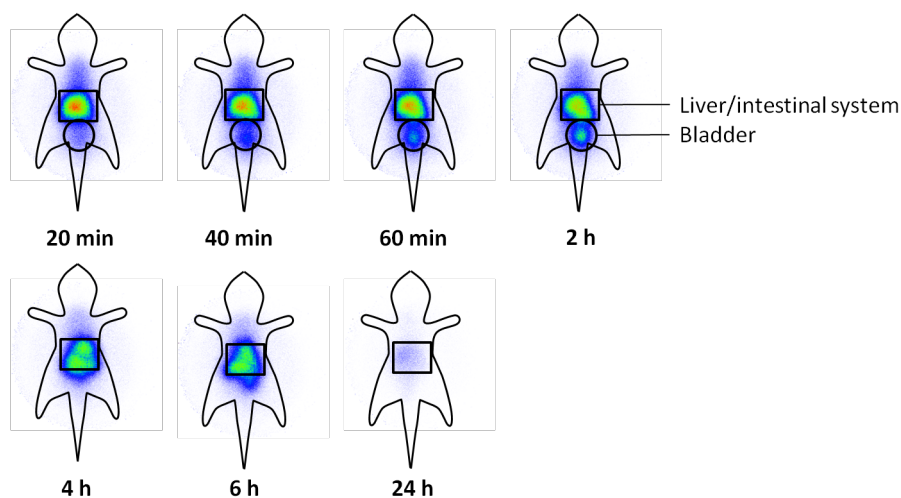


Figure 5.6: Scintigrams of ^{125}I -FFF loaded ^{111}In -DOTA-HN-PEG-PLGA. Presentation of the ^{125}I traces. Scintigrams were recorded simultaneously to the ^{111}In traces of the polymeric carrier. Consequently biodistribution could be followed qualitatively within the same animal.

activity in the bladder upon injection and a signal loss after stopping narcosis of the animal. So far, the incorporated radioactively labeled drug (Fig. 5.6) showed a similar biodistribution pattern compared to the polymeric carrier. For comparison purposes the animal was sacrificed after 24 h and the organs were resected and analyzed on radioactivity of ^{111}In and ^{125}I . Fig. 5.7 reports the actual quantitative distribution.

Whereas nearly no activity of ^{125}I after 24 h post injection was detectable, there was a lot of activity remaining from ^{111}In . Unexpectedly the ^{111}In activity resulting from carrier labeling was remarkably high in liver, lungs, spleen, heart and kidneys compared to the ^{125}I signals from drug labeling. Interestingly ^{125}I activity in the stomach was higher than that of ^{111}In .

5.5 Discussion

The purpose of this study was to develop a suitable micellar formulation of compound A to solubilize the drug and finally to change pharmacokinetics and biodistribution in terms of decreasing heart accumulation and increasing tumor drug concentrations. To reach this goal the development candidate was encapsulated into biodegradable PEG-PLGA micelles as a commercially available block copolymer. The goal of encapsulation and consequently solubilization was successfully gained. For this purpose varying amphiphilic block copolymers were screened on drug-polymer compatibility. This screen revealed a reasonable compatibility with PEG-PVPy and PEG-PLGA compared to PEG-PLA and PEG-PCL. At this point it must be admitted that the resulting drug loads $<0.6\%$ were very low compared to other

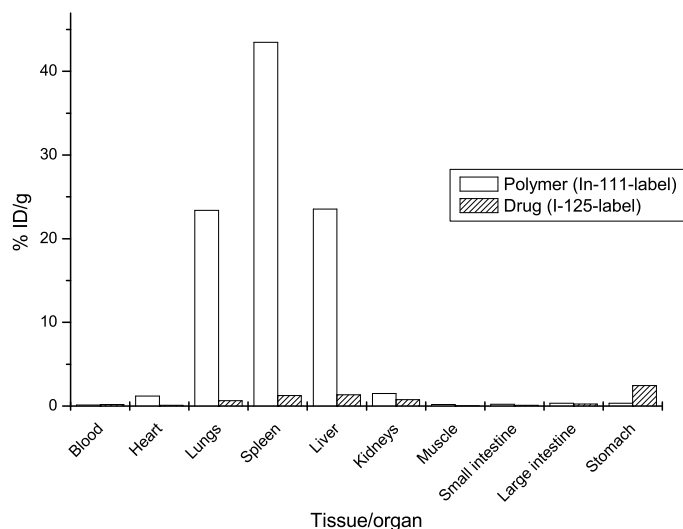


Figure 5.7: Biodistribution of ^{125}I FF loaded ^{111}In -DOTA-HN-PEG-PLGA species 24 h upon injection. The data were recorded from the original animal of the bioimaging study. As previously stated, to reduce the number of animal experiments the micelles were followed on biodistribution in one NMRI mouse.

micellar systems (e.g. Genexol-PM[®] 16.6%). Due to the biodegradability of PEG-PLGA in favour of PEG-PVPy, the encapsulation and animal studies were conducted with PEG-PLGA micelles. Encapsulation in PEG-PLGA micelles increased drug solubility from 1 $\mu\text{g}/\text{mL}$ (PBS buffer pH 7.4) to $\sim 180 \mu\text{g}/\text{mL}$ (PEG-PLGA micelles in PBS buffer pH 7.4); consequently drug solubility increased by factor 180. It is remarkable that although the drug-polymer compatibility was quite low (drug loads $< 0.6\%$), the drug was solubilized with concentrations up to $\sim 180 \mu\text{g}/\text{mL}$. The previously developed method for loading DXM into PEG-PVPy micelles (chapter 2) was successfully employed and derived for this development compound. Moreover, the overall procedure consisting of 1) solvent screen prior to cosolvent evaporation, 2) cosolvent evaporation and 3) dialysis for purification delivered micelles with therapeutically relevant drug concentrations.

As a next step the micelles were tested on their *in vivo* performance. In this experiment the micellar formulation was compared to a drug solution of a soluble salt (dimesylate) in terms of their biodistribution. According to the theory of the enhanced permeation and retention (EPR) effect, long circulating nanoparticles are able to target tumors more effectively than small molecule drugs [122, 131, 140]. A wide-spread approach to achieve long circulation properties was the selection of PEGylated polymers for formulation that present the PEG “stealth” shield to the surrounding biological media. Such micelle forming block copolymers were utilized in the studies. Therefore it was expected that the micellar

formulation would have enhanced circulation properties and consequently a significantly increased tumor accumulation compared to the drug solution. As a result of this experiment there were less distinct differences between both types of formulations in terms of their biodistribution found. Completely unexpected was the high drug accumulation in the lungs, liver and spleen compared to drug solution. This accumulation can be seen as responsible for the low circulation times of the micelles. Simultaneously overall exposure of the formulated and unformulated drug was nearly similar, indicating no enhanced circulation and therefore no utilization of the EPR effect. However, what reasons could lead to such a distribution pattern? Generally, there are 3 varying scenarios that lead to these observations [246]: 1) insufficient stealthiness of the micelles and therefore rapid opsonization and cell phagocytosis, 2) insufficient stability of the micelles in presence of blood and consequently rapid dissolution and 3) insufficient stability of the incorporated drug that led to rapid drug extraction from the carriers toward proteins and continued circulation of “empty” carriers. Stealthiness of the particles was usually achieved by a complete PEG-coverage of the nanoparticles. Typical block lengths for the PEG parts had already been investigated and scattered between 2 kDa and 5 kDa PEG and was most effective in weight portions of at least 5% [216]. In the study PEG-PLGA [5-b-28] with a 5 kDa PEG and a weight portion of around ~15% w/w was employed, consequently PEGylation as the basic requirement for stealthiness was matched. However, surface properties of nanoparticles were not only determined by the presence of PEG molecules. Drug encapsulation often had a strong influence also on the surface. As reported by Brigger et al. [247] drug incorporation changed surface charge and therefore aggregation tendency of the nanoparticles. Compound A had a pK_a of 3.2 (corresponding acid) and consequently was non-ionic (free base) at pH 7.4. Therefore particle precipitation due to surface charge changes caused by the encapsulated drug could not be the reason for this observation. Stability of the investigated PEG-PLGA micelles was previously analyzed with a FRET probing technique [57]. In this study an intermediate stability of the micelles in presence of serum proteins was revealed. A residual micellar fraction upon 3 h of incubation was found to be ~66%. Consequently one could assume stability in the range of a few hours for the micellar system in serum. Rapid release properties should have been also prevented by the selection of a long PLGA block that imparted the resulting micelles enhanced thermodynamic and kinetic stability [8]. It was known that micelles formed from polymers with short hydrophobic block lengths disassemble rapidly upon injection as had been shown for Paclitaxel in PEG-PLA micelles [7].

The second part of this study dealt with the investigation of the mechanisms that lead to the observed biodistribution of compound A loaded PEG-PLGA micelles. For this purpose the study was designed with a dual-label to simultaneously track carrier and drug *in vivo*. Due to the limited access to the development compound A, IFF was selected as a suitable model drug which is similar hydrophobic (compound A logP: 4.5, IFF logP: 5.5) compared

to compound A. Since IFF was labeled with ^{125}I and consequently there was the need of another label for the polymer that allowed for discrimination between drug and carrier. So far, mPEG-PLGA beared a methoxy-group at the end of the PEG chain and was therefore not accessible for a labeling step. Consequently a H_2N -PEG-PLGA was *de novo* synthesized for finally coupling covalently a chelator with a radioactive metal cation to the polymer chain. Polymer synthesis by ring opening polymerization was successfully done and H_2N -PEG-PLGA [5.5-b-20.4] was prepared with high purity and low residual monomers (Fig. 5.4). The aimed and resulting polymer was slightly shorter in terms of hydrophobic block length compared to the commercially available mPEG-PLGA [5-b-28]. The goal for this experimental design was that the final ^{111}In -DOTA-NH-PEG-PLGA should not exceed strongly the micellar surface composed of mPEG-PLGA. In the following bioimaging experiment the formulation was prepared by mixing mPEG-PLGA with the radioactively labeled H_2N -PEG-PLGA. Drug loading procedure was kept constant for this preparation step. Upon formulation preparation, the drug loaded micelles were injected into a healthy animal. As indicated by the bioimaging scintigrams of ^{111}In (carrier), a certain percentage of the injected dose accumulated in the lungs, liver and spleen directly upon injection. However, due to the diffusivity of the scintigrams, one can conclude on circulating micelles for a few hours. In contrast to this the ^{125}I labeled drug accumulated rapidly in the liver and spleen. Consequently, the encapsulated drug did not follow the biodistribution of the carrier. This observation was supported by the biodistribution data from quantification of radioactivity 24 hours upon injection. Whereas nearly all ^{125}I was cleared from the animal, there were strong ^{111}In signals detected in liver, spleen and lungs. Summarizing this, encapsulation of the drug was not maintained upon injection and similar distribution pattern had been found for micelles and solution which was supported by the data of the biodistribution experiment with the development compound. In future studies it has to be clarified if this observation depends on the polymeric carrier material (e.g. polyester based micelles), on the intrinsic properties of the encapsulated drug (e.g. hydrophobicity, lipophilicity) or on the type of preparation (e.g. physical drug incorporation).

5.6 Conclusions

In this study a previously developed drug loading technique was successfully applied to the hydrophobic compound A. Furthermore, based on the loading results a development project was supported with the micellar formulation (PEG-PLGA/compound A). The pharmaceutical quality of this formulation was suitable for a biodistribution study. Whereas drug solubilization in physiological pH (pH 7.4) was possible (solubilization factor: 180) by the micellar delivery system, unfortunately the desired change of pharmacokinetic properties and increase in tumor accumulation of the drug was not achieved. This was probably due to the dissociation of

drug and carrier systems rapidly upon injection.

Chapter 6

Radiolabeling of PEGylated poly-(4-vinylpyridine) and its biodistribution

6.1 Abstract

The purpose of this study was the investigation of the *in vivo* distribution of PEGylated poly-(4-vinylpyridine). The *in vivo* experiments were designed to reveal micellar circulation and body clearance of the polymer. For this purpose, the PEG-PVPy materials are labeled with an iodine isotope after pyridine N quaternization with an electron-rich phenol derivative. The animal experiments revealed a short circulation time (<1 h) of the micelles and a long liver residence time (half life ~ 56 h) of the polymer. Dechloro-4-Iodo-Fenofibrate (IFF) was encapsulated into non-labeled PEG-PVPy micelles and investigated via bioimaging. From the scintigrams a fast accumulation of the drug in the liver was obtained. As both drug and polymeric carrier were bearing identical radioactive isotopes, a discrimination between carrier and drug effects was not possible.

6.2 Introduction

PEGylated poly-(4-vinylpyridine) (PEG-PVPy) material is an interesting material for encapsulation of hydrophobic drugs. In this connection excellent drug loading results with dexamethasone were obtained (chapter 2). But the material was not under previous investigation on biodistribution, metabolization and excretion yet. Since *in vitro* cytotoxicity and complement activation data (chapter 4) did not reveal severe issues which pose an obstacle against animal experiments, this *in vivo* route is followed in the present study.

Radiolabeling is an appropriate mean to investigate the *in vivo* properties of drugs and polymeric materials. Generally, radiolabeling of PEG-PVPy can be achieved at the pyridine part or at the PEG part. Both procedures will alter the micellar properties: the pyridine labeling changes the micellar core properties (e.g. critical association concentration) whereas shell labeling could change the surface charge and PEG brush density. In this context, labeling at the pyridine part is much easier to achieve because the methoxy-endcapping (H₃CO-endcapping) at the commercially available PEG-PVPy does not allow direct coupling to radioactive isotopes. Consequently for the shell labeling a *de novo* synthesis must be applied that maintains an endgroup for coupling to labeling moieties. In this study as a starting point the pyridine labeling was achieved by quaternization of the pyridine N in the hydrophobic region of the polymer. This approach delivers a stably coupling to radioactive isotopes.

6.3 Materials and methods

6.3.1 Materials

Dechloro-4-Iodo-Fenofibrate (IFF) was prepared by *de novo* synthesis and provided by Breyer et al. [245]. mPEG-PVPy [5-b-20] was purchased from Polymersource, Inc, Montreal, Canada. 4-(2-bromoethyl)-phenol, chloramin T (CAT), dithiothreitol (DTT) and PBS buffer concentrate (10x) were obtained from Sigma Aldrich, Rossdorf, Germany. Dichlormethane, methanol, ether, dimethylformamide (DMF) were purchased from VWR, Darmstadt, Germany. Na¹²⁵I and Na¹³¹I were purchased from Perkin Elmer, Waltham, MA, USA. Float-A-Lyzer dialysis tubes MWCO 3.5 kDa were purchased from Spectrumlabs, Breda, The Netherlands. Female NMRI mice were obtained from Charles River, Wilmington, MA, USA. Water was of MilliQ grade.

6.3.2 Methods

6.3.2.1 PEG-PVPy quaternization and labeling with radioactive iodine isotopes

General approach PEG-PVPy is not subject to direct labeling with iodine isotopes due to the low electron density of the pyridine hetero-aromates. Consequently, an effective way of radiolabeling with iodine is the coupling to electron-rich aromates which can be reacted with iodine isotopes. For this purpose the PEG-PVPy was quaternized at the pyridine N with 4-(2-bromoethyl)-phenol and in a second step labeled with iodine. Fig. 6.1 summarizes this approach.

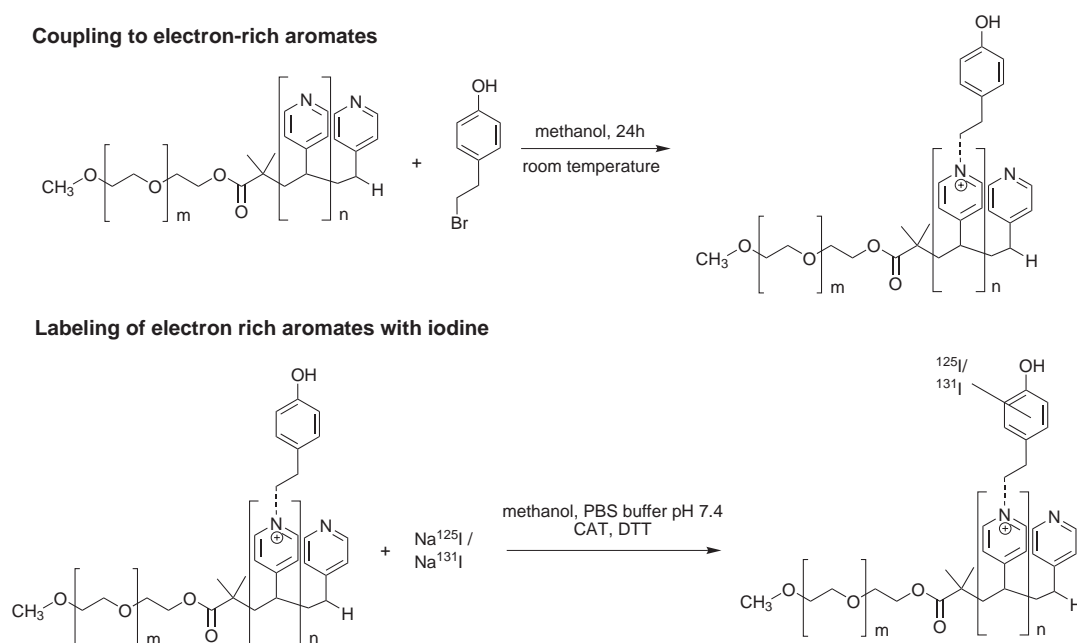


Figure 6.1: Quaternization and labeling of PEG-PVPy.

Quaternization reaction 210 mg PEG-PVPy was dissolved in 13 mL methanol and 4-(2-bromoethyl)-phenol was added under constant stirring. This mixture was stirred over 24 h at room temperature. Then the polymer was precipitated in 35 mL ether, cooled to -20°C for 35 min and centrifuged at 2900 rpm (10 min at 4°C). The precipitate was dissolved in methanol and the precipitation step was repeated in triplicate. The resulting quaternized polymer was dried over night under reduced pressure.

Radiolabeling of quaternized polymer 10 mg of the quaternized polymer were dissolved in 1 mL methanol. To this solution 50 μL PBS buffer (pH 7.4), 10 μL Na^{125}I or Na^{131}I solution (~ 100 MBq and 50 μL chloramine T solution (CAT) (5 mg/mL w/v in methanol)

were added. After 30 s the reaction was stopped by a solution of dithiothreitol (DTT) (10 mg/30 μ L), precipitated in ether and washed three times. The resulting polymer was dissolved in methanol and dialyzed against PBS buffer pH 7.4 containing non-radioactive sodium iodide (1 g in 450 mL PBS buffer).

6.3.2.2 Bioimaging of labeled PEG-PVPy micelles

All animal experiments in the bioimaging and biodistribution study were conducted following the German law.

100 μ L of each of the formulations were injected into the tail vein of the animals. For bioimaging study the animals were anesthetized with isoflurane and analyzed on γ -imager SCT (Biospace Lab, Paris, France). In the biodistribution study the animals were sacrificed and organ radioactivity was measured with a berthold LB951G counter (Berthold Technologies, Bad Wildbad, Germany).

Drug-free PEG-PVPy micelles 10 mg ^{125}I labeled polymer (20 MBq) was dissolved in methanol. This solution was dialyzed against PBS buffer overnight to remove the solvent and free iodine.

IFF-loaded PEG-PVPy micelles Labeled ^{125}I IFF (25 MBq) and 10 mg PEG-PVPy were dissolved in 1 mL THF and diluted with 1 mL water. Finally to prepare the micelles, this mixture was dialyzed against PBS buffer overnight and concentrated by centrifugation with Amicon microtubes (MWCO 10 kDa).

6.3.2.3 Biodistribution of labeled PEG-PVPy micelles

Biodistribution was investigated in healthy NMRI mice (Charles River Corp., Wilmington, MA, USA). The preparation procedure of micelles was carried out as described above with the exception of using Na^{131}I rather than Na^{125}I .

6.4 Results

6.4.1 Preparation of labeled PEG-PVPy

The polymer was labeled successfully with a resulting activity of ~ 9 MBq in 400 μ L PBS buffer. 100 μ L of this colloidal dispersion was injected into the animal for bioimaging. For the biodistribution study this dispersion was diluted to 2 mL with non-labeled PEG-PVPy

micelles in PBS buffer and 100 μL of this mixed micellar solution was injected into each animal.

6.4.2 Bioimaging of labeled PEG-PVPy micelles

Polymeric micellar formulations were successfully prepared by employing a dialysis method. The formulation was then intravenously injected into mice and biodistribution was followed over time. For comparison purposes the IFF solution was injected in the study of Breyer et al. [245].

6.4.2.1 IFF in unlabeled PEG-PVPy micelles

The encapsulated drug was tracked whereas the carrier remained unlabeled. The scintigrams were presented in Fig. 6.2.

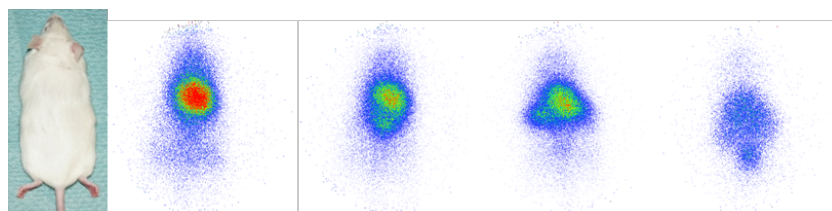


Figure 6.2: ^{125}I FF in PEG-PVPy micelles 10 min, 60 min, 6 h and 24 h post injection.

Form the scintograms it is remarkable that directly upon injection a strong radioactive signal can be found in the liver-spleen region of the animal. Until 1 h post injection the scintigrams looked quite diffuse, indicating still circulating micelles. This diffusivity decreased strongly after 1 h. Over time the liver signal decreased and splitted up into two “green” regions. The lower “green” center represented the intestinal system of the mouse. The drug was cleared from the body by using this route. 24 h upon injection a radioactive signal was still detectable.

6.4.2.2 Labeled PEG-PVPy micelles

The labeled polymer was investigated on biodistribution in γ -scintigraphy and quantitative biodistribution. The results were reported in Fig. 6.3 and Fig. 6.4.

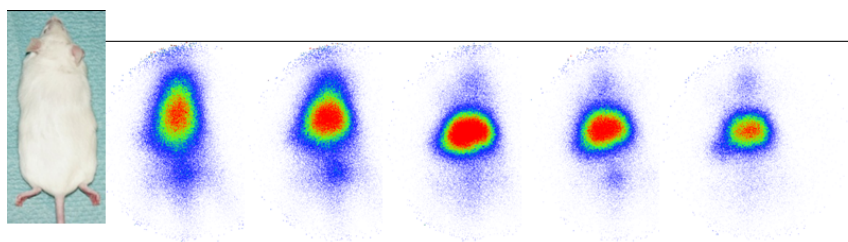


Figure 6.3: ^{125}I -PEG-PVPy micelles 10 min, 60 min, 6 h, 24 h and 7 d post injection.

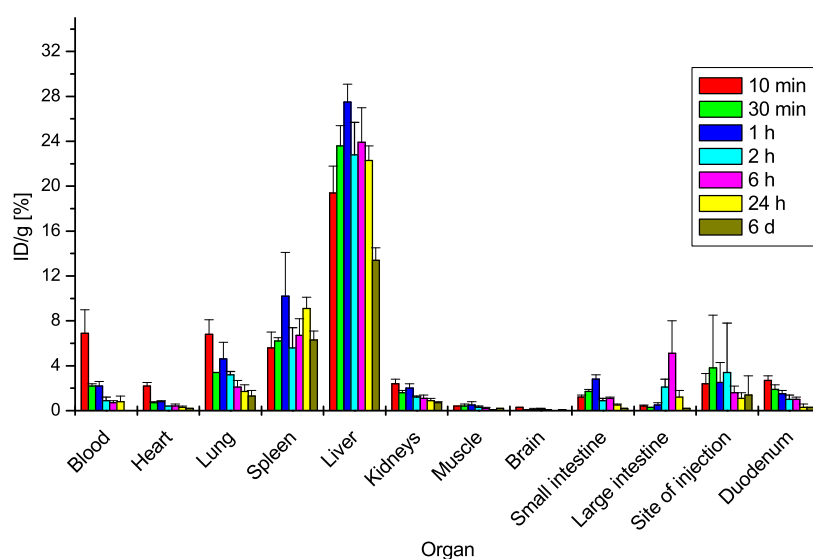


Figure 6.4: ^{131}I -PEG-PVPy micelles in a biodistribution experiment (each bar $n=3$).

The scintigrams showed a strong radioactive signal upon injection in the liver-spleen region. But in contrast to the scintigrams at 1 h post injection, the signal was not centered as a circle. This and the diffusivity of the scintigrams indicated still circulating micelles. 1 h post injection the signal was centered in the liver and remained until 7 d post injection. The biodistribution data showed a similar pattern: strong accumulation in the liver which increased from injection to 1 h post injection and remained for more than 6 d. Simultaneously in blood and lungs the radioactivity decreased rapidly upon injection.

6.4.2.3 Elucidation of PEG-PVPy body clearance

For this purpose the remaining activity in the animals was recorded in dependence of time. The data were isotope half-life corrected. The results were reported by Fig. 6.5.

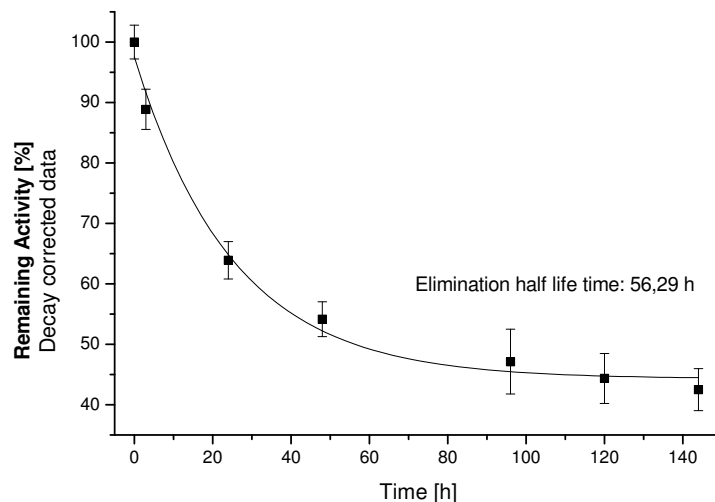


Figure 6.5: Body clearance of PEG-PVPy in dependence of time ($n=3$).

The body clearance half-life was found to be ~ 56 h and followed a first-order decay.

6.5 Discussion

The purpose of this study was the preparation and *in vivo* detection of radiolabeled polymeric PEG-PVPy carriers with their encapsulated drugs. The central question was the elucidation of pharmacokinetic properties combined with elimination routes of the polymeric carrier. Preparation of radiolabeled materials followed by micellization and encapsulation of drugs generally is quite challenging. Radiolabeling of a polymer for micellization is possible via two different routes: 1) labeling in the micellar core and 2) labeling of the micellar shell. Option 1) has the advantage that the surface properties of the particles remain unchanged (e.g. charge) whereas option 2) does not affect the stability of the micellar cores. Core labeling was received by coupling an electron-rich phenol derivative to the hydrophobic domain of the PEG-PVPy. This phenol derivative was then accessible for direct labeling with iodine isotopes. The labeled polymeric carrier showed a strong accumulation in the liver directly upon injection (Fig. 6.3 and 6.4). The blood compartment showed a strong decrease of the micellar/polymeric concentration within 60 min upon injection. This indicates that the circulation of the micelles was less than 1 h. It is remarkable that the residence time in the liver was very long compared to the circulation time of the micellar system. Isotope half-life corrected radioactivity measurements of the animals revealed an elimination half-life of ~ 56 h upon a single injection of the micelles. Excretion of the polymeric species via the kidneys, as expected for polymeric chains with molar masses below 40 kDa [12, 248], did not

play a major role for micellar systems. Furthermore, micellar/polymeric exposure was found in organs with high blood flows [4] and strong activity of the reticulo endothelial system (RES), as expected. For example, spleen and lungs showed strong signals of radioactivity. Although the micellar stability in biofluids [57] was investigated prior to this *in vivo* experiment which was found to be reasonably stable, the circulation of the micelles was strongly limited. From this experiment the question remains open whether the micelles disassembled prematurely into single polymeric chains or if the RES cleared the intact particles rapidly upon injection. Loading the micelles with IFF drug and tracking this drug *in vivo* was selected to reveal information about the drug payload (Fig. 6.2). As IFF is a very hydrophobic model compound, it was previously shown upon injection of an organic drug solution that metabolism and excretion followed the liver-bile-intestine route [245]. The drug-loaded micelles showed similar properties as can be seen from the bioimaging scintigrams. Consequently a separation between carrier and drug effects was not possible.

6.6 Conclusions

The radiolabeling experiment of PEG-PVPy is very important in several dimensions: 1) although the materials showed excellent drug-loading results and reasonable *in vitro* stability, the *in vivo* influence on drug pharmacokinetics was insufficient, 2) elimination of polymers via the kidneys (single chains below 25 kDa) is only a minor route for excretion of micellar assemblies and 3) information about drug payload and polymer can only be received by different isotope labeling. Taking these conclusions into account, the design of further *in vivo* experiments can be optimized.

6.7 Outlook

To overcome the disadvantages of the iodine labels it can be suggested to change the experimental design: labeling of drug and polymeric carrier had to be different to allow for a discrimination *in vivo*. For this purpose a different radiolabel apart from iodine isotopes had to be included into the polymeric chain. The previously investigated option for PEG-PLGA (chapter 5) of micellar shell labeling could be a valuable option for the design of potential ^{111}In labeled PEG-PVPy. This option requires a functional group at the PEG end of the polymeric chain. The idea could be to synthesize a H_2N -PEG-PVPy that is not commercially available yet. Polymerization can be carried out starting from H_2N -PEG and 4-vinylpyridine. The polymerization technique of choice is Atom Transfer Radical Polymerization (ATRP).

In 1995 the ATRP technology was independently discovered as a special type of radical polymerization by the groups of Matyjaszewski [249, 250, 251] and Sawamoto [252, 253,

254]. The groups leveraged this technology as one option to prepare polymeric materials with high conversion rates in a reasonable time frame. Unique features of ATRP are: 1) preparation of polymeric vinyl backbones with high molar masses (e.g 100 kDa), 2) reaction in aqueous/organic solvent mixtures, 3) short reaction times (few hours maximum), 4) good control of polymeric chain length distributions ($M_w/M_n < 1.5$) compared to other radical polymerization techniques and 5) usage of transition metals as catalysts.

However, this technology was described in literature for polymerization with H_3CO -PEGs [255, 256, 257] whereas in this case an amino-PEG should be used. To ensure that the polymerization is not carried out at the amino group, a protected amino-PEG derivative should be selected for polymerization.

Chapter 7

The fate of carriers and encapsulated drugs upon injection of self-assembling polymeric micellar systems

Tobias Miller^{1,3}, Sandra Breyer², Gwenaëlle van Colen¹, Simon Geissler¹, Walter Mier², Uwe Haberkorn², Senta Uezguen¹, Markus Weigandt¹, Achim Goepferich³

¹ Merck KGaA, Exploratory Pharmaceutical Development, Frankfurter Str. 250, 64293 Darmstadt, Germany

² Department of Nuclear Medicine, University Hospital Heidelberg, Im Neuenheimer Feld 400, 69120 Heidelberg, Germany

³ University of Regensburg, Department of Pharmaceutical Technology, Universitätsstrasse 31, 93040 Regensburg, Germany

To be submitted

7.1 Abstract

The solubilization of hydrophobic drugs, controlling the pharmacokinetics by a carrier system as well as drug targeting are the driving forces for exploring drug-loaded polymeric micelles. In this study these issues were investigated for PEGylated poly-(lactic acid) (PEG-PLA) micelles which incorporated the hydrophobic model drug dechloro-4-iodo-fenofibrate (IFF). For this purpose amino-PEG-PLA (H_2N -PEG-PLA) was synthesized, coupled to 1,4,7,10-tetraazacyclododecane-1,4,7,10-tetraacetic acid (DOTA) and labeled with ^{111}In . From this polymeric species, mixed micelles with methoxy-PEG-PLA (H_3CO -PEG-PLA) were prepared which encapsulated the ^{125}I -Iodine or ^{131}I -Iodine labeled drug IFF. Bioimaging and biodistribution experiments in healthy and tumor bearing mice (AR42J model) were carried out and the uptake of the drug and its carrier was quantified in single organs (Fig. 7.1). As a result successful solubilization of IFF by physical incorporation into the micelles was possible. Upon injection of this system a rapid dissociation of the polymeric carrier and the incorporated drug (<10 min post inj.) was found. Furthermore, drug and carrier exhibited completely different biodistribution patterns; both showed no enhanced tumor accumulation. As a conclusion, the self-assembling system allowed for successful solubilization of the hydrophobic drug by physical incorporation into micelles, however, *in vivo* a rapid dissociation of drug and carrier was detectable.

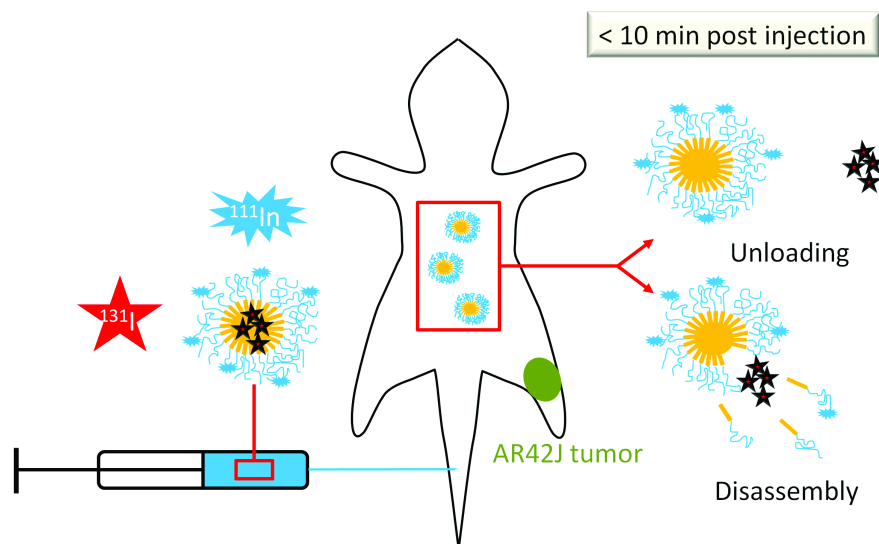


Figure 7.1: Summary of the biodistribution study with ^{111}In -HN-PEG-PLA micelles.

7.2 Introduction

The development of cytostatic agents for the treatment of life-threatening diseases like cancer excited the scientific community and gave hope for cure to patients. Despite the progress made, cancer treatment still requires improvements. Major drawbacks of cytostatic therapies were and still are strong off-target effects caused by adverse drug pharmacokinetics. This leads to severe side-effects and frequently only limited success in the treatment of the disease [258, 211]. Nanoparticles with their sufficiently small particle size, variable morphology and surface charge as well as multiple chemical composition are expected to overcome the lack of drug efficacy since they change the drug pharmacokinetics by a carrier system [259, 260]. A flicker of hope in this context were the liposomal product Doxil[®] [20] and the micellar products Genexol-PM[®] [7] and Nanoxel-PM[®] [261]. Doxil[®] was the first reasonable treatment option for patients suffering from Kaposi sarcoma that led to complete remission of the tumors combined with low side effects [262, 263, 264]. In contrast to this, Genexol-PM[®] and Nanoxel-PM[®] sufficiently solubilized highly effective taxol-derivatives which previous formulations were dose limiting due to strong excipient toxicity [265]. Finally the tolerated doses as well as the treatment success increased [266]. As can be seen with the products that encapsulate Taxol-derivatives, many anticancer agents are hydrophobic and, therefore, require solubilization technologies prior to administration. A very promising approach that combines the challenges, both in drug targeting and solubilization, are polymeric micelles. These self-assembling systems generally exhibit a hydrophilic shell and a hydrophobic core [210]. Consequently they are ideal for solubilizing hydrophobic drugs by encapsulation in their hydrophobic regions whereas the hydrophilic shell interacts with the biological environment. One intention is to fend off opsonizing agents by a steric barrier that finally prevents premature blood clearance of the micelles by the reticulo-endothelial system (RES) [106]. This leads to an increased blood circulation of the particles and enables the accumulation in tumors by the enhanced permeability and retention effect (EPR) [131, 140]. The amount of drug solubilization is not to only increase a substance's solubility. The idea behind the drug incorporation is based on the sufficiently stable cargo encapsulation in the micellar core. This assumption, however, remains questionable because self-assembling micelles are dynamic systems which encounter multiple stresses upon injection [246]. Therefore, in this study the fate of micellar carriers and their drug payloads was investigated in biodistribution experiments by means of radiolabeling. For this purpose the model drug dechloro-4-iodo-fenofibrate was selected which was derived from the highly hydrophobic drug fenofibrate [245]. The radiolabeled model drug was encapsulated into micelles composed of PEGylated polylactic acid (PEG-PLA). These micelles were known to form stable associates in water and serum [57] and were accessible for radiolabeling via synthesis of H₂N-PEG-PLA. The terminal amino-group was then modified with 1,4,7,10-tetraazacyclododecane-1,4,7,10-tetraacetic acid (DOTA) [267] which is able to

chelate several metallic radioactive isotopes such as indium. Consequently tracking of the drug delivery system within the same animal was made possible by employing and detecting an iodine isotope for the drug cargo and a metal isotope for the micellar carrier. These systems were investigated in tumor-bearing mice on their efficacy of tumor targeting as well as their *in vivo* fate. The results are intended to give a deeper understanding on the *in vivo* properties of such self-assembling systems.

7.3 Materials and methods

7.3.1 Materials

Amino-polyethyleneglycole (H_2N -PEG) with a molar mass of 5 kDa was purchased from Rapp Polymere Inc, Tübingen, Germany. Dilactide, stannous diethylhexanoate ($Sn(EtHex)_2$), tetrabutylammonium bromide (TBABr) and dried toluene (water content <50 ppm) were obtained from Sigma-Aldrich, Rossdorf, Germany. H_3CO -PEG-PLA [5-b-23] was purchased from Polymersource Inc., Montreal, Canada. DOTA-2,5-difluorophenyl-ester was synthesized according to Mier et al. [267]. Acetone, tetrahydrofuran (THF), $CDCl_3$, HCl, acetonitrile, dimethylsulfoxide (DMSO), polyethyleneglycole 200 (PEG-200), ethanol (96% v/v) and dimethylformamide (DMF) were delivered from VWR, Darmstadt, Germany. Water was of MilliQ grade. Float-A-Lyzer G2 8-10 kDa dialysis tubes were purchased from Spectrumlabs Inc., Breda, the Netherlands. Dechloro-4-iodo-fenofibrate (IFF) was prepared as reported by Breyer et al. [245]. Sodium 125-iodide, sodium 131-iodide and 111-indium chloride were obtained from Perkin Elmer, USA. NMRI mice and nude mice were delivered by Charles River Inc, Wilmington, MA; USA.

7.3.2 Methods

7.3.2.1 Synthesis of H_2N -PEG-PDLLA

For radiolabeling purposes a strategy proposed by Lee et al. [268] and Hoang et al. [269] was followed. Both groups described radiolabeling of PEGylated block copolymers at the terminal amino functionality of the PEG part. The amino group was used for chemical modification by coupling of chelators like DOTA via forming a stable amide bond. Therefore H_2N -PEG-PLA with H_2N -PEG as macroinitiator was synthesized via ring opening polymerization (ROP). Generally the method of Tessmar et al. [270] was applied. In brief, H_2N -PEG, the dilactide and the catalyst $Sn(EtHex)_2$ were dissolved in dried toluene under nitrogen atmosphere in a round bottom flask. Protection of the amino functionality from polymerization reaction was carried out by addition of 1 M HCl. Then the round bottom flask was equipped with

a condensor and the reaction mixture was heated to 115°C under constant stirring. After 4 h, the mixture was cooled to room temperature and the organic solvent was removed under reduced pressure. The crude polymer was dissolved in 2 mL acetone and precipitated upon addition of 8 mL water. The resulting dispersion was dialyzed twice overnight against 5 L water to remove unbound PEG and monomers/dimers. The purified premicellar formulation was lyophilized overnight to receive a dry polymer product.

7.3.2.2 Polymer analytics

Molar masses and mass distributions of the resulting polymers were determined on a Viscotek GPCmax system equipped with a TDA 302 triple detector system (full system provided by Malvern Instruments Ltd., Worcestershire, UK). 0.1% TBABr in DMF served as a solvent mixture on a Tosoh TSK Gel 3000 HHR column (Tosoh Biosciences GmbH, Stuttgart, Germany). Calibration was carried out by using a set of polystyrene standards. For ^1H -NMR analysis the polymers were dissolved in CDCl_3 . Spectra were recorded on a Bruker 400 MHz NMR spectrometer (Bruker BioSpin GmbH, Rheinstetten, Germany).

7.3.2.3 Radioactive labeling of H_2N -PEG-PLA

The chelator DOTA was conjugated to the H_2N -PEG-PLA by reaction of the primary amino group with DOTA-2,5-difluorophenyl-ester [245] to form a stable amide bond. In a typical procedure 10 mg of the block copolymer and 1.3 mg DOTA-2,5-difluorophenyl-ester were dissolved in a mixture of 500 μL acetonitrile and 0.4 μL triethylamine. The mixture was stirred at room temperature for 48 h and precipitated by addition of an excess of ethanol (EtOH) (5 mL). The solid was collected, washed twice with EtOH and water and dried under vacuum overnight. The polymer conjugate was dissolved in 500 μL acetonitrile and 1.0 mL NH_4OAc buffer solution (0.5 M, pH 6) followed by addition of $^{111}\text{InCl}_3$ -solution (~ 30 MBq). The mixture was heated to 95°C for 2 h, cooled to room temperature and the solvent was evaporated. The residue was washed with EtOH and water (3 x 1 mL each) and dried in vacuum to yield ~ 20 MBq of the ^{111}In -labeled polymer. Radiochemical purity was evaluated by instant thin layer chromatography (ITLC) as follows: A glass fiber strip was spotted with the sample and developed in NH_4OAc buffer (0.5 M, pH 6). The strip was sectioned and counted for radioactivity at the baseline (retention factor = 0) and at the solvent front (retention factor = 1). Unbound ^{111}In and unbound ^{111}In -DOTA migrated with the solvent front whereas ^{111}In -DOTA-NH-PEG-PLA remained at the baseline. The radiolabeling efficiency was calculated as ratio between detected radioactivity at baseline and solvent front in percent.

7.3.2.4 Radiolabeling of H₂N-PEG

The amino-PEG species was injected into a healthy NMRI mouse for reference purposes. H₂N-PEG (20 mg) and DOTA-2,5-difluorophenylester (5 mg) were dissolved in a mixture of 1 mL acetonitrile and 375 μ L triethylamine. The solution was stirred for 48 h at room temperature and evaporated to dryness. The residue was washed with EtOH (3 x 3 mL) and dried under vacuum. 10 mg of the polymeric conjugate and ¹¹¹InCl₃ were dissolved in 500 μ L acetonitrile and 1 mL NH₄OAc buffer solution (0.5 M, pH 6). The mixture was stirred at 95°C for 2 h and cooled to room temperature. The mixture was concentrated and the crude polymer solution was purified using Amicon[®] Ultra Centrifugal Filters with 3 kDa cutoff. After washing with water (3 x 100 μ L) the product was dried in vacuum. Radiochemical purity was analyzed as described above.

7.3.2.5 Formulation preparation for biodistribution and bioimaging

Preparation of ¹²⁵IFF or ¹³¹IFF encapsulated in ¹¹¹In-HN-PEG-PLA micelles The preparation of the formulation was performed by employing a modified cosolvent evaporation method. Briefly, for preparation of 0.4 mL micellar formulation, 1 mg IFF with 8 MBq ¹²⁵IFF and a mixture of 20 mg mPEG-PLA and 5 mg ¹¹¹In-DOTA-NH-PEG-PLA (activity: 8 MBq) was dissolved in a mixture of 6 mL THF and 1 mL water. Evaporation of THF was performed under reduced pressure (25 mbar) to load the micelles. Removal of residual solvents was achieved by a dialysis step against IFF saturated PBS buffer to reduce drug distribution from the micellar core towards the surrounding dialysis medium. For this purpose Float-A-Lyzer dialysis tubes with a cutoff between 8-10 kDa were used. This formulation was injected into the animal. In Fig. 7.2 the concept of the resulting labeled polymeric micelles was portrayed.

Characterization of micelles Particle sizes and size distributions were measured by employing the dynamic light scattering (DLS) technique. For this purpose the sample was diluted 1:100 and measured with the Zetasizer Nano ZS90, Malvern Instruments, Worcestershire, UK. Additionally, the zeta potential of the resulting micelles was investigated with this method: a 1:10 dilution of micelles with 0.1% sodium chloride solution was prepared and analyzed.

¹¹¹In-DOTA-HN-PEG and ¹¹¹In-DOTA-HN-PEG-PLA solutions The radiolabeled polymers were dissolved in a mixture of 5% DMSO, 45% PEG-200 and 50% PBS buffer. This solution was then taken for injection.

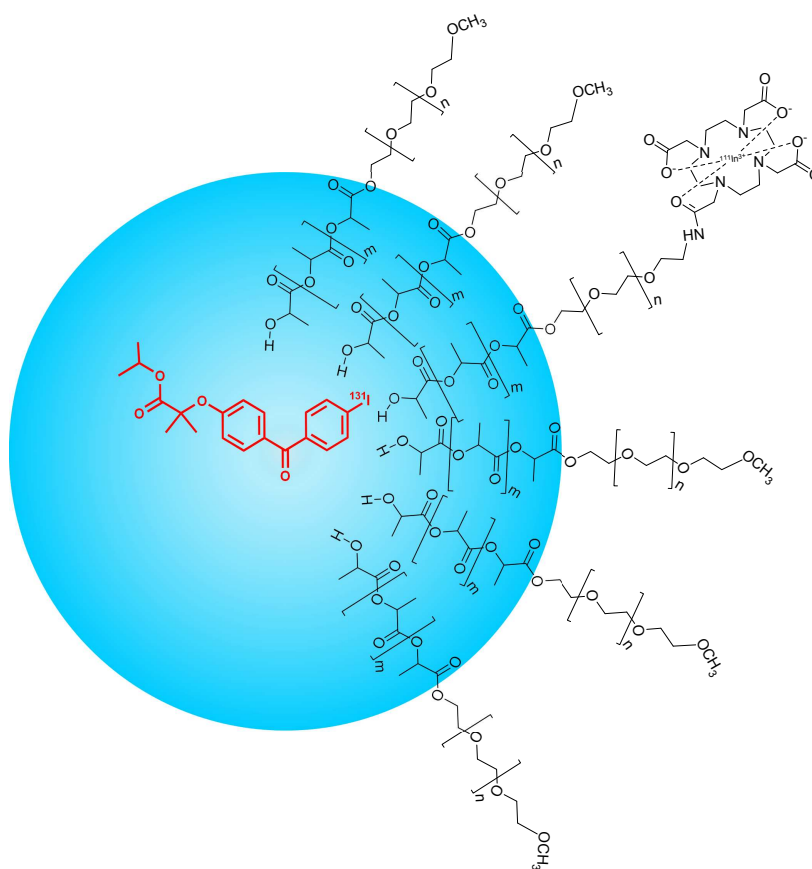


Figure 7.2: Micellar composition and morphology. The core components consisted of polylactic acid which hosted the radioactively labeled drug ^{131}I IFN. The particle shell was covered with PEG chains. The surfaces showed a mixture of ^{111}In -DOTA-HN-PEG-PLA and H_3CO -PEG-PLA.

7.3.2.6 Animal preparation and *in vivo* studies

The approach of the *in vivo* studies was summarized in Fig. 7.3. According to the experimental setup, the polymeric solutions were injected for reference purposes in healthy NMRI mice. For the micellar formulation loaded with IFN drug a biodistribution study was carried out with tumor-modified animals. All animal experiments were carried out according to German law requirements on *in vivo* experiments.

For bioimaging studies with single animal biodistribution Investigation of biodistribution for ^{111}In -DOTA-HN-PEG and ^{111}In -DOTA-HN-PEG-PLA solutions as well as ^{125}I IFN-loaded ^{111}In -DOTA-HN-PEG-PLA micelles was carried out by bioimaging in one healthy, female NMRI mouse (6 weeks old, ~ 30 g) per specimen. For this purpose, the animal was anaesthetized with isoflurane prior to the bioimaging experiment. Then 100 μL of the radioactive micellar formulation was injected into the tail vein of the mice. Bioimaging was carried

out on a γ -imager SCT, Biospace Lab, Houston, TX, USA. After finishing the bioimaging experiments, each animal was sacrificed and radioactivity of ^{111}In and ^{125}I was quantified in different organs with a berthold LB951G γ -counter (Berthold Technologies, Bad Wildbad, Germany).

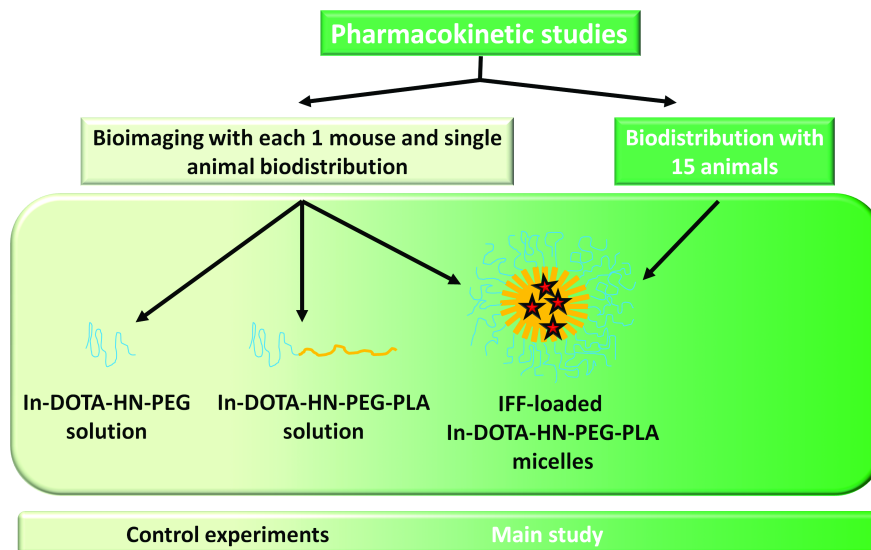


Figure 7.3: Summary of the animal study approach.

For biodistribution studies with drug loaded micelles: tumor inoculation in mice The AR42J cell line which was derived from a rat exocrine pancreas neuroendocrine tumor was used. For inoculation of the tumors, a Matrigel matrix/cell suspension was injected subcutaneously into the flank of the animals (5×10^6 cells per animal). Tumors were grown up to a size of $\sim 1.0 \text{ cm}^3$. 100 μL of the formulations were injected into the tail vein of the mice. Groups of 3 animals each were sacrificed 10 min, 30 min, 1 h, 2 h, 24 h upon injection. The following tissues/organs were extracted and prepared for further analysis: plasma, heart, lungs, kidneys, liver, spleen, intestines, stomach and where appropriate tumor. The organs were analyzed for radioactivity of ^{111}In and ^{131}I with a berthold LB951G γ -counter.

7.4 Results

7.4.1 Polymer synthesis, analytics and micelle characterization

Amino functionalized PEG-PLA was successfully synthesized with the following characteristics obtained from GPC and NMR (Tab. 1).

Table 7.1: Characterization of H₂N-PEG-PLA.

	M_n [calc]	M_n [¹ H-NMR]	M_n [GPC]	M_w [GPC]	M_w/M_n
H ₂ N-PEG-PLA	28.000	29.300	28.300	32.600	1.15

The chemical shifts for the resulting polymer obtained from ¹H-NMR confirmed identity and structure of the polymer. H₂N-PEG-PLA, CDCl₃: δ 1.55 ppm (1H, -OCHCH₃CO-), δ 2.7 ppm (2H, H₂N-), δ 3.6 ppm (4H, -OCH₂CH₂-), δ 5.35 ppm (3H, -OCHCH₃CO). Particle sizes, size distributions as well as zeta potential of the prepared micelles are reported in Table 7.2.

Table 7.2: Characterization of the resulting micelles composed of a mixture of ¹¹¹In-DOTA-NH-PEG-PLA and mPEG-PLA (mean \pm SD).

Particle size [nm]	PdI	Zeta-potential [mV]
110 \pm 3	0.24 \pm 0.02	0 \pm 4

7.4.2 Bioimaging

The imaging experiment was carried out prior to the biodistribution study to identify the scarification time-points. Moreover, for the control experiments with ¹¹¹In-DOTA-NH-PEG-PLA and ¹¹¹In-DOTA-NH-PEG distribution was only followed by bioimaging. 24 h upon injection the animals were sacrificed and the organs analyzed for radioactivity.

7.4.2.1 Drug-loaded polymeric micelles

Radiochemical purity was obtained from ITLC and found to be 92.4% for the ¹¹¹In-DOTA-NH-PEG-PLA (data not shown). This labeled species was taken for further preparation of micelles followed by *in vivo* studies. The scintigrams for the drug loaded micelles are shown in Fig. 7.4. The scintigrams obtained for the carrier immediately upon injection show a rather diffuse radioactivity pattern indicating the circulation of the carrier system (Fig. 7.4A). Moreover, the liver-region was clearly detectable in the center of the scintigrams. Over time the diffuse signal vanished and the radioactivity strongly focused on the liver. 24 h upon injection radioactivity was still detectable. A different distribution pattern could be found for the encapsulated drug IFF (Fig. 7.4B): Initially, a strong signal was rather centered in the liver-region (red spot) but simultaneously showed a diffuse corona around this region. The scintigrams 1 h to 6 h nicely reveal the rapid liver clearance of the drug from the liver via the bile into the intestinal system. In contrast to the carrier the drug was cleared rapidly and nearly no radioactivity could be detected 24 h post injection. Clarification of the question at

which time point the biodistribution pattern of the drug still followed the carrier system was revealed by analyzing the radioactivity in different organs (Fig. 7.4C). The biodistribution results 24 h after injection revealed a clear accumulation of the polymer in spleen, liver and lungs whereas the drug only followed the carrier system in liver and lungs.

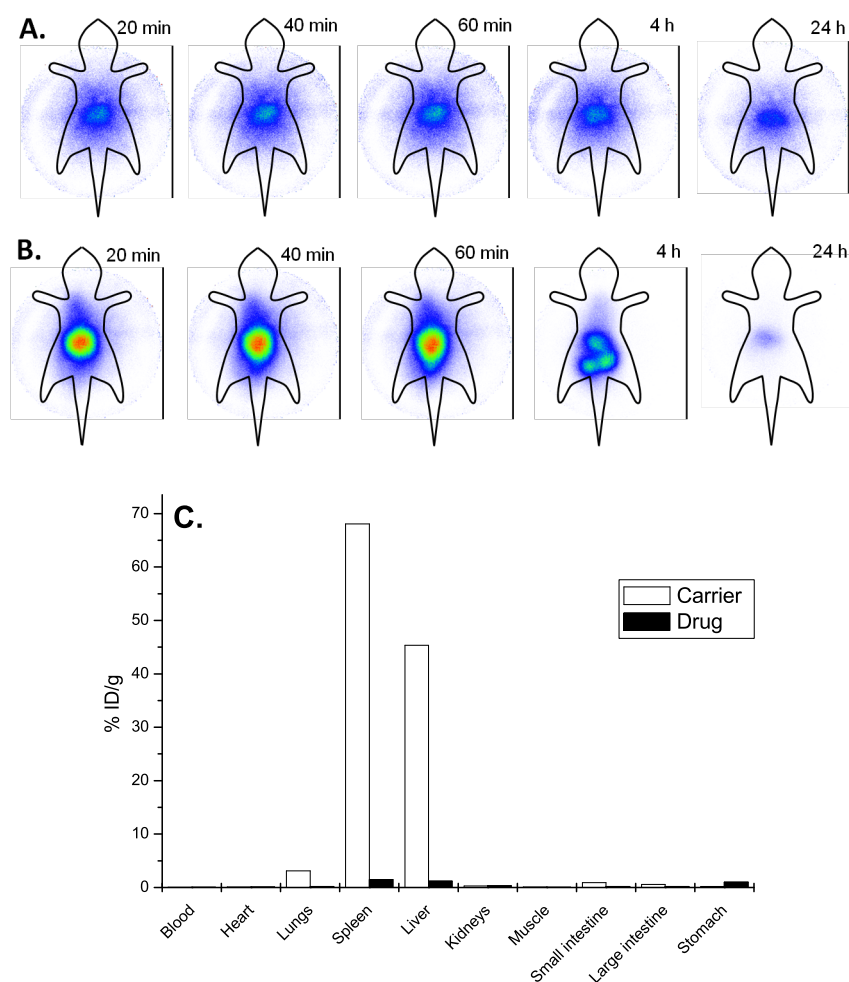


Figure 7.4: **A.** Bioimaging of ^{125}I FF loaded ^{111}In -DOTA-HN-PEG-PLA micelles showing carrier distribution. **B.** Bioimaging of ^{125}I FF loaded ^{111}In -DOTA-HN-PEG-PLA micelles showing drug distribution. **C.** Preliminary biodistribution of ^{125}I FF loaded ^{111}In -DOTA-HN-PEG-PLA micelles (n=1). Based on these distribution results the time points for the final biodistribution experiment was determined.

7.4.2.2 ^{111}In -DOTA-NH-PEG-PLA solution

The polymeric solution was dissolved in a formulation containing 5% DMSO, 45% PEG-200 and 50% PBS buffer as a control experiment. Bioimaging in Fig. 7.5A reported the recorded

scintigrams. Immediately upon injection (0-20 min) the liver-region and kidneys were stained by radioactivity. Simultaneously a strong signal was detectable in the bladder. Most of the injected activity was cleared from the organism within 2 h upon injection. Moreover, a weak signal was still detectable in the liver-region after 24 h. Subsequently the animal was sacrificed and the organs were analyzed (Fig. 7.5B). Biodistribution of radioactivity revealed a strong preference of lungs, spleen and liver for the radioactively labeled polymer. As expected from the scintigrams a signal in the kidneys was detected.

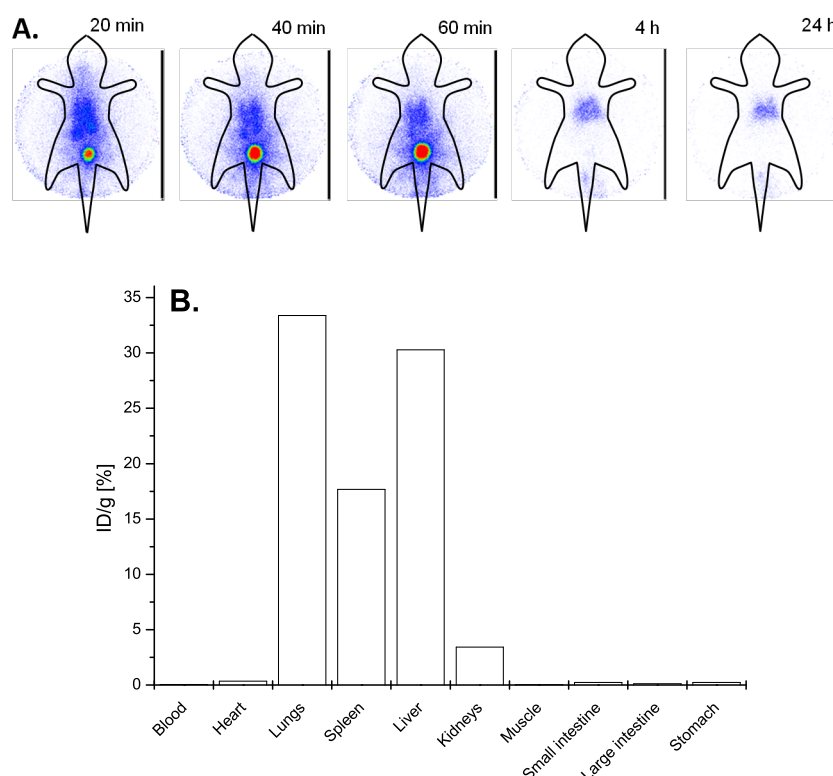


Figure 7.5: **A.** Bioimaging of ^{111}In -DOTA-NH-PEG-PLA solution (non-micellar). **B.** Biodistribution of ^{111}In -DOTA-HN-PEG-PLA polymer 24 h upon injection (n=1). This experiment was a control for the drug-loaded micelles group.

7.4.2.3 ^{111}In -DOTA-NH-PEG solution

As an additional control experiment the radioactively labeled hydrophilic part of the investigated block copolymer was investigated on biodistribution. The radiochemical purity for ^{111}In -DOTA-NH-PEG detected by ITLC was 80.9% (data not shown). This polymer was taken for further *in vivo* studies. The scintigrams in Fig. 57.6 showed the very rapid clearance of the labeled PEG (5.5 kDa) from the body. Clearly the kidneys were detectable 5 min upon

injection followed by a strong radioactive signal in the bladder (>20 min). As expected the biodistribution pattern 2 h upon injected showed a small remaining signal of radioactivity in the kidneys from which the major blood clearance mechanism appeared (Fig. 7.6B).

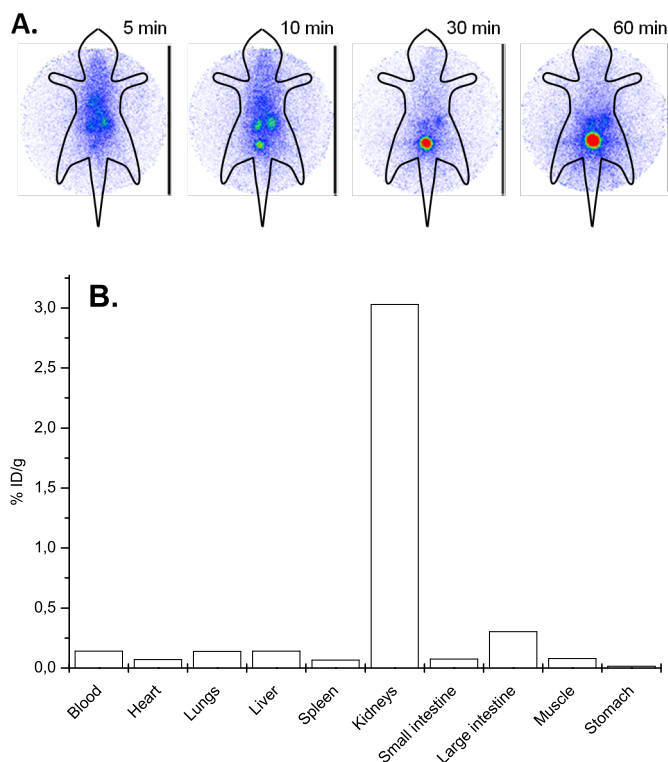


Figure 7.6: **A.** Bioimaging of ^{111}In -DOTA-NH-PEG solution. **B.** Biodistribution of ^{111}In -DOTA-NH-PEG 24 h upon injection (n=1). This experiment was a control for the biodistribution of drug-loaded micelles.

7.4.3 Biodistribution of dual-labeled polymeric micelles with ^{131}I FF payload in several animal groups of tumor-bearing mice

Based on the bioimaging data of the drug-loaded formulation the following time points for the biodistribution study were selected: 10 min, 30 min, 60 min, 2h and 24 h. At each of these time points 3 animals were sacrificed and analyzed for organ radioactivity. The results from the analyses are shown in Fig. 7.7.

Generally two methods were selected to present the acquired biodistribution data: %ID/g and %ID. Both modes of presentation offer different insights into the experiment. The %ID/g presentation respects the tissue selectivity of a drug/carrier system whereas %ID reported the quantitative distribution per organ. The data are presented in Fig. 7.7A and 7.7B

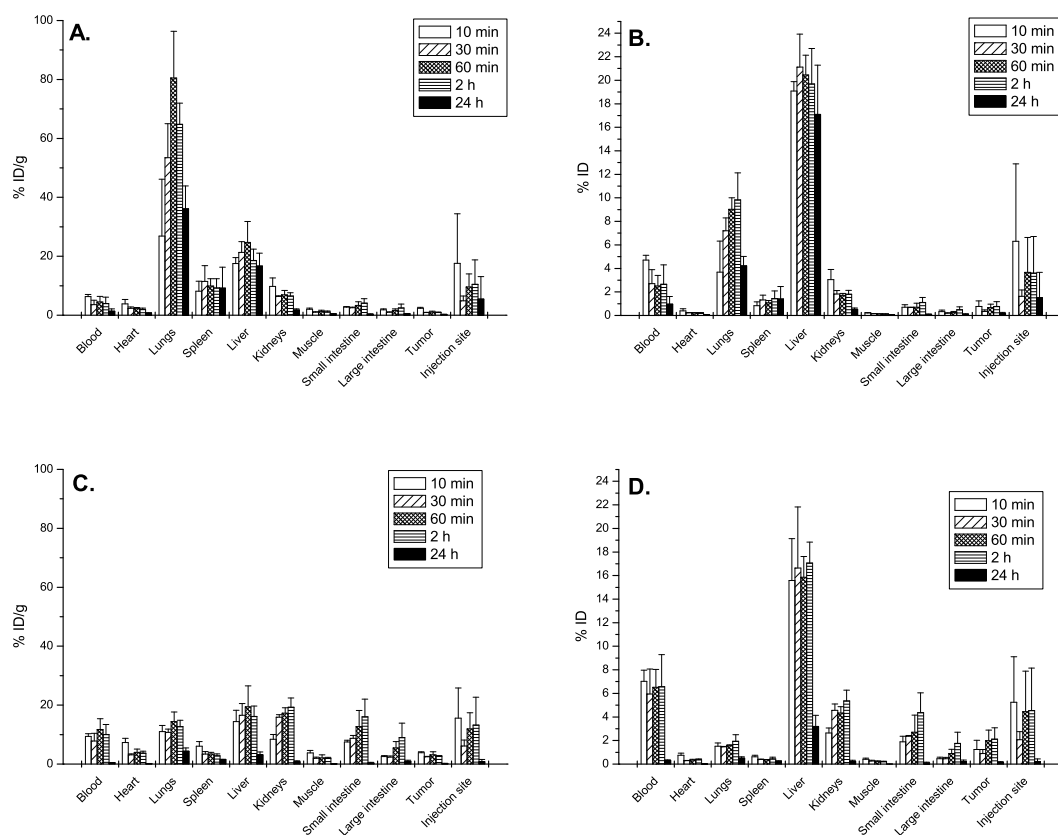


Figure 7.7: **A.** Biodistribution of polymeric carrier in % ID/g. **B.** Biodistribution of polymeric carrier in % ID. **C.** Biodistribution of IFF drug payload in % ID/g. **D.** Biodistribution of IFF drug payload in % ID.

for the biodistribution of the carrier system whereas Fig. 7.7C and 7.7D summarize drug biodistribution. It was obvious from the biodistribution data of the carrier that the lungs strongly accumulated the injected micelles (Fig. 7.7A). The signal in the lungs increased starting from 10 min upon injection ($\sim 26\%$ ID/g) to 1 h ($\sim 80\%$ ID/g) and decreased again until 24 h ($\sim 35\%$ ID/g). A similar progression of this trend could also be detected in the liver. In contrast to this, blood concentrations decreased over time compared to the initial concentration measured at 10 min. However, an increased tumor accumulation of the nanoparticles could not be detected. Focusing on the absolute biodistribution values of the carrier (Fig. 7.7B) the data revealed the strongest accumulation of the carrier in the liver followed by the lungs. 2 h post injection the quantitative radioactivity in lungs ($\sim 12\%$ ID) was more than half of that in the liver ($\sim 20\%$ ID). It was remarkable that radioactivity in the kidneys followed the trend of progression in the blood. Moreover, a certain percentage of ID remained at the site of injection.

The biodistribution for IFF was quite different to that of the carrier. The strong preference for the liver compared to the micellar carrier could not be found here (Fig. 7.7C). The organ preferences for the drug in lungs, liver and kidneys were quite equal over time. Unexpectedly the blood concentrations of the drug did not show a strong decay upon injection. Until 2 h post injection there was a drug plateau phase in the blood compartment which vanished after 24 h. Interestingly the tumor preference for the drug was similarly low as for the carrier (drug: $\sim 2\%$ ID/g, carrier: $\sim 1.5\%$). The absolute biodistribution pattern in Fig. 7.7D for the drug showed a strong overall accumulation of the drug in the liver which also resulted in a plateau over the first 2 h post injection. This plateau-phase was also present in blood and lungs. The absolute blood concentration was higher compared to the carrier (drug: $\sim 7\%$ ID, carrier: 2-5% ID). Unexpectedly an increasing progression of drug concentration over time could be found in the kidneys. Excretion and elimination of the drug could be followed by increasing concentrations in the intestinal system.

7.5 Discussion

The idea of successful passive drug targeting to disease modified tissue is based on 1) the long circulation of particles within the blood stream to utilize the EPR effect [131] and 2) the stability of drug encapsulation into the nanoparticulate cores [57]. Long circulation of polymeric micelles is achieved by covering the particle core with PEG [64] whereas the stability of encapsulation is generally assumed to be sufficiently high. However, when it was investigated that premature drug release could occur when the micelles' integrity was lost, the results pointed at blood components that could be responsible for this effect. Based on this hypothesis a couple of studies investigated the stability of micelles in serum [57, 45, 53] or blood [53]. For the selected polymeric materials in this study, a serum stability study prior to performing animal experiments was also employed and PEG-PLA micelles were found to be reasonably stable [57]. Besides a lack in colloidal stability, some groups already doubted that micelles stability would be the only mechanism which leads to premature drug release. They argued for diffusion/distribution of the drug from the micelles [214, 58]. Such observations were made from *in vivo* experiments by comparing the pharmacokinetic properties of the nanoparticulate carriers to those of drug solutions. A recent investigation by Letchford and Burt [87] had shown that rapid distribution processes upon injection of Paclitaxel loaded PEGylated polycaprolactone (PEG-PCL) micelles occurred. In their *in vivo* experiments the pharmacokinetic properties of drug encapsulated in PEG-PCL micelles were similar compared to the standard Taxol[®]-formulation which is composed of ethanol/Cremophor EL[®] as solubilizers. Given the lower stability of low molar mass surfactants (Cremophor EL[®]) these results were rather disappointing. Considering these findings, the goal of the study was to investigate the fate of the micellar carrier components and the encapsulated

drug simultaneously. For this purpose, H₂N-PEG-PLA was synthesized which was labeled via coupling ¹¹¹In-DOTA to the polymer backbone whereas the drug payload IFF was labeled with a radioactive iodine isotope (¹³¹I for biodistribution, ¹²⁵I for bioimaging). The different emission energies of the two iodine and indium labels allowed for the discrimination of carrier and drug distribution in a single *in vivo* experiment. Bioimaging was carried out to obtain a qualitative picture of the biodistribution. Furthermore, bioimaging allowed for checking the experimental setup and concept of dual-labeling: carrier distribution should be distinguishable from drug payload distribution in a single animal. The scintigrams confirmed that this was possible: The carrier (Fig. 7.4A) seemed to distribute directly upon injection into the liver while its rather diffuse distribution indicated empty circulating micelles. The IFF payload was found in the liver with a strong radioactive signal directly upon injection (Fig. 7.4B). The scintigrams showed a much lower diffusivity compared to the carrier scintigrams which is a first hint on the separation of drug and carrier distribution rapidly post injection. Concerning the strong liver accumulation of the carrier it is remarkable that, besides the lungs and kidneys, the liver is one of the organs with the highest blood flow [4]. Nanoparticles are known to preferentially accumulate in tissues with high perfusion [4]. Additional information which can be extracted from the bioimaging scintigrams are the excretion routes of the injected species. 24 h post injection the radioactivity for both species, carrier and payload, decreased compared to the initial imaging time points and for IFF drug nearly no activity was remaining in the animal. Once accumulated in the liver, the drug payload was excreted via the liver-bile-intestine pathway. This was expected due to the biodistribution results from IFF solution which were acquired in a previous study [245]. For the polymeric carrier this information was difficult to obtain from the scintigrams. For quantitative analyses a preliminary biodistribution experiment was performed at 24 h upon injection (Fig. 7.4C). The distribution pattern shows that the drug biodistribution did not follow the carrier system: this could be seen in several organs in which the carrier persisted (e.g. spleen, lungs, liver) but simultaneously nearly no drug was detectable in those organs. To confirm the separation of drug and carrier further biodistribution studies were performed. These studies especially focused on the elucidation of the time points at which this separation of biodistribution takes place *in vivo* and if carrier or drug reach tumor tissue sufficiently. Based on the bioimaging results a decision was made for investigating primarily earlier time points upon injection (<1 h). Consequently the first time point of analysis was set to 10 min post injection to portray the possible early differences. Drug-free ¹¹¹In-DOTA-NH-PEG-PLA solution was rapidly cleared from the blood and finally stained the kidneys and the liver-heart-lung-region (Fig. 7.5A). Shortly upon injection (20 min) the excretion of the polymer from the urinary bladder was detectable which increased up to 2 h upon injection. This observation was expected from the literature that single polymeric chains with molar masses below approximately 40-45 kDa were able to be excreted by free

renal filtration [12, 248]. Besides renal filtration, the polymer accumulated in liver and spleen (Fig. 7.5B). This was also not unexpected due to the known rapid blood clearance of macromolecules by the mononuclear phagocyte system (MPS) and was previously found for PAMAM dendrimers and HPMA [271]. ^{111}In -DOTA-NH-PEG solutions (Fig. 7.6A) in contrast are cleared extremely fast from blood and the body. 5 min upon injection the polymer was detectable in the kidneys and 10 min upon injection radioactivity could be found in the urinary bladder. 1 h post injection most of the radioactivity seemed to have been excreted into the urine. Moreover, 2 h post injection there was nearly no radioactivity remaining in the animal (kidneys $\sim 3\%$ ID/g, Fig. 7.6B). Summarizing both experiments from ^{111}In -DOTA-NH-PEG and ^{111}In -DOTA-NH-PEG-PLA it was obvious that the PLA derivative with a higher molar mass (~ 28 kDa) was partly excreted via the kidneys but increasingly accumulated in the organs with high activity of the RES. ^{111}In -DOTA-NH-PEG with a molar mass of ~ 5.5 kDa was excreted by free renal filtration. The biodistribution of the PEG derivative differed strongly from that of micelles whereas the PEG-PLA derivative came closer to it. This was probably a matter of using organic polymer solutions. Rapidly upon injection the organic solvent is diluted and PEG-PLA micelles form *in situ*. Pure PEGs are, however, not amphiphilic and therefore not able to form micelles. Bearing these biodistribution data of the control groups in mind, the drug loaded micellar system was investigated on its biodistribution and tumor targeting properties in disease modified mice. For this purpose the AR42J xenograft model for pancreatic cancer was selected. This model was previously selected for nanoparticle accumulation studies [272, 273]. Comparing carrier (Fig. 7.7A) and drug (Fig. 7.7C) biodistribution for organ selectivity it was clear that major differences could be found in the values for the lungs and the excretion mechanisms of drug and carrier (kidneys, intestines). The carrier accumulated strongly in the lungs whereas the drug concentration did not follow the carrier in this organ. Similar observations were found for the kidneys: carrier excretion via the kidneys decreased over time whereas drug excretion increased. Due to the hydrophobic nature of the drug and the previous study of intravenous injection (strong liver accumulation) [245] it was most probable that not the intact drug was renally excreted but a water soluble metabolite: IFF was derived from fenofibrate which was known to encounter an ester hydrolysis and was consequently metabolized to fenofibric acid and is usually coupled in rodents to glucuronic acid [274, 275]. These species were completely water soluble and consequently renally excreted. However, only a part of the drug was excreted renally in the studies, most prominent was excretion via the bile into the intestines. Apart from this, a very unusual distribution pattern was found in the blood: carrier concentration decreased over time (Fig. 7.7A and B) whereas drug concentration remained on a plateau for the first 2 h upon injection (Fig. 7.7C and D). An explanation for this could be the high hydrophobicity of IFF: The derivative fenofibrate already was highly hydrophobic ($\log P \sim 5.24$) [276]. Consequently the modification of the drug molecule by

substitution of the chlorine atom in fenofibrate in favour of iodine in IFF increased the drugs' hydrophobicity. Therefore it is not unlikely that distribution into adipose tissue appeared. Drug in adipose tissue served as a reservoir and could lead to the observed plateau phase. The general positive correlation between drug hydrophobicity and adipose tissue distribution was confirmed *in silico* and *in vivo* by Poulin et al. [277, 278]. Moreover, very remarkable issues were the tumor targeting properties of the injected particles. The biodistribution patterns clearly demonstrated that the micelles were not able to deliver the drug efficiently into the tumor. The overall exposure for carrier and drug was far below 5% ID/g at each investigated time point. As was shown by other groups, the blood circulation determined the tumor accumulation properties by the EPR effect: Heneweir et al. [279] described effective accumulation above 20 h of circulation whereas Pirollo and Chang [280] suggested necessary circulation times between 24 h and 48 h. Compared to these numbers in the present study, the circulation times were much lower (<24 h) and, therefore, an enhanced tumor accumulation could not be observed. As previously mentioned, encapsulation of the drug was carried out physically and based on hydrophobic interaction or π - π stacking between drug and polymer. Generally, even when the particles might have reached the tumor target, the question remained if they would be still drug loaded. As clearly demonstrated by the results, this physical encapsulation technique was not suitable to deliver a stable incorporation of the drug in the micellar core. Consequently a more direct interaction will be needed e.g. ionic interaction or chemical coupling of the drug to single polymer chains. Great success of the latter method even in humans was found for cisplatin which was attached to PEGylated poly-(glutamic acid) [281]. Compared to these results the concept of physical incorporation of drugs into self-assembling systems for targeted delivery seems to be difficult to reduce to practice.

7.6 Conclusion

The results of this study clearly demonstrate that self-assembling polymeric micelles are a suitable carrier for the solubilization of the hydrophobic model drug IFF. The encapsulation process was based on physical interactions between drug and carrier (no chemical coupling). Although the investigated PEG-PLA micelles exhibited a high stability in serum (*in vitro*) which was shown in the previous study, the *in vivo* experiments led to a completely different picture: Investigation of the loaded carrier in biodistribution experiments revealed that the carrier and the encapsulated drug followed different distribution routes rapidly upon injection. These separation processes of drug and carrier were very fast (<10 min). Moreover, due to these reasons an effective tumor targeting was not possible. Consequently physical loading of drugs by non-specific interactions (hydrogen bonding, π - π stacking) to the polymeric carrier seems to be a difficult approach to achieve an effective change on drug pharmacokinetics or

tumor accumulation. Stronger drug-polymer interactions (e.g. electrostatic encapsulation, chemical coupling) might be more appropriate to reach this goal.

Chapter 8

Summary and conclusion

Summary

This thesis focussed on the encapsulation of hydrophobic drugs into polymeric micelles and was intended to show the strengths and limitations of these self-assembling systems in terms of solubilization and drug targeting. Characterization of hydrophobic drug solubilization prior to intravenous injection was one of the key goals of this thesis. For this purpose a novel drug loading procedure was developed based on mechanistic considerations during the loading processes (**Chapter 2**). The cosolvent evaporation combined with appropriate solvent selection prior to preparation was found to be superior to other well investigated methods like direct dialysis and O/W emulsion techniques. This loading procedure was successfully developed for dexamethasone as a model drug but was further applied to all other investigated drugs in this thesis. Furthermore, storage stability of the micellar systems was acquired by lyophilization with excipients, showing that β -cyclodextrin derivatives are versatile lyoprotectors for these purposes.

Besides solubilization, the fate of micelles in biofluids was seen to hamper their application [8, 29]. For this purpose the existing literature was revisited especially on the question of micellar *in vivo* stability and accumulation into tumor tissue (**Chapter 1**). As a result it was found that colloidal systems undergo several stress factors upon injection that questions their stability of drug incorporation as well as the colloidal integrity itself. Moreover, tumor accumulation of colloidal systems with native appearance (before injection) of the particle shell was found to be very unlikely. It was argued for an active uptake mechanism into tumor tissue which could be triggered by the protein corona (e.g. albumin via gp-60 receptors in highly SPARC expressing tissues [150, 151]).

Based on these results it was reasonable to develop adequate *in vitro* tests prior to *in vivo* experiments to assess the micelles' stability and safety in biological systems. A serum incubation assay was selected to investigate stability which was based on FRET (Foerster Resonance Energy Transfer) (**Chapter 3**) and was previously described by Chen and Savic [53, 282]. Unfortunately, this assay lacked the possibility of quantifying micellar integrity and therefore to compare different micellar compositions. Consequently this test was further developed for this thesis and direct comparison between different micellar species could be made possible. Micellar safety and potential immunological responses were assessed with cytotoxicity studies and complement activation assays (**Chapter 4**). The results showed impressively that polymers like mPEG-PDLLA were non-toxic in the selected concentrations (up to 10 mg/mL) whereas already approved non-ionic surfactants (Cremophor EL[®], Tween 80[®]) showed distinct cytotoxicity on both tested cell types (HepG2 cell line, primary rat hepatocytes). The test polymer species PEG-PVPy which was not under previous investigations, showed a slight cytotoxicity in both assays. The complement activation assays revealed the liposomal product Doxil[®] as a stronger *in vitro* complement activator compared

to the investigated block copolymers. Consequently the safety and toxicity of micelles and their block copolymers did not exceed existing products based on colloidal carrier systems.

The experimental and theoretical results were very relevant prior to the conduction of *in vivo* experiments. Animal experiments were intended to show the potential of self-assembling micelles in drug targeting and altering pharmacokinetics of drugs compared to simple solutions. The first evidence that this concept of altering the pharmacokinetic profile might not fit to the polymeric micelles used in this thesis were delivered from compound A encapsulated in mPEG-PLGA micelles (**Chapter 5**). Besides successful preparation and solubilization (solubility increase by factor 180) the *in vivo* properties of the micellar formulation were identical to the drug solution of compound B (mesylate salt solution of compound A). An enhanced circulation and therefore drug targeting into tumors was not observed. The reasons for this *in vivo* observation of the compound A loaded micelles were not that clear so far from this experiment because only the drug was tracked *in vivo* by using an LC-MS method. No information was acquired about the polymeric carrier. For this reason a follow-up study was designed: drug and carrier should be tracked simultaneously. A H₂N-PEG-PLGA derivative was prepared, coupled to DOTA and labeled with ¹¹¹In. This procedure was quite successful and allowed for simultaneous detection with ¹²⁵IFF. Compound A and IFF are similarly hydrophobic but indeed show structural differences. Regardless of these differences, IFF is a model compound to probe the fate of micellar drugs upon injection. The bioimaging revealed remarkable qualitative biodistribution differences between polymeric carrier and encapsulated drug.

Different approaches were followed with the PEG-PVPy material: excellent drug loads with hydrophobic compounds were achieved but only little information was available concerning the *in vivo* properties of such micelles. To reveal biodistribution and clearance, as a first step the PEG-PVPy polymer was labeled within the hydrophobic part of the block copolymer because this species was easily accessible for radiolabeling by quarterization of the pyridine N (**Chapter 6**). As a disadvantage of this experimental setup can be seen that both species, polymer and drug, were labeled with a radioactive iodine isotope and consequently could not be discriminated. However, this approach showed that PEG-PVPy micelles circulated only within a short time frame (<1 h) but sustained over weeks in RES organs (e.g. liver: half life ~56 h). These results indicated the poor biodegradability of PEG-PVPy.

However, the approach for PEG-PLGA was further utilized to reveal the *in vivo* fate of carrier and drug (**Chapter 7**): the block copolymer was *de novo* synthesized and labeled at the PEG part by coupling to DOTA and chelating ¹¹¹In. In these ¹¹¹In labeled micelles, ¹³¹I or ¹²⁵I labeled IFF drug was incorporated. The different emission energies enabled to distinguish between drug and polymeric carrier. The major outcome of this study was the biodistribution difference of carrier and payload within the same animal. Rapidly upon injection the drug

exhibited a different biodistribution pattern compared to its carrier. As previously indicated in the chapters 5 and 6 the polymeric associates disassembled quickly.

Conclusive remarks and future perspective

Self-assembling polymeric micelles consisting of linear block copolymers are ideal systems for the solubilization of hydrophobic drugs and were pharmaceutically characterized in this thesis based on the following: 1) high drug loads were achieved e.g. with DXM in PEG-PVPy (~19%), 2) storage stability of this drug incorporation could be maintained by removing any water from the micelles by freeze-drying and 3) the selected block copolymers were toxicologically unproblematic.

From the *in vivo* studies it could be concluded that self-assembling systems like these polymeric micelles consisting of linear block copolymers were not able to carry the drug to its target site and/or to alter the pharmacokinetic properties compared to free drug. Premature release from these micelles due to the presence of blood proteins and other components was observed. These observations were not made with the *in vitro* test assaying micellar stability in serum. Consequently this experiment was revealed to be non-predictive for premature *in vivo* drug release. Possible reasons for this are the general differences between a static *in vitro* assay and a dynamic, complex *in vivo* system (e.g. blood volume and flow, particle opsonization followed by premature clearance). The idea of passive drug targeting is based on the long-circulating properties of particles assuming the stability of drug incorporation. However, self-assembling polymeric micelles do not seem to justify this expectation due to their fast release as shown in several animal studies within this thesis. Currently there are several strategies available to enhance the stability of the particles including their drug-loaded properties. These strategies focus on 1) increasing drug-polymer interactions (e.g. ionic interactions, covalent attachment of drug) or 2) increasing the particulate core rigidity (e.g. crosslinking). Both options are reasonable whereas for the latter one potential toxic chemical residues should be considered from particle preparation. Consequently the first approach will achieve more attention which can be seen in ongoing clinical trials with polypeptidic block copolymers and oppositely charged drugs (e.g. cisplatin, product in clinical trials: NK 6004 [281, 90]).

Generally from this thesis the questions remain open, if the concept of passive targeting based on the EPR effect can be successfully utilized by “simple” size/surface adjustment of the nanoparticles. Firstly, superior tumor accumulation could not be shown within the results from animal experiments although the often proposed size limits for nanoparticles below 200 nm [131] were always met. Secondly, it is generally questionable whether nanoparticles with their molar masses which are at least by factor 10^3 times higher compared to serum

proteins can extravasate effectively from the bloodstream only in artificial tumors (e.g. mice models). The currently available information concerning an EPR effect in natively growing tumor in humans is extremely limited. Regardless of these concerns, the achievement of long-circulating particles could be a valuable option to prolong the blood circulation of rapidly metabolized drugs or by reducing the free drug fraction of toxic drugs. In this connection, nanoparticles will pose a treatment advance by the formation of blood drug depots with sustained release. Future investigations will show if this is the major active principle of the already approved nanomedicines.

Bibliography

- [1] Mullard, A. (2011) 2010 FDA drug approvals. *Nature Reviews Drug Discovery* 10, 82–85.
- [2] Dimasi, J., Hansen, R., and Grabowski, H. (2003) The price of innovation: new estimates of drug development costs. *Journal of Health Economics* 22, 151–185.
- [3] Kola, I., and Landis, J. (2004) Can the pharmaceutical industry reduce attrition rates? *Nature Reviews Drug Discovery* 3, 711–715.
- [4] Bertrand, N., and Leroux, J. (2011) The journey of a drug-carrier in the body: An anatomo-physiological perspective. *J.Control Release* *In press*.
- [5] Lipinski, C. (2002) Poor aqueous solubility - an industry wide problem in drug discovery. *Am.Pharm.Rev.* 5, 82–85.
- [6] Di, L., Fish, P., and Mano, T. (2011) Bridging solubility between drug discovery and development. *Drug Discov.Today* 17, 486–495.
- [7] Kim, S., Kim, D., Shim, Y., Bang, J., Oh, H., Wan, K. S., and Seo, M. (2001) In vivo evaluation of polymeric micellar paclitaxel formulation: toxicity and efficacy. *J.Control Release* 72, 191–202.
- [8] Jones, M., and Leroux, J. (1999) Polymeric micelles - a new generation of colloidal drug carriers. *Eur.J.Pharm.Biopharm.* 48, 101–111.
- [9] Trivedi, R., and Kompella, U. (2010) Nanomicellar formulations for sustained drug delivery: strategies and underlying principles. *Nanomedicine (Lond)* 5, 485–505.
- [10] Hamidi, M., Shahbazi, M., and Rostamizadeh, K. (2012) Copolymers: efficient carriers for intelligent nanoparticulate drug targeting and gene therapy. *Macromol.Biosci.* 12, 144–164.
- [11] Miyata, K., Christie, R., and Kataoka, K. (2011) Polymeric micelles for nano-scale drug delivery. *Reactive & Functional Polymers* 71, 227–234.
- [12] Greish, K. (2010) Enhanced permeability and retention (EPR) effect for anticancer nanomedicine drug targeting. *Methods Mol.Biol.* 624, 25–37.

- [13] Kedar, U., Phutane, P., Shidhaye, S., and Kadam, V. (2010) Advances in Polymeric Micelles for Drug Delivery and Tumor Targeting. *Nanomedicine*. 6, 714–729.
- [14] Wang, J., Sui, M., and Fan, W. (2010) Nanoparticles for tumor targeted therapies and their pharmacokinetics. *Curr.Drug Metab* 11, 129–141.
- [15] Wang, D., Miller, S., Liu, X., Anderson, B., Wang, X., and Goldring, S. (2007) Novel dexamethasone-HPMA copolymer conjugate and its potential application in treatment of rheumatoid arthritis. *Arthritis Research & Therapy* 9, 1–9.
- [16] Matsumura, Y., and Maeda, H. (1986) A New Concept for Macromolecular Therapeutics in Cancer-Chemotherapy - Mechanism of Tumoritropic Accumulation of Proteins and the Antitumor Agent Smanacs. *Cancer Research* 46, 6387–6392.
- [17] Maeda, H., Sawa, T., and Konno, T. (2001) Mechanism of tumor-targeted delivery of macromolecular drugs, including the EPR effect in solid tumor and clinical overview of the prototype polymeric drug SMANCS. *Journal of Controlled Release* 74, 47–61.
- [18] Maeda, H. (2001) The enhanced permeability and retention (EPR) effect in tumor vasculature: The key role of tumor-selective macromolecular drug targeting. *Advances in Enzyme Regulation, Vol 41* 41, 189–207.
- [19] Tsukioka, Y., Matsumura, Y., Hamaguchi, T., Koike, H., Moriyasu, F., and Kakizoe, T. (2002) Pharmaceutical and biomedical differences between micellar doxorubicin (NK911) and liposomal doxorubicin (Doxil). *Japanese Journal of Cancer Research* 93, 1145–1153.
- [20] Bao, A., Goins, B., Klipper, R., Negrete, G., and Phillips, W. (2004) Direct Tc-99m labeling of pegylated liposomal doxorubicin (Doxil) for pharmacokinetic and non-invasive imaging studies. *Journal of Pharmacology and Experimental Therapeutics* 308, 419–425.
- [21] Patel, H., and Moghimi, S. (1998) Serum-mediated recognition of liposomes by phagocytic cells of the reticuloendothelial system - The concept of tissue specificity. *Adv.Drug Deliv.Rev.* 32, 45–60.
- [22] Moghimi, S., Muir, I., Illum, L., Davis, S., and Kolbachofen, V. (1993) Coating Particles with A Block-Copolymer (Poloxamine-908) Suppresses Opsonization But Permits the Activity of Dysopsonins in the Serum. *Biochimica et Biophysica Acta* 1179, 157–165.
- [23] Thiele, L., Diederichs, J., Reszka, R., Merkle, H., and Walter, E. (2003) Competitive adsorption of serum proteins at microparticles affects phagocytosis by dendritic cells. *Biomaterials* 24, 1409–1418.
- [24] Elwing, H., Askendal, A., and Lundstrom, I. (1987) Competition between adsorbed fibrinogen and high-molecular-weight kininogen on solid surfaces incubated in human

- plasma (the Vroman effect): influence of solid surface wettability. *J.Biomed.Mater.Res.* 21, 1023–1028.
- [25] Szebeni, J., Bedocs, P., Rozsnyay, Z., Weiszhar, Z., Urbanics, R., Rosivall, L., Cohen, R., Garbuzenko, O., Bathori, G., Toth, M., Bunger, R., and Barenholz, Y. (2012) Liposome-induced complement activation and related cardiopulmonary distress in pigs: factors promoting reactogenicity of Doxil and AmBisome. *Nanomedicine* 8, 176–184.
- [26] Chanan-Khan, A., Szebeni, J., Savay, S., Liebes, L., Rafique, N., Alving, C., and Muggia, F. (2003) Complement activation following first exposure to pegylated liposomal doxorubicin (Doxil): possible role in hypersensitivity reactions. *Ann.Oncol.* 14, 1430–1437.
- [27] Ishida, T., Atobe, K., Wang, X., and Kiwada, H. (2006) Accelerated blood clearance of PEGylated liposomes upon repeated injections: Effect of doxorubicin-encapsulation and high-dose first injection. *Journal of Controlled Release* 115, 251–258.
- [28] Torchilin, V. (2001) Structure and design of polymeric surfactant-based drug delivery systems. *Journal of Controlled Release* 73, 137–172.
- [29] Gaucher, G., Dufresne, M., Sant, V., Kang, N., Maysinger, D., and Leroux, J. (2005) Block copolymer micelles: preparation, characterization and application in drug delivery. *Journal of Controlled Release* 109, 169–188.
- [30] Mondon, K., Gurny, R., and Moller, M. (2008) Colloidal Drug Delivery Systems - Recent Advances With Polymeric Micelles. *Chimia* 62, 832–840.
- [31] Shi, B., Fang, C., You, M., Zhang, Y., Fu, S., and Pei, Y. (2005) Stealth MePEG-PCL micelles: effects of polymer composition on micelle physicochemical characteristics, in vitro drug release, in vivo pharmacokinetics in rats and biodistribution in S-180 tumor bearing mice. *Colloid and Polymer Science* 283, 954–967.
- [32] Cerritelli, S., O’Neil, C., Velluto, D., Fontana, A., Adrian, M., Dubochet, J., and Hubbell, J. (2009) Aggregation behavior of poly(ethylene glycol-bi-propylene sulfide) di- and triblock copolymers in aqueous solution. *Langmuir* 25, 11328–11335.
- [33] Yang, L., Zhao, Z., Wei, J., El, G. A., and Li, S. (2007) Micelles formed by self-assembling of polylactide/poly(ethylene glycol) block copolymers in aqueous solutions. *J.Colloid Interface Sci.* 314, 470–477.
- [34] Kim, S., Tan, J., Nederberg, F., Fukushima, K., Colson, J., Yang, C., Nelson, A., Yang, Y., and Hedrick, J. (2010) Hydrogen bonding-enhanced micelle assemblies for drug delivery. *Biomaterials* 31, 8063–8071.
- [35] Li, G., and Cho, C. (2008) CMC and dynamic properties of poly(VA-b-St) copolymer micelles for drug delivery. *Korean Journal of Chemical Engineering* 25, 1444–1447.

- [36] Yam, V., Hu, Y., Chan, K., and Chung, C. (2009) Reversible pH- and solvent-responsive micelle-mediated self-assembly of platinum(II) terpyridyl-based metallo-supramolecular diblock copolymers. *Chemical Communications* 6216–6218.
- [37] Attia, A., Ong, Z., Hedrick, J., Lee, P., Ee, P., Hammond, P., and Yang, Y. (2011) Mixed micelles self-assembled from block copolymers for drug delivery. *Current Opinion in Colloid & Interface Science* 16, 182–194.
- [38] Cao, J., Chen, Y., Chen, N., and Luo, X. (2010) The preparation of phosphorylcholine-containing poly(L-lactide) nanoparticles with solvent evaporation method. *E-Polymers e-resource*.
- [39] Zhang, J., Men, K., Gu, Y., Wang, X., Gou, M., Guo, G., Luo, F., and Qian, Z. (2011) Preparation of Core Cross-Linked PCL-PEG-PCL Micelles for Doxorubicin Delivery In Vitro. *Journal of Nanoscience and Nanotechnology* 11, 5054–5061.
- [40] Xiong, J., Meng, F., Wang, C., Cheng, R., Liu, Z., and Zhong, Z. (2011) Folate-conjugated crosslinked biodegradable micelles for receptor-mediated delivery of paclitaxel. *Journal of Materials Chemistry* 21, 5786–5794.
- [41] Wilhelm, M., Zhao, C., Wang, Y., Xu, R., Winnik, M., Mura, J., Riess, G., and Croucher, M. (1991) Poly(Styrene-Ethylene Oxide) Block Copolymer Micelle Formation in Water - A Fluorescence Probe Study. *Macromolecules* 24, 1033–1040.
- [42] Hans, M., Maxwell, C., Ehrlichman, R., Metzger, K., Liang, Y., Siegel, S., and Lowman, A. (2007) Evaluation of in vitro release and in vivo efficacy of mPEG-PLA-haloperidol conjugate micelle-like structures. *Journal of Biomedical Materials Research Part B-Applied Biomaterials* 83B, 422–430.
- [43] Cerritelli, S., Velluto, D., Hubbell, J. A., and Fontana, A. (2008) Breakdown kinetics of aggregates from poly(ethylene glycol-bi-propylene sulfide) di- and triblock copolymers induced by a non-ionic surfactant. *J.Polym.Sci.A Polym.Chem.* 46, 2477–2487.
- [44] Kastantin, M., Missirlis, D., Black, M., Ananthanarayanan, B., Peters, D., and Tirrell, M. (2010) Thermodynamic and Kinetic Stability of DSPE-PEG(2000) Micelles in the Presence of Bovine Serum Albumin. *Journal of Physical Chemistry B* 114, 12632–12640.
- [45] Lu, J., Owen, S., and Shoichet, M. (2011) Stability of Self-Assembled Polymeric Micelles in Serum. *Macromolecules* 44, 6002–6008.
- [46] Theodoly, O., Jacquin, M., Muller, P., and Chhun, S. (2009) Adsorption kinetics of amphiphilic diblock copolymers: from kinetically frozen colloids to macrosurfactants. *Langmuir* 25, 781–793.

-
- [47] Newkome, G. R., Moorefield, C. N., Baker, G. R., Saunders, M. J., and Grossman, S. H. (1991) Unimolecular Micelles. *Angew.Chem.Int.Ed.Engl.* 30, 1178–1180.
- [48] Liu, M., Kono, K., and Frechet, J. (2000) Water-soluble dendritic unimolecular micelles: their potential as drug delivery agents. *J Control Release* 65, 121–131.
- [49] Heise, A., Hedrick, J. L., Frank, C. W., and Miller, R. D. (1999) Starlike Block Copolymers with Amphiphilic Arms as Models for Unimolecular Micelles. *J.Am.Chem.Soc.* 121, 8647–8648.
- [50] Kainthan, R., Mugabe, C., Burt, H., and Brooks, D. (2008) Unimolecular micelles based on hydrophobically derivatized hyperbranched polyglycerols: ligand binding properties. *Biomacromolecules* 9, 886–895.
- [51] Matsumura, Y., Hamaguchi, T., Ura, T., Muro, K., Yamada, Y., Shimada, Y., Shirao, K., Okusaka, T., Ueno, H., Ikeda, M., and Watanabe, N. (2004) Phase I clinical trial and pharmacokinetic evaluation of NK911, a micelle-encapsulated doxorubicin. *British Journal of Cancer* 91, 1775–1781.
- [52] Hamaguchi, T., Kato, K., Yasui, H., Morizane, C., Ikeda, M., Ueno, H., Muro, K., Yamada, Y., Okusaka, T., Shirao, K., Shimada, Y., Nakahama, H., and Matsumura, Y. (2007) A phase I and pharmacokinetic study of NK105, a paclitaxel-incorporating micellar nanoparticle formulation. *British Journal of Cancer* 97, 170–176.
- [53] Chen, H., Kim, S., He, W., Wang, H., Low, P., Park, K., and Cheng, J. (2008) Fast release of lipophilic agents from circulating PEG-PDLLA micelles revealed by in vivo forster resonance energy transfer imaging. *Langmuir* 24, 5213–5217.
- [54] Blunk, T., Hochstrasser, D., Sanchez, J., Muller, B., and Muller, R. (1993) Colloidal carriers for intravenous drug targeting: plasma protein adsorption patterns on surface-modified latex particles evaluated by two-dimensional polyacrylamide gel electrophoresis. *Electrophoresis* 14, 1382–1387.
- [55] Luck, M., Paulke, B., Schroder, W., Blunk, T., and Muller, R. (1998) Analysis of plasma protein adsorption on polymeric nanoparticles with different surface characteristics. *J.Biomed.Mater.Res.* 39, 478–485.
- [56] Thode, K., Luck, M., Schroder, W., Semmler, W., Blunk, T., Muller, R., and Kresse, M. (1997) The influence of the sample preparation on plasma protein adsorption patterns on polysaccharide-stabilized iron oxide particles and N-terminal microsequencing of unknown proteins. *J.Drug Target* 5, 35–43.
- [57] Miller, T., Rachel, R., Besheer, A., Uezguen, S., Weigandt, M., and Goepferich, A. (2012) Comparative Investigations on In Vitro Serum Stability of Polymeric Micelle Formulations. *Pharm.Res.* 29, 448–459.

- [58] Aliabadi, H., Brocks, D., Mahdipoor, P., and Lavasanifar, A. (2007) A novel use of an in vitro method to predict the in vivo stability of block copolymer based nano-containers. *J.Control Release* 122, 63–70.
- [59] Jette, K., Law, D., Schmitt, E., and Kwon, G. (2004) Preparation and drug loading of poly(ethylene glycol)-block-poly(epsilon-caprolactone) micelles through the evaporation of a cosolvent azeotrope. *Pharm.Res.* 21, 1184–1191.
- [60] Vroman, L. (1962) Effect of Adsorbed Proteins on the Wettability of Hydrophilic and Hydrophobic Solids. *Nature* 196, 476–477.
- [61] Slack, S., Bohnert, J., and Horbett, T. (1987) The effects of surface chemistry and coagulation factors on fibrinogen adsorption from plasma. *Ann.N.Y.Acad.Sci.* 516, 223–243.
- [62] Horbett, T. (1984) Mass action effects on competitive adsorption of fibrinogen from hemoglobin solutions and from plasma. *Thromb.Haemost.* 51, 174–181.
- [63] Brash, J., and ten, H. P. (1984) Effect of plasma dilution on adsorption of fibrinogen to solid surfaces. *Thromb.Haemost.* 51, 326–330.
- [64] Owens, D., and Peppas, N. (2006) Opsonization, biodistribution, and pharmacokinetics of polymeric nanoparticles. *International Journal of Pharmaceutics* 307, 93–102.
- [65] Weber, M., Bujotzek, A., Andrae, K., Weinhart, M., and Haag, R. (2011) Computational entropy estimation of linear polyether-modified surfaces and correlation with protein resistant properties of such surfaces. *Molecular Simulation* 37, 899–906.
- [66] Lasic, D. D., Woodle, M. C., and Papahadjopoulos, D. (1992) On the Molecular Mechanism of Steric Stabilization of Liposomes in Biological Fluids. *Journal of Liposome Research* 2, 335–353.
- [67] Moghimi, S., and Patel, H. (1989) Serum opsonins and phagocytosis of saturated and unsaturated phospholipid liposomes. *Biochim.Biophys.Acta* 984, 384–387.
- [68] Patel, H., Tuzel, N., and Ryman, B. (1983) Inhibitory Effect of Cholesterol on the Uptake of Liposomes by Liver and Spleen. *Biochimica et Biophysica Acta* 761, 142–151.
- [69] Moghimi, S., and Patel, H. (1988) Tissue specific opsonins for phagocytic cells and their different affinity for cholesterol-rich liposomes. *FEBS Lett.* 233, 143–147.
- [70] Moghimi, S., and Patel, H. (1996) Altered tissue-specific opsonic activities and opsonorecognition of liposomes in tumour-bearing rats. *Biochim.Biophys.Acta* 1285, 56–64.
- [71] Moghimi, S., and Patel, H. (1990) Calcium as a possible modulator of Kupffer cell phagocytic function by regulating liver-specific opsonic activity. *Biochim.Biophys.Acta* 1028, 304–308.

-
- [72] Ogawara, K., Yoshida, M., Takakura, Y., Hashida, M., Higaki, K., and Kimura, T. (1999) Interaction of polystyrene microspheres with liver cells: roles of membrane receptors and serum proteins. *Biochimica et Biophysica Acta-General Subjects* 1472, 165–172.
- [73] Johnstone, S., Masin, D., Mayer, L., and Bally, M. (2001) Surface-associated serum proteins inhibit the uptake of phosphatidylserine and poly(ethylene glycol) liposomes by mouse macrophages. *Biochimica et Biophysica Acta-Biomembranes* 1513, 25–37.
- [74] Vert, M., and Domurado, D. (2000) Poly(ethylene glycol): Protein-repulsive or albumin-compatible? *Journal of Biomaterials Science-Polymer Edition* 11, 1307–1317.
- [75] Tenzer, S. et al. (2011) Nanoparticle Size Is a Critical Physicochemical Determinant of the Human Blood Plasma Corona: A Comprehensive Quantitative Proteomic Analysis. *Acs Nano* 5, 7155–7167.
- [76] Emmenegger, C., Brynda, E., Riedel, T., Sedlakova, Z., Houska, M., and Alles, A. (2009) Interaction of Blood Plasma with Antifouling Surfaces. *Langmuir* 25, 6328–6333.
- [77] Schmaier, A., Silver, L., Adams, A., Fischer, G., Munoz, P., Vroman, L., and Colman, R. (1984) The effect of high molecular weight kininogen on surface-adsorbed fibrinogen. *Thromb.Res.* 33, 51–67.
- [78] Unsworth, L., Sheardown, H., and Brash, J. (2005) Polyethylene oxide surfaces of variable chain density by chemisorption of PEO-thiol on gold: adsorption of proteins from plasma studied by radiolabelling and immunoblotting. *Biomaterials* 26, 5927–5933.
- [79] Goppert, T., and Muller, R. (2005) Adsorption kinetics of plasma proteins on solid lipid nanoparticles for drug targeting. *Int.J.Pharm.* 302, 172–186.
- [80] Goppert, T., and Muller, R. (2005) Protein adsorption patterns on poloxamer- and poloxamine-stabilized solid lipid nanoparticles (SLN). *Eur.J.Pharm.Biopharm.* 60, 361–372.
- [81] Harada, Y., Yamamoto, T., Sakai, M., Saiki, T., Kawano, K., Maitani, Y., and Yokoyama, M. (2011) Effects of organic solvents on drug incorporation into polymeric carriers and morphological analyses of drug-incorporated polymeric micelles. *International Journal of Pharmaceutics* 404, 271–280.
- [82] Diezi, T., Bae, Y., and Kwon, G. (2010) Enhanced Stability of PEG-block-poly(N-hexyl stearate L-aspartamide) Micelles in the Presence of Serum Proteins. *Molecular Pharmaceutics* 7, 1355–1360.
- [83] Woodle, M., Newman, M., and Cohen, J. (1994) Sterically Stabilized Liposomes - Physical and Biological Properties. *Journal of Drug Targeting* 2, 397–403.

- [84] Ritchie, T., and Macdonald, S. (2009) The impact of aromatic ring count on compound developability - are too many aromatic rings a liability in drug design? *Drug Discovery Today* 14, 1011–1020.
- [85] Burt, H., Zhang, X., Toleikis, P., Embree, L., and Hunter, W. (1999) Development of copolymers of poly(D,L-lactide) and methoxypolyethylene glycol as micellar carriers of paclitaxel. *Colloids and Surfaces B-Biointerfaces* 16, 161–171.
- [86] Letchford, K., Liggins, R., Wasan, K., and Burt, H. (2009) In vitro human plasma distribution of nanoparticulate paclitaxel is dependent on the physicochemical properties of poly(ethylene glycol)-block-poly(caprolactone) nanoparticles. *European Journal of Pharmaceutics and Biopharmaceutics* 71, 196–206.
- [87] Letchford, K., and Burt, H. (2012) Copolymer micelles and nanospheres with different in vitro stability demonstrate similar Paclitaxel pharmacokinetics. *Mol.Pharm.* 9, 248–260.
- [88] Kumar, G., Walle, U., Bhalla, K., and Walle, T. (1993) Binding of Taxol to Human Plasma, Albumin and Alpha-1-Acid Glycoprotein. *Research Communications in Chemical Pathology and Pharmacology* 80, 337–344.
- [89] Liu, J., Zeng, F., and Allen, C. (2005) Influence of serum protein on polycarbonate-based copolymer micelles as a delivery system for a hydrophobic anti-cancer agent. *J.Control Release* 103, 481–497.
- [90] Uchino, H., Matsumura, Y., Negishi, T., Koizumi, F., Hayashi, T., Honda, T., Nishiyama, N., Kataoka, K., Naito, S., and Kakizoe, T. (2005) Cisplatin-incorporating polymeric micelles (NC-6004) can reduce nephrotoxicity and neurotoxicity of cisplatin in rats. *Br.J.Cancer* 93, 678–687.
- [91] Rybak-Smith, M., and Sim, R. (2011) Complement activation by carbon nanotubes. *Advanced Drug Delivery Reviews* 63, 1031–1041.
- [92] Meerasa, A., Huang, J., and Gu, F. (2011) CH(50): A Revisited Hemolytic Complement Consumption Assay for Evaluation of Nanoparticles and Blood Plasma Protein Interaction. *Current Drug Delivery* 8, 290–298.
- [93] Karmali, P., and Simberg, D. (2011) Interactions of nanoparticles with plasma proteins: implication on clearance and toxicity of drug delivery systems. *Expert Opinion on Drug Delivery* 8, 343–357.
- [94] Zolnik, B., Gonzalez-Fernandez, A., Sadrieh, N., and Dobrovolskaia, M. (2010) Minireview: Nanoparticles and the Immune System. *Endocrinology* 151, 458–465.
- [95] Vasir, J., and Labhasetwar, V. (2006) Polymeric nanoparticles for gene delivery. *Expert.Opin.Drug Deliv.* 3, 325–344.

-
- [96] Szebeni, J. (2005) Complement activation-related pseudoallergy: a new class of drug-induced acute immune toxicity. *Toxicology* 216, 106–121.
- [97] Szebeni, J. (2001) Complement activation-related pseudoallergy caused by liposomes, micellar carriers of intravenous drugs, and radiocontrast agents. *Crit Rev. Ther. Drug Carrier Syst.* 18, 567–606.
- [98] Szebeni, J., Muggia, F., Gabizon, A., and Barenholz, Y. (2011) Activation of complement by therapeutic liposomes and other lipid excipient-based therapeutic products: Prediction and prevention. *Adv. Drug Deliv. Rev.* 63, 1020–1030.
- [99] Szebeni, J., Baranyi, L., Savay, S., Milosevits, J., Bodo, M., Bunger, R., and Alving, C. (2003) The interaction of liposomes with the complement system: in vitro and in vivo assays. *Methods Enzymol.* 373, 136–154.
- [100] Szebeni, J., Baranyi, L., Savay, S., Milosevits, J., Bunger, R., Laverman, P., Metselaar, J., Storm, G., Chanan-Khan, A., Liebes, L., Muggia, F., Cohen, R., Barenholz, Y., and Alving, C. (2002) Role of complement activation in hypersensitivity reactions to doxil and HYNICPEG liposomes: Experimental and clinical studies. *Journal of Liposome Research* 12, 165–172.
- [101] Yang, A., Liu, W., Li, Z., Jiang, L., Xu, H., and Yang, X. (2010) Influence of Polyethyleneglycol Modification on Phagocytic Uptake of Polymeric Nanoparticles Mediated by Immunoglobulin G and Complement Activation. *Journal of Nanoscience and Nanotechnology* 10, 622–628.
- [102] Shan, X., Yuan, Y., Liu, C., Tao, X., Sheng, Y., and Xu, F. (2009) Influence of PEG chain on the complement activation suppression and longevity in vivo prolongation of the PCL biomedical nanoparticles. *Biomed. Microdevices.* 11, 1187–1194.
- [103] Yang, A., Liu, W., Li, Z., Jiang, L., Xu, H., and Yang, X. (2010) Influence of Polyethyleneglycol Modification on Phagocytic Uptake of Polymeric Nanoparticles Mediated by Immunoglobulin G and Complement Activation. *Journal of Nanoscience and Nanotechnology* 10, 622–628.
- [104] Chen, A., Kozak, D., Battersby, B., and Trau, M. (2008) Particle-by-particle quantification of protein adsorption onto poly(ethylene glycol) grafted surfaces. *Biofouling* 24, 267–273.
- [105] Gaucher, G., Asahina, K., Wang, J., and Leroux, J. (2009) Effect of Poly(N-vinylpyrrolidone)-block-poly(D,L-lactide) as Coating Agent on the Opsonization, Phagocytosis, and Pharmacokinetics of Biodegradable Nanoparticles. *Biomacromolecules* 10, 408–416.

- [106] Moghimi, S., and Szebeni, J. (2003) Stealth liposomes and long circulating nanoparticles: critical issues in pharmacokinetics, opsonization and protein-binding properties. *Progress in Lipid Research* 42, 463–478.
- [107] Richter, A., and Akerblom, E. (1983) Antibodies against polyethylene glycol produced in animals by immunization with monomethoxy polyethylene glycol modified proteins. *Int.Arch.Allergy Appl.Immunol.* 70, 124–131.
- [108] Richter, A., and Akerblom, E. (1984) Polyethylene glycol reactive antibodies in man: titer distribution in allergic patients treated with monomethoxy polyethylene glycol modified allergens or placebo, and in healthy blood donors. *Int.Arch.Allergy Appl.Immunol.* 74, 36–39.
- [109] Ganson, N., Kelly, S., Scarlett, E., Sundy, J., and Hershfield, M. (2006) Control of hyperuricemia in subjects with refractory gout, and induction of antibody against poly(ethylene glycol) (PEG), in a phase I trial of subcutaneous PEGylated urate oxidase. *Arthritis Res.Ther.* 8, R12.
- [110] Armstrong, J., Hempel, G., Koling, S., Chan, L., Fisher, T., Meiselman, H., and Garratty, G. (2007) Antibody against poly(ethylene glycol) adversely affects PEG-asparaginase therapy in acute lymphoblastic leukemia patients. *Cancer* 110, 103–111.
- [111] Ishida, T., Ichihara, M., Wang, X., and Kiwada, H. (2006) Spleen plays an important role in the induction of accelerated blood clearance of PEGylated liposomes. *Journal of Controlled Release* 115, 243–250.
- [112] Ishida, T., Ichihara, M., Wang, X., Yamamoto, K., Kimura, J., Majima, E., and Kiwada, H. (2006) Injection of PEGylated liposomes in rats elicits PEG-specific IgM, which is responsible for rapid elimination of a second dose of PEGylated liposomes. *Journal of Controlled Release* 112, 15–25.
- [113] Koide, H., Asai, T., Hatanaka, K., Akai, S., Ishii, T., Kenjo, E., Ishida, T., Kiwada, H., Tsukada, H., and Oku, N. (2010) T cell-independent B cell response is responsible for ABC phenomenon induced by repeated injection of PEGylated liposomes. *Int.J Pharm.* 392, 218–223.
- [114] Romberg, B., Oussoren, C., Snel, C., Carstens, M., Hennink, W., and Storm, G. (2007) Pharmacokinetics of poly(hydroxyethyl-L-asparagine)-coated liposomes is superior over that of PEG-coated liposomes at low lipid dose and upon repeated administration. *Biochimica et Biophysica Acta-Biomembranes* 1768, 737–743.
- [115] Ishihara, T. et al. (2009) Accelerated Blood Clearance Phenomenon Upon Repeated Injection of PEG-modified PLA-nanoparticles. *Pharmaceutical Research* 26, 2270–2279.

-
- [116] Tagami, T., Uehara, Y., Moriyoshi, N., Ishida, T., and Kiwada, H. (2011) Anti-PEG IgM production by siRNA encapsulated in a PEGylated lipid nanocarrier is dependent on the sequence of the siRNA. *J Control Release* 151, 149–154.
- [117] Koide, H., Asai, T., Hatanaka, K., Urakami, T., Ishii, T., Kenjo, E., Nishihara, M., Yokoyama, M., Ishida, T., Kiwada, H., and Oku, N. (2008) Particle size-dependent triggering of accelerated blood clearance phenomenon. *Int.J Pharm.* 362, 197–200.
- [118] Liu, Y., Reidler, H., Pan, J., Milunic, D., Qin, D., Chen, D., Vallejo, Y., and Yin, R. (2011) A double antigen bridging immunogenicity ELISA for the detection of antibodies to polyethylene glycol polymers. *J Pharmacol.Toxicol.Methods* 64, 238–245.
- [119] Talekar, M., Kendall, J., Denny, W., and Garg, S. (2011) Targeting of nanoparticles in cancer: drug delivery and diagnostics. *Anti-Cancer Drugs* 22, 949–962.
- [120] Barreto, J., O'Malley, W., Kubeil, M., Graham, B., Stephan, H., and Spiccia, L. (2011) Nanomaterials: Applications in Cancer Imaging and Therapy. *Adv.Mater.* 23, H18–H40.
- [121] Maeda, H., Bharate, G., and Daruwalla, J. (2009) Polymeric drugs for efficient tumor-targeted drug delivery based on EPR-effect. *European Journal of Pharmaceutics and Biopharmaceutics* 71, 409–419.
- [122] Maeda, H. (2010) Tumor-selective delivery of macromolecular drugs via the EPR effect: background and future prospects. *Bioconjg.Chem.* 21, 797–802.
- [123] Maeda, H., Greish, K., and Fang, J. (2006) The EPR effect and polymeric drugs: A paradigm shift for cancer chemotherapy in the 21st century. *Polymer Therapeutics II: Polymers As Drugs, Conjugates and Gene Delivery Systems* 193, 103–121.
- [124] Maeda, H., Fang, J., Inutsuka, T., and Kitamoto, Y. (2003) Vascular permeability enhancement in solid tumor: various factors, mechanisms involved and its implications. *Int.Immunopharmacol.* 3, 319–328.
- [125] Maeda, H., Bharate, G., and Daruwalla, J. (2009) Polymeric drugs for efficient tumor-targeted drug delivery based on EPR-effect. *Eur.J Pharm.Biopharm.* 71, 409–419.
- [126] Iyer, A., Khaled, G., Fang, J., and Maeda, H. (2006) Exploiting the enhanced permeability and retention effect for tumor targeting. *Drug Discov.Today* 11, 812–818.
- [127] Dellian, M., Yuan, F., Trubetskoy, V., Torchilin, V., and Jain, R. (2000) Vascular permeability in a human tumour xenograft: molecular charge dependence. *Br.J.Cancer* 82, 1513–1518.
- [128] Kobayashi, A., Oda, T., and Maeda, H. (1988) Protein Binding of Macromolecular Anticancer Agent SMANCS: Characterization of Poly(styrene-co-maleic acid) Derivatives as an Albumin Binding Ligand. *Journal of Bioactive and Compatible Polymers* 3, 319–333.

- [129] Maeda, H. (2001) SMANCS and polymer-conjugated macromolecular drugs: advantages in cancer chemotherapy. *Advanced Drug Delivery Reviews* 46, 169–185.
- [130] Pimm, M., and Hudecz, F. (1996) Biodistribution in tumour-bearing mice of polycationic, amphoteric and polyanionic branched polypeptides with a poly(L-lysine) backbone labelled with I-125 and In-111: Tumour accumulation less than that of labelled serum proteins. *Journal of Cancer Research and Clinical Oncology* 122, 45–54.
- [131] Torchilin, V. (2007) Micellar nanocarriers: pharmaceutical perspectives. *Pharm.Res.* 24, 1–16.
- [132] Dreher, M., Liu, W., Michelich, C., Dewhirst, M., Yuan, F., and Chilkoti, A. (2006) Tumor vascular permeability, accumulation, and penetration of macromolecular drug carriers. *Journal of the National Cancer Institute* 98, 335–344.
- [133] Kwon, G., Suwa, S., Yokoyama, M., Okano, T., Sakurai, Y., and Kataoka, K. (1994) Enhanced Tumor Accumulation and Prolonged Circulation Times of Micelle-Forming Poly(Ethylene Oxide-Aspartate) Block Copolymer-Adriamycin Conjugates. *Journal of Controlled Release* 29, 17–23.
- [134] Iyer, A., Greish, K., Seki, T., Okazaki, S., Fang, J., Takeshita, K., and Maeda, H. (2007) Polymeric micelles of zinc protoporphyrin for tumor targeted delivery based on EPR effect and singlet oxygen generation. *J Drug Target* 15, 496–506.
- [135] Ahmed, F., Pakunlu, R., Srinivas, G., Brannan, A., Bates, F., Klein, M., Minko, T., and Discher, D. (2006) Shrinkage of a rapidly growing tumor by drug-loaded polymersomes: pH-triggered release through copolymer degradation. *Mol.Pharm.* 3, 340–350.
- [136] Savla, R., Taratula, O., Garbuzenko, O., and Minko, T. (2011) Tumor targeted quantum dot-mucin 1 aptamer-doxorubicin conjugate for imaging and treatment of cancer. *Journal of Controlled Release* 153, 16–22.
- [137] Ishida, O., Maruyama, K., Sasaki, K., and Iwatsuru, M. (1999) Size-dependent extravasation and interstitial localization of polyethyleneglycol liposomes in solid tumor-bearing mice. *Int.J.Pharm.* 190, 49–56.
- [138] Hobbs, S., Monsky, W., Yuan, F., Roberts, W., Griffith, L., Torchilin, V., and Jain, R. (1998) Regulation of transport pathways in tumor vessels: role of tumor type and microenvironment. *Proc.Natl.Acad.Sci.U.S.A* 95, 4607–4612.
- [139] Zhao, M., Yang, M., Ma, H., Li, X., Tan, X., Li, S., Yang, Z., and Hoffman, R. (2006) Targeted therapy with a Salmonella typhimurium leucine-arginine auxotroph cures orthotopic human breast tumors in nude mice. *Cancer Res.* 66, 7647–7652.
- [140] Yuan, F., Dellian, M., Fukumura, D., Leunig, M., Berk, D., Torchilin, V., and Jain, R.

- (1995) Vascular permeability in a human tumor xenograft: molecular size dependence and cutoff size. *Cancer Res.* 55, 3752–3756.
- [141] Xiao, K., Luo, J., Li, Y., Xiao, W., Lee, J., Gonik, A., and Lam, K. (2010) The Passive Targeting of Polymeric Micelles in Various Types and Sizes of Tumor Models. *Nanoscience and Nanotechnology Letters* 2, 79–85.
- [142] Feng, D., Nagy, J., Dvorak, A., and Dvorak, H. (2000) Different pathways of macromolecule extravasation from hyperpermeable tumor vessels. *Microvasc.Res.* 59, 24–37.
- [143] Stehle, G., Sinn, H., Wunder, A., Schrenk, H., Stewart, J., Hartung, G., Maier-Borst, W., and Heene, D. (1997) Plasma protein (albumin) catabolism by the tumor itself—implications for tumor metabolism and the genesis of cachexia. *Crit Rev.Oncol.Hematol.* 26, 77–100.
- [144] Wunder, A., Stehle, G., Sinn, H., Schrenk, H., Hoffbiederbeck, D., Bader, F., Friedrich, E., Peschke, P., Maierborst, W., and Heene, D. (1997) Enhanced albumin uptake by rat tumors. *Int.J.Oncol.* 11, 497–507.
- [145] Wilkinson, P., Jeremy, R., Brooks, F., and Hollander, J. L. (1965) Mechanism of Hypoalbuminemia in Rheumatoid Arthritis. *Annals of Internal Medicine* 63, 109–114.
- [146] Wang, D., and Goldring, S. (2011) The bone, the joints and the Balm of Gilead. *Mol.Pharm.* 8, 991–993.
- [147] Zhou, Q., Wood, R., Schwarz, E., Wang, Y., and Xing, L. (2010) Near-infrared lymphatic imaging demonstrates the dynamics of lymph flow and lymphangiogenesis during the acute versus chronic phases of arthritis in mice. *Arthritis Rheum.* 62, 1881–1889.
- [148] Maruotti, N., Cantatore, F., Crivellato, E., Vacca, A., and Ribatti, D. (2006) Angiogenesis in rheumatoid arthritis. *Histol.Histopathol.* 21, 557–566.
- [149] Quan, L., Purdue, P., Liu, X., Boska, M., Lele, S., Thiele, G., Mikuls, T., Dou, H., Goldring, S., and Wang, D. (2010) Development of a macromolecular prodrug for the treatment of inflammatory arthritis: mechanisms involved in arthrotropism and sustained therapeutic efficacy. *Arthritis Res.Ther.* 12, R170–.
- [150] Desai, N., Trieu, V., Yao, Z., Louie, L., Ci, S., Yang, A., Tao, C., De, T., Beals, B., Dykes, D., Noker, P., Yao, R., Labao, E., Hawkins, M., and Soon-Shiong, P. (2006) Increased antitumor activity, intratumor paclitaxel concentrations, and endothelial cell transport of cremophor-free, albumin-bound paclitaxel, ABI-007, compared with cremophor-based paclitaxel. *Clin.Cancer Res.* 12, 1317–1324.
- [151] Desai, N., Trieu, V., Damascelli, B., and Soon-Shiong, P. (2009) SPARC Expression Correlates with Tumor Response to Albumin-Bound Paclitaxel in Head and Neck Cancer Patients. *Transl.Oncol.* 2, 59–64.

- [152] Jendraschak, E., and Sage, E. (1996) Regulation of angiogenesis by SPARC and angiostatin: implications for tumor cell biology. *Semin.Cancer Biol.* 7, 139–146.
- [153] Sage, H., Johnson, C., and Bornstein, P. (1984) Characterization of a novel serum albumin-binding glycoprotein secreted by endothelial cells in culture. *J.Biol.Chem.* 259, 3993–4007.
- [154] Greish, K., Nagamitsu, A., Fang, J., and Maeda, H. (2005) Copoly(styrene-maleic acid)-pirarubicin micelles: high tumor-targeting efficiency with little toxicity. *Bioconjug.Chem.* 16, 230–236.
- [155] Monopoli, M., Walczyk, D., Campbell, A., Elia, G., Lynch, I., Bombelli, F., and Dawson, K. (2011) Physical-chemical aspects of protein corona: relevance to in vitro and in vivo biological impacts of nanoparticles. *J Am.Chem.Soc.* 133, 2525–2534.
- [156] Walczyk, D., Bombelli, F., Monopoli, M., Lynch, I., and Dawson, K. (2010) What the cell "sees" in bionanoscience. *J Am.Chem.Soc.* 132, 5761–5768.
- [157] Ehrenberg, M., Friedman, A., Finkelstein, J., Oberdorster, G., and McGrath, J. (2009) The influence of protein adsorption on nanoparticle association with cultured endothelial cells. *Biomaterials* 30, 603–610.
- [158] Ogawara, K., Furumoto, K., Nagayama, S., Minato, K., Higaki, K., Kai, T., and Kimura, T. (2004) Pre-coating with serum albumin reduces receptor-mediated hepatic disposition of polystyrene nanosphere: implications for rational design of nanoparticles. *Journal of Controlled Release* 100, 451–455.
- [159] Furumoto, K., Yokoe, J., Ogawara, K., Amano, S., Takaguchi, M., Higaki, K., Kai, T., and Kimura, T. (2007) Effect of coupling of albumin onto surface of PEG liposome on its in vivo disposition. *Int.J Pharm.* 329, 110–116.
- [160] Crielaard, B., Yousefi, A., Schillemans, J., Vermehren, C., Buyens, K., Braeckmans, K., Lammers, T., and Storm, G. (2011) An in vitro assay based on surface plasmon resonance to predict the in vivo circulation kinetics of liposomes. *J.Control Release* 156, 307–314.
- [161] Kratz, F. (2008) Albumin as a drug carrier: Design of prodrugs, drug conjugates and nanoparticles. *Journal of Controlled Release* 132, 171–183.
- [162] Pierri, E., and Avgoustakis, K. (2005) Poly(lactide)-poly(ethylene glycol) micelles as a carrier for griseofulvin. *J.Biomed.Mater.Res.A* 75, 639–647.
- [163] Carstens, M., De Jong, P., van Nostrum, C., Kemmink, J., Verrijck, R., De Leede, L., Crommelin, D., and Hennink, W. (2008) The effect of core composition in biodegradable oligomeric micelles as taxane formulations. *European Journal of Pharmaceutics and Biopharmaceutics* 68, 596–606.

-
- [164] Velluto, D., Demurtas, D., and Hubbell, J. (2008) PEG-b-PPS diblock copolymer aggregates for hydrophobic drug solubilization and release: cyclosporin A as an example. *Mol.Pharm.* 5, 632–642.
- [165] Chen, H., Kim, S., Li, L., Wang, S., Park, K., and Cheng, J. (2008) Release of hydrophobic molecules from polymer micelles into cell membranes revealed by Forster resonance energy transfer imaging. *Proc.Natl.Acad.Sci.U.S.A* 105, 6596–6601.
- [166] Moghimi, S., Hunter, A., Dadswell, C., Savay, S., Alving, C., and Szebeni, J. (2004) Causative factors behind poloxamer 188 (Pluronic F68, Flocor)-induced complement activation in human sera. A protective role against poloxamer-mediated complement activation by elevated serum lipoprotein levels. *Biochim.Biophys.Acta* 1689, 103–113.
- [167] Hamad, I., Al-Hanbali, O., Hunter, A., Rutt, K., Andresen, T., and Moghimi, S. (2010) Distinct Polymer Architecture Mediates Switching of Complement Activation Pathways at the Nanosphere-Serum Interface: Implications for Stealth Nanoparticle Engineering. *Acs Nano* 4, 6629–6638.
- [168] Hamad, I., Hunter, A., Szebeni, J., and Moghimi, S. (2008) Poly(ethylene glycol)s generate complement activation products in human serum through increased alternative pathway turnover and a MASP-2-dependent process. *Mol.Immunol.* 46, 225–232.
- [169] Lipinski, C., Lombardo, F., Dominy, B., and Feeney, P. (1997) Experimental and computational approaches to estimate solubility and permeability in drug discovery and development settings. *Advanced Drug Delivery Reviews* 23, 3–25.
- [170] Lipinski, C. (2000) Drug-like properties and the causes of poor solubility and poor permeability. *Journal of Pharmacological and Toxicological Methods* 44, 235–249.
- [171] Di, L., Kerns, E., and Carter, G. (2009) Drug-Like Property Concepts in Pharmaceutical Design. *Current Pharmaceutical Design* 15, 2184–2194.
- [172] Marupudi, N., Han, J., Li, K., Renard, V., Tyler, B., and Brem, H. (2007) Paclitaxel: a review of adverse toxicities and novel delivery strategies. *Expert Opinion on Drug Safety* 6, 609–621.
- [173] Tyrrell, Z., Shen, Y., and Radosz, M. (2010) Fabrication of micellar nanoparticles for drug delivery through the self-assembly of block copolymers. *Progress in Polymer Science* 35, 1128–1143.
- [174] Kim, S., Shi, Y., Kim, J., Park, K., and Cheng, J. (2010) Overcoming the barriers in micellar drug delivery: loading efficiency, in vivo stability, and micelle-cell interaction. *Expert.Opin.Drug Deliv.* 7, 49–62.
- [175] Sant, V., Smith, D., and Leroux, J. (2005) Enhancement of oral bioavailability of poorly

- water-soluble drugs by poly(ethylene glycol)-block-poly(alkyl acrylate-co-methacrylic acid) self-assemblies. *J.Control Release* 104, 289–300.
- [176] Avgoustakis, K., Beletsi, A., Panagi, Z., Klepetsanis, P., Karydas, A., and Ithakissios, D. (2002) PLGA-mPEG nanoparticles of cisplatin: in vitro nanoparticle degradation, in vitro drug release and in vivo drug residence in blood properties. *J.Control Release* 79, 123–135.
- [177] Song, C., Labhasetwar, V., Murphy, H., Qu, X., Humphrey, W., Shebuski, R., and Levy, R. (1997) Formulation and characterization of biodegradable nanoparticles for intravascular local drug delivery. *Journal of Controlled Release* 43, 197–212.
- [178] Jeon, H., Jeong, J., Jang, M., Park, Y., and Nah, J. (2000) Effect of solvent on the preparation of surfactant-free poly(DL-lactide-co-glycolide) nanoparticles and norfloxacin release characteristics. *International Journal of Pharmaceutics* 207, 99–108.
- [179] Aliabadi, H., Elhasi, S., Mahmud, A., Gulamhusein, R., Mahdipoor, P., and Lavasanifar, A. (2007) Encapsulation of hydrophobic drugs in polymeric micelles through co-solvent evaporation: the effect of solvent composition on micellar properties and drug loading. *Int.J.Pharm.* 329, 158–165.
- [180] Fournier, E., Dufresne, M., Smith, D., Ranger, M., and Leroux, J. (2004) A novel one-step drug-loading procedure for water-soluble amphiphilic nanocarriers. *Pharm.Res.* 21, 962–968.
- [181] Jansook, P., and Loftsson, T. (2008) gamma CD/HP gamma CD: Synergistic solubilization. *International Journal of Pharmaceutics* 363, 217–219.
- [182] Moretton, M., Chiappetta, D., and Sosnik, A. (2012) Cryoprotection-lyophilization and physical stabilization of rifampicin-loaded flower-like polymeric micelles. *J.R Soc.Interface* 9, 487–502.
- [183] Richter, A., Olbrich, C., Krause, M., Hoffmann, J., and Kissel, T. (2010) Polymeric micelles for parenteral delivery of Sagopilone: physicochemical characterization, novel formulation approaches and their toxicity assessment in vitro as well as in vivo. *Eur.J.Pharm.Biopharm.* 75, 80–89.
- [184] Abdelwahed, W., Degobert, G., Stainmesse, S., and Fessi, H. (2006) Freeze-drying of nanoparticles: formulation, process and storage considerations. *Adv.Drug Deliv.Rev.* 58, 1688–1713.
- [185] Sander, B., Golas, M., and Stark, H. (2003) Corrim-based alignment for improved speed in single-particle image processing. *Journal of Structural Biology* 143, 219–228.
- [186] EMA, European Medicines Agency: ICH Topic Q3C (R4) Impurities: Guideline for Residual Solvents CPMP/ICH/283/95. 2009.

-
- [187] Wang, W. (2000) Lyophilization and development of solid protein pharmaceuticals. *Int.J.Pharm.* 203, 1–60.
- [188] Li, X., Yang, H., Xu, L., Fu, X., Guo, H., and Zhang, X. (2010) Janus Micelle Formation Induced by Protonation/Deprotonation of Poly(2-vinylpyridine)-block-Poly(ethylene oxide) Diblock Copolymers. *Macromolecular Chemistry and Physics* 211, 297–302.
- [189] Leson, A., Hauschild, S., Rank, A., Neub, A., Schubert, R., Forster, S., and Mayer, C. (2007) Molecular exchange through membranes of poly(2-vinylpyridine-block-ethylene oxide) vesicles. *Small* 3, 1074–1083.
- [190] Selb, J., and Gallot, Y. (1975) Micelle Formation in Polystyrene-Poly(Vinyl-N-Alkylpyridinium Bromide) Block Copolymer Solutions in Methanol-Water Mixtures. *Journal of Polymer Science Part C-Polymer Letters* 13, 615–619.
- [191] Cinelli, S., Freda, M., Onori, G., Paciaroni, A., and Santucci, A. (2005) Hydration-dependent internal dynamics of macromolecules: a neutron scattering study. *Journal of Molecular Liquids* 117, 99–105.
- [192] Zhao, J., Allen, C., and Eisenberg, A. (1997) Partitioning of pyrene between "crew cut" block copolymer micelles and H₂O/DMF solvent mixtures. *Macromolecules* 30, 7143–7150.
- [193] Vangeyte, P., Gautier, S., and Jerome, R. (2004) About the methods of preparation of poly(ethylene oxide)-b-poly(epsilon-caprolactone) nanoparticles in water analysis by dynamic light scattering. *Colloids and Surfaces A-Physicochemical and Engineering Aspects* 242, 203–211.
- [194] Lee, M., Kim, M., Kim, S., and Lee, J. (2009) Cryoprotectants for freeze drying of drug nano-suspensions: effect of freezing rate. *J.Pharm.Sci.* 98, 4808–4817.
- [195] Miyajima, K. (1997) Role of saccharides for the freeze-thawing and freeze drying of liposome. *Advanced Drug Delivery Reviews* 24, 151–159.
- [196] Tanaka, K., Takeda, T., Fujii, K., and Miyajima, K. (1992) Cryoprotective Mechanism of Saccharides on Freeze-Drying of Liposome. *Chemical & Pharmaceutical Bulletin* 40, 1–5.
- [197] Abdelwahed, W., Degobert, G., and Fessi, H. (2006) Investigation of nanocapsules stabilization by amorphous excipients during freeze-drying and storage. *Eur.J.Pharm.Biopharm.* 63, 87–94.
- [198] Allison, S., Molina, M., and Anchordoquy, T. (2000) Stabilization of lipid/DNA complexes during the freezing step of the lyophilization process: the particle isolation hypothesis. *Biochim.Biophys.Acta* 1468, 127–138.

- [199] Guo, M., and Jiang, M. (2007) Macromolecular self-assembly based on inclusion complexation of cyclodextrins. *Progress in Chemistry* 19, 557–566.
- [200] Dreiss, C., Nwabunwanne, E., Liu, R., and Brooks, N. (2009) Assembling and de-assembling micelles: competitive interactions of cyclodextrins and drugs with Pluronics. *Soft Matter* 5, 1888–1896.
- [201] Qin, J., Meng, X., Li, B., Ha, W., Yu, X., and Zhang, S. (2010) Self-assembly of beta-cyclodextrin and pluronic into hollow nanospheres in aqueous solution. *Journal of Colloid and Interface Science* 350, 447–452.
- [202] Becheri, A., Lo Nostro, P., Ninham, B. W., and Baglioni, P. (2003) The Curious World of Polypseudorotaxanes: Cyclodextrins As Probes of Water Structure. *J. Phys. Chem. B* 107, 3979–3987.
- [203] He, L., Huang, J., Chen, Y., Xu, X., and Liu, L. (2005) Inclusion Interaction of Highly Densely PEO Grafted Polymer Brush and α -Cyclodextrin. *Macromolecules* 38, 3845–3851.
- [204] Plumridge, T., and Waigh, R. (2002) Water structure theory and some implications for drug design. *Journal of Pharmacy and Pharmacology* 54, 1155–1179.
- [205] Lerbret, A., Bordat, P., Affouard, F., Descamps, M., and Migliardo, F. (2005) How Homogeneous Are the Trehalose, Maltose, and Sucrose Water Solutions? An Insight from Molecular Dynamics Simulations. *J. Phys. Chem. B* 109, 11046–11057.
- [206] Sano, H., Ichi, T., Kumashiro, Y., Kontani, K., Kuze, T., Mizutani, G., Ooya, T., and Yui, N. (2003) Raman scattering study of water clusters around polyrotaxane and pseudopolyrotaxane supramolecular assemblies. *Spectrochimica Acta Part A: Molecular and Biomolecular Spectroscopy* 59, 285–289.
- [207] Liu, K. L., Goh, S. H., and Li, J. (2008) Threading α -Cyclodextrin through Poly[(R,S)-3-hydroxybutyrate] in Poly[(R,S)-3-hydroxybutyrate]-Poly(ethylene glycol)-Poly[(R,S)-3-hydroxybutyrate] Triblock Copolymers: Formation of Block-Selected Polypseudorotaxanes. *Macromolecules* 41, 6027–6034.
- [208] Adams, M., Lavasanifar, A., and Kwon, G. (2003) Amphiphilic block copolymers for drug delivery. *J. Pharm. Sci.* 92, 1343–1355.
- [209] Kataoka, K., Harada, A., and Nagasaki, Y. (2001) Block copolymer micelles for drug delivery: design, characterization and biological significance. *Adv. Drug Deliv. Rev.* 47, 113–131.
- [210] Aliabadi, H., Shahin, M., Brooks, D., and Lavasanifar, A. (2008) Disposition of drugs in block copolymer micelle delivery systems: from discovery to recovery. *Clin. Pharmacokinet.* 47, 619–634.

-
- [211] Wiradharma, N., Zhang, Y., Venkataraman, S., Hedrick, J., and Yang, Y. (2009) Self-assembled polymer nanostructures for delivery of anticancer therapeutics. *Nano Today* 4, 302–317.
- [212] Hamaguchi, T. (2009) [Cancer chemotherapy utilizing nanotechnology]. *Gan To Kagaku Ryoho* 36, 372–376.
- [213] Chung, T.-W., Liu, D.-Z., Hsieh, J.-H., Fan, X.-C., Yang, J.-D., and Chen, J.-H. (2006) Characterizing Poly(-caprolactone)-b-Chitooligosaccharide-b-Poly(ethylene glycol) (PCP) Copolymer Micelles for Doxorubicin (DOX) Delivery: Effects of Crosslinked of Amine Groups. *Journal of Nanoscience and Nanotechnology* 6, 2902–2911.
- [214] Gaucher, G., Marchessault, R., and Leroux, J. (2010) Polyester-based micelles and nanoparticles for the parenteral delivery of taxanes. *J.Control Release* 143, 2–12.
- [215] Kamat, P., and Fox, M. (1984) Photophysics and Photochemistry of Xanthene Dyes in Polymer-Solutions and Films. *Journal of Physical Chemistry* 88, 2297–2302.
- [216] Gref, R., Luck, M., Quellec, P., Marchand, M., Dellacherie, E., Harnisch, S., Blunk, T., and Muller, R. (2000) 'Stealth' corona-core nanoparticles surface modified by polyethylene glycol (PEG): influences of the corona (PEG chain length and surface density) and of the core composition on phagocytic uptake and plasma protein adsorption. *Colloids Surf.B Biointerfaces* 18, 301–313.
- [217] Savic, R., Luo, L., Eisenberg, A., and Maysinger, D. (2003) Micellar nanocontainers distribute to defined cytoplasmic organelles. *Science* 300, 615–618.
- [218] Kalyanasundaram, K., and Thomas, J. (1977) Environmental Effects on Vibronic Band Intensities in Pyrene Monomer Fluorescence and Their Application in Studies of Micellar Systems. *Journal of the American Chemical Society* 99, 2039–2044.
- [219] Berney, C., and Danuser, G. (2003) FRET or no FRET: a quantitative comparison. *Biophys.J.* 84, 3992–4010.
- [220] Fraunhofer, W., and Winter, G. (2004) The use of asymmetrical flow field-flow fractionation in pharmaceuticals and biopharmaceuticals. *Eur.J.Pharm.Biopharm.* 58, 369–383.
- [221] Zimm, B. (1948) The Scattering of Light and the Radial Distribution Function of High Polymer Solutions. *Journal of Chemical Physics* 16, 1093–1099.
- [222] Zheng, Z., and Obbard, J. (2002) Evaluation of an elevated non-ionic surfactant critical micelle concentration in a soil/aqueous system. *Water Res.* 36, 2667–2672.
- [223] Allen, C., Maysinger, D., and Eisenberg, A. (1999) Nano-engineering block copolymer aggregates for drug delivery. *Colloids and Surfaces B-Biointerfaces* 16, 3–27.

- [224] Sagalowicz, L., Leser, M., Watzke, H., and Michel, M. (2006) Monoglyceride self-assembly structures as delivery vehicles. *Trends in Food Science & Technology* 17, 204–214.
- [225] Wang, L., Zeng, R., Li, C., and Qiao, R. (2009) Self-assembled polypeptide-block-poly(vinylpyrrolidone) as prospective drug-delivery systems. *Colloids Surf.B Biointerfaces*. 74, 284–292.
- [226] EMA, European Medicines Agency: Reflection paper on the pharmaceutical development of intravenous medicinal products containing active substances solubilised in micellar systems (non-polymeric surfactants). EMA/CHMP/QWP/574767/2010, 2010.
- [227] Ahyauch, H., Bennouna, M., Alonso, A., and Goni, F. (2010) Detergent Effects on Membranes at Subsolubilizing Concentrations: Transmembrane Lipid Motion, Bilayer Permeabilization, and Vesicle Lysis/Reassembly Are Independent Phenomena. *Langmuir* 26, 7307–7313.
- [228] Lasseter, K., Gambale, J., Jin, B., Bergman, A., Constanzer, M., Dru, J., Han, T., Majumdar, A., Evans, J., and Murphy, M. (2007) Tolerability of fosaprepitant and bioequivalency to aprepitant in healthy subjects. *J.Clin.Pharmacol.* 47, 834–840.
- [229] Riley, T., Govender, T., Stolnik, S., Xiong, C., Garnett, M., Illum, L., and Davis, S. (1999) Colloidal stability and drug incorporation aspects of micellar-like PLA-PEG nanoparticles. *Colloids and Surfaces B-Biointerfaces* 16, 147–159.
- [230] Jacquin, M., Muller, P., Cottet, H., and Theodoly, O. (2010) Self-Assembly of Charged Amphiphilic Diblock Copolymers with Insoluble Blocks of Decreasing Hydrophobicity: From Kinetically Frozen Colloids to Macrosurfactants. *Langmuir* 26, 18681–18693.
- [231] Toncheva, V., Schacht, E., Ng, S., Barr, J., and Heller, J. (2003) Use of Block Copolymers of Poly(Ortho Esters) and Poly (Ethylene Glycol) Micellar Carriers as Potential Tumour Targeting Systems. *Journal of Drug Targeting* 11, 345–353.
- [232] Lin, Z., and Will, Y. (2012) Evaluation of drugs with specific organ toxicities in organ-specific cell lines. *Toxicol.Sci.* 126, 114–127.
- [233] Lu, S., Jessen, B., Strock, C., and Will, Y. (2012) The contribution of physicochemical properties to multiple in vitro cytotoxicity endpoints. *Toxicol.In Vitro* 26, 613–620.
- [234] Scheers, E., Ekwall, B., and Dierickx, P. (2001) In vitro long-term cytotoxicity testing of 27 MEIC chemicals on Hep G2 cells and comparison with acute human toxicity data. *Toxicology in Vitro* 15, 153–161.
- [235] WANG, K., SHINDOH, H., INOUE, T., and HORII, I. (2002) Advantages of in vitro Cytotoxicity Testing by using Primary Rat Hepatocytes in Comparison with established Cell Lines. *The Journal of Toxicological Sciences* 27, 229–237.

-
- [236] Szebeni, J., Muggia, F., Gabizon, A., and Barenholz, Y. (2011) Activation of complement by therapeutic liposomes and other lipid excipient-based therapeutic products: Prediction and prevention. *Adv. Drug Deliv. Rev.* 63, 1020–1030.
- [237] Hong, J., Park, J., Huh, K., Chung, H., Kwon, I., and Jeong, S. (2004) PEGylated polyethylenimine for in vivo local gene delivery based on lipiodolized emulsion system. *J. Control Release* 99, 167–176.
- [238] Scripture, C., Szebeni, J., Loos, W., Figg, W., and Sparreboom, A. (2005) Comparative in vitro properties and clinical pharmacokinetics of Paclitaxel following the administration of taxol(r) and paxene(r). *Cancer Biol. Ther.* 4, 555–560.
- [239] Gao, X., Yao, L., Song, Q., Zhu, L., Xia, Z., Xia, H., Jiang, X., Chen, J., and Chen, H. (2011) The association of autophagy with polyethylenimine-induced cytotoxicity in nephritic and hepatic cell lines. *Biomaterials* 32, 8613–8625.
- [240] Engels, F., Mathot, R., and Verweij, J. (2007) Alternative drug formulations of docetaxel: a review. *Anticancer Drugs* 18, 95–103.
- [241] Gelderblom, H., Verweij, J., Nooter, K., and Sparreboom, A. (2001) Cremophor EL: the drawbacks and advantages of vehicle selection for drug formulation. *Eur. J. Cancer* 37, 1590–1598.
- [242] Zhou, D., Zhang, M., Ye, X., Gu, C., Piser, T. M., Lanoue, B. A., Schock, S. A., Cheng, Y.-F., and Grimm, S. W. (2011) In vitro metabolism of $\alpha 7$ neuronal nicotinic receptor agonist AZD0328 and enzyme identification for its N-oxide metabolite. *Xenobiotica* 41, 232–242.
- [243] Kim, S., Williams, D., Schuetz, E., Guzelian, P., and Novak, R. (1988) Pyridine induction of cytochrome P-450 in the rat: role of P-450j (alcohol-inducible form) in pyridine N-oxidation. *J. Pharmacol. Exp. Ther.* 246, 1175–1182.
- [244] Anuszevska, E., and Koziorowska, J. (1995) Role of pyridine N-oxide in the cytotoxicity and genotoxicity of chloropyridines. *Toxicol. In Vitro* 9, 91–94.
- [245] Breyer, S., Semmler, A., Miller, T., Hill, A., Geissler, S., Haberkorn, U., and Mier, W. (2012) Radioiodinated dechloro-4-iodofenofibrate: a hydrophobic model drug for molecular imaging studies. *Int. J. Pharm.* In press.
- [246] Miller, T., Hill, A., Uezguen, S., Weigandt, M., and Goepferich, A. (2012) Analysis of immediate stress mechanisms upon injection of polymeric micelles and related colloidal drug carriers: implications on drug targeting. *Biomacromolecules* In press.
- [247] Brigger, I., Morizet, J., Laudani, L., Aubert, G., Appel, M., Velasco, V., Terrier-Lacombe, M., Desmaele, D., d’Angelo, J., Couvreur, P., and Vassal, G. (2004) Negative

- preclinical results with stealth nanospheres-encapsulated Doxorubicin in an orthotopic murine brain tumor model. *J. Control Release* 100, 29–40.
- [248] Seymour, L., Duncan, R., Strohalm, J., and Kopecek, J. (1987) Effect of Molecular-Weight (Mbarw) of N-(2-Hydroxypropyl)Methacrylamide Copolymers on Body Distribution and Rate of Excretion After Subcutaneous, Intraperitoneal, and Intravenous Administration to Rats. *Journal of Biomedical Materials Research* 21, 1341–1358.
- [249] Wang, J. S., and Matyjaszewski, K. (1995) Controlled/"living" radical polymerization. atom transfer radical polymerization in the presence of transition-metal complexes. *Journal of the American Chemical Society* 117, 5614–5615.
- [250] Wang, J. S., and Matyjaszewski, K. (1995) "Living"/Controlled Radical Polymerization. Transition-Metal-Catalyzed Atom Transfer Radical Polymerization in the Presence of a Conventional Radical Initiator. *Macromolecules* 28, 7572–7573.
- [251] Wang, J. S., and Matyjaszewski, K. (1995) Controlled/"Living" Radical Polymerization. Halogen Atom Transfer Radical Polymerization Promoted by a Cu(I)/Cu(II) Redox Process. *Macromolecules* 28, 7901–7910.
- [252] Fukui, H., Sawamoto, M., and Higashimura, T. (1995) Multifunctional Coupling Agents for Living Cationic Polymerization .5. Synthesis of Amphiphilic Tetraarmed Star Poly(Vinyl Ethers) by Coupling Reactions with Tetrafunctional Silyl Enol Ether. *Macromolecules* 28, 3756–3765.
- [253] Katayama, H., Kamigaito, M., Sawamoto, M., and Higashimura, T. (1995) In-Situ C-13 and H-1-Nmr Analysis of the Growing Species in Living Cationic Polymerization of Isobutyl Vinyl Ether by the Hcl/Sncl₄ Initiating System in the Presence of A Nbu(4)Ncl Salt. *Macromolecules* 28, 3747–3755.
- [254] Kato, M., Kamigaito, M., Sawamoto, M., and Higashimura, T. (1995) Polymerization of Methyl-Methacrylate with the Carbon-Tetrachloride Dichlorotris(Triphenylphosphine)Ruthenium(Ii) Methylaluminum Bis(2,6-Di-Tert-Butylphenoxide) Initiating System - Possibility of Living Radical Polymerization. *Macromolecules* 28, 1721–1723.
- [255] Ishizu, K., Satoh, J., and Sogabe, A. (2004) Architecture and solution properties of AB-type brush-block-brush amphiphilic copolymers via ATRP techniques. *J Colloid Interface Sci.* 274, 472–479.
- [256] Tan, B., Hussain, H., Liu, Y., He, C., and Davis, T. (2010) Synthesis and self-assembly of brush-type poly[poly(ethylene glycol)methyl ether methacrylate]-block-poly(pentafluorostyrene) amphiphilic diblock copolymers in aqueous solution. *Langmuir* 26, 2361–2368.

-
- [257] Hussain, H., Mya, K., and He, C. (2008) Self-assembly of brush-like poly[poly(ethylene glycol) methyl ether methacrylate] synthesized via aqueous atom transfer radical polymerization. *Langmuir* 24, 13279–13286.
- [258] Brannon-Peppas, L., and Blanchette, J. (2004) Nanoparticle and targeted systems for cancer therapy. *Adv. Drug Deliv. Rev.* 56, 1649–1659.
- [259] Vasir, J., and Labhasetwar, V. (2005) Targeted drug delivery in cancer therapy. *Technol. Cancer Res. Treat.* 4, 363–374.
- [260] De Jong, W., and Borm, P. (2008) Drug delivery and nanoparticles: applications and hazards. *Int. J. Nanomedicine* 3, 133–149.
- [261] Lee, S. W., Yun, M. H., Jeong, S. W., In, C. H., Kim, J. Y., Seo, M. H., Pai, C. M., and Kim, S. O. (2011) Development of docetaxel-loaded intravenous formulation, Nanoxel-PM using polymer-based delivery system. *Journal of Controlled Release* 155, 262–271.
- [262] Bogner, J., Kronawitter, U., Rolinski, B., Truebenbach, K., and Goebel, F. (1994) Liposomal doxorubicin in the treatment of advanced AIDS-related Kaposi sarcoma. *J Acquir. Immune. Defic. Syndr.* 7, 463–468.
- [263] Goebel, F., Goldstein, D., Goos, M., Jablonowski, H., and Stewart, J. (1996) Efficacy and safety of Stealth liposomal doxorubicin in AIDS-related Kaposi's sarcoma. The International SL-DOX Study Group. *Br. J Cancer* 73, 989–994.
- [264] James, N., Coker, R., Tomlinson, D., Harris, J., Gompels, M., Pinching, A., and Stewart, J. (1994) Liposomal doxorubicin (Doxil): an effective new treatment for Kaposi's sarcoma in AIDS. *Clin. Oncol. (R Coll. Radiol.)* 6, 294–296.
- [265] Utreja, P., Jain, S., Yadav, S., Khandhuja, K., and Tiwary, A. (2011) Efficacy and toxicological studies of cremophor el free alternative Paclitaxel formulation. *Curr. Drug Saf* 6, 329–338.
- [266] Lim, W., Tan, E., Toh, C., Hee, S., Leong, S., Ang, P., Wong, N., and Chowbay, B. (2010) Phase I pharmacokinetic study of a weekly liposomal paclitaxel formulation (Genexol-PM) in patients with solid tumors. *Ann. Oncol.* 21, 382–388.
- [267] Mier, W., Hoffend, J., Kramer, S., Schuhmacher, J., Hull, W., Eisenhut, M., and Haberkorn, U. (2005) Conjugation of DOTA using isolated phenolic active esters: the labeling and biodistribution of albumin as blood pool marker. *Bioconjug. Chem.* 16, 237–240.
- [268] Lee, H., Hoang, B., Fonge, H., Reilly, R., and Allen, C. (2010) In vivo distribution of polymeric nanoparticles at the whole-body, tumor, and cellular levels. *Pharm. Res.* 27, 2343–2355.

- [269] Hoang, B., Lee, H., Reilly, R., and Allen, C. (2009) Noninvasive monitoring of the fate of ^{111}In -labeled block copolymer micelles by high resolution and high sensitivity microSPECT/CT imaging. *Mol.Pharm.* 6, 581–592.
- [270] Tessmar, J., Mikos, A., and Gopferich, A. (2002) Amine-reactive biodegradable diblock copolymers. *Biomacromolecules* 3, 194–200.
- [271] Sadekar, S., Ray, A., Janat-Amsbury, M., Peterson, C., and Ghandehari, H. (2011) Comparative Biodistribution of PAMAM Dendrimers and HPMA Copolymers in Ovarian-Tumor-Bearing Mice. *Biomacromolecules* 12, 88–96.
- [272] Helbok, A., Rangger, C., von, G. E., Saba-Lepek, M., Radolf, T., Thurner, G., Andrae, F., Prassl, R., and Decristoforo, C. (2012) Targeting properties of peptide-modified radiolabeled liposomal nanoparticles. *Nanomedicine* 8, 112–118.
- [273] Surujpaul, P., Gutierrez-Wing, C., Ocampo-Garcia, B., Ramirez, F. M., rteaga de, M. C., Pedraza-Lopez, M., Camacho-Lopez, M., and Ferro-Flores, G. (2008) Gold nanoparticles conjugated to [Tyr3]octreotide peptide. *Biophys.Chem.* 138, 83–90.
- [274] Weil, A., Caldwell, J., and Strolin-Benedetti, M. (1988) The metabolism and disposition of fenofibrate in rat, guinea pig, and dog. *Drug Metabolism and Disposition* 16, 302–309.
- [275] Liu, A., Patterson, A., Yang, Z., Zhang, X., Liu, W., Qiu, F., Sun, H., Krausz, K., Idle, J., Gonzalez, F., and Dai, R. (2009) Fenofibrate metabolism in the cynomolgus monkey using ultraperformance liquid chromatography-quadrupole time-of-flight mass spectrometry-based metabolomics. *Drug Metab Dispos.* 37, 1157–1163.
- [276] Najib, J. (2002) Fenofibrate in the treatment of dyslipidemia: A review of the data as they relate to the new suprabioavailable tablet formulation. *Clinical Therapeutics* 24, 2022–2050.
- [277] Poulin, P., and Theil, F. (2000) A priori prediction of tissue:plasma partition coefficients of drugs to facilitate the use of physiologically-based pharmacokinetic models in drug discovery. *J.Pharm.Sci.* 89, 16–35.
- [278] Poulin, P., Schoenlein, K., and Theil, F. (2001) Prediction of adipose tissue: plasma partition coefficients for structurally unrelated drugs. *J.Pharm.Sci.* 90, 436–447.
- [279] Heneweer, C., Holland, J., Divilov, V., Carlin, S., and Lewis, J. (2011) Magnitude of enhanced permeability and retention effect in tumors with different phenotypes: ^{89}Zr -albumin as a model system. *J.Nucl.Med.* 52, 625–633.
- [280] Pirollo, K., and Chang, E. (2008) Does a targeting ligand influence nanoparticle tumor localization or uptake? *Trends Biotechnol.* 26, 552–558.
- [281] Plummer, R., Wilson, R., Calvert, H., Boddy, A., Griffin, M., Sludden, J., Tilby, M., Eatock, M., Pearson, D., Ottley, C., Matsumura, Y., Kataoka, K., and Nishiya, T.

- (2011) A Phase I clinical study of cisplatin-incorporated polymeric micelles (NC-6004) in patients with solid tumours. *Br.J.Cancer* 104, 593–598.
- [282] Savic, R., Azzam, T., Eisenberg, A., and Maysinger, D. (2006) Assessment of the integrity of poly(caprolactone)-b-poly(ethylene oxide) micelles under biological conditions: a fluorogenic-based approach. *Langmuir* 22, 3570–3578.

List of abbreviations

ACN	Acetonitrile
AF4	Asymmetrical Flow Field Flow Fractionation
ATP	Adenosine triphosphate
ATRP	Atom Transfer Radical Polymerization
CAC	Critical Association Concentration
CARPA	C-Activation Related Pseudoallergy
CAT	Chloramine T
cryo-EM	Cryo Transmission Electron Microscopy
DCM	Dichlormethane
DiI	1,1'-Diocetyl-3,3',3'-tetramethylindocarbocyanine perchlorate
DiO	3,3'-Diocetylloxacarbocyanine perchlorate
DLS	Dynamic Light Scattering
DMAc	Dimethylacetate
DMF	Dimethylformamide
DMSO	Dimethylsulfoxide
DOTA	1,4,7,10-tetraazacyclododecane-1,4,7,10-tetraacetic acid
DTT	Dithiothreitol
DXM	Dexamethasone
ELISA	Enzyme Linked Immuno Sorbent Assay
EPR	Enhanced Permeability and Retention
FDA	Food and Drug Administration
FRET	Foerster Resonance Energy Transfer
GPC	Gel Permeation Chromatography
HP β CD	Hydroxy Propyl β -Cyclodextrin
IFF	Dechloro-4-iodo-fenofibrate
LOQ	Limit Of Quantification
MALS	Multiple Angle Light Scattering
MBq	Mega Bequerel
MPS	Mononuclear Phagocyte System

MWCO	Molecular Weight Cut-Off
NMR	Nuclear Magnetic Resonance
O/W	Oil in water
PBS	Phosphate Buffered Saline
mPEG-PCL	methoxy PEGylated poly-(ϵ -caprolactone)
PDI	Poly Dispersity Index
mPEG-PDLLA	methoxy PEGylated poly-(D,L-lactic acid)
mPEG-PLA	methoxy PEGylated poly-(lactic acid)
mPEG-PLGA	methoxy PEGylated poly-(lactic acid-co-glycolic acid)
mPEG-PLLA	methoxy PEGylated poly-(L-lactic acid)
PTA	Phosphor Tungstic Acid
mPEG-PVPy	methoxy PEGylated poly-4-(vinylpyridine)
RES	Reticulo Endothelial System
RMF	Residual Micellar Fraction
RMS	Root Mean Square
ROP	Ring Opening Polymerization
SANS	Small Angle Neutron Scattering
SBE β CD	Sulfobutyl Ether β -Cyclodextrin
TEM	Transmission Electron Microscopy
TFA	Trifluoroacetic acid
THF	Tetrahydrofuran

List of Figures

1.1	Summary of stress factor analysis.	6
1.2	Scenario analysis of protein-carrier interactions.	11
1.3	Immunological responses that could lead to premature particle clearance. . . .	17
2.1	Summary of cosolvent evaporation and lyophilization.	30
2.2	Solubility screen of DXM in organic solvents.	36
2.3	T _g ' determination of lyoprotectors.	38
2.4	Polymeric micelles upon lyophilization: size and size distributions.	39
2.5	Lyoprotector optimum for lyophilized for DXM-loaded PEG-PVPy micelles. .	40
2.6	Cryo-EM analysis of PEG-PVPy micelles.	41
2.7	Cryo-EM micrograph analysis regarding particle sizes and size distributions. .	42
2.8	Schematic drawing of the O/W emulsion process.	45
2.9	Schematic drawing of the direct dialysis process.	46
2.10	Schematic drawing of the cosolvent evaporation process.	47
2.11	Schematic drawing of the β -cyclodextrin inclusion complexes with PEGylated surfaces (pseudopolyrotaxane formation).	49
3.1	CAC values for block copolymers.	59
3.2	TEM micrographs of block copolymer micelles.	62
3.3	FRET fluorescence spectra of Tween 80 [®] micelles.	63
3.4	Residual micellar fractions of Tween 80 [®] micelles.	63
3.5	Residual micellar fractions of block copolymer micelles upon serum incubation.	64
3.6	AF4 fractograms of PEG-PVPy micelles upon serum incubation.	66
4.1	Preparation steps for PEG-PEI derivatives.	75
4.3	EC ₅₀ cruve for Cremophor EL [®] micelles on HepG2 cells.	79
4.4	Results of the complement activation assays.	83
4.2	¹ H-NMR spectrum of PEG-PEI.	86
5.1	Solubility screen of compound A in organic solvents.	93
5.2	Biodistribution of compound A loaded PEG-PLGA micelles compared to compound B solution.	96

5.3	Recorded drug plasma concentrations over time upon injection of micellar drug or drug solution.	97
5.4	^1H -NMR spectrum of H_2N -PEG-PLGA.	98
5.5	Scintigrams of dual-labeled IFF-loaded PEG-PLGA micelles. Indium traces. .	99
5.6	Scintigrams of dual-labeled IFF-loaded PEG-PLGA micelles. Iodine traces. .	100
5.7	Biodistribution of dual-labeled IFF-loaded PEG-PLGA micelles.	101
6.1	Quaternization and labeling of PEG-PVPy.	108
6.2	Scintigrams of IFF-labeled PEG-PVPy micelles.	110
6.3	Scintigrams of PEG-PVPy labeled micelles.	111
6.4	Biodistribution of labeled PEG-PVPy micelles.	111
6.5	Body clearance of PEG-PVPy in mice.	112
7.1	Summary of the biodistribution study with ^{111}In -HN-PEG-PLA micelles. . . .	116
7.2	Concept of micellar dual-label with IFF encapsulated in PEG-PLA micelles. .	121
7.3	Summary of the animal study approach.	122
7.4	Scintigrams and biodistribution of IFF-loaded dual labeled PEG-PLA micelles.	124
7.5	Scintigrams and biodistribution of labeled PEG-PLA as solution.	125
7.6	Scintigrams and biodistribution of labeled PEG as solution.	126
7.7	Biodistribution study of dual-labeled IFF-loaded PEG-PLA micelles.	127

List of Tables

2.1	Loading results of DXM in PEG-PVPy micelles.	37
2.2	Particle size distribution parameters obtained from cryo-EM micrograph analysis.	43
3.1	Physical state of block copolymers.	60
3.2	Particle sizes of micelles in negative staining TEM vs DLS.	61
3.3	Residual micellar fraction of block copolymer micelles upon serum incubation.	64
3.4	AF4 results of PEG-PVPy micelles upon serum incubation.	65
4.1	Testing materials/particles in the cytotoxicity and complement assays.	76
4.2	PEG-PEI characteristics obtained from ¹ H-NMR spectroscopy.	79
4.3	Particle sizes and size distributions of micelles/particles in cytotoxicity and immunogenicity assays.	80
4.4	EC ₅₀ values for micelles on rat hepatocytes and HepG2 cells.	81
4.5	Evaluation of the complement activation results.	84
5.2	Physicochemical characterization of the injected formulations.	94
5.1	Loading results of compound A in varying block copolymer micelles.	95
5.3	Pharmacokinetic parameters of compound A and compound B in different tissues/organs.	97
5.4	Molar mass characterizations of H ₂ N-PEG-PLGA.	98
7.1	Characterization of H ₂ N-PEG-PLA.	123
7.2	Characterization of labeled PEG-PLA micelles.	123

Appendix

Curriculum vitae

Personal information

Name: Tobias Miller
Date of birth: 1/14/1984
Place of birth: Potsdam, Germany
Nationality: German

Professional experience

4/2009 - 6/2012	PhD student at Merck Serono, Darmstadt, Germany, in collaboration with Prof. A. Goepferich, University of Regensburg, Germany
11/2008 - 3/2009	Scientific coworker at University of Brunswick, Germany
5/2008 - 10/2008	Pharmacy internship in Kaenguruh-Apotheke, Potsdam, Germany (public pharmacy)
11/2007 - 4/2008	Pharmacy internship at Haupt Pharma Wuelfing GmbH, Gronau (Leine), Germany (CMO)
7/2004 - 8/2004	Internship in dispensary of Ernst-von-Bergmann Klinikum, Potsdam, Germany
03/2004	Internship Linden Apotheke, Werder, Germany (public pharmacy)

Education

10/2003 - 10/2007	Studies of Pharmaceutical Sciences at the Free University of Berlin, Germany
06/2003	General qualification for university entrance ("Allgemeine Hochschulreife")

List of publications

Peer-reviewed scientific articles

Tobias Miller, Reinhard Rachel, Ahmed Besheer, Senta Uezguen, Markus Weigandt, Achim Göpferich: Comparative investigations on *in vitro* serum stability of polymeric micelles formulations. *Pharm Research* 29 (2): 448-459, 2012. (**Chapter 3**)

Tobias Miller, Alexandra Hill, Senta Uezguen, Markus Weigandt, Achim Göpferich: Analysis of stress mechanisms occurring immediately upon injection of polymeric micelles and their potential implications on passive drug targeting. Published in: *Biomacromolecules*. In press. (**Section 1.2**)

Tobias Miller, Gwenaëlle van Colen, Mariola Monika Golas, Bjoern Sander, Senta Uezguen, Markus Weigandt, Achim Goepferich: Drug loading of polymeric micelles. Submitted to: *Pharm Research*. (**Chapter 2**)

Tobias Miller, Sandra Breyer, Gwenaëlle van Colen, Walter Mier, Uwe Haberkorn, Senta Uezguen, Markus Weigandt, Achim Goepferich: Dual-label of carrier micelle and payload revealed biodistribution differences rapidly occurring upon injection. To be submitted. (**Chapter 7**)

Sandra Breyer, Angelika Semmler, **Tobias Miller**, Alexandra Hill, Simon Geissler, Uwe Haberkorn, Walter Mier: Radioiodinated dechloro-4-iodofenofibrate: a hydrophobic model drug for molecular imaging studies. Published in: *Int J Pharm*.

Conference abstracts

Tobias Miller, Ahmed Besheer, Markus Weigandt, Achim Goepferich: Preparation and *in vitro* serum stability testing of polymeric PEG-PLA micelles by Foerster Resonance Energy Transfer (FRET). 7th World Meeting on Pharmaceutics, Biopharmaceutics and Pharmaceutical Technology, Valletta, Malta (2010).

Angelika Semmler, Simon Geissler, **Tobias Miller**, Uwe Haberkorn, Walter Mier: Synthese des hydrophoben Modellwirkstoffes Deschlor-4-iodfenofibrat. 18. Jahrestagung der Arbeitsgemeinschaft Radiochemie/Radiopharmazie, Bad Boll, Germany (2010).

Tobias Miller, Ahmed Besheer, Senta Uezguen, Markus Weigandt, Achim Goepferich: *In vitro* serum stability of polymeric micelles. 38th Annual Meeting & Exposition of the Controlled Release Society. National Harbor, MD, USA (2011).

Tobias Miller, Angelika Semmler, Sandra Breyer, Walter Mier, Senta Uezguen, Markus Weigandt, Achim Goepferich: Challenges in nanoparticulate drug delivery: What fate

do polymeric micelles encounter upon injection? 8th World Meeting on Pharmaceutics, Biopharmaceutics and Pharmaceutical Technology, Istanbul, Turkey (2012).

Poster and oral presentations

Tobias Miller, Ahmed Besheer, Markus Weigandt, Achim Goepferich: Preparation and *in vitro* serum stability testing of polymeric PEG-PLA micelles by Förster resonance energy transfer (FRET). 7th Worldmeeting on Pharmaceutics and Biopharmaceutics, Valletta, Malta (2010). Poster presentation.

Tobias Miller, Ahmed Besheer, Senta Uezguen, Markus Weigandt, Achim Goepferich: *In vitro* serum stability of polymeric micelles. 38th Annual Meeting of the Controlled Release Society, National Harbor, MD, USA (2011). Poster presentation.

Tobias Miller, Angelika Semmler, Sandra Breyer, Walter Mier, Senta Uezguen, Markus Weigandt, Achim Goepferich: What fate do polymeric micelles encounter upon injection? 8th World Meeting on Pharmaceutics and Biopharmaceutics, Istanbul, Turkey (2012). Oral presentation.

Patents

Applications

Tobias Miller, Senta Uezguen, Markus Weigandt, Achim Goepferich: Verfahren zur Herstellung wirkstoffbeladener Nanopartikel. Deutsches Patent- und Markenamt (German Patent and Trademark Office), Munich, Germany (2012). Preliminary application #: DE102012004099

Acknowledgements

An dieser Stelle möchte ich die Möglichkeit nutzen, all den Menschen zu danken, die mich sowie diese Arbeit in den letzten Jahren begleitet haben.

Allen voran geht dieser Dank an Achim Göpferich, der diese Arbeit hervorragend betreut hat und trotz der permanenten geografischen Entfernung zwischen uns stets als überaus kompetenter Gesprächspartner erreichbar war. Ich danke ihm insbesondere für das Interesse an der Arbeit, die konstruktive Kritik an den Experimenten sowie Manuskripten und darüber hinaus für seine Ideen, die zum Gelingen dieser Arbeit wesentlich beigetragen haben.

Besonderer Dank gebührt weiterhin Senta Üzgün und Markus Weigandt (Merck Serono, Darmstadt) die diese Arbeit organisatorisch und inhaltlich betreut haben. Ohne die wissenschaftlichen Diskussionen, das kritische Hinterfragen der experimentellen Ergebnisse sowie die Sichtbarkeit innerhalb der Firma wären einige Möglichkeiten verschlossen geblieben.

Die enge Zusammenarbeit mit Alexandra Hill sowie Simon Geissler (Merck Serono, Darmstadt) war ebenfalls Triebkraft für das vorliegende Manuskript. Ich danke Alexandra für ihre stetige konstruktive Kritik, die aufmunternden Worte sowie besonders für ihre persönliche Begleitung während der Hochs und Tiefs in den vergangenen Jahren. Simon danke ich für seine persönliche, labororganisatorische sowie fachliche Unterstützung in dieser Zeit. Beide sind hervorragende Wissenschaftler und es war ein großer Lichtblick, mit ihnen zusammen zu arbeiten.

Dem Radiologie-Team an der Universität Heidelberg gebührt sehr großer Dank, insbesondere Sandra Breyer, Angelika Semmler, Karin Leotta und Walter Mier, das an der Durchführung der Tierversuche mit radioaktiv markierten Polymeren/Wirkstoffen beteiligt war.

Weiterhin danke ich Finn Bauer und dem gesamten Team von EMD Millipore in Woburn (MA, USA) für die freundliche Aufnahme am Standort und die Möglichkeit, dort intensiv Serumexperimente durchzuführen. Die 2 Monate in einem US-Labor waren sehr erfahrungsreich, fachlich sowie persönlich und haben mich und die Arbeit erheblich positiv beeinflusst.

Besonderer Dank geht ebenfalls an Ahmed Besheer, LMU München, der die Idee für diese Doktorarbeit entwickelte, mich in den ersten 6 Monaten der Arbeit fachlich begleitete und für mich persönlich über die gesamte Arbeit ein wissenschaftliches Vorbild war.

Dem Team der *in vitro* Toxikologie am Standort Merck Serono, Darmstadt, möchte ich für ihre Unterstützung bei den Zytotoxizitätsexperimenten danken. Hier haben mich bei den Zellkulturexperimenten Johanna Sebbel und Stefan O. Müller unterstützt.

Reinhard Rachel an der Universität Regensburg danke ich für die Aufnahme der negativ-kontrastierten TEM Bilder.

Bjoern Sander und Monika Golas (Universität Aarhus) danke ich für die Aufnahme der cryo-EM Bilder.

Frank Zenke, Christiane Amendt sowie Gerhard Schuster (Merck Serono, Darmstadt) danke ich für die Durchführung der Tierversuche mit compound A-beladenen Mizellen.

Weiterhin möchte den Mitdoktoranden sowie allen Kollegen in ED (Merck Serono, Darmstadt) danken, insbesondere:

- Gwenaëlle van Colen für ihre Leidenschaft, Mitarbeit, Ideen und Interesse an meiner Arbeit.
- Katharina Anhalt, Stefan Schiller, Bernd Sterner für die fachlichen Diskussionen und die gemeinsame Zeit während der Doktorarbeit.
- Andrea Hanefeld, Patrizia Boniforte sowie Nadja Foster für Labororganisation.
- Dirk Schiroky für gelegentliche MS-Experimente.

Darüber hinaus möchte ich dem Team von WL-ACP-7 (Merck KGaA, Darmstadt) danken, insbesondere Christoph Hoffmann und Sven Brüninghoff für die Möglichkeit der Durchführung von Fluoreszenzexperimenten.

Am Lehrstuhl für Pharmazeutische Technologie, Regensburg, danke ich Miriam Breunig und Sonja Bauhuber. Miriam für die Zell- und FACS-Experimente und Sonja für Aufnahme von NMR Spektren.

Abschließend, aber nicht minder bedeutend, danke ich meinen Eltern, die mich immer auf jedem meiner Wege und in jeder Entscheidung unterstützt haben. Ohne sie wäre ich wohl niemals so weit gekommen. Leider wird auch in Zukunft die räumliche Entfernung zwischen uns nicht kleiner.